https://ntrs.nasa.gov/search.jsp?R=19700019404 2020-03-12T02:05:32+00:00Z

N 70 28712

NASA CR-72675

57

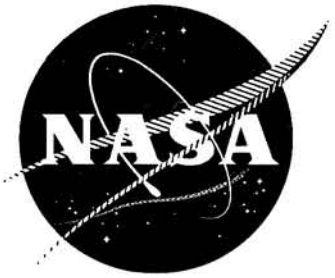

HIGH VOLTAGE SOLAR ARRAY STUDY

By

W. Knauer, J.R. Bayless, G.T. Todd, and J.W. Ward

HUGHES RESEARCH LABORATORIES

Prepared for

NATIONAL AERONAUTICS AND SPACE ADMINISTRATION

NASA Lewis Research Center
Contract NAS 3-11535
S. Domitz, Project Manager

CASE FILE COPY

NOTICE

This report was prepared as an account of Government-sponsored work. Neither the United States, nor the National Aeronautics and Space Administration (NASA), nor any person acting on behalf of NASA:

A.) Makes any warranty or representation, expressed or implied, with respect to the accuracy, completeness, or usefulness of the information contained in this report, or that the use of any information, apparatus, method, or process disclosed in this report may not infringe privately-owned rights; or

B.) Assumes any liabilities with respect to the use of, or for damages resulting from the use of, any information, apparatus, method or process disclosed in this report.

As used above, "person acting on behalf of NASA" includes any employee or contractor of NASA, or employee of such contractor, to the extent that such employee or contractor of NASA or employee of such contractor prepares, disseminates, or provides access to any information pursuant to his employment or contract with NASA, or his employment with such contractor.

Requests for copies of this report should be referred to

National Aeronautics and Space Administration
Scientific and Technical Information Facility
P. O. Box 33
College Park, Md. 20740

NASA CR-72675

FINAL REPORT

HIGH VOLTAGE SOLAR ARRAY STUDY

by

W. Knauer, J. R. Bayless, G. T. Todd, and J. W. Ward

Hughes Research Laboratories
A Division of Hughes Aircraft Company
3011 Malibu Canyon Road
Malibu, California 90265

Prepared for

NATIONAL AERONAUTICS AND SPACE ADMINISTRATION

May 1970

CONTRACT NAS 3-11535

NASA Lewis Research Center
Cleveland, Ohio 44135
S. Domitz, Project Manager

FOREWORD

The following persons contributed to the preparation of this report: W. C. Dunkerly, R. W. Opjorden, R. J. Holbrook, and C. R. Buckey.

TABLE OF CONTENTS

ABSTRACT

A detailed feasibility study of high voltage solar arrays, capable of 15 kW at 2 to 16 kV, has been performed. The major areas considered are (1) plasma power losses; (2) dielectric stresses; and (3) questions relating to high voltage design, fabrication, and testing. The general conclusion reached is that, except for minor modifications, conventional array designs can be utilized on most missions. Missions which require operation in the lower regions of the ionosphere at the higher voltages or for extended time periods can involve severe plasma power losses. Methods are discussed for reducing such losses.

LIST OF ILLUSTRATIONS

I. INTRODUCTION AND SUMMARY

Present spacecraft which incorporate high voltage devices such as ion thrusters and microwave power tubes must employ power conditioning units to convert the low voltage output from conventional solar arrays to the required high voltage levels. For this type of spacecraft attractive systems simplifications and perhaps savings in weight could be accomplished with the use of solar arrays which produce the high voltages directly. In principle, the transition from low to high voltage should be straightforward. By placing large numbers of cells in series and few in parallel, instead of the reverse as in conventional arrays, output voltages of several kilovolts should be easily achievable with panels having output powers on the order of kilowatts. However, the presence of high voltages leads to a number of electric insulation problems; some of these are common to high voltage gear in general, while others are unique to operation in space. Much of the effort under this contract was devoted to problems of the latter type.

Operation in space involves, first and foremost, the interaction of the array with its space environment. The following facets of this interaction were considered of particular importance: (a) power losses due to collection of space plasma particles, (b) power losses due to discharges initiated and sustained by the neutral and charged particle environment, (c) dielectric breakdown and damage to solar cells as a result of environmental charge accumulation on insulator surfaces, and (d) sputter and radiation damage to solar cells due to incident energetic particles.

In addition to these environment-induced problems, questions relating to the design, fabrication and testing of high voltage solar arrays were investigated. Furthermore, a conceptual design of a high voltage array was worked out. Finally, a description of further efforts required to assure feasibility of such arrays was prepared.

The results obtained may be summarized as follows. The computed power losses of arrays with standard solar cells (cover slides and open tabs) are acceptably low throughout space, except in the ionosphere. Even there, arrays which are required to produce 2000 V or less can be operated with losses not exceeding 20 to 30% of their output power. For missions that include orbit raising maneuvers the spacecraft passes through the densest regions of the ionosphere in a matter of days, and for such short periods losses of the described magnitude may be acceptable. An additional favorable factor is that, in the ionosphere, the arrays have not yet suffered any radiation degradation and therefore can deliver their maximum power. For missions where high voltages must be provided over long periods at ionospheric altitudes, several alternative methods can be used to decrease plasma losses to acceptable levels. One possibility is to hermetically seal all high voltage portions of the array with an insulating layer. This method works reliably only if pinhole breakdown (arc-like discharges issuing from pinholes across the insulating layer) can be avoided. Pinhole arcs have been observed in several laboratory experiments; however, the evidence is insufficient for determining whether pinhole arcs will adversely affect the operation of high voltage

solar arrays. For this reason, total insulation cannot, at this time, be considered a safe approach toward reduced plasma leakage. Other possibilities include "depressed plasma collectors" and biased screens. The depressed collector method is a very interesting, new concept combining the prevention of pinhole breakdown with reduced plasma losses. However, further effort is required to prove its effectiveness. The biased screen method is conceptually straightforward. It decreases the plasma leakage in much the same way that biasing a triode grid will lower the anode current. Because the effectiveness of this method is not in doubt, a conceptual screen design has been evolved.

An investigation of dielectric array surfaces has disclosed that all insulating surfaces, including those of cover slides, adopt a potential very near, but slightly negative with respect to space plasma potential. This raises the question whether tabs, which are located between cover slides, are shielded by their negative surroundings and consequently draw smaller electron currents than would be expected otherwise. An evaluation of the field configuration near tabs shows, however, that a noticeable decrease in tab current cannot be expected on standard arrays. For this to occur the cover slides would have to be far more negatively biased than space environmental conditions permit, or the tabs would have to be far more recessed than is the case on conventional arrays.

Because all dielectric surfaces are near space potential, large voltage gradients can be expected to exist across the dielectric layers which cover the array. Static voltage breakdown data collected for dielectric materials of interest for the present application suggest that comparatively small layer thicknesses (about 6 to 8 mils for quartz and 3 to 4 mils for kapton) should be sufficient to withstand the maximum anticipated dielectric stresses. This conclusion is based on the assumption that all insulating layers are free of large voids and have clean surfaces, and that breakdown does not occur through pinholes created by micrometeoroids. A further assumption is that the dielectric strength does not deteriorate under energetic particle radiation. The validity of some of these assumptions is in doubt, and suitable experimental investigations should be conducted in order that more reliable values for safe insulating layer thicknesses can be established.

Impact of energetic particles on the solar array may not only affect the dielectric strength but also lead to surface erosion and deterioration of solar cell performance. Sufficient experimental data are available to allow predictions for these two types of damage. From known sputtering rates for oxygen, nitrogen, and hydrogen on quartz, one can conclude that even in the ionosphere the erosion rates should not exceed about 10^4 atom layers per year. This amount is believed too small to adversely affect the optical quality of quartz cover slides. Damage caused to solar cells by energetic radiation belt particles is considered to be much more serious. Radiation dose computations for an orbit raising maneuver which employs ion thrusters predict that the solar cell power output may have deteriorated by about 30 to 40% by the time the spacecraft reaches synchronous orbit, and that less than 50% of the original power output will remain at the end of a 5 year mission. This result, which is not peculiar to high voltage solar arrays, suggests that emphasis be given to methods for healing radiation damage by cell annealing techniques.

Design studies performed under this contract have led to the conclusion that, in general, high voltage arrays can be built along rather conventional lines. The layout of cells within cell-groups, cell-sectors, cell-blocks, and panels can be chosen according to circuit needs and is affected little by environmental factors. To be sure, cell blocks of different potentials which border each other must be kept at a safe distance (about 1 in.). The same is true for busses which operate at large potential differences. Because only a few cells are connected in parallel, the problem of open circuits is more serious here than with low voltage arrays. In order to provide the required high reliability in this case, short-circuit diodes must be incorporated in sufficient numbers. To facilitate manufacture and handling and to minimize electrical shock hazards, the array should be composed of smaller units or "sectors" which would be manufactured separately. Their output voltage should not exceed about 100 V and they should be interconnected with other sectors only at the end of the manufacturing process.

The work reported here permits the following over-all conclusions:

- high voltage arrays appear to be quite feasible
- high voltage arrays are not expected to be much heavier than standard arrays (when power conditioning, switching, and regulation circuitry is included the high voltage array will weigh considerably less than an equivalent low voltage array)
- relatively conventional cell configurations should be satisfactory for most missions
- for some missions plasma leakage may have to be reduced by such methods as biased screens, total cell insulation, or depressed plasma collectors
- future study efforts should be concentratedon (a) dielectric strength tests in a plasma and radiation environment, (b) plasma leakage computations and measurements in the presence of insulating surface portions, and (c) bread-board panel performance and life tests in a plasma environment.

II. ARRAY CURRENT LOSSES

A. PLASMA LOSSES

1. Basic Rules

The situation of a high voltage solar array in space can be compared with that of an electrostatic probe in a laboratory plasma. A biased probe is surrounded by a plasma sheath. A sheath is the region across which the potential rises (or falls) from the level of the plasma to that of the probe. At the outer edge of the sheath, particles of one polarity are rejected while those of the other sign are attracted.

A major interest in studying the plasma probe properties of high voltage solar arrays is to determine current-voltage characteristics for the array-plasma interaction. In general, probe characteristics depend upon the geometry of a probe and upon the energy and density of the surrounding plasma particles. In the case of a solar array in space, additional complications arise from (a) motions of the array against the space plasma (primarily in the ionosphere), (b) the presence of the earth's magnetic field, (c) potential structures on the array, (d) differences between floating and ion beam biased operation, and (e) trapping and reflection of attracted particles. In this section we will ignore these complicating factors and discuss the situation of a unipotential array in an isotropic plasma at rest, which by itself is a nontrivial problem.

The width of a plasma sheath depends significantly upon plasma density. At high densities the sheath is thin, and at low densities it is thick. Analytic determination of the I-V characteristics for probes which are as irregularly shaped as an array is possible only in the extremes where the plasma sheath is either small or large in comparison with the array dimensions. In the former case the sheath can be considered a one-dimensional layer; in the latter case it is very nearly spherical (see Fig. 1).

The size and configuration of the sheath which surrounds a high voltage solar array in space depends much upon the charged particle flux at the location of the array. In Appendix A a detailed description is given of the special distributions of various types of environmental charged particle components. Near earth, the most important component is the so called "thermal" plasma. Its spatial distribution is shown in Fig. 2. The density of this plasma has been used in an analysis (see Appendix B) to compute the sheath thickness as a function of distance from earth. The results show (see Fig. 3) that in the ionosphere the sheath width is comparable to or smaller than the array dimensions (order of 10^3 cm). Farther out into space the sheath width increases rapidly and, at synchronous orbit, it can be considered large compared with the array dimensions.

Based upon the described dependence of the sheath width on location we elect to compute I-V characteristics in the ionosphere from a one-dimensional sheath model. For distances in excess of 2 earth radii from earth, a spherical sheath model will be used. Between both regions we interpolate data obtained at the two extremes. To assess the validity of this interpolation we solve selected cases with intermediate sheath width, using a self-consistent computational technique involving an electrolytic tank simulation (see Appendix B for details).

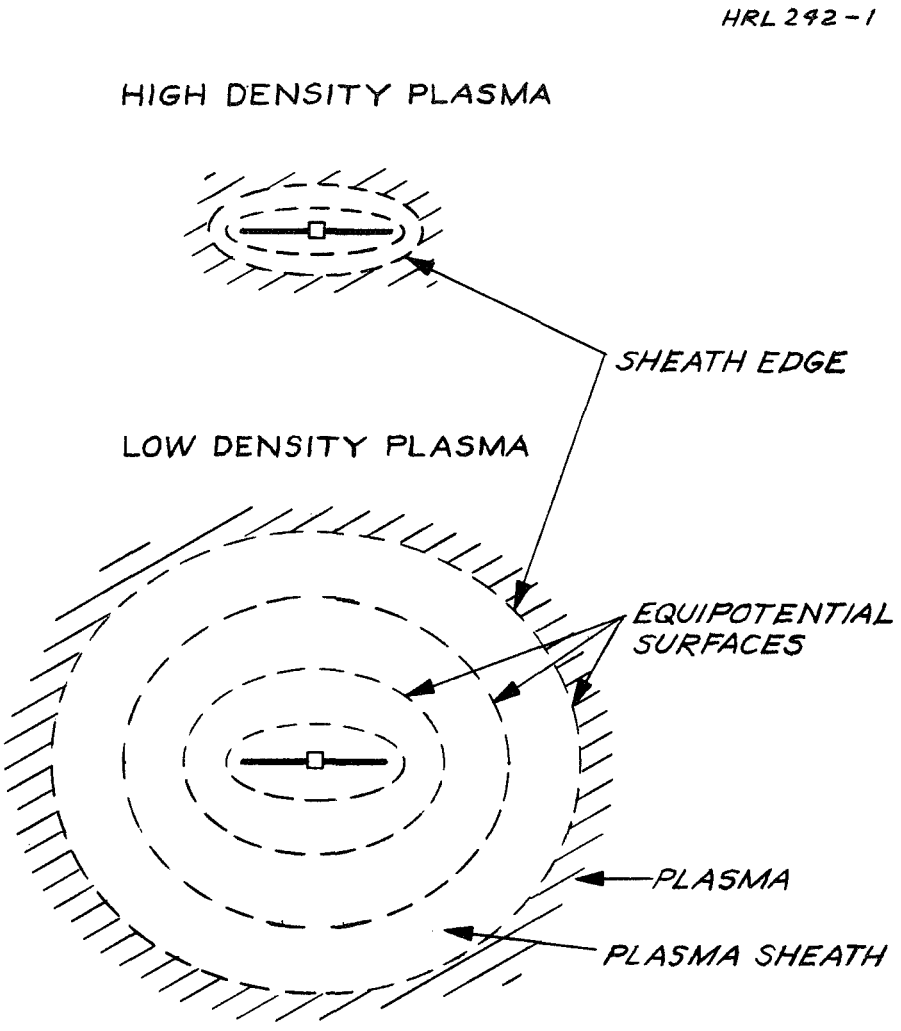

Fig. 1. Approximate plasma sheath configurations for arrays at a unipotential.

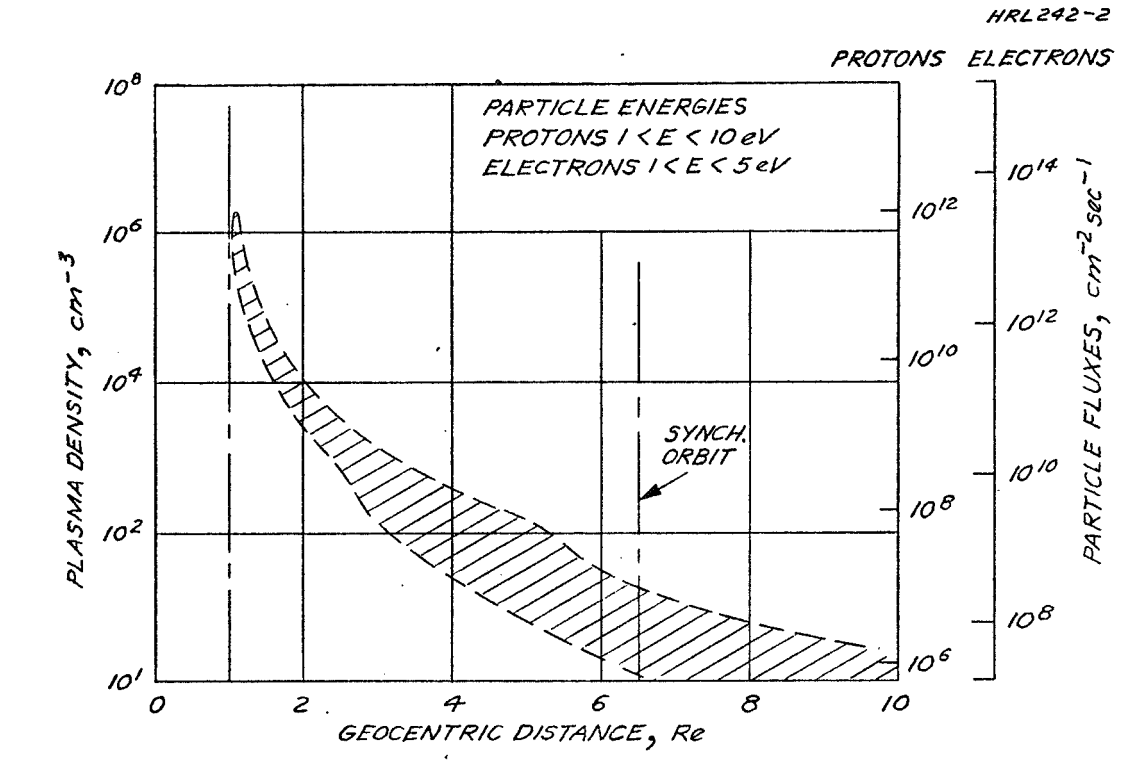

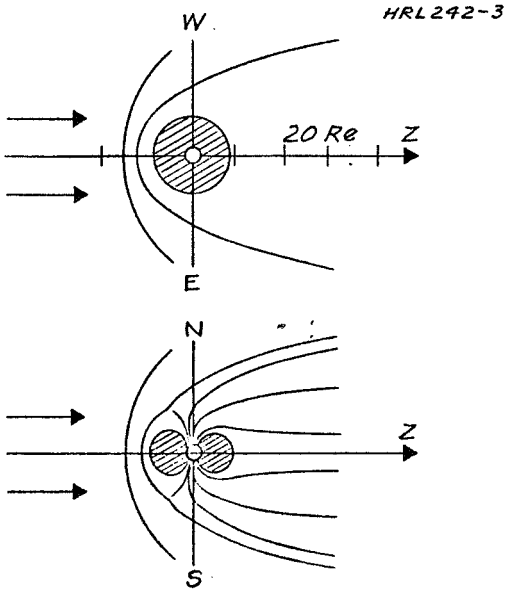

Fig. 2. Thermal plasma distribution along the z-axis within the geomagnetic cavity. The range shown indicates temporal fluctuations and measurement uncertainties.

The I-V characteristic of a one-dimensional sheath configuration can be determined very simply. If A is the surface area of the array, counting both sides, and if j_r is the random current of the particle species that is attracted by the array, the total collected current I is

$$I = A\, j_r \quad . \tag{1}$$

Equation (1) does not contain V, i.e., the current collection is independent of voltage. It is obvious that this is true only within limits. As the voltage is increased to very high levels the sheath width becomes so large that the assumption of a one-dimensional array breaks down. Current collection then begins to increase with voltage.

In the case of a large sheath, determination of the I-V characteristics is more complicated. Under conditions of free ballistic particle flow (no collisions) the attracted particles must conserve energy and angular momentum (with respect to the probe) while they approach the probe. This leads to an "impact" parameter p which determines the maximum passing distance from which a particle can be attracted to the probe.[1] Particles entering a sphere of radius p concentric with the probe can (but need not) be collected. Whether they are indeed collected depends upon the potential distribution around the probe.[1] If the surrounding plasma is tenuous the space charge of the attracted species distorts the vacuum potential distribution of the probe very little. In this case all particles that penetrate the sphere p are collected. However, if the plasma density is large, the potential distribution is strongly affected by space charge. In this case the probe fields extend only to a distance r_o which is smaller than p and only those particles that move randomly to within radius r_o are attracted. The value of r_o is determined by the rules for space charge limited flow. In Appendix B an expression is derived for r_o as functions of array voltage V, plasma density n, and electron and ion temperatures T_e and T_i. Figure 3 gives numerical results for r_o and p. It can be seen that to distances on the order of 8 earth radii the impact parameter p is larger than the space charge sheath radius r_o. Therefore, I-V characteristics must be determined on the basis of r_o and not p. The collection current I is then simply given by

$$I = 4\pi r_o^{\,2}\, j_r \tag{2}$$

where j_r is the random current density of the attracted species. If the expression for r_o (given in Appendix B) is introduced into (2), one obtains (in cgs units)

$$I = 4\pi \left[\frac{1.08}{\pi}\left(\frac{e}{m}\right)^{1/2}\right]^{4/7} (aV)^{6/7}\, j_r^{\,3/7} \tag{3}$$

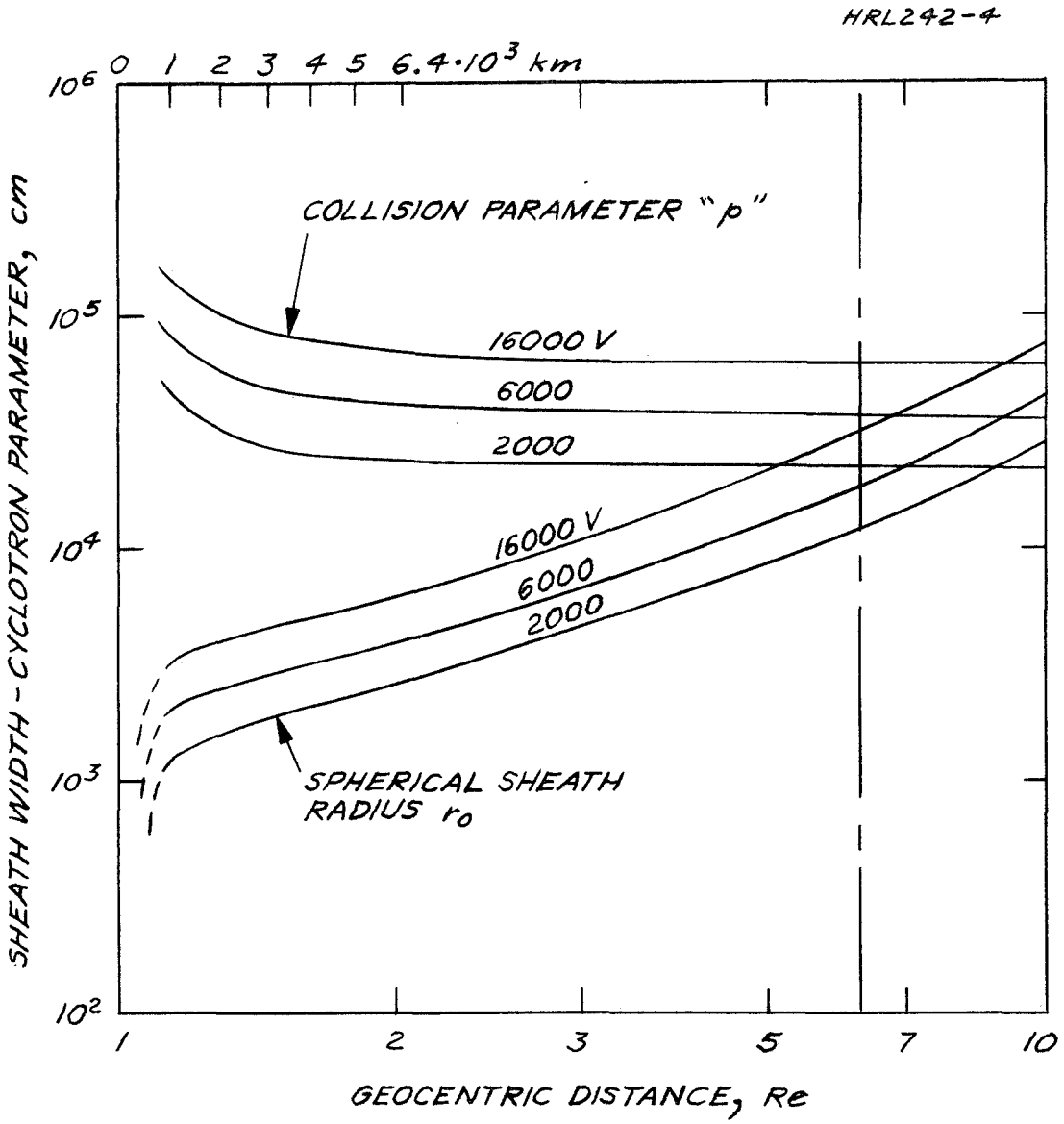

Fig. 3. Sheath width and collision parameter as a function of distance from earth with the array voltage (assumed unipotential) as a parameter.

where V is the array potential and a is the effective array diameter. For distances beyond 8 R_e where $p < r_o$, the collection current can be determined from the following expression, first derived by Langmuir[2]:

$$I = 4\pi a^2 \left(1 + \frac{V}{kT}\right) j_r \qquad (4)$$

where T is the temperature of the attracted species. Again, it should be emphasized that (4) is not applicable to the space regions near earth which are predominantly of interest here. Indeed, use of (4) for regions below synchronous altitude yields currents which are in error by as much as two orders of magnitude.

The array power loss W which results from the collection of plasma particles can be computed simply by multiplying the collector currents I, given by (2) and (4), with the array voltage V. Figure 4 gives power losses W for an array of $A \cong 6 \times 10^6$ cm^2 total surface area ($a \cong 7 \times 10^2$ cm) which is maintained at voltages between 2000 and 16000 V. The low altitude loss power curves are based on (2) and the high altitude curves on (4). The dashed portions in between are best estimates. The validity of such an interpolation is suggested by the satisfactory agreement between one of the dashed curves and two power loss points (marked by circles) which were derived with the help of a computer simulation technique. The details of this technique, which involves an electrolytic tank test, are described in Appendix C.

For comparison, Fig. 4 also gives the power W_o generated by the array. The numerical value for W_o used in Fig. 4 and elsewhere in this report is based upon an array sizing exercise described below, which includes radiation deterioration. According to Fig. 4 the power losses W, computed by the described first order method, tend to exceed the array power output W_o throughout the ionosphere. It will be seen below, however, that a more sophisticated approach leads to much smaller power losses which, for array voltages of 2000 V, remain significantly below the power output even in the densest regions of the ionosphere.

Thus far the large sheath case has been treated as if the array were a sphere of radius a. The question arises whether the actual, irregularly shaped array should collect plasma particles at comparable rates. On the following grounds, the answer should be affirmative. The vacuum fields generated by a charged probe of irregular shape tend to become radial in shape at distances from the probe body which are large compared with the over-all probe dimensions. If such a probe is immersed in an environmental plasma, the vacuum fields are modified by the space charge of the attracted particle species. Most of the field modifications take place in the region near the plasma boundary, where the particles are still moving slowly. Because the boundary is far from the probe (where the fields are radial regardless of probe shape), the space charge should have the same effect in both cases which implies that the same number of particles are attracted. The only remaining question is the following: how large is the radius r_o of a sphere which can be substituted for the actual, irregularly shaped probe? The answer is given in Appendix D, where numbers for the present case of interest are given. The power losses, so derived, have been entered

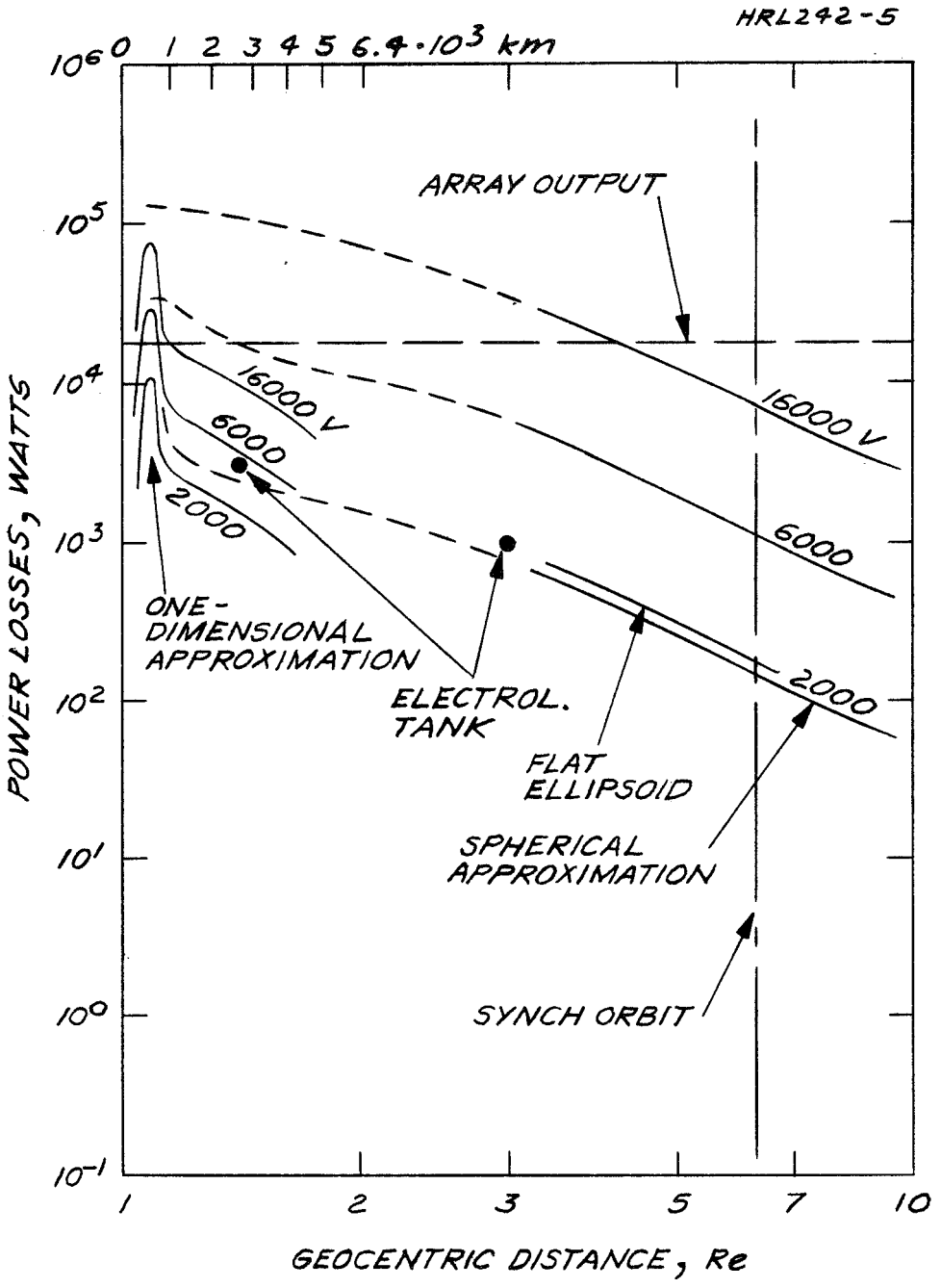

Fig. 4. Power losses of a positively charged array, first order computations.

into Fig. 4 (flat ellipsoid). Because these losses are very close to the earlier computed losses, it appears permissible to consider the array as a sphere with the same surface areas as that of the actual array.

2. Refined Plasma Loss Computations

In this section a number of factors are taken into account which significantly affect the collection rates of charged particles by a high voltage solar array and which make necessary a revision of the basic treatment given in the last section. These factors include (a) the geomagnetic field, (b) spacecraft velocities, (c) array surface potential distributions, (d) presence of insulators on the array surfaces, and (c) nonintercepting particle trajectories. As in the last section the loss currents are computed on the basis of the thermal plasma fluxes (see Fig. 2). Contributions due to Auger electrons (emitted by incident excited neutrals), secondary and photoelectrons and ions are neglected because they are small in comparison.

a. Geomagnetic Field

In the presence of a magnetic field the trajectories of charged particles are coiled. The geomagnetic field can be expected to influence array current collection rates when the orbits of the attracted particle species are comparable to or smaller than the width of the plasma sheath. The orbit diameter is given by

$$d = 2\frac{m}{e}\frac{vc}{B} \tag{5}$$

where m is the mass of the particle, e is its charge, v is its velocity, c is the light velocity, and B is the magnetic field (all in cgs units). A quick calculation shows that the orbital diameters of the ions in space are generally larger than the anticipated array sheath widths. The situation is different for the electrons. Figure 5 shows sheath width s and electron cyclotron diameters d as a function of distance from earth. The cyclotron diameters are given for a range of energies since, depending upon the location and way of entry into the sheath, electrons may have widely differing orbital energies. The sheath widths are given for array voltages between 2000 and 16000 V and for conducting as well as 95% insulating array surfaces (details are given below). It can be seen that at low and medium altitudes the cyclotron orbits of the less energetic particles are comparable to or even smaller than the sheath widths. For a discussion of the influence which this may have upon the current collection rates, refer to Fig. 6. In a situation where the array surfaces are transverse to the direction of the geomagnetic field and at low altitudes, where the plasma sheath can be considered one-dimensional, the collection rates should not be affected because the attracted particles are accelerated along the lines of force of the B-field. In a situation where array surface and magnetic field run parallel, a maximum change in the collection rates can be expected. There is some question whether only those particles are collected which approach the array with an impact parameter smaller than the cyclotron diameter, or whether particles can be collected from larger distances, as a result of instabilities.[3] Judging from the situation in a Penning discharge, which configurationally is similar to a high voltage array and which has been studied in great detail,

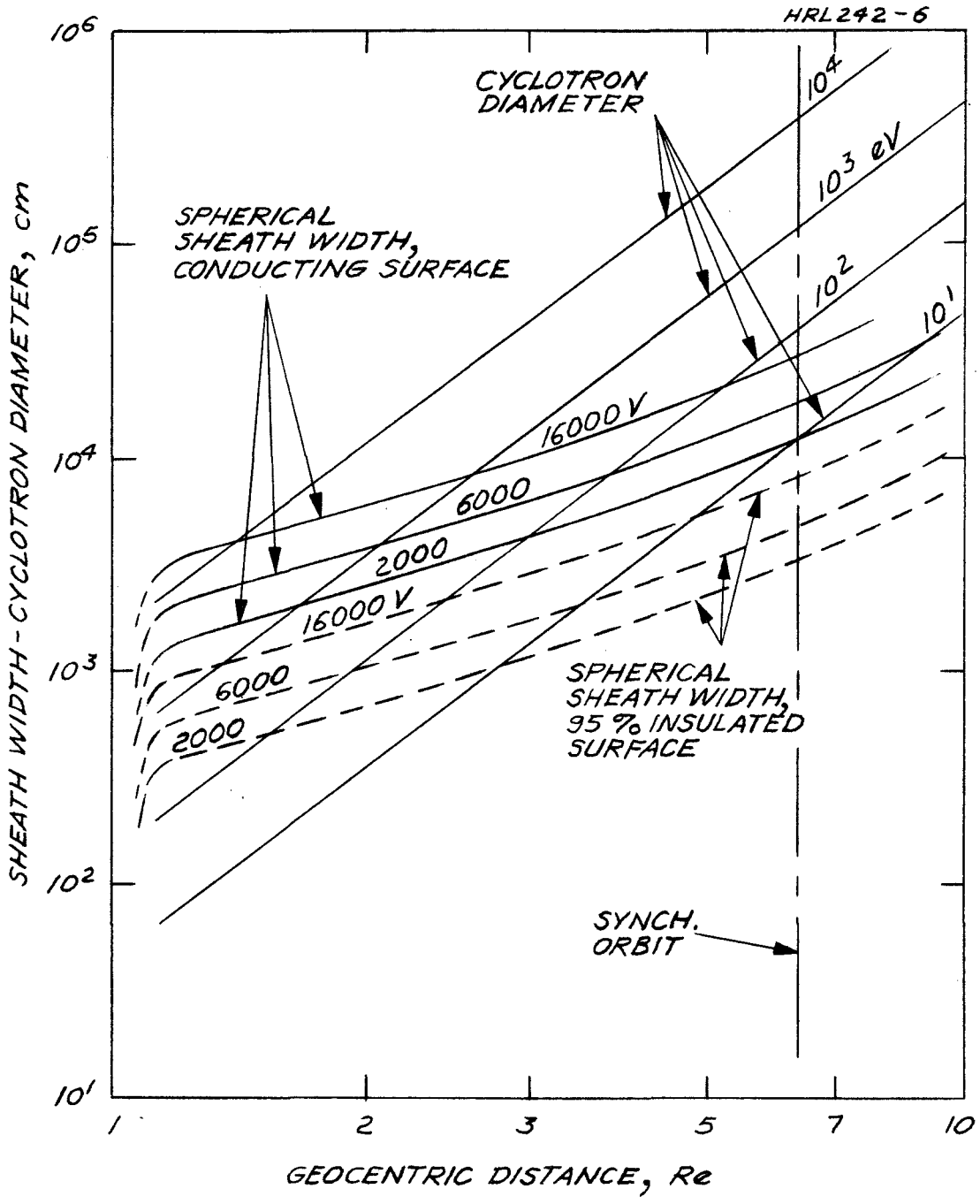

Fig. 5. Comparison of sheath width and cyclotron diameter.

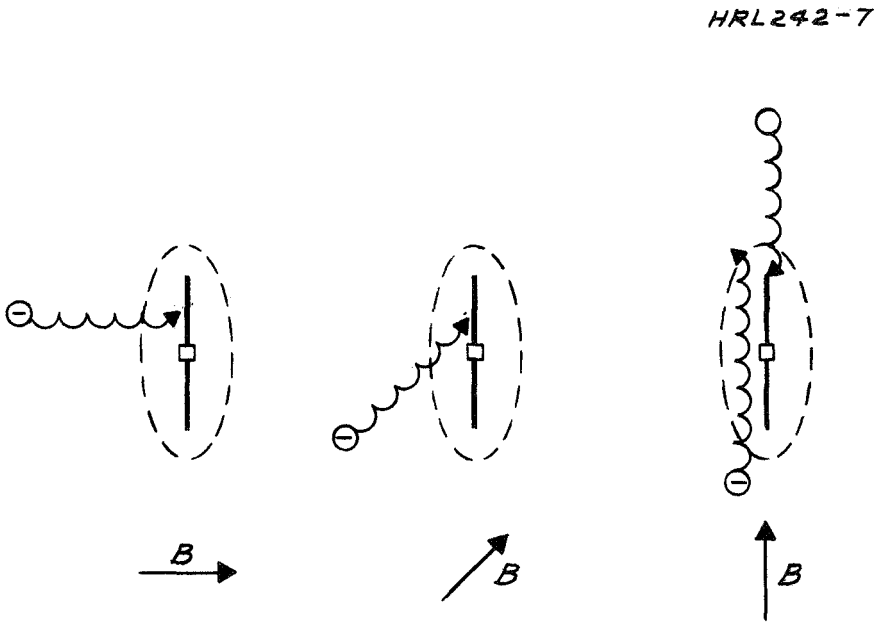

Fig. 6. Dependence of the electron trajectories upon magnetic field orientation.

one may conclude that instabilities will, indeed, increase the distances from which particles are collected. In Penning discharges the so-called "diocotron instability" collects particles at the anode from distances greater than the electron cyclotron diameter but always less than the space charge sheath width.[4] We can conclude that even with an instability present in the case where the array surface and B-field are parallel to each other, generally less current is collected than if they are at right angles. It is difficult to estimate the amount by which the current collection is reduced.

Conclusions: The effect of the geomagnetic field is to reduce the current collection of a positive array for certain array orientations at low altitudes. In other orientations the same full current as without magnetic field is collected. Because an orbiting array passes through all orientations with respect to the geomagnetic field during each orbit, the full collection current must be considered as a realistic upper limit. The ion collection current of a negatively charged array is not affected by the geomagnetic field.

b. Spacecraft Motions

A low altitude satellite moves through the ionosphere with an orbital velocity v_o of about 7×10^5 cm/sec. It moves past ions with thermal velocities v_m on the order of 10^5 cm/sec and electrons with 2×10^7 cm/sec. Because the satellite velocity is considerably higher than the average ion velocity, the region behind the satellite is rarefied (see Fig. 7). What happens in front depends upon the potential of the satellite (array). A positively charged array generates a detached "bow shock", where the ion density at the center point in front is increased by a factor 2. A negatively charged array collects all ions through which it sweeps, and because the reflected electrons move much faster than the array, a normal sheath boundary is formed. The described situation is not just a theoretical mode; recent satellite experiments have confirmed this picture.[5] In particular, they have demonstrated the existence of a rarefied region in the rear. Probe measurements yielded current collection ratios between front and rear which were as high as 100:1.

Because of the odd shape of high voltage solar arrays the current collection rates in low orbit should depend upon the orientation with respect to the direction of motion. A positive array which moves broadside through the ionosphere can be expected to collect only about half as much current as if it were at rest. The rear portion collects very little current because the absence of ions prevents electrons from passing through the rarefied region in large numbers. In front, despite a local increase in ion density, electrons are collected at the same rates as on an array at rest. The reason is that the geomagnetic field confines the electrons to field lines and thereby limits the influx to the random flux of the undisturbed plasma. A positive array which moves through the ionosphere with its narrow profile can be expected to collect approximately the same current as an array at rest. In this case the ions are displaced only at the edge of the plasma sheath and the array can collect electrons along its entire surface.

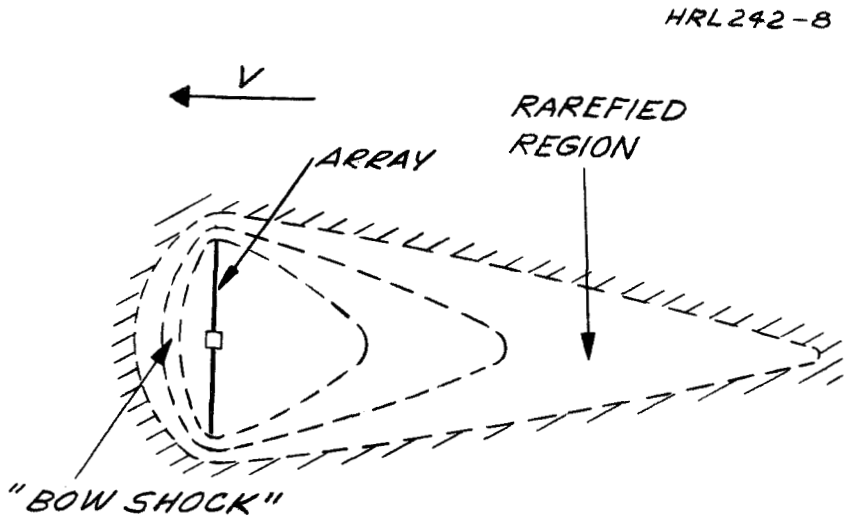

Fig. 7. Sheath distortion when the spacecraft moves faster than the environmental ions.

A negative array moving broadside through the ionosphere collects more than an array at rest, even though few ions can reach the rear of the array. In front, ions are swept up at the rate

$$I_m = \frac{A}{2} en v_o \qquad (6)$$

where A/2 is the front area, n is the ionospheric plasma density, v_o is the orbit velocity, and e is the ionic charge. I_m can be several times ^{o}larger than the current I given by (2) for an array at rest. This can be seen readily if (2) is expressed as

$$I = \frac{A}{4} en v_{thi}$$

whereby v_{thi} is the thermal ion velocity. In the case where the negatively charged array moves lengthwise through the ionosphere, again the collection should not differ much from that of an array at rest.

Conclusions: If a positively charged array moves broadside through the ionosphere, it will collect about half the current that it would collect at rest. One cannot take full advantage of this saving because during part of each orbit the array moves lengthwise whereby the full electron current is collected. In the case of a negative array the broadside orientation leads to ion collection rates which are enhanced by the factor $v_o/2\ v_{thi}$ over those for an array at rest.

c. Potential Structures on the Array

High voltage solar arrays incorporate large numbers of series connected solar cells as a result of which the surface potential varies significantly from location to location. In fact, depending upon cell layout within each array block and upon block layout within each solar panel, an infinite number of different surface potential distributions can be created. The question arises whether some of the layouts are more conducive to low plasma leakage than others. The answer is complicated by the fact that even individual cells do not constitute equipotential surfaces. It will be seen below that insulating cell cover slides, comprising about 95% of the surface area, adopt a potential very near to that of the space plasma. Only the exposed interconnecting tabs with about 5% surface area are at high voltage. The array surface potential therefore can be characterized by a periodic "micro"-structure, associated with the individual cells, and a "macro"-structure, linked to the array layout.

To deal with such a complex potential distribution we resort to a method recently advanced by Heil in connection with a basic study of the secondary electron emission from "patchy" surfaces.[6] Heil treated such surfaces as "checkerboards." He assumed a periodic potential distribution and used Fourier analysis to determine the electric field distribution

adjacent to the surface. A basic conclusion to be drawn from this analysis is that the near-field structure associated with a checkerboard potential distribution affects particles only over distances on the order of e-folding length of the periodic checker potential which is equal to $d/2\pi$ for quadratic checkers of width. At larger distances from the surface, charge motions are determined primarily by fields which derive from the average value of the surface potential. For the case of quadratic checkers, which alternate in potential between v_1 and v_2, this average potential is simply $0.5\ (v_1 + v_2)$. For the case of solar cells where 95% of the surface is at zero potential (with respect to space) and where 5% is at a high potential v, the average value of the surface potential becomes 0.05 V. The potential distribution across and away from such a surface is shown in Figs. 8 and 9.

According to this picture particles are attracted to a checkerboard array by fields which are much smaller than those associated with a unipotential array. In the case of large sheath widths where the collection rate depends upon voltage, eq. (4) yields much reduced plasma currents. In the case of small sheath widths, where the collection rates are independent of voltage, a checkered potential pattern will not help to reduce the plasma currents. This conclusion is subject to a more detailed examination of particle trajectories in the neighborhood of the array surface where the microfields affect the trajectories. Indeed, it is conceivable that a portion of the attracted particles is reflected locally by insulating surface elements and returns to the plasma. This possibility is discussed below.

The above description applies primarily to the cell microstructure that is present on any panel using conventional cells with cover slides and open tabs. The earlier mentioned macrostructure can be expected to further reduce the current collection in cases of large sheath widths, but to have no effect upon leakage currents where the sheath is thin. Because the current collection rates for large sheath widths are tolerably small even without a special layout for the macrostructure, the configuration for cells and cell blocks therefore may be chosen without regard for current losses.

Thus far the discussion has been concerned with the front side of the array. Consistent with dielectric strength requirements, to be described below, it will be assumed that the back is covered with a layer of Kapton or its equivalent. This layer must be sufficiently thick to withstand the potential difference between solar cells and space at all locations of the array. It will be assumed, furthermore, that small, conductive strips are attached to the outside of the Kapton layer. These strips are maintained at the same potential as the solar cells across the Kapton layer. The reason for this arrangement will be described below in the discussion of the pinhole effect. For simplicity, it will be assumed that the strips constitute 5% of the back surface. Front and back surfaces then generate identical electric field patterns and associated leakage losses.

Conclusions: Insulating coverslides and exposed cell tabs result in a checkered potential distribution that reduces the current collection rates when the sheath width is large but has no effect when the sheath width is small. Cell and cell block layouts have an insignificant influence on leakage currents, and therefore, any layout is acceptable.

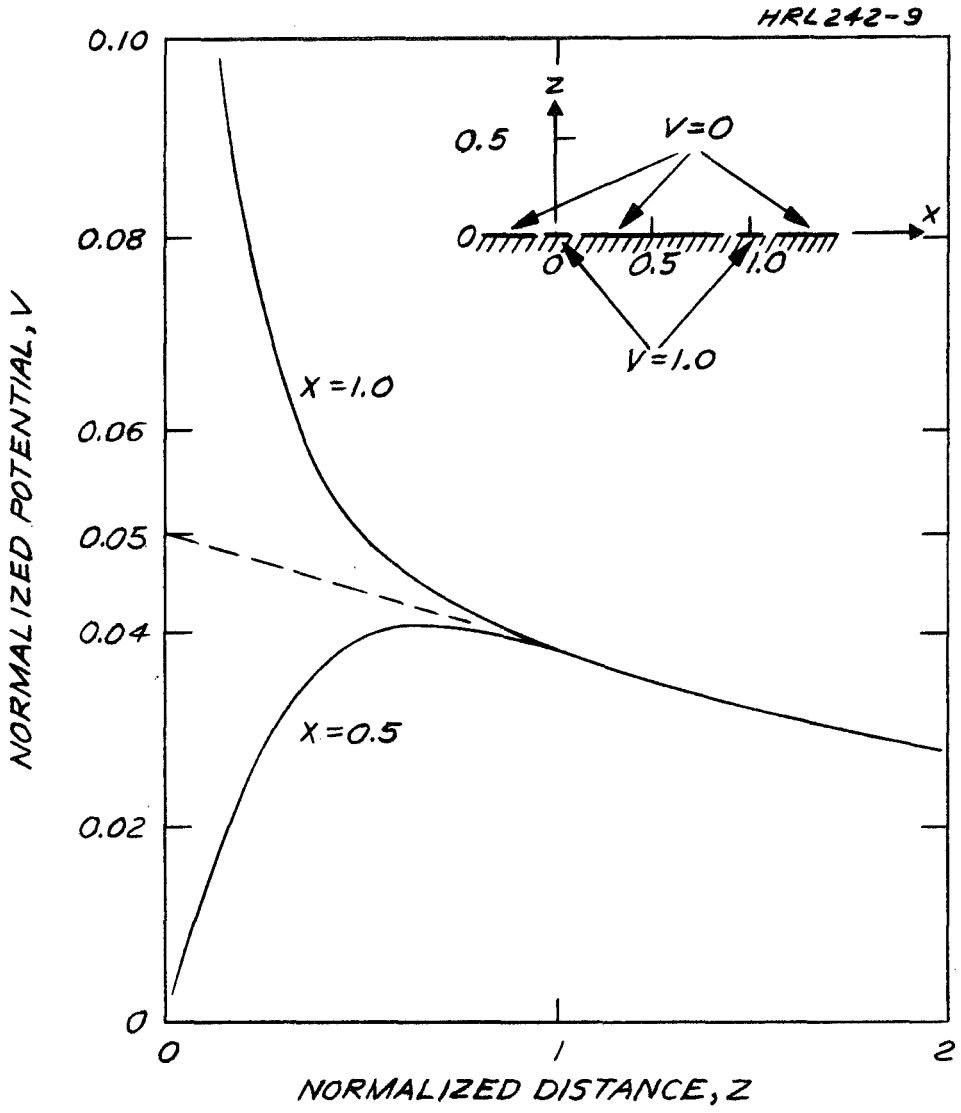

Fig. 8. Potential in front of a surface with periodically varying potential (5 % at potential 1, 95% at potential 0).

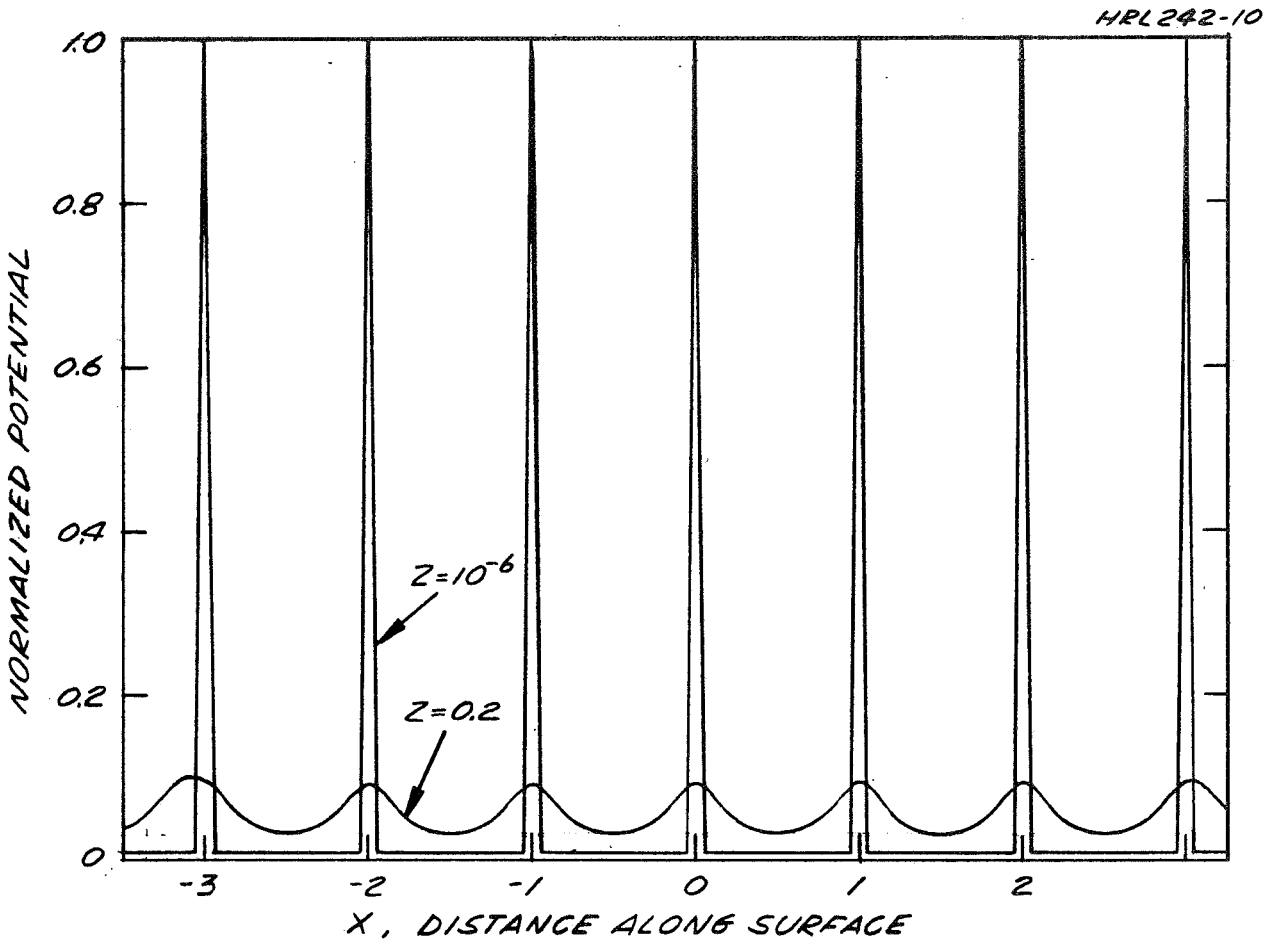

Fig. 9. Normalized potential in front of a surface with periodic potentials (5% at potential 1, 95% at potential 0); parameter: distance z from surface.

d. Floating and Ion Beam-Biased Arrays

In order to derive collection rates for the various situations of interest, still another factor must be considered. A solar array may either float (electrically) with respect to the environmental plasma or be maintained artificially at a biased potential. The array floats when the array output is used internally to power the spacecraft electronics. The array becomes biased when an electric propulsion system is activated. Both cases are discussed below.

(1) Floating Array - A high voltage array, left to itself in space, will act as a floating probe and adopt an equilibrium state at which the total current to and from the array becomes zero. Ignoring for the moment photoelectric currents and other secondary currents, equilibrium is achieved when the ion currents to the more negative array portions equal the electron currents to the more positive portions. In space, the random ion currents are much smaller than the random electron currents. Therefore, an array will tend to float predominantly negative with respect to space. Actually, this is true only for situations where the sheath width is small (see Fig. 10 (a)). In case of large sheath width the array potentials extend equally for positive and negative (see Fig. 10(b)). The reason for this is that over large distances from the array any net potential bias results in electric fields which reject all particles of one polarity and attract those of the other. However, this is in conflict with the requirement that electrons and ions must arrive at equal rates on a floating array. Therefore, the array will float so that its center potential is nearly equal to space potential (within several volts).

(2) Biased Array - If a high voltage array is used primarily to power ion thrusters, the exhausted ion beam establishes a voltage link between space plasma and array. The neutralized ion beam can be considered as a highly conductive plasma bridge that forces the potential of the electron emitting neutralizer to stay within about 30 V of space potential. To eject ions at space potential requires that they be accelerated from an ion source which is at a high positive potential. Thus, most of the solar array output must be delivered to a terminal at high positive potential, and most of the array will therefore be at positive potentials with respect to space. Figure 11 shows the sheath configurations for a positive array when the sheath width is either small or large with respect to the array.

If the various factors discussed here are incorporated into the loss current relations given in Appendix B, more reliable plasma loss estimates than given in Fig. 4 can be made. The computed power losses of floating and positively biased arrays are shown in Figs. 12 and 13. They pertain to standard arrays with 95% insulating surface areas and include the effects of array velocities (important only for floating arrays).

Conclusions: The plasma leakage losses of floating arrays with standard, slide-covered cells remain generally small even for potentials as high as 16000 V. For arrays charged to plus 2000 V (when ion thrusters are operated), the power losses amount to a maximum of 20 to 30% of the output powers in low orbit. During part of each orbit when the array

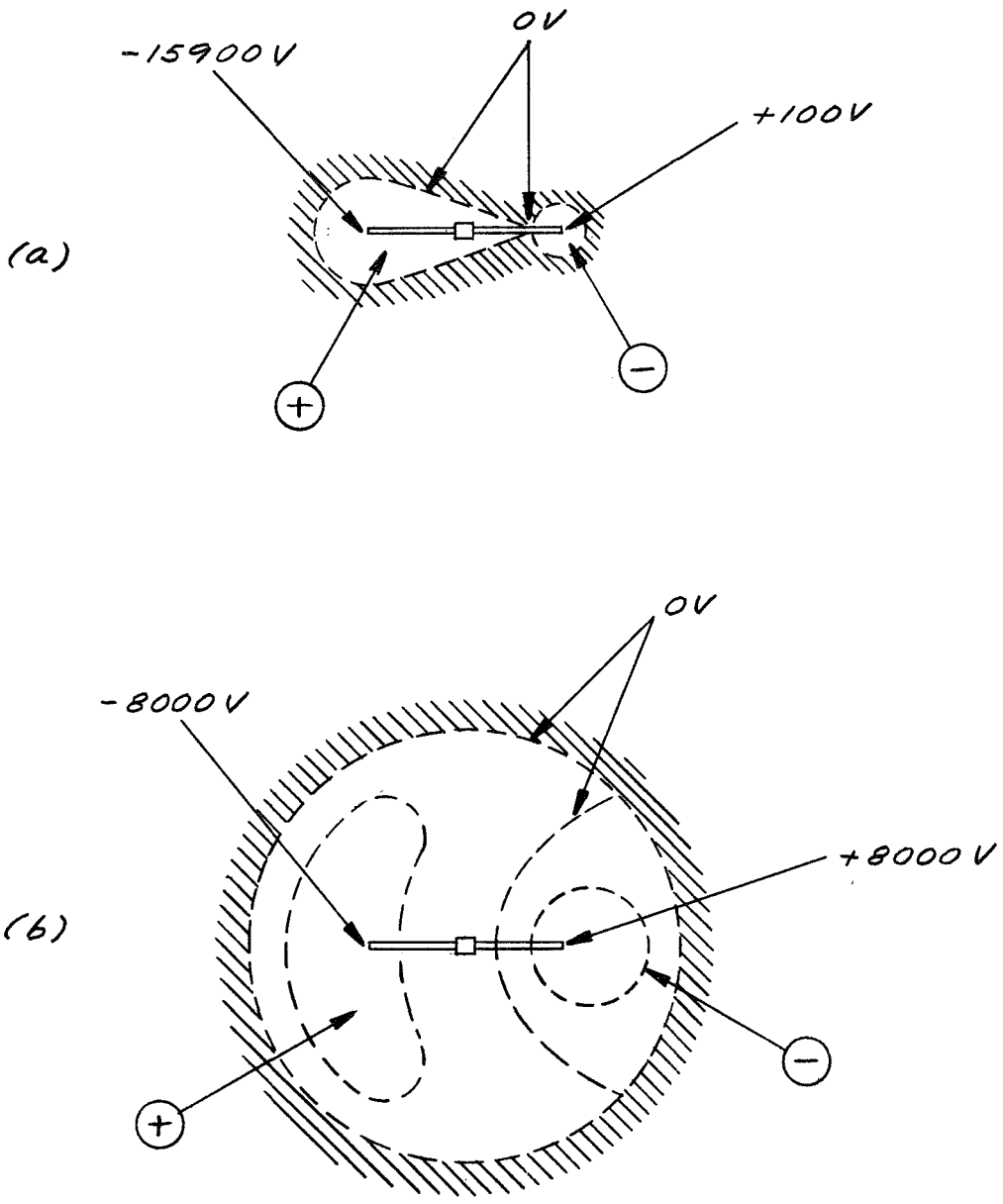

Fig. 10. Approximate plasma sheath configurations of a floating array with a graded potential surface. (a) Dense plasma. (b) Tenuous plasma.

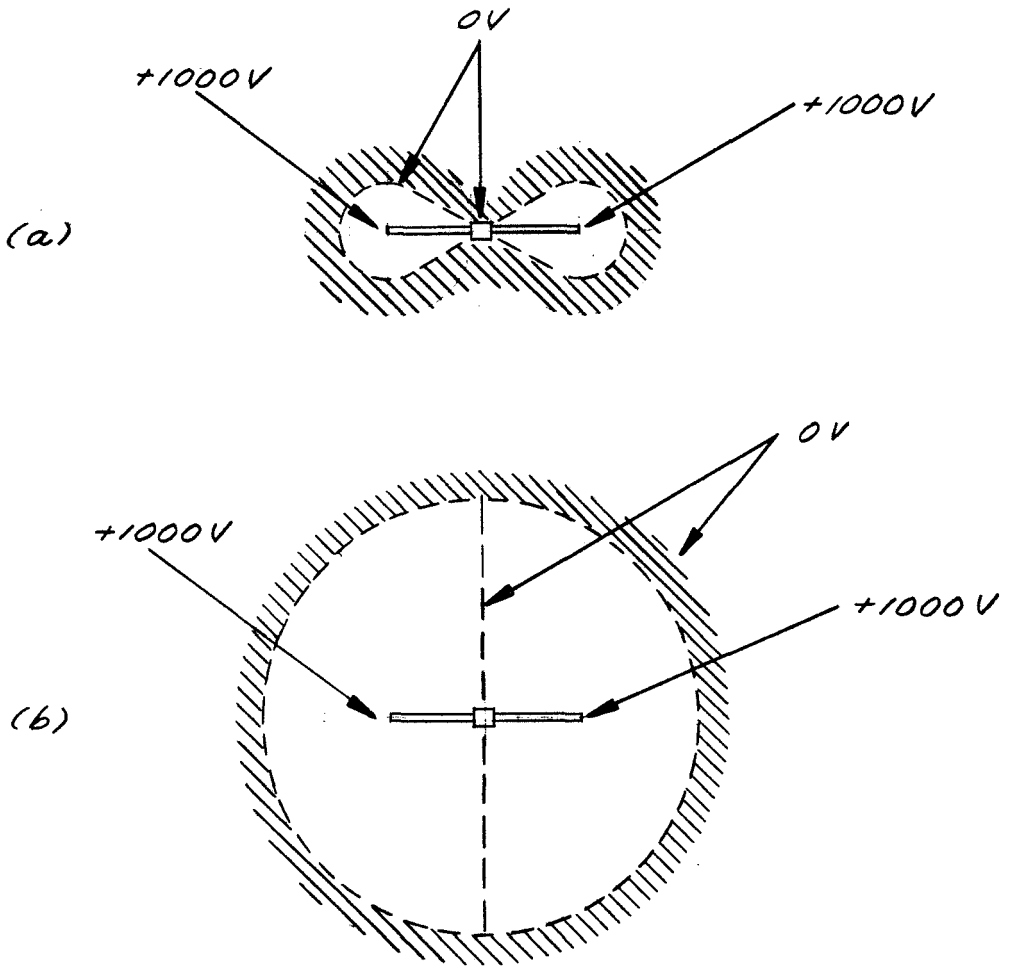

Fig. 11. Approximate plasma sheath configurations of a positively biased array with graded potential surface. (a) Dense plasma. (b) Tenuous plasma.

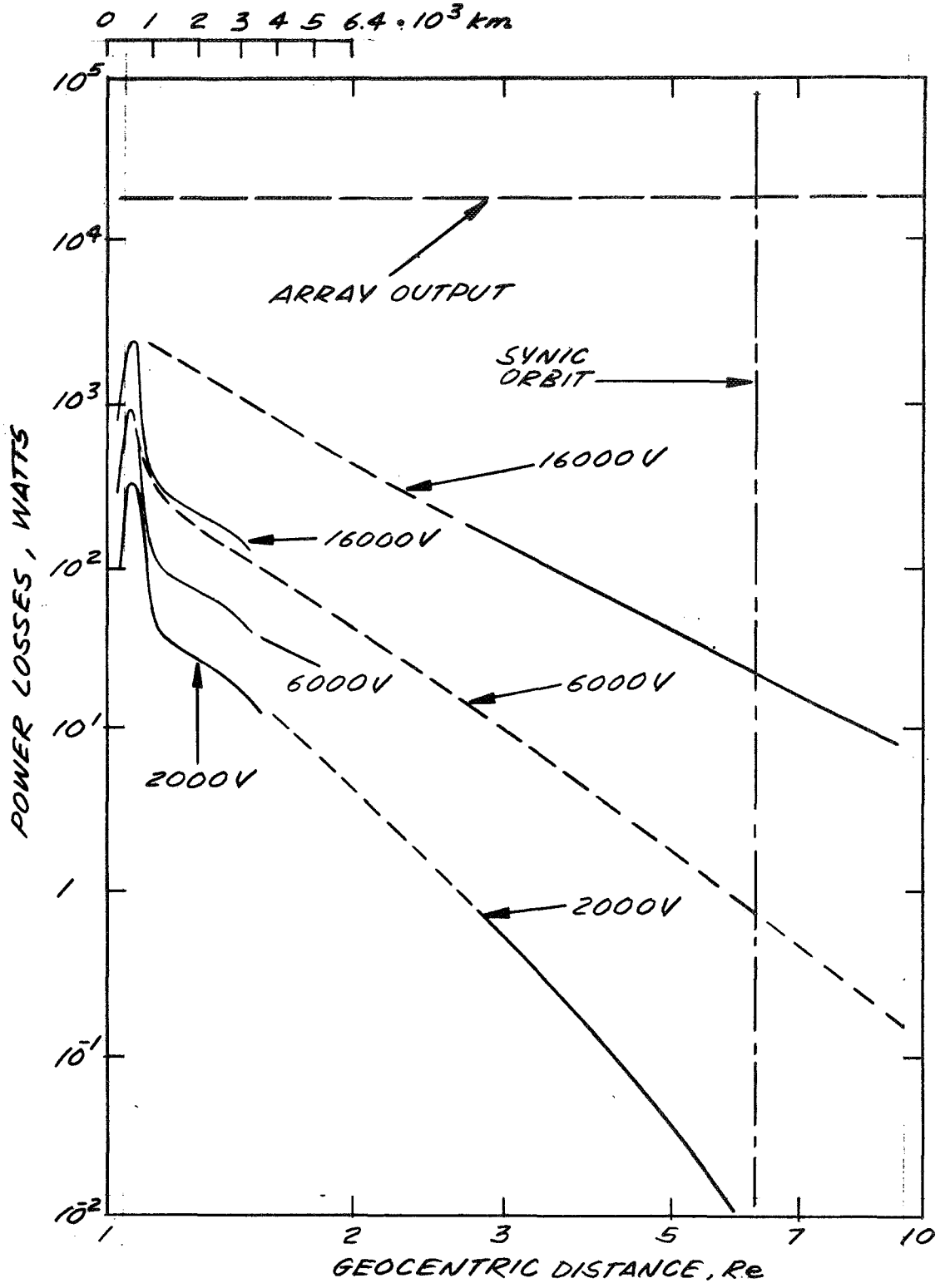

Fig. 12. Power losses of a floating array, with 95% insulating surface.

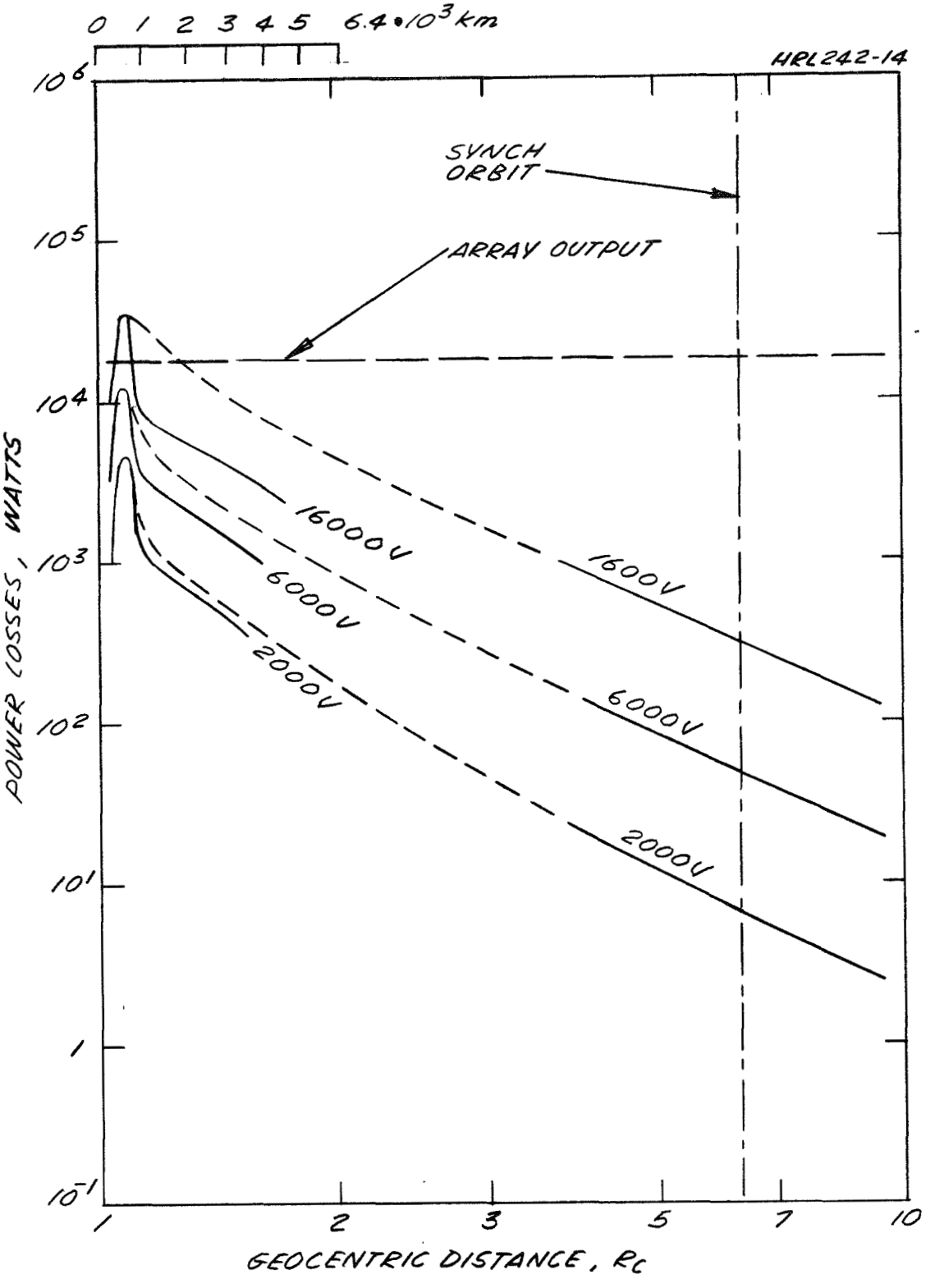

Fig. 13. Power losses of a positively biased array, with 95% insulating surface.

collects on one side only, the losses will be lower by as much as a factor of two. At higher voltages the power losses become larger and, in low orbit, eventually reach the full output power.

e. Particle Trajectories

Thus far it has been assumed that all particles which enter the plasma sheath (and are attracted) move to the array on directly intercepting trajectories. This is true in general for unipotential probes in cases where the collision parameter p is larger than the spacecharge sheath radius r_o (see above). Significantly modified trajectories may be expected if portions of the array surface are insulating. As will be seen below, the surface potential of an insulator in space can be expected to be a few volts below space potential. If the array itself is positive with respect to space, some of the approaching electrons will be attracted to and impact directly on exposed conducting array surfaces. Others will move in the direction of insulating surface sections. However, only few will be able to land there. Those electrons that are reflected back can be divided into the following two groups:

(1) electrons which return more or less straight toward the sheath edge; these have sufficient outward directed energy to return to the space plasma; (2) electrons which move back under an angle; electrons of this group cannot reach the sheath edge because part of their energy is directed parallel to the sheath edge. They are trapped and may bounce back and forth several times before they reach one of the tabs. The following questions arise: what are the probabilities for the three different types of electron trajectories (direct impact, reflection into space, and trapping), and how many bounces will a trapped particle make before it is collected?

In order to obtain answers to these questions, a digital computer program was written which gives solutions for electron trajectories in the sheath of a checkerboard array. The details are described in Appendix E. A representative set of electron trajectories obtained by this method is shown in Fig. 14. Evaluation of a number of such sets for different launching conditions at the sheath edge leads to the following results: A substantial portion of the attracted electrons (on the order of 75%) impacts on the tabs, even though these constitute only about 5% of the surface area. Few of the remaining electrons (on the order of 7.8% of all electrons entering) escape back into space. Most of the reflected electrons are trapped and execute, on the average, one bounce before reaching the tabs.

The results given here should be considered only a qualitative indication of what may actually occur. They are based upon a first order approximation with respect to space charge. The trajectories of the multiply reflected electrons are so complicated that a detailed assessment of their space charge would have been a major undertaking. It is recommended that more elaborate computations be performed during future studies,and that they be complemented by laboratory experiments.

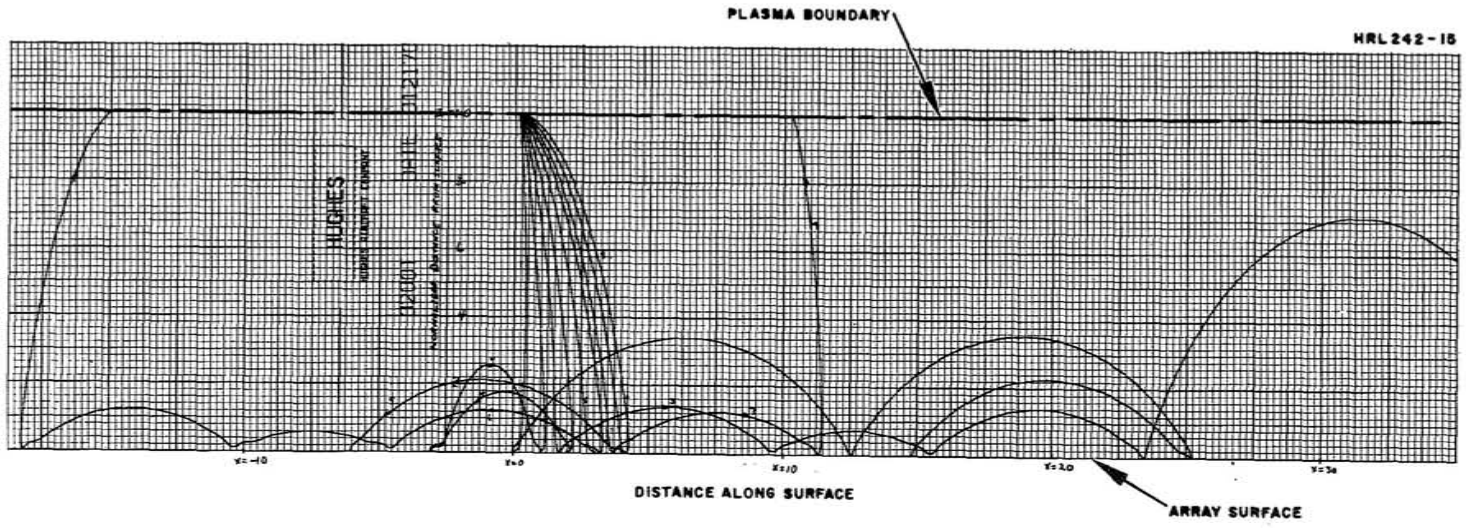

Fig. 14. Trajectories of attracted plasma electrons; surface is 95% insulating, tabs are at 2000 V.

Conclusions: It can be concluded that an array with standard cells (for which about 95% of the surface is insulated) collects a large majority of those electrons which have entered the plasma sheath. In other words, the insulator surfaces with their slightly negative bias (order of volts) cannot prevent electrons from being attracted to highly positive tabs. Even those electrons which miss the tabs on their first approach are collected with high probability later because most of them become trapped within the sheath.

B. THRUST BEAM LOSSES

During the operation of ion thrusters, power losses can be expected to occur as a result of charged particle currents flowing from the ion beam to the array (see Fig.15). This is not intended to imply that the array intercepts portions of the ion beam, but rather that the difference in potential between beam and array causes space charge limited flow across a gap between beam and array. The situation for primary propulsion is expected to be different from that with beams serving altitude control and station keeping functions. The cases will be discussed separately.

1. Main Thrust Beam

It was pointed out above that when most of the array output is used to power the main thrust beam, much of the array will be positive with respect to space and therefore with respect to the ion beam. Only electrons then may reach the array. In principle, the number of electrons which can be drawn from the ion beam to the array could be limited either by the number of electrons available in the beam or by the space charge limits for flow to the array. However, because present plasma neutralizers can provide almost unlimited numbers of electrons, space charge is assumed to limit the outflow of electrons from the ion beam.

The beam-array flow problem is too complex to be solved analytically. Therefore, a computer program for space charge limited flow (Stanford Program) was utilized (see Appendix F). The array was approximated by a circular disk at constant potential (representing either the full array potential in the case of a conducting array surface or a reduced "average" potential in the case of a mostly insulating surface with exposed tabs). The ion beam was simulated by a circular cone of 15° aperture, and electron extraction was assumed to take place from the entire beam surface. The computations were performed without regard for the space plasma sheaths. In other words, these sheaths were assumed to be far away. In this situation the ion beam losses can be expected to reach their highest levels. The electron trajectories obtained are shown in Fig. 16. It can be seen that most of the electrons are collected near the outer array edge and not, as might intuitively be expected, on the array sections closest to the ion beam. The power losses resulting from the electron flow pattern of Fig. 16 are shown in Fig. I7. It can be concluded that the losses of an array with standard cells are acceptably small.

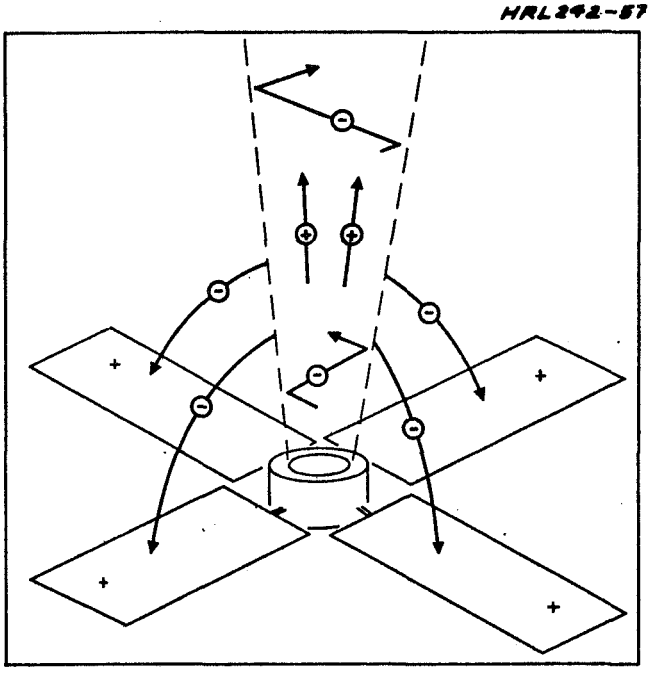

Fig. 15. Attraction of thrust beam electrons to high voltage solar array.

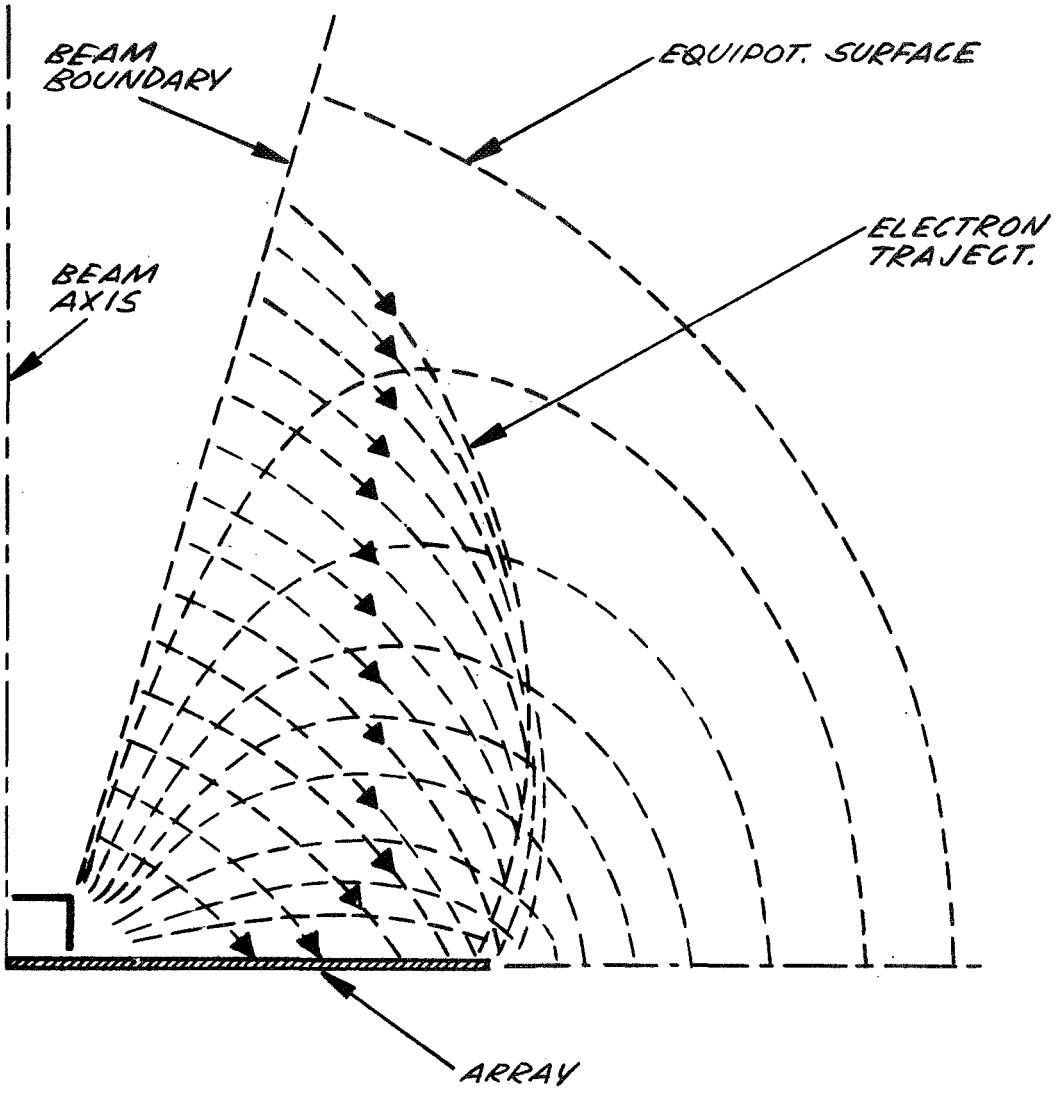

Fig. 16. Electron trajectories between ion beam boundary and array; the array is at unipotential (2000 V), and the electrons are launched with zero energy.

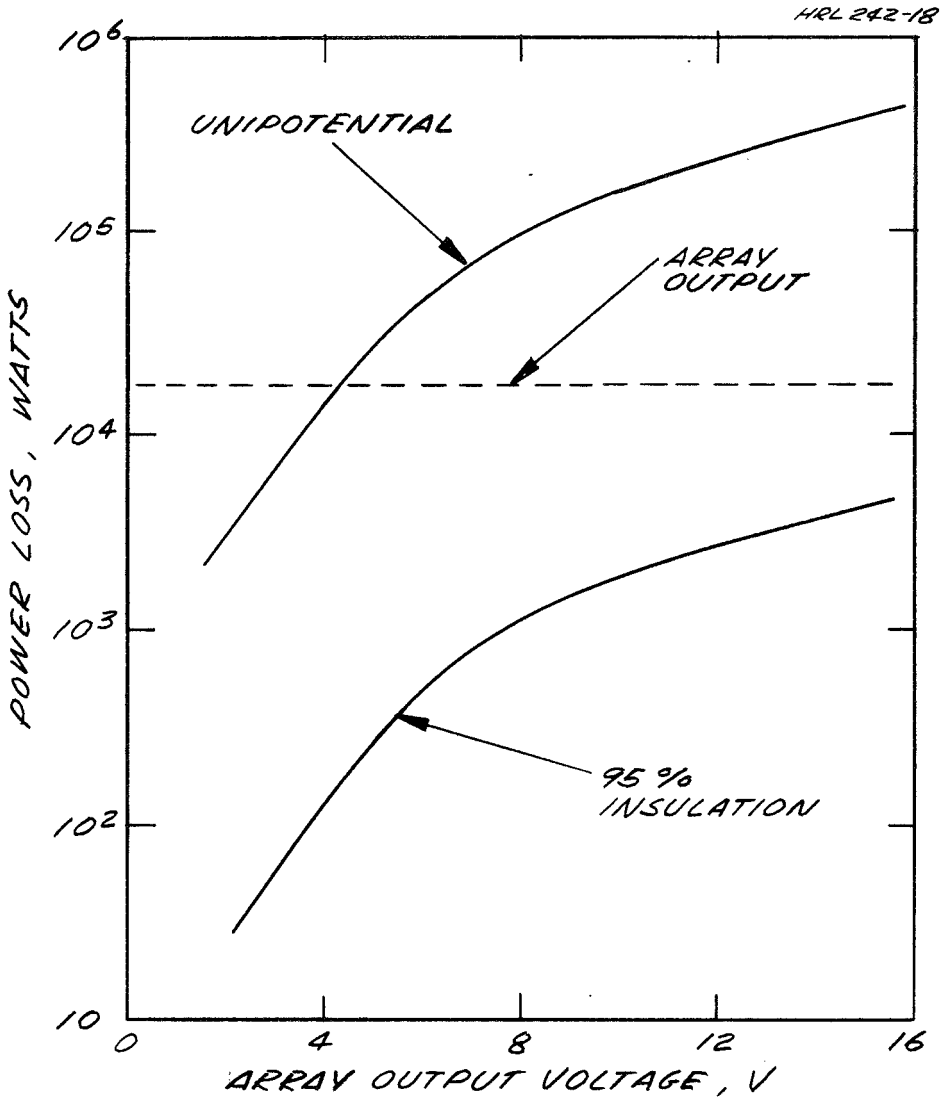

Fig. 17. Power losses associated with the main thrust beam.

One assumption made in the above computations was that the electrons leave the ion beam with zero velocity. This is not fully justified because the commonly used plasma neutralizers inject electrons with diagonally outward directed energies on the order of 15 eV. To account for this, it was assumed that, at the beam edge, electrons possess a kinetic energy of 10 eV tangential to the beam boundary. Figure 18 shows the electron trajectories for this case. It can be seen that sufficiently far downstream electrons drawn from the beam are not attracted to the array but pass into space. However, this happens at such large distances from the array that the number of escaping electrons is small. Therefore, the currents collected by the array are practically unchanged from the cold electron case and the power loss curves shown in Fig. 17 remain valid.

2. Ion Beams used for Control Functions

The power consumed during operation of ion beams for attitude control and station keeping is a small fraction of the power generated by the array. Consequently, the neutralizer need not be attached to the most negative point of the array. However, the ion beam must still be ejected close to space potential. In cases where the plasma leakage currents are small compared with the ion beam current, the neutralizer can be attached to any potential on the array. When a beam is ejected it will automatically bias the entire array such that the neutralizer potential is brought close to space potential. In cases where the plasma leakage currents are comparable to or larger than the ion beam current, the neutralizer must be attached to a potential on the array which is either level with or above space potential. Otherwise, the ion beam will not eject properly.

With some portions of the array more positive than the ion beam and others more negative, both electron and ion leakage currents can occur. In principle, the ion leakage currents can consist of deflected primary ions as well as accelerated charge exchange ions. Ion beams are launched with such high directional energy that it seems unlikely that many of these fast ions will find their way back to the array. Charge exchange ions are more likely to hit the array. However, their total number also should be small. With an ion beam of, e.g., 10 mA the charge exchange ion generation rate should not exceed 1 mA. Most of these slow ions will be attracted to thruster electrodes. The number of ions drawn to the array can be estimated again by the rules for space charge limited flow. For a quick estimate we utilize the results obtained for the main thrust beam, taking into account that ions are slower than electrons (by a factor of 600 in the case of mercury) and that ion beams used for control purposes are smaller in diameter (by a factor of approximately 30). For an array with 95% insulating surface this leads to leakage currents on the order of 10^{-2} mA at 8 kV. (A voltage of 8 kV was chosen under the assumption that the full array output is 16 kV and that the thruster operates from the center level). It is evident that the power losses resulting from such small currents are totally negligible. However, the question remains whether the impact of ions may cause some damage to the array surface. As it turns out, sputtering would amount to an average of less than 10^{-6} atom layers/sec. This would lead to a total of only 100 atom layers during an array lifetime of 3 years if the thruster were to operate full time. Material removal of this magnitude would appear to be acceptable.

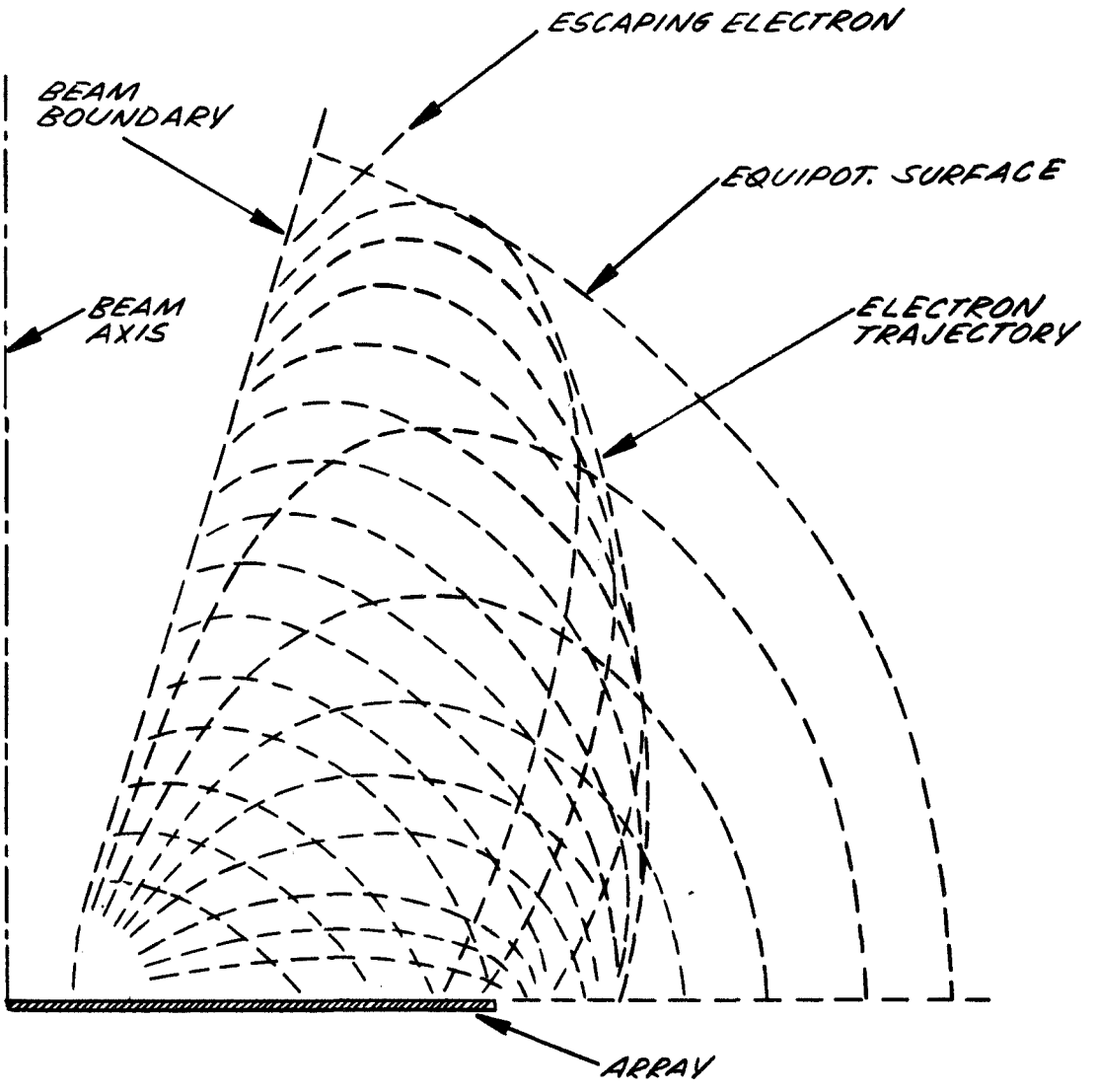

Fig. 18. Electron trajectories between ion beam and array; unipotential array (2000 V); the electrons are launched with 15 eV energy tangential to the beam boundary.

Leakage currents resulting from the attraction of electrons from a small control beam to positive array sections may be estimated by the same procedure used to determine ion currents. By this method, one obtains leakage currents of about 3 mA at 8 kV. The associated power losses should be less than 25 W, which is acceptably small.

It should be emphasized that the numbers given for both electron and ion loss currents represent upper limits. They were obtained under the conservative assumption that the ion beam leaves an array, 5% of which is at the full high potential (+ 8kV for electron collection, - 8 kV for ions).

Conclusions: The power losses associated with the electron and ion collection from either the main thrust beam or from attitude control and station keeping ion beams are tolerably small for arrays with predominantly insulated surfaces. Ion impact on negative array portions is too infrequent to cause noticeable sputter damage.

C. DISCHARGE LOSSES

Thus far only those leakage losses have been considered which are associated with the collection of charges from an existing, natural and spacecraft generated plasma environment of the array. In this section, additional losses are discussed which result from self-sustained discharges between sections of the array. In principle, the following types of discharge modes could occur on HV solar arrays: glow discharges, crossed-field discharges, and vacuum arcs. All three discharge types are sufficiently different from each other to warrant separate discussions.

1. Glow Discharges

Glow discharges require a suitable gas environment. The conditions under which a glow discharge can be ignited are established by the so-called Paschen characteristics. Figure 19 shows a Paschen curve for N_2. Similar curves are obtained for other gases. According to Fig.19 the breakdown voltage is a function of the product of gas pressure p and electrode separation d. Because of the low gas pressures in space only the left side of the Paschen curve is of interest here. For an array of about 10^3cm length and for a maximum potential difference of 16 kV, Fig. 19 yields a pressure limit for breakdown of about 5×10^{-5} Torr. Only at pressures above this limit can a glow discharge be ignited.

The gas pressure in the upper atmosphere is strongly dependent upon altitude and falls below 5×10^{-5} Torr at about 100 km. Therefore, the natural atmospheric environment should not lead to breakdown on HV arrays at altitudes above about 100 km. In addition to the natural environment, one must consider also gas atmospheres produced by the array itself. The potential gas generation mechanisms come to mind: (a) outgassing of materials used on the array, and (b) jets from cold gas attitude control rockets. As will be seen in a later section, the outgassing rates of most array materials are too small to produce pressures anywhere near the level of 5×10^{-5} Torr. The only exception is R. T. V. If the entire array surface would be covered with R. T. V. and were maintained at a temperature of 200°C, a period of a few minutes would elapse before the pressure would fall below 5×10^{-5} Torr.

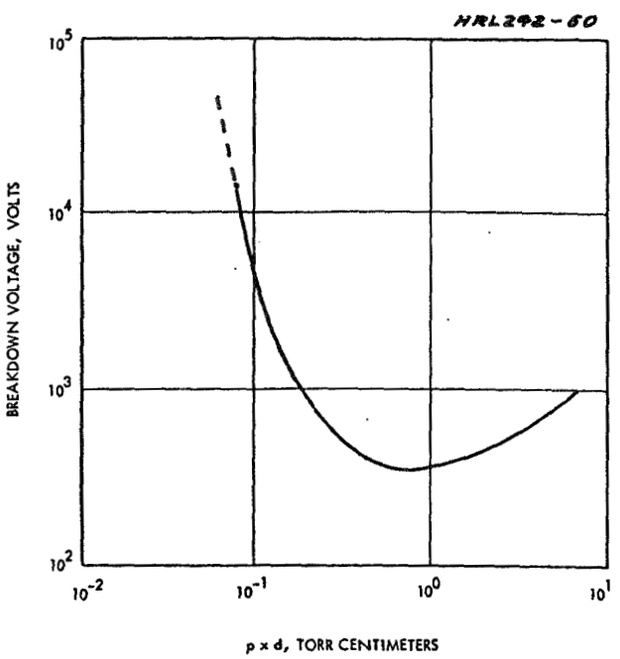

Fig. 19. Paschen breakdown characteristics for molecular nitrogen.

In order to study the dangers posed by cold gas rocket exhausts, we consider the case of a hydrogen peroxide rocket with a specific impulse of 100 sec and a thrust level of 1 lb. Such a rocket exhausts H_2O at a mean velocity v of about 10^5 cm/sec. The rate of gas flow amounts to 10^{-2} lb/sec, equivalent to $n = 8 \times 10^{22}$ molecules/sec. If it is assumed that the exhaust spreads into a cone with an aperture angle of 90°, the pressure variation with distance from the nozzle becomes

$$p = 2.85 \times 10^{-17} \frac{n}{\pi v} \frac{1}{\ell^2}$$

where p is the pressure (Torr) and ℓ is the distance (centimeters). As can be seen from Fig. 20, the pressure is sufficiently high to initiate breakdown up to distances of several meters from the nozzle. Accordingly, the rocket nozzle should be directed so that the exhaust streams past the array at a distance of several meters. The same considerations apply to hydrazine (N_2H_4), which has a molecular weight similar to hydrogen peroxide.

2. Crossed-Field Discharges

In the presence of a magnetic field of sufficient strength, discharges can be sustained to very low pressures. In the laboratory, the so-called "Penning" discharge has been observed to operate at pressure levels as low as 10^{-14} Torr. For crossed-field discharges the parameter $B \cdot d$ is as important as $p \cdot d$ for ordinary glow discharges. Figure 21 shows the breakdown characteristics of air as a function of Bd. It can be seen that with an array of about 10^3 cm length and a magnetic field of 0.5 gauss breakdown is possible, even though the situation is marginal. Furthermore, there is considerable uncertainty as to how well an array can serve as a crossed-field discharge configuration even if it is aligned properly with respect to the geomagnetic field (see Fig. 22). It would seem desirable to explore the existence range of this discharge mode on solar arrays with a suitably scaled laboratory plasma experiment.

3. Vapor Arcs

As the name implies, vapor arcs do not require the presence of an ambient gas background. Instead, they generate their own gas in the form of vapor jets issuing from the cathode surface at the location of the arc spot. Unlike glow discharges, vapor arcs cannot be ignited by raising the applied voltage to the operating level. Rather, a high voltage spark or similarly dense plasma must be provided. Once ignited, the arc burns with quite low voltages which are in the range between 4 and 100 V, depending upon cathode material.

The possibility that vapor arcs may arise on HV solar arrays is suggested by laboratory experiments performed by Sellan, et al.[7] These investigators found that fully insulated solar panels after immersion into a plasma of about 10^6 particles/cm^3 suffered from excessive leakage losses when the panel was maintained at a sufficiently high, positive potential (on the order of 1000 V). It was found that the leakage was initiated by dielectric breakdown through the insulator.

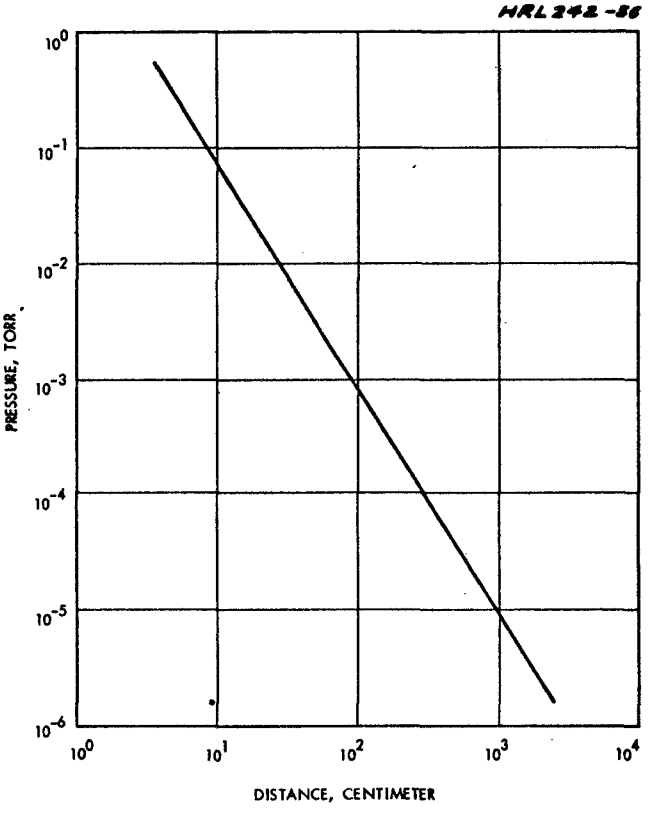

Fig. 20. Gas pressure in the exhaust of hydrogen peroxide attitude control rockets.

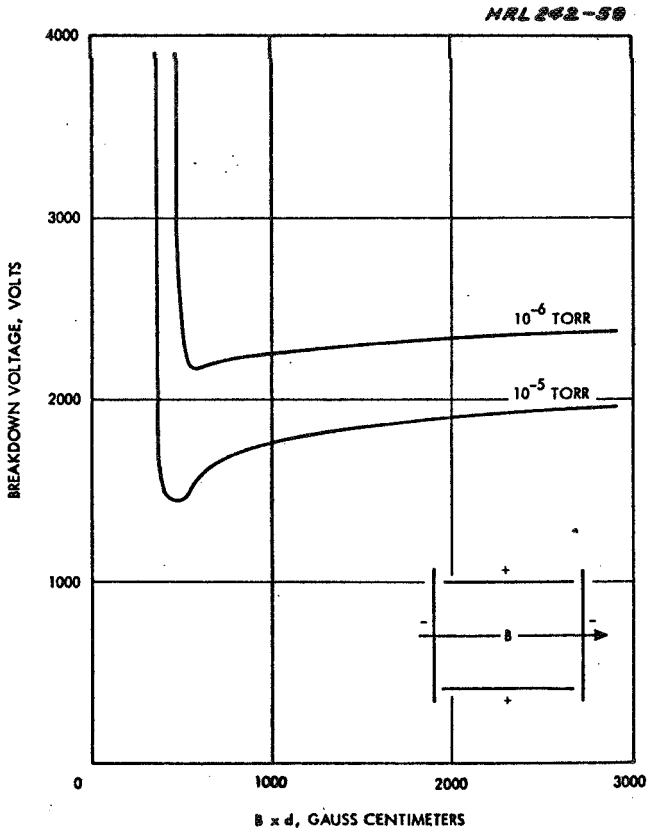

Fig. 21. Breakdown characteristics for a transverse magnetic field geometry in air.

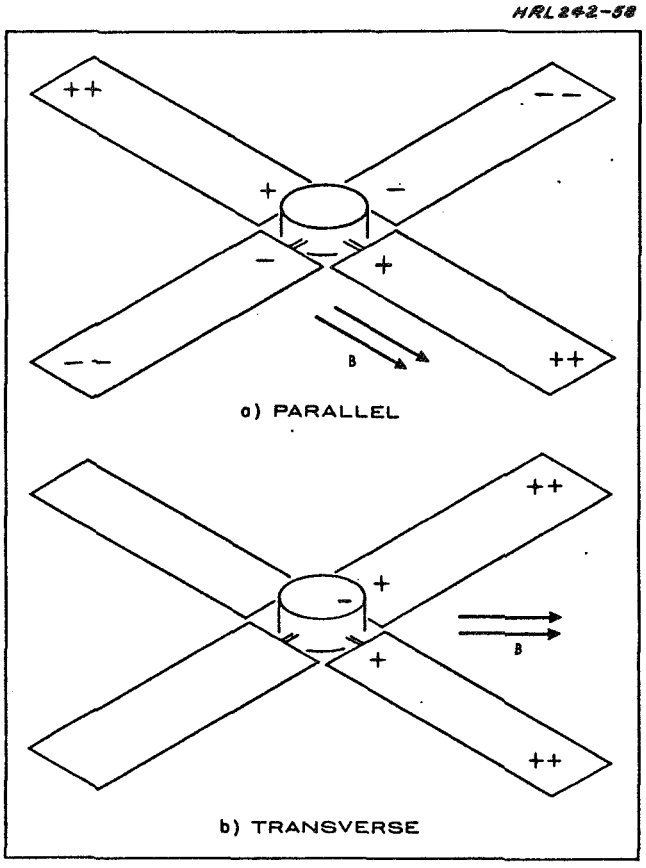

Fig. 22. Electrical breakdown possibilities in the presence of a magnetic field.

The resulting tiny pinhole appeared to attract large plasma currents.

It is not unreasonable to explain these currents in terms of a vapor arc. Figure 23 shows a proposed qualitative discharge model. The arc is attached to the front of the pinhole; it utilizes the insulator as cathode and the solar cell (which is the most positive electrode) as anode. Current continuity at the arc spot is provided by ion flow to and electron flow from the environmental plasma. The combination of plasma electron and arc ion bombardment of the insulator surface adjacent to the arc spot provides the heat necessary to feed the arc with the vapor.

The situation in Sellan's laboratory tests was not fully equivalent to that existing in space. Therefore, it is not certain at this time that pinhole arcs will occur. There is no doubt, however, that even with an insulating layer of sufficient thickness to prevent dielectric breakdown, there will always be some pinholes as a result of micrometeorite impacts. (For a 15 kW array, which has an area of approximately 400 m^2, it can be seen from Fig. A-10 (Appendix A) that an insulating layer with a typical thickness of 0.015 cm (0.006 in.) will be penetrated roughly ten times per day.) Therefore, caution demands that the possibility of pinhole arcs not be overlooked. Indeed, further laboratory experiments should be performed under conditions that closely match those in space. Furthermore, preventative measures should be considered and tested in the laboratory (see following section). Finally, experiments should be conducted to determine whether the maximum leakage currents resulting from pinhole arcs are limited by the spacecharge currents across the plasma sheath.

Conclusions: Ordinary glow discharges are not considered a major hazard to HV arrays. Crossed-field discharges may occur under some conditions; however, the associated leakage currents are likely to be low. Vapor arcs are potentially dangerous. However, experimental work is required to better assess the magnitude of this danger and to explore possible remedial measures.

D. REDUCTION OF LEAKAGE CURRENT LOSSES

It would be very desirable if HV arrays could utilize standard cells with insulating cover slides and open tabs. The earlier derived leakage losses suggest that, indeed, for some missions standard cells would be acceptable. For example, missions in which the array is operated at altitudes above about 3000 km and at voltages up to 16 kV, when floating, or 6 kV, when positively biased, should suffer less than 5% power loss. Similarly, the power loss on orbit raising missions, during which the array must supply ion thrusters with a relatively low voltage (approximately 1000 to 2000 V) is acceptably low for most of the mission. During the initial portion of the orbit raising maneuver, while the spacecraft passes through the ionosphere, leakage losses may reach values as high as 20 to 30% of the output power. The period of large losses lasts only a few days. In addition, it occurs during a phase of the mission where the array still has a power reserve, since radiation degradation has not yet affected the performance.

For missions in which high voltages (on the order of 16 kV)

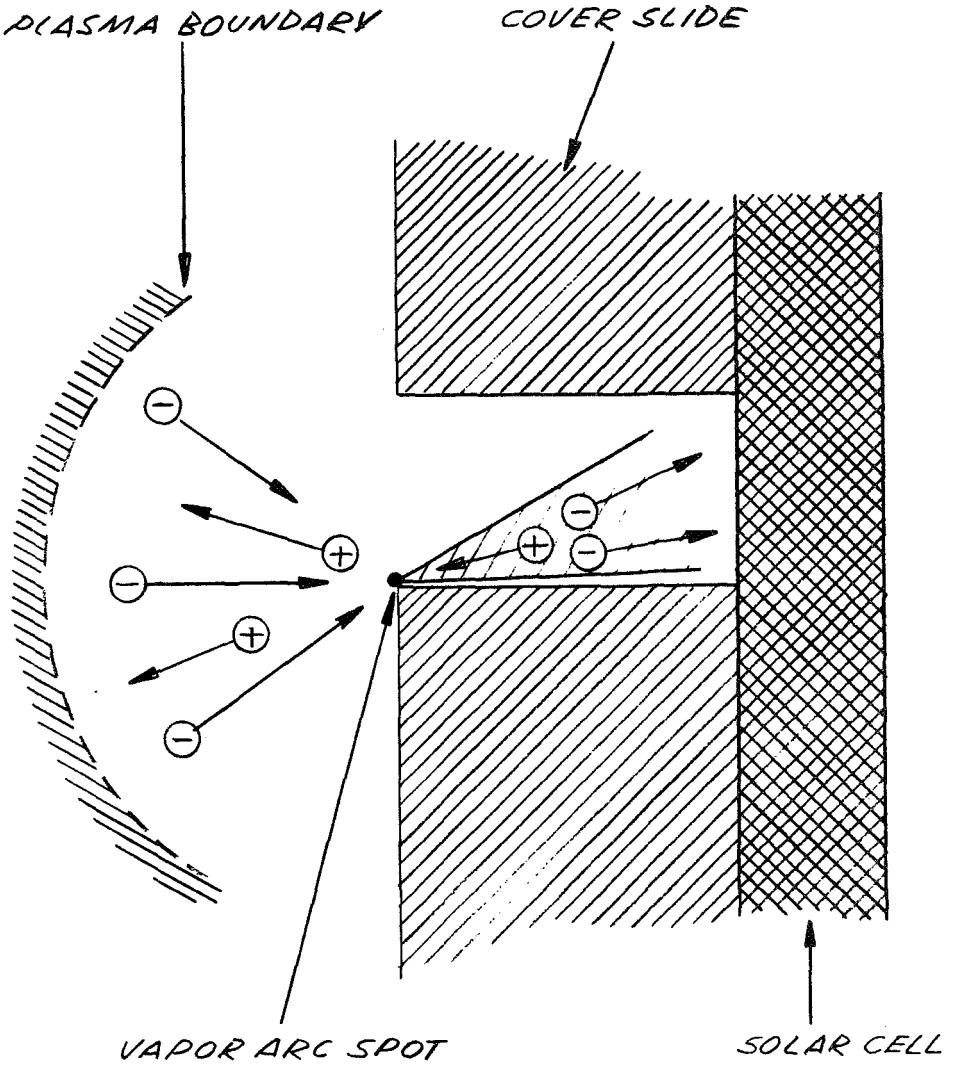

Fig. 23. Possible pinhole-arc mechanism.

must be supplied on low orbits; however, the plasma losses with standard cells can be expected to be prohibitively large. Several methods are described below which promise to reduce these losses substantially.

1. Totally Insulated Array

It is evident that an array that is totally enclosed by an insulating layer should not suffer any leakage losses. The question is whether inevitable cracks (due to mechanical stresses) and holes (due to micrometeorite impacts) eventually will lead to pinhole arcs and thereby to gradually increasing losses. At this time, a conclusive answer cannot be given; it is premature to propose total insulation as a final solution. However, should future experiments show that pinhole arcs can be ruled out, an effort should be initiated to investigate and evolve methods for sealing the array.

2. Depressed Plasma Collectors

The earlier described vapor arc model for pinholes suggests that an arc can arise only when sufficient plasma electrons are attracted to the pinhole. If neighboring electrodes of a sufficiently high voltage compete with the pinhole for electrons, the currents arriving at the pinhole may be insufficient to sustain the arc. If this hypothesis is correct, pinhole arcs may be prevented by the use of collecting electrodes, suitably distributed over the surface of the array. On arrays with exposed tabs, the tabs themselves should suppress pinhole arcs. In fact, solar panels tested by Sellan failed to show arcs when the tabs were exposed (even though the tabs attracted large leakage currents).

The following method not only may eliminate pinhole arcs, but also may reduce tab losses. Consider an array on which the tabs are covered by an insulating layer and assume that a conductor ("collector") is attached to the outer surface of this layer. The potential of this collector is chosen just high enough to collect all electrons entering the plasma sheath. The array power losses are then determined by the collector voltage instead of the array voltage. Because several hundred volts should suffice for the collection of all arriving electrons, power savings by a factor of 10 or more may be realized. It is evident that the described concept requires further study. Computer simulations and laboratory experiments must be performed to prove its effectiveness and practicality.

3. Biased Screens

A third method to reduce plasma leakage losses is to surround the array with a biased screen. If, in conjunction with a positively biased array, the screen is biased negatively with respect to space potential, most plasma electrons are reflected before they can slip through the screen meshes. The ratio of reflected to attracted electrons depends upon a number of geometrical factors and upon array and screen voltages. To some degree it also depends upon trapping of particles in the space between screen and array. Except for this latter effect the details of

of this approach have been worked out; they are presented in Appendix G. Here it is sufficient to state that a reduction of the losses by an order of magnitude may be achieved. A conceptual design for a screen has been worked out and will be described in a later section. Care must be exercised in the design to prevent contact between the array and the screen, which would result in short circuiting of the array and possible catastrophic failure. Future computational and experimental efforts on screens are indicated.

4. Natural Bias of Cover Slides

According to an analysis of the surface potentials on dielectrics (see the following section), dielectric array surfaces are expected to adopt a potential that is slightly negative with respect to space. This leads to the possibility that fewer electrons than expected will be collected by tabs as a result of electrostatic shielding. The magnitude of this effect will depend upon several factors: (1) upon the geometrical situation (i.e., width and recess of the tabs), (2) upon the negative bias of the surrounding dielectric surfaces.

It is assumed that the tabs are 20 mils wide and that they are recessed 6 mils below the cover slide surface. The bias potential of the cover slide surface can be determined as follows. With positive tabs the potential rises from the sheath boundary toward the array, as shown in Fig. 8. Accordingly, all positive ions are reflected before reaching the array. The equilibrium potential of the surface is therefore determined by a balance between arriving plasma electron and emitted photoelectron current. This balance can be expressed as

$$j_{ph} = j_r \, e^{-\frac{eV}{kT_e}}$$

where j_{ph} is the photoelectron current density, j_r is the random plasma electron current density, T_e is the plasma electron temperature, and V is the equilibrium surface potential. With $j_{ph} = 5 \times 10^{-11}$ A/cm^2 (see Appendix H), $j_r = 10^{-6}$ A/cm^2 (at 400 km altitude), and $kT_e = 0.2$ eV, the equilibrium potential V_{equ} becomes about -2 V. This is the approximate bias potential which cover slide surfaces will adopt in the densest region of the ionosphere.

To derive the electron flow to the array under these conditions, a self-consistent computer solution was obtained, based upon the program described in Appendix F. It was found that the flow pattern is much the same as without negative cover slide bias and without tab recess. This result becomes quite plausible if the computed potential distribution across a tab in the plane of the coverslide surface is considered. Figure 24 shows that the "effective" potential V_{eff} across this plane is at least one half of the tab potential. It is evident that the resulting net checkerboard potential V_{net} which is determined by

$$V_{net} = 0.05 \, V_{eff} + 0.95 \, V_{equ}$$

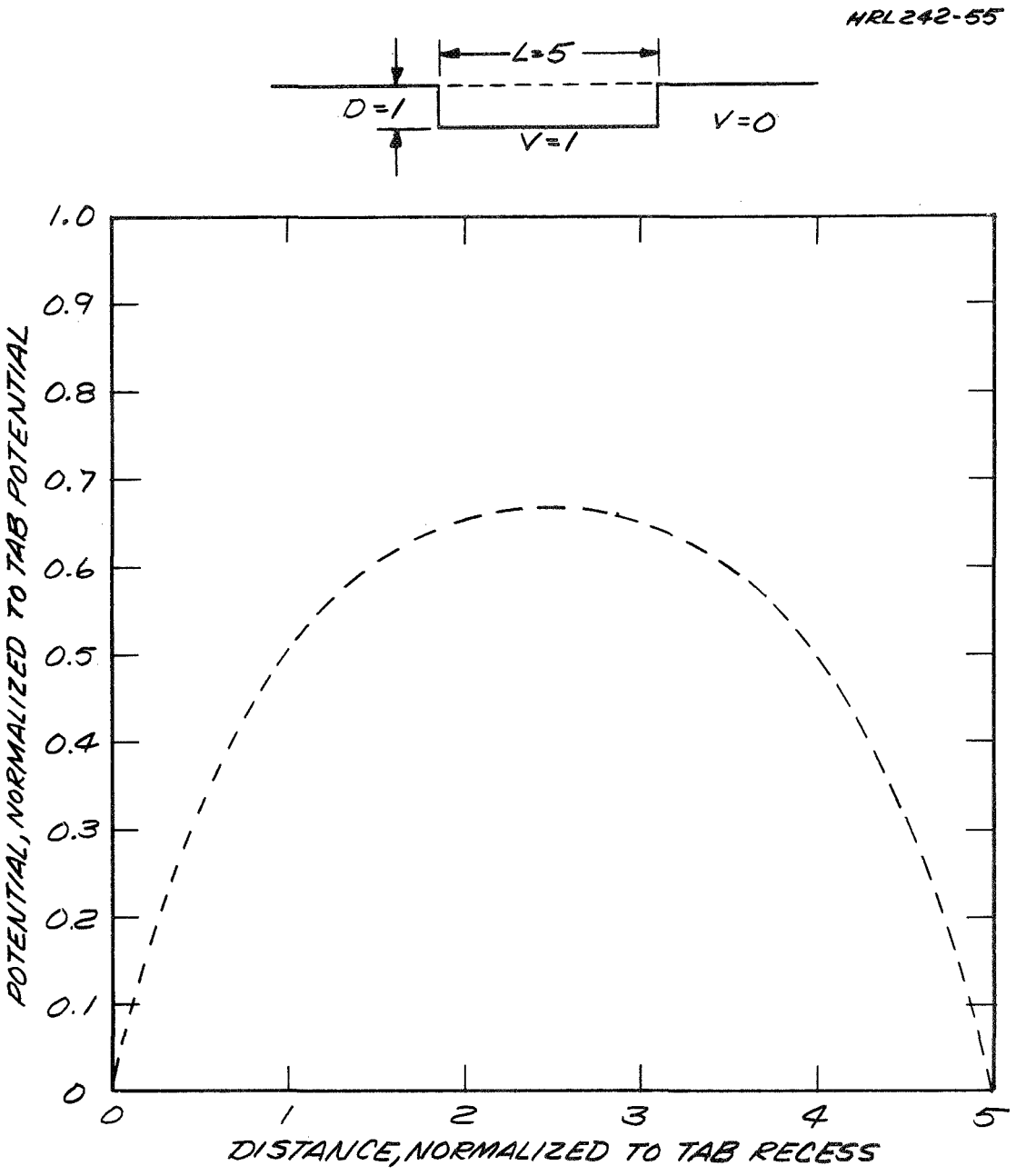

Fig. 24. Computed potential across a tab, in the plane of the cover slide surface. Space charge effects by attracted charges are taken into account.

is still quite positive (order of 48 V), and therefore able to attract electrons in undiminished numbers. It should be noted that the current density carried across a one-dimensional plasma sheath is independent of applied potential as long as the applied potential is large compared with $kT_{e/e}$.

Conclusions: Fully insulated arrays would avoid all plasma losses if pinhole breakdown could be precluded. One possibility to prevent pinhole arcs is to provide so-called "plasma collectors" on the array surface. The potential of these collectors is depressed (with respect to the array potential) and current collection is associated with much reduced power losses. Alternatively, leakage currents may be reduced with the aid of a biased screen surrounding the array. The shielding of the tabs by the natural negative bias of the cover slides cannot be relied upon as a means to reduce leakage currents.

III. SURFACE EFFECTS

This section discusses the physical effects associated with the surfaces of a high voltage solar array. The main areas of interest are surface charging of insulators, sputtering, and propellant condensation.

A. SURFACE CHARGING OF INSULATORS

A dielectric surface that is exposed to a plasma will tend to accumulate electrical charge through the collection of plasma ions and electrons and the emission of charged particles from the surfaces by secondary emission and photoemission processes. This situation occurs when the insulating surfaces of a high voltage solar array are exposed to the space plasma. If the resultant surface potential is sufficiently different from that of the conducting substrate, electrical breakdown may occur within the insulating layers or along their surfaces.

A conventional solar array consists of solar cells interconnected by metal tabs that are exposed to space. The active area of the individual solar cell is protected from the space environment by a thin transparent insulating layer or cover slide which is usually composed of fused silica. The back surface of the array may be partially or totally covered with a material such as Kapton which provides electrical insulation as well as structural support.

A simple model, which is based on this conventional array design, has been adopted in order to study the surface charging processes of insulators. The model assumes a plane insulating layer that is infinite in two dimensions and continuous. It is bounded on one side by a conducting substrate and on the other by the space environment. The problem of determining the potential of the exposed surface is divided in two parts. The charge transfer processes between the insulating surface and the space plasma is determined first, and the modes for current leakage between the surface and substrate are then considered. The final surface potential and leakage current density are obtained from the equilibrium condition that the sum of all the currents arriving at a given surface is zero.

1. Current Flow Between Plasma and Insulator

The current density collected by an insulating surface is now obtained as a function of the surface potential which is referenced to the plasma potential and allowed to range from large positive to large negative values. For the moment the surface potential will be assumed to be maintained by some means, such as conduction to the substrate, which will be discussed later.

The total current density arriving at an insulating surface is the sum of the incident primary current density and the current density resulting from secondary emission and photoemission. These processes are illustrated in Fig. 25. The primary currents arriving at an insulating surface from space consist mainly of ions and electrons originating

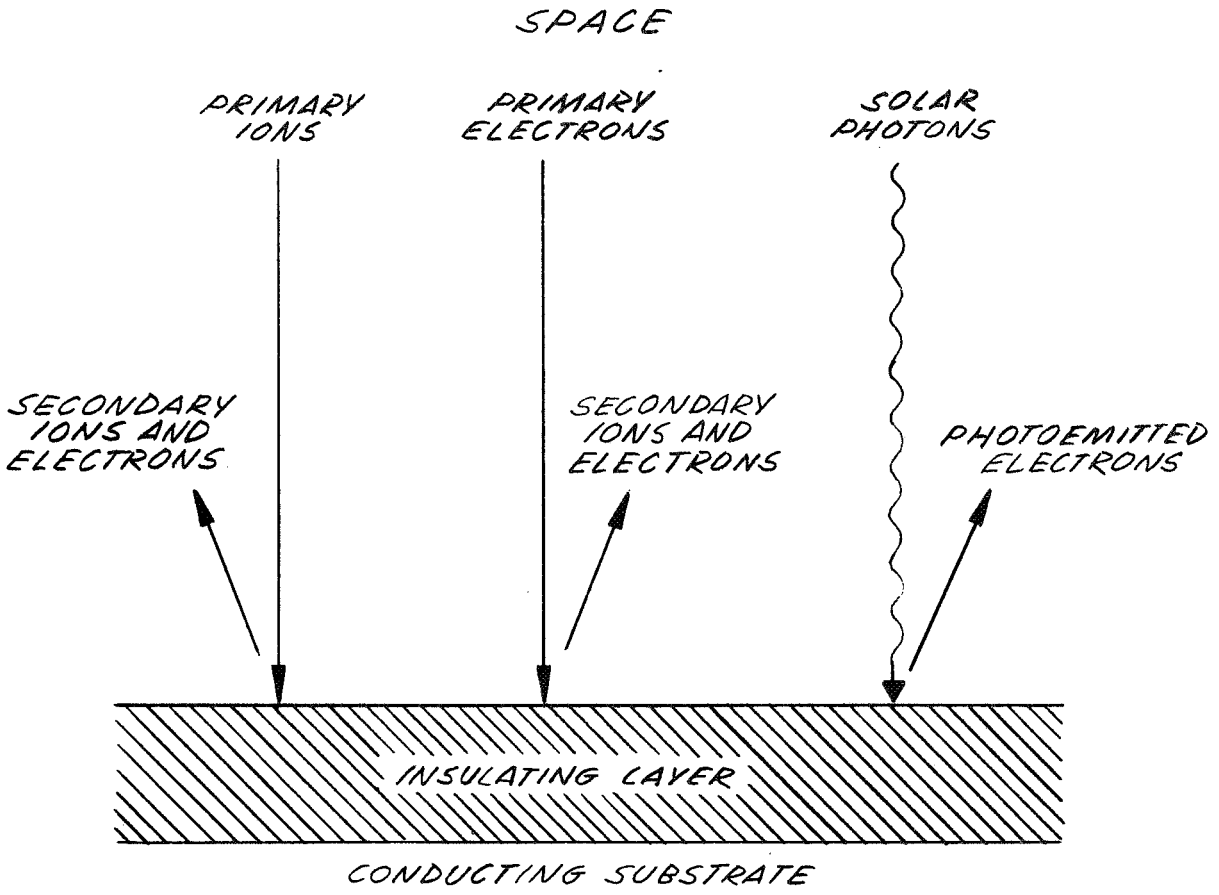

Fig. 25. Charge transfer processes between an insulating layer and the space plasma.

from the environmental space plasma. High energy particles such as encountered in the radiation belts and the effects of a streaming plasma, or spacecraft motion, are neglected for the moment. The maximum current density which can be extracted from an equilibrium plasma is denoted by the random current density and is given by

$$j_r = \frac{1}{4} en\, v_{th}$$

where n is the plasma density and e and v_{th} are the electronic charge and average velocity of the charge species which is drawn from the plasma. If a current collecting surface is highly positive with respect to the plasma, ions will be repelled and electrons will be collected at the electron saturation current density. The opposite is true for a negative surface. Fig. 4 in Appendix A illustrates how the maximum expected ion and electron saturation fluxes (current density/e) depend on altitude.

For a charge species whose motion is retarded by the potential at the surface, the incident current density is given by:

$$j = j_r \quad e^{\frac{-eV}{kT}} \quad \text{with } eV \geq 0, \tag{7}$$

where j is the collected current density of the retarded charge specie, j_r is the associated random current density, T is the temperature of the species, and V is the potential of the collecting surface with respect to the plasma.

Because the quantity kT for the photoplasma ions and electrons is on the order of 10 eV or less, the collected primary particle current density will differ from the random values only for surface potentials within approximately 100 V of the plasma potential.

The primary charged particles are incident on an insulating surface with an energy that is the sum of the random kinetic energy associated with the equilibrium space plasma and the energy gained in passing from the plasma to the surface. The impact of these particles will result in the emission of various secondary charged particles. (The release of neutral particles will be discussed later when the effects of sputtering are considered.) In addition, incident solar radiation will cause photoemission of electrons from illuminated surfaces. The various emission processes which must be considered are

1. Secondary electrons generated by ion impact
2. Secondary electrons due to electron impact
3. Photoemission of electrons
4. Secondary ions generated by ion impact
5. Secondary ions resulting from electron impact (this is an extremely rare process and it will be neglected.)
6. Secondary electrons released by incident metastable atoms (this does not occur for insulating surfaces.[8])

For insulating materials there are few data on these phenomena. Fortunately, fused silica is an exception and a set of data is summarized in Appendix H. Other insulating materials can be expected to possess secondary coefficients of the same order of magnitude as quartz. According to Appendix H, the most important among the above listed phenomena are the first four.

The current density of secondary particles emitted from a surface (they may return to the surface after emission) is simply given as the product of the flux density of incident primary particles, the electronic charge of the emitted particles, and the secondary particle yield (number of secondary particles generated per incident primary particle). Determination of the photoemitted current density is discussed in Appendix H. Once emitted, the motion of secondary and photogenerated particles is influenced by the surface potential; some leave the surface and others are attracted back to the surface from which they originated, thus giving no contribution to the net surface current density. The latter case occurs when the energies of the emitted particles are not sufficient to overcome the potential barrier between the insulating surface and the plasma. From the discussion in Appendix A, it is seen that the bulk of the emitted particles associated with each process have relatively low energies (less than 40 eV). Thus, for a surface potential greater than a few tens of volts, emitted particles of the appropriate electronic charge cannot leave the insulating surface.

A qualitative representation of the contribution of the above processes to the current density transferred between an insulating surface and the space plasma is illustrated in Fig. 26. In this figure, the current density j collected by the surface is plotted as a function of the surface potential V_S; the altitude is unspecified. The dashed curves represent the primary currents incident upon the surface. When V_S is much greater than zero, primary electrons are attracted to the surface and are collected at the electron random current density. As the surface potential becomes negative, more and more electrons are repelled, as described by (7). For a potential greater than approximately kTe/e, very little primary electron current is collected. Similar considerations are applicable to primary ions.

The thin solid curves represent contributions to the current density by secondary and photoemitted charged particles. Secondary electrons generated by electron impact tend to be attracted back to the surface from which they originate. Therefore, for surface potentials greater than several volts (see Appendix A), this contribution to the surface current density drops to zero. At surface potentials for which the secondaries can escape, the primary electron flux and/or energy is so small that few secondary electrons are generated. Thus, the contribution of secondary electrons resulting from electron impact is almost negligible, as shown in Fig. 26.

Similar considerations are applicable to secondary ions generated by primary ion impact (the space plasma contains mainly positive ions which in turn generate primarily positive secondary ions as discussed in Appendix H.); however, the yield for this process does not drop to zero at low incident primary ion energies, with the result illustrated in Fig. 26.

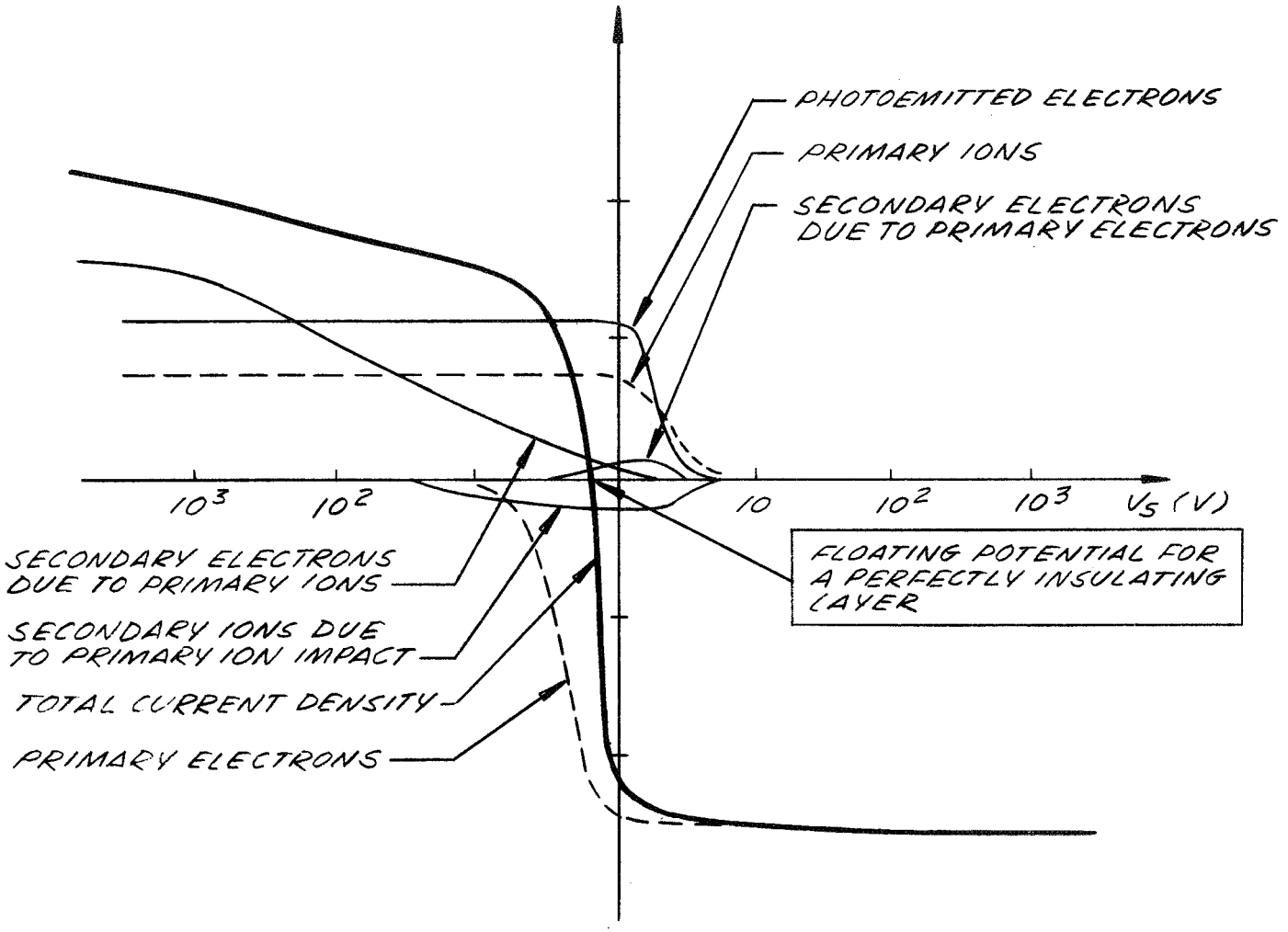

Fig. 26. Current density components at an insulating surface.

Electrons emitted by ion impact are repelled from a surface which has a negative potential and, therefore, give a positive contribution to the current density.

Photons reach the illuminated array surface independent of the surface potential and release photoelectrons which contribute to the surface current density as shown in Fig. 26. For negative surface potentials the electrons are repelled, giving a positive contribution to the surface current density; for positive potentials, however, the emitted electrons return to the surface and given no contribution. The photoelectric contribution to the surface current density will only be important at high altitudes where it can become comparable to and greater than other contributions.

The heavy solid curve in Fig. 26 represents the summation of all the current densities. The "S" shaped current-voltage characteristic is a general property of the charging process of an insulating surface. It is seen that, for a perfectly insulating layer, the steady state current density must be zero and the surface potential is fixed to within a few volts of the plasma potential.

Figure 27 demonstrates the expected quantitative current-voltage characteristics for a fused silica surface at low and high altitudes. It should be noted that, for convenience, the surface potential scale used in Figs. 26 and 27 is linear from 0 to 10 V and logarithmic thereafter. The ordinate in Fig. 26, which expresses the current density delivered to the surface in amperes per square centimeter, is calibrated in a similar manner. At an altitude of 300 km, the surface current density has a maximum value of approximately 2×10^{-6} A/cm^2 for positive surface potentials. The increase in current density with rising negative surface potential is due to the increase in secondary electron yield with incident primary ion energy. The current density becomes zero at approximately -2 V. For synchronous altitude the current densities are several orders of magnitude smaller. The solid curve in Fig. 27(b) represents the total current density for an unilluminated fused silica surface. The dashed curve includes the photoemitted current due to solar illumination at 1 AU. At synchronous altitude the surface current density becomes zero for surface potentials of from -5 to -10 V due to the higher plasma electron temperature. It should be reiterated that these results are for an infinite, plane, insulating surface. In actuality the surface is finite and the collected current density will be influenced by the plasma sheath thickness as discussed in Section II.

The high energy particle population associated with the space environment has been neglected thus far. These particles are not expected to significantly alter the surface charging characteristics of an insulating layer unless fluctuations occur, at high altitudes, which cause the high energy particle current density to exceed the ion and/or electron saturation current densities associated with the thermal space plasma. Under these conditions the insulator surface potential will differ from zero by an amount necessary to achieve a plasma sheath sufficiently thick that the thermal plasma currents can neutralize the high energy particle currents. For the altitudes region where high energy particle currents may

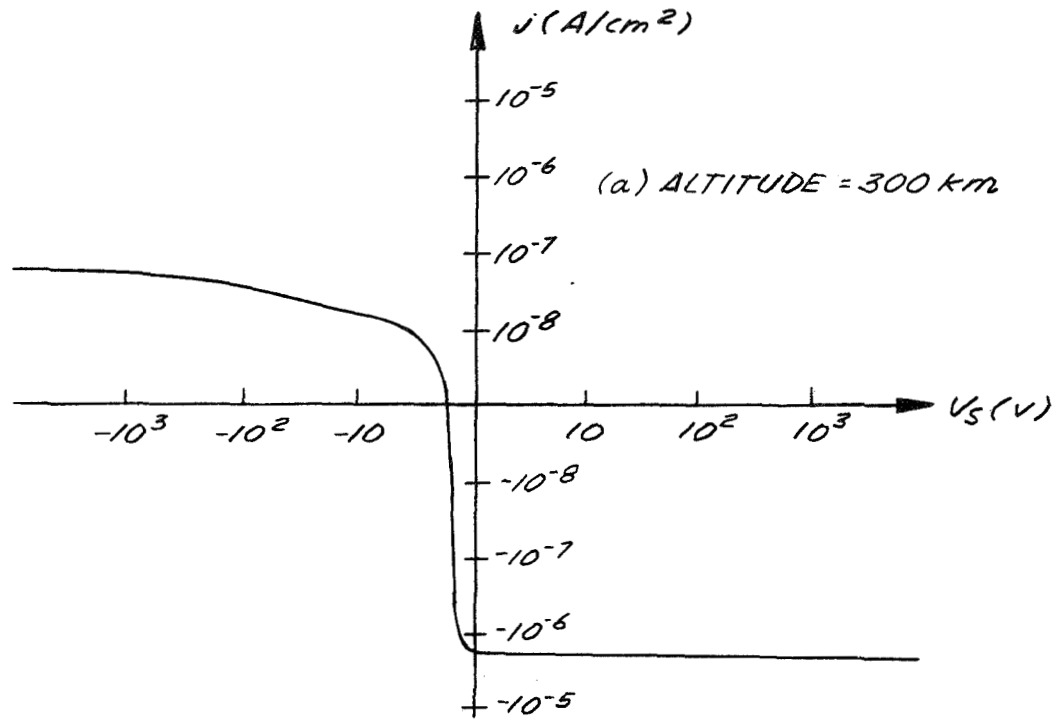

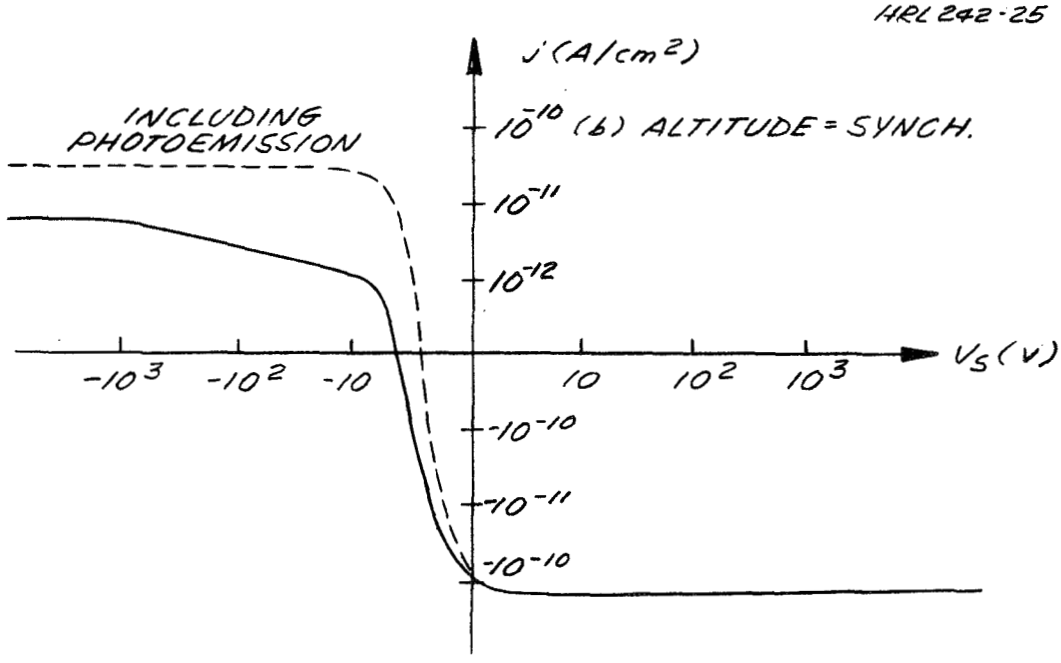

Fig. 27. Current density-surface potential characteristics for a fused silica surface.

be significant (~ 20,000 km), the surface potential could be altered by as much as a few hundred volts. Because this alteration is small in relation to the total array voltage, it can be neglected.

Spacecraft motion will influence the current collection process primarily at low altitudes, where the vehicle velocity can be as much as ten times greater than the average ion velocity. In this case, as discussed in Section II, the effective ion random current to the leading edge surfaces will be approximately four times greater than for a stationary craft. The trailing edge surfaces will collect orders of magnitude less ion current density. The collection of electrons will be unaffected, however, because they travel at much higher velocities than does the spacecraft. At the higher altitudes the average ion velocities are greater than the spacecraft velocity and the effects of motion will be negligible. Thus, it is seen that spacecraft motion is important only at low altitudes; however, the current-voltage characteristic of an insulating surface is not altered in a fundamental way, i.e., the "S" shaped characteristic is maintained and the collected current density becomes zero at a surface potential which is still close (within less than 100 V) to the plasma potential.

2. Current Leakage to the Substrate

The mechanisms for current transfer between an insulating surface and the space plasma have been discussed. To determine the equilibrium potential of the exposed surface of an insulating layer, it is necessary to consider also the various modes of current leakage between the surface and the conducting substrate. The surface potential is then obtained from the equilibrium requirement that the leakage current density is equal to the current density collected by the insulating surface.

The naturally occurring conduction mechanisms which can exist for the model of an insulating layer described earlier are

- Bulk conductivity
- Photoconductivity
- Bombardment induced conductivity

These three processes are illustrated in Fig. 28 for a conductive substrate which, for example, is assumed to have a positive potential with respect to the space plasma.

For most insulating materials considered for use in high voltage solar arrays (fused silica cover slides, kapton, etc.), the bulk resistivities are very high (10^{18} Ω -cm[9, 10]) for the expected operating temperature range of -190 to 65°C. For material thicknesses (0.01 cm) and voltage differences (10^4V) of interest, the maximum leakage current density through such insulating layers is less than 10^{-12} A/cm^2. Also, for insulators such as fused silica, the conduction process is partially ionic and the current is carried, in part, by impurity ions with the result that the effective resistivity will increase in time due to a depletion of impurities at the anode surface. In any case, it is seen from Fig. 27 that the expected bulk leakage currents are less than the collected currents with the result that the influence on the surface potential is expected to be negligible.

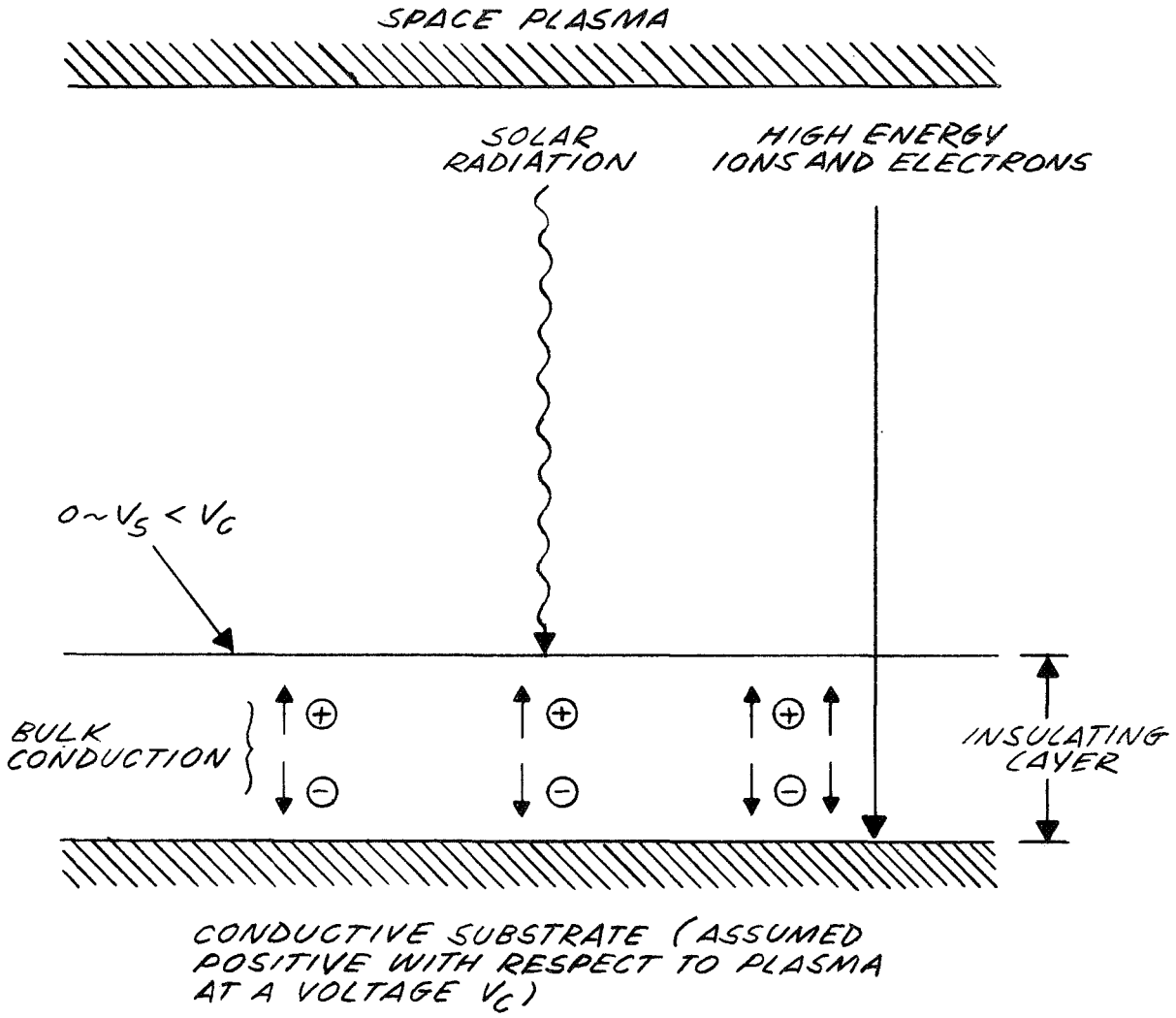

Fig. 28. Naturally occurring conduction mechanisms in insulating layers.

Photoconduction has not been observed in fused silica and will be neglected here[11].

The process in which the conductivity of a material is increased due to bombardment by energetic ions or electrons is termed bombardment induced conductivity(BIC).[12-14] In this process electron-hole pairs are released within the solid and carry current (only during periods of bombardment). Because the electrons and holes released in this manner become immobilized through trapping in a very short distance, it is necessary for the incident particle beam to have sufficient energy to penetrate most of the insulating layer. For a layer with a thickness of interest for a solar array (0.01 cm), the energy required for penetration far exceeds the energy available from acceleration by the electric fields of the array. Therefore, photoplasma particles accelerated by the array will not cause any significant increase in conductivity. However, high energy radiation belt particles can penetrate such insulating layers and enhance the conductivity of the insulator. Ehrenberg[12] has studied BIC in fused silica specimens having thicknesses similar to those of interest for a solar array. He used a yttrium-strontium source to produce an energetic electron current density of 10^{-11} A/cm^2. The electrons generated by this source have energies in the range between 0 and 2.1 MeV with a broad peak at approximately 0.8 MeV, and completely penetrate the samples. The gain, which is the ratio of the current passing through the insulating layer to that incident upon it, is proportional to the potential across the layer. For 500 V applied across a 0.02 cm thick sample the gain ranged from 1 to 5; a gain of 50 would be expected for a voltage drop of 10 kV. Assuming a similar gain for radiation belt electrons with energies greater than 40 keV at synchronous altitude, this implies an induced reduction in resistivity to a value of approximately 10^{16} Ω cm for a 0.01 cm thick fused silica cover slide. This can result in a large decrease in the potential across such an insulating layer. However, the results of Brown[15] indicate that the energetic electron flux density at synchronous orbit can decrease from the average value by more than an order of magnitude for time intervals of days. For fused silica, this will cause the leakage current density to decrease to such a value that the surface potential will be close to the value expected when BIC is not present. Thus the phenomenon of BIC cannot be relied upon to provide a consistent decrease in the potential appearing across an insulating layer.

The contribution of energetic ions to these processes is unknown. Also, specific results for other insulating materials are not available.

Only continuous insulating layers have been considered thus far. It is of interest to determine the influence of the presence of exposed conducting areas which have the same potential as the substrate of the insulating layers. This situation occurs for a conventional array design in which the conducting tabs, which interconnect the individual solar cells, are exposed to the space environment. Secondary and photoemitted particles generated at the conducting surfaces may be collected by the insulating surface, and vice versa. These processes are equivalent to current leakage between the surface of an insulating layer and its conducting substrate and thus may affect the insulator surface potential.

A digital computer analysis has been performed in an effort to determine the effective leakage currents and resulting influence on the surface potentials of insulating layers. The analysis, which is described in Appendix E, assumes a distribution of conducting surfaces similar to that for a conventional array where the solar cells are 2 cm wide and the exposed tabs comprise approximately 5% of the array area. In considering the motion of particles released from the tabs by secondary or photoemission processes, it was found that none of the particles were collected on insulating surfaces. This was true for all particles and array potentials. Conversely, it was determined that a substantial fraction of the particles released from insulating surfaces are collected by the tabs (50% for a sheath thickness of 40 cm with the conducting areas at 2000 V with respect to the insulating surfaces and the plasma).

It is easily seen that electrons generated by photoemission and ion impact are the only particles of importance in this type of leakage process (ions are seldom released from a surface). Therefore, referring to the above results, it can be concluded that this mode of leakage is important only for positive sectors of the array where electrons which are photoemitted from insulating surfaces reach the tabs. In this case there is the possibility that the surface potential of the insulating layers will become substantially positive if the photoelectron current density emitted from the surface and collected by the tabs is greater than the collected plasma electron current density. This can occur only at high altitudes.

Therefore, it is seen that the above process does not provide a consistent mode of current leakage between the exposed insulating surfaces of a high voltage solar array and their substrates.

3. Conclusion

Combination of the above considerations concerning current collection and leakage for insulating layers indicates that because no consistent naturally occurring leakage mechanism exists, insulator surface potentials will be close to the space plasma potential. Therefore, the entire array potential at any point on the array can be expected to appear across an insulating layer, independent of altitude.

It should be noted that the above result is nearly independent of the existence of surrounding biased conductors. At most, a conductor would tend to cause the potential of a nearby insulating surface to shift toward the potential of that conductor. This implies that exposed tabs may collect slightly larger currents due to the presence of insulating surfaces; however, this would be significant only at very high altitudes where plasma losses are quite small.

B. SPUTTERING

A high voltage solar array that is not fully electrically insulated from the space environment can incur damage due to sputtering, which is much greater than that experienced by a low voltage array or a fully

insulated high voltage solar array. The increased sputtering results from the incidence of photoplasma ions which are accelerated to high energies by the intense electric fields of the array. Figures 29 and 30 illustrate how the sputtering rate, in Angstroms per year, depends on altitude for a characteristic conductor (silver) and a typical insulator (fused silica), respectively. At low altitudes the major contribution to sputtering is from the O^+ ions; at high altitudes H^+ gives the main contribution. The detailed calculations from which these results were obtained are presented in Appendix I. The range of values for the sputtering rate at a given altitude results from the experimental error and temporal variation of the space plasma density. These results are applicable for ion energies in the range 2 to 16 keV. For ion energies lower than 2 keV the sputtering yield (number of atoms per incident ion) and, therefore, the sputtering rate, decreases. It is seen that the sputtering rates are quite small at high altitudes but can become significant at low altitudes. For example, an estimated six months are required to remove a 4000 A thick magnesium fluoride antireflection film at an altitude of 300 km provided, of course, that it is energetically possible for ions to reach the insulating portions of the array that are covered by such a film. Results for conducting surfaces other than silver are given in Appendix I.

In contrast to the partially insulated high voltage solar array, the low voltage array and the fully insulated high voltage solar array are subject to sputtering only by misdirected thrust ions, low energy thermal plasma ions, and radiation belt ions. Presumably the spacecraft could be designed to minimize the interception of the thrust beam. Plasma ions cause little damage because the bulk of these particles do not have energies greater than the sputtering threshold.[16,17] Finally, the radiation belt ions have flux densities which, at most, are approximately equal to the photoplasma ion flux at high altitudes. Because the sputtering yields of these particles are approximately equal to those of photoplasma ions, with energies in the range 2 to 16 keV, it is expected that the associated sputtering rates are very small.

In addition to surface erosion by sputtering, there is the possibility that sputtered material can be deposited on solar cell cover slides and reduce their transparency. However, sputtered material travels in straight trajectories and, therefore, only material released from central spacecraft surfaces, which do not lie in the plane of the array, must be considered. However, it is probable that this portion of the spacecraft will be maintained at plasma potential, with the result that the flux of sputtered material will be very small.

Conclusion: Sputtering is not expected to be a problem except at low altitudes where proper design and operation should prevent harmful effects.

C. PROPELLANT CONDENSATION

It is of interest to consider the effects of propellant condensation on the surfaces of a solar-electric spacecraft. Such condensation is not peculiar to spacecraft utilizing high voltage solar arrays however, the existence of a thin surface film of propellent may have a marked importance in the following areas:

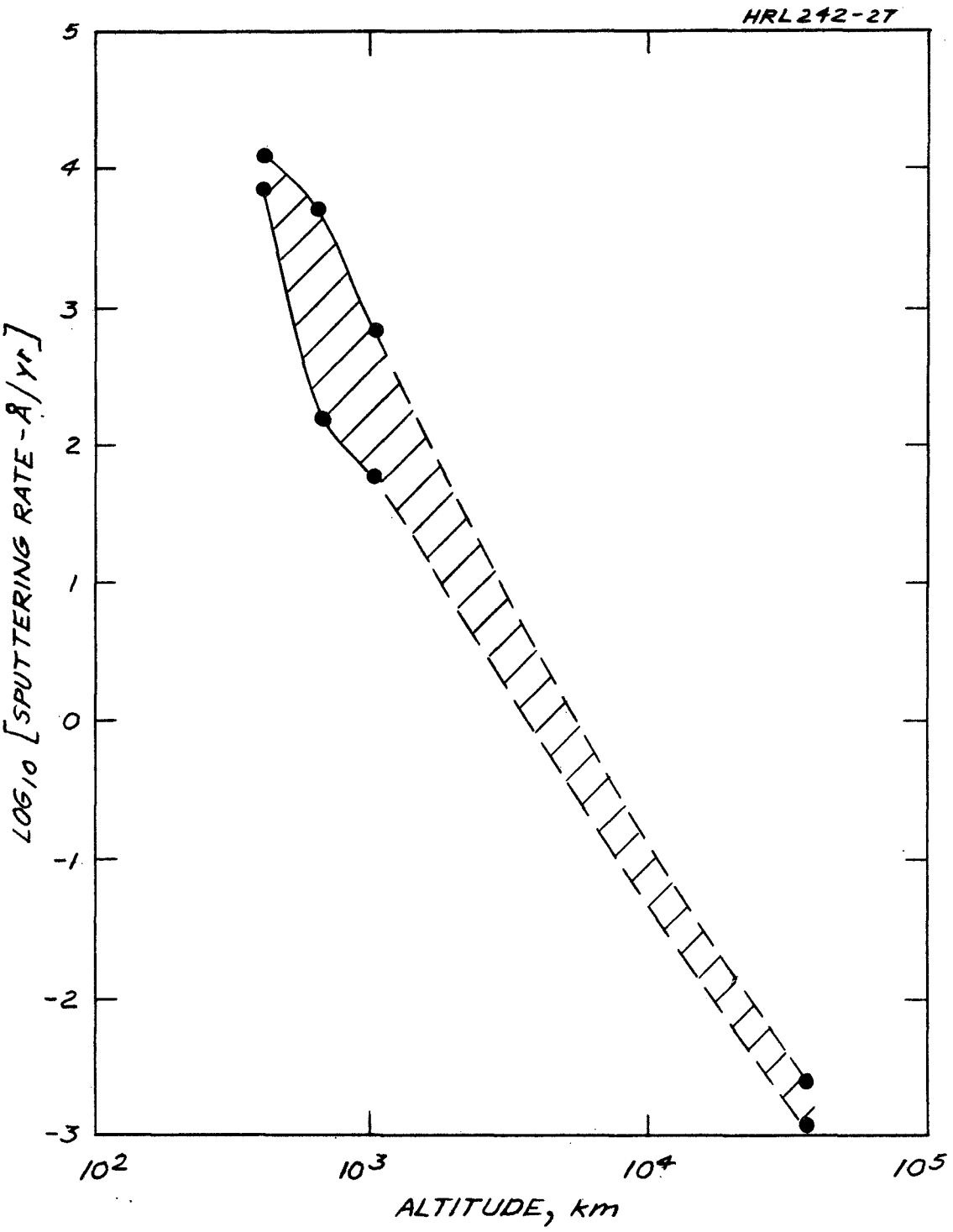

Fig. 29. Sputtering rate of a silver surface (semi-infinite) having a potential of 2 to 16 keV below plasma potential.

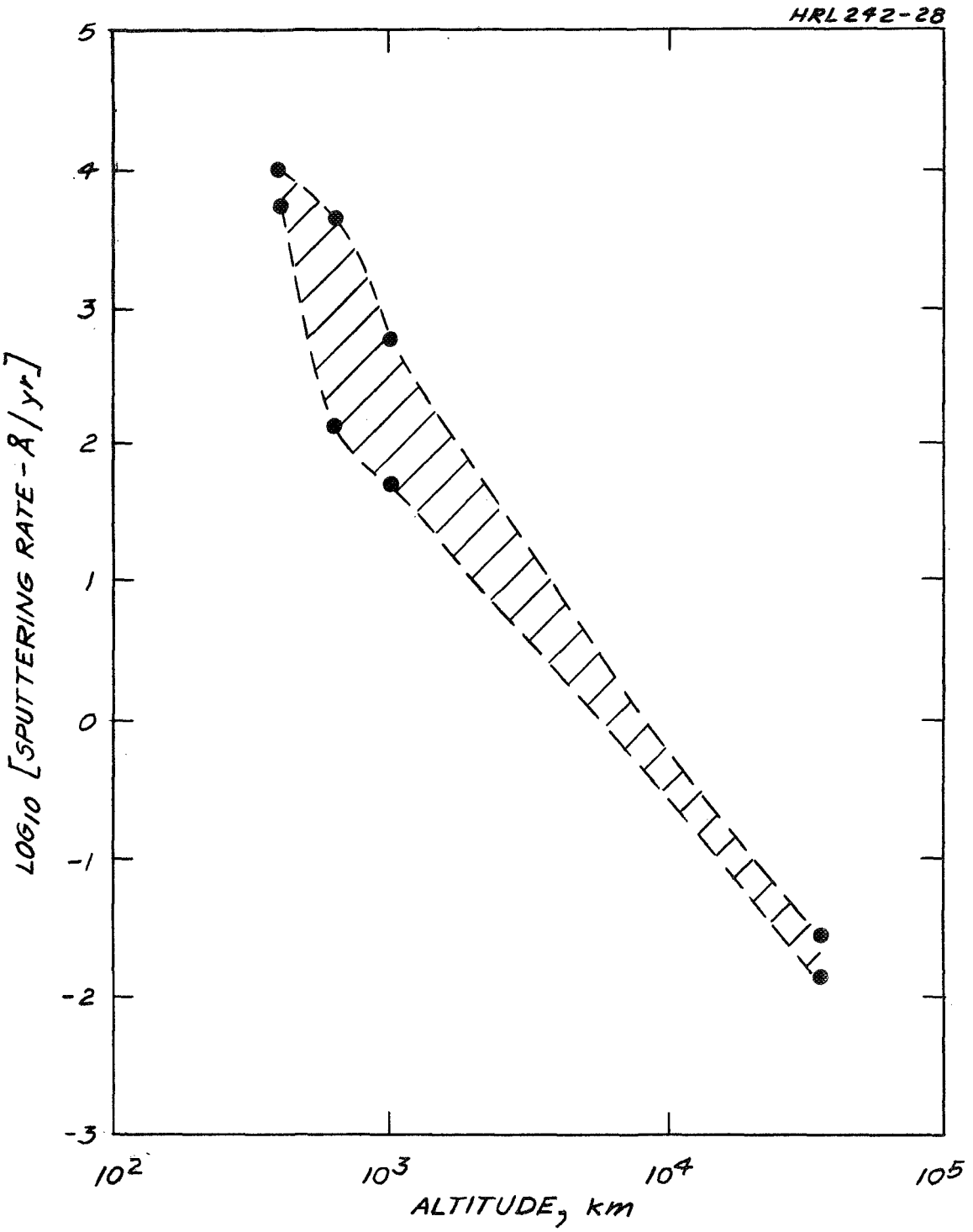

Fig. 30. Sputtering rate of fused silica for ion energies in the range 2 to 16 keV.

- The possibility of increased surface conductivity of insulating layers may result in increased leakage to conductive substrates and a decrease in the potentials across the layers. Based on the results of Reynolds and Richley[18] it is expected that, except for operation at large distances from the sun ($>$ 2 AU), only a monolayer of propellant will exist on array surfaces. This is not expected to appreciably alter the surface conductivity of insulating layers.

- Contamination of the various solar array surfaces can alter the secondary and photoemission characteristics, which in turn can cause a change by as much as a factor of two or three in the plasma leakage currents. Experimentation is required in this area.

- Alteration of the array surface properties could influence the surface breakdown characteristics. Experiments would be necessary to determine the importance of these effects.

There are a number of other areas concerning the influence of propellant condensation on the optical, electrical, and chemical properties of contaminated surfaces; however, these are not peculiar to high voltage solar arrays and will not be discussed.

Conclusion: Propellant condensation should not be important except at distances from the sun greater than 2 AU.

IV. SOLAR ARRAY DESIGN

A. INTRODUCTION

The primary purpose of this section is to define the problems associated with the design, fabrication, testing, and flight operation of high voltage solar arrays. This purpose is accomplished through the examination of basic design parameters and the development of a conceptual design. The array being considered is one which supplies 16 kV and 15 kW at end of life. Power is available to the loads in at least six voltage increments from 2 kV to 16 kV. The study will assume a common basic block producing 0.94 A at 1 kV at end of life. Smaller building blocks would have little impact on the proposed design. Table I describes the modular components of the array.

B. BASIC DESIGN CONSIDERATIONS

A number of considerations are now presented which are basic to the design of a high voltage solar array. Some factors are discussed which are not peculiar to the high voltage array; however, their consideration is necessary in order to establish a basis for design. The following areas will be considered:

1. Thermal Environment
2. Radiation Degradation of Solar Cell Performance
3. Materials
4. Array Configuration
5. Reliability
6. Fabrication
7. Testing
8. Safety

1. Thermal Environment

The thermal environment experienced by a solar array as it travels from a low earth orbit to synchronous altitude has been analyzed. Temperatures were computed for three conditions as a function of altitude, with the results shown in Figs. 31 and 32. These results are based upon a typical deployable array with a Kapton substrate and are not peculiar to the high voltage case.

As indicated in Fig. 31, the temperature of the solar array is higher at lower altitude. This is the result of the increased influence of the earth's albedo at low altitudes where the earth presents a larger area view factor. The same phenomenon applies in eclipse, as shown in Fig. 32, where radiation from the earth elevates the array temperature during the lower orbits.

2. Radiation Degradation of Solar Cell Performance

Solar cell radiation damage has been analyzed for an orbit raising mission, and the results are shown in Fig. 33. It is important and significant to note that both backside and frontside radiation effects have been considered; backside effects must be included for the thin flexible substrate proposed for this design. The total degradation

TABLE I

Array Modules

Solar Cell	Smallest electrical producing element, single crystal silicon, 2 cm x 2 cm, 0.015 cm thick, 10Ω-cm, 0.015 cm thick fused quartz coverslides, exposed tabs.
Group	Basic cell assembly, a total of 350 solar cells, 14 in parallel by 25 in series.
Sector	8 groups of solar cells connected in series, a total of 2800 solar cells, the largest tested unit prior to final assembly.
Block	22 sectors of solar cells connected in series, a total of 61,600 solar cells, the basic assembly for providing power to the spacecraft loads, provides 1 kV at 0.94 A at end of life.
Panel	4 blocks, switchable in series/parallel combinations, one of four physical entities of the power producing configuration, a total of 246,400 solar cells. Approximately 15 ft by 85 ft.
Array	4 panels, the full power configuration, a total of 985,600 solar cells.
Panel Segment	Basic fabrication unit, full panel width by one sector, with 8 sectors attached, 11 panel segments are joined together to form a panel as the final step in assembly.
Bypass Module	The set of cells wired in parallel with a diode for the purpose of failure isolation, primarily open circuit failures.

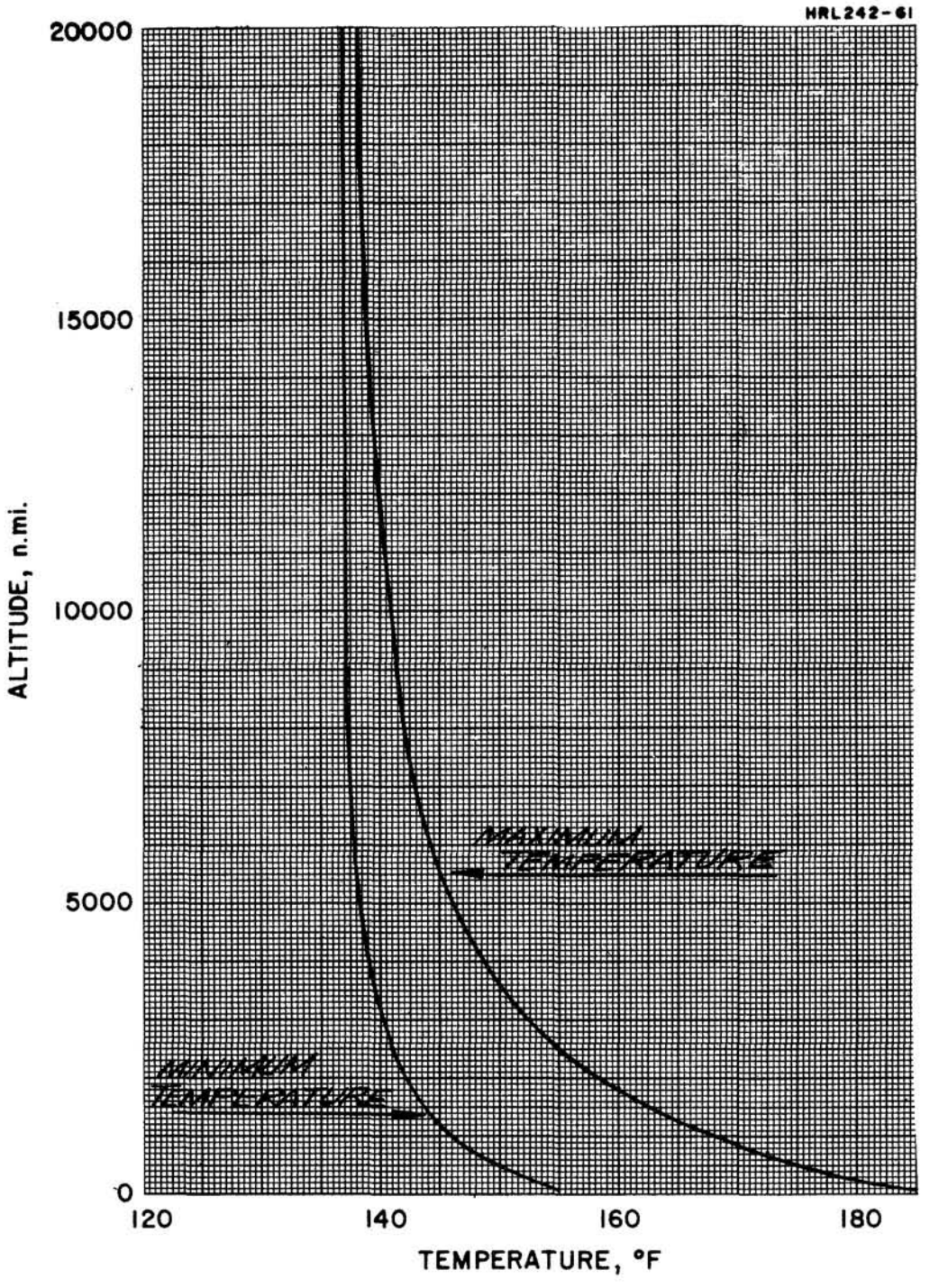

Fig. 31. Maximum and minimum temperatures during circular orbit as a function of orbit altitude.

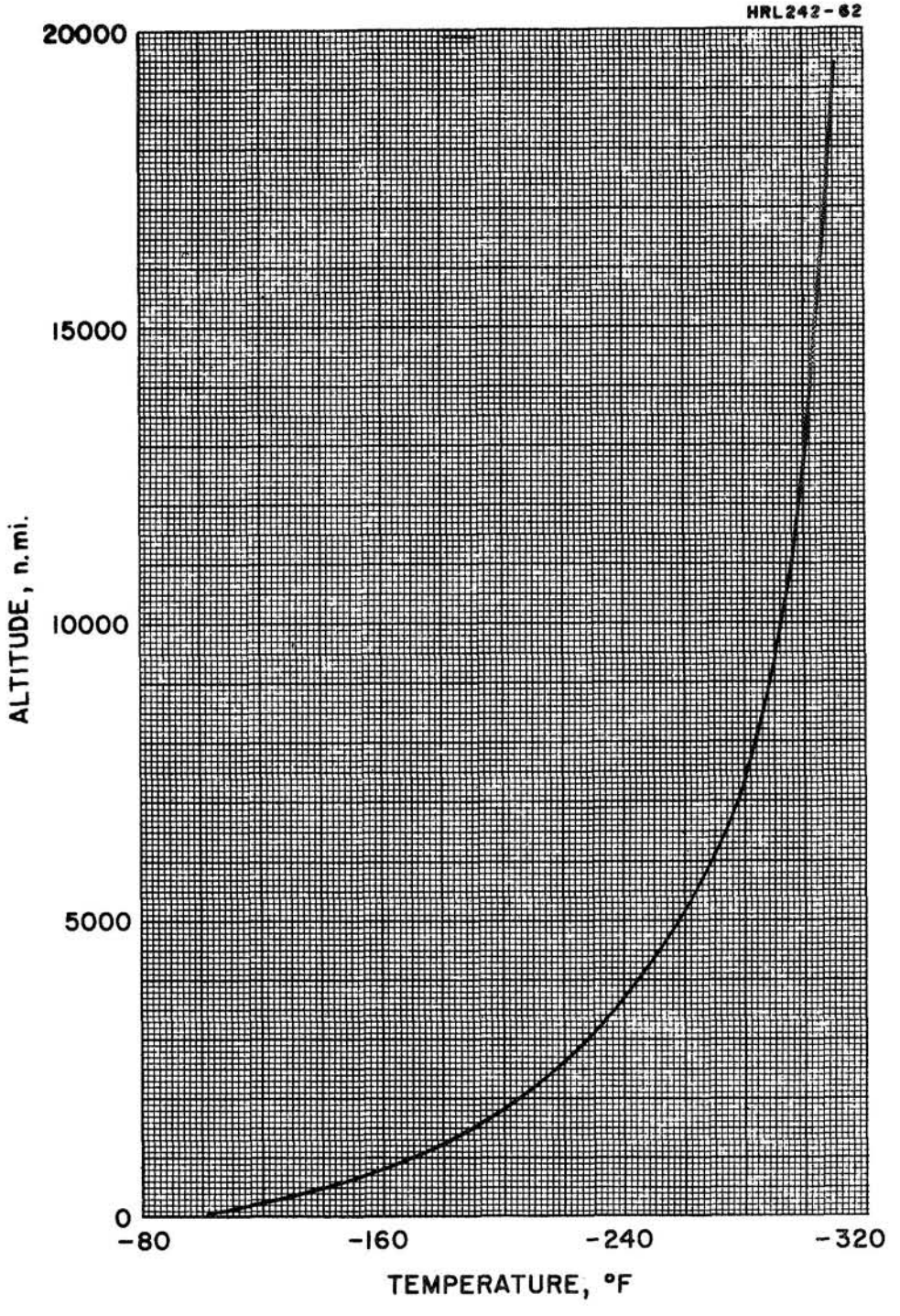

Fig. 32. Minimum eclipse temperature for maximum duration eclipse during circular orbit as a function of orbit altitude.

expected for 6 mil solar cells with 6 mil coverslides is 58%. If the panel were raised directly to synchronous orbit, the end of life degradation would be 30%. The greater degradation associated with orbit raising results from passage through the severe environment in the heart of the Van Allen belts. These results are equally applicable to both high and low voltage arrays.

As indicated in Fig. 33, the degradation decreases as the solar cell and cover slide thickness increase. However, increased thickness causes the array weight to increase as indicated in Fig. 34. For this reason, a 6 mil (0.015 cm) silicon solar cell with a 6 mil cover slide was chosen. This cell satisfies the following requirement: (1) sufficient dielectric strength, as will be discussed later; (2) backside radiation protection equal to frontside protection; (3) minimum array weight for end of life power requirements; and (4) ease of fabrication (thinner assembly would complicate the fabrication procedure).

3. Materials

The design of a high voltage solar array is strongly dependent on the characteristics of materials, particularly with regard to electrical breakdown, outgassing, mechanical strength, and sensitivity to temperature and radiation. This subsection discusses the various important material aspects and is concluded with a selection of materials which are most suitable for high voltage solar array applications.

a. Electrical Breakdown Considerations

A high voltage solar array is subject to severe electrical stresses which result from surface charging by plasma currents as well as from electric fields generated between various active components of the array by photoelectric means. The effects of electrical breakdown, which may result from these stresses, vary from minor current leakage losses to partial or total catastrophic array failure. The severity will depend on the array design, the location of the failure, and the nature of the electrical discharge.

Electrical breakdown through a material generally will result in permanent change, with a resultant loss in both dielectric and mechanical properties. If the failure is generated between nonactive areas such as between the array and the plasma, the most probable effect would be a power loss, which is not expected to be catastrophic. Discharges through a dielectrical material cause a progressive material erosion which may propagate between active elements and result in catastrophic electrical failure or greatly weaken structural integrity.

The effects of surface breakdown depend upon the nature of the discharge. If the discharge is intermittent and does not cause deterioration of the dielectric surface, it may actually increase the potential required for subsequent breakdown by conditioning the surface. However, if the discharge is sustained and/or the surface is degraded,

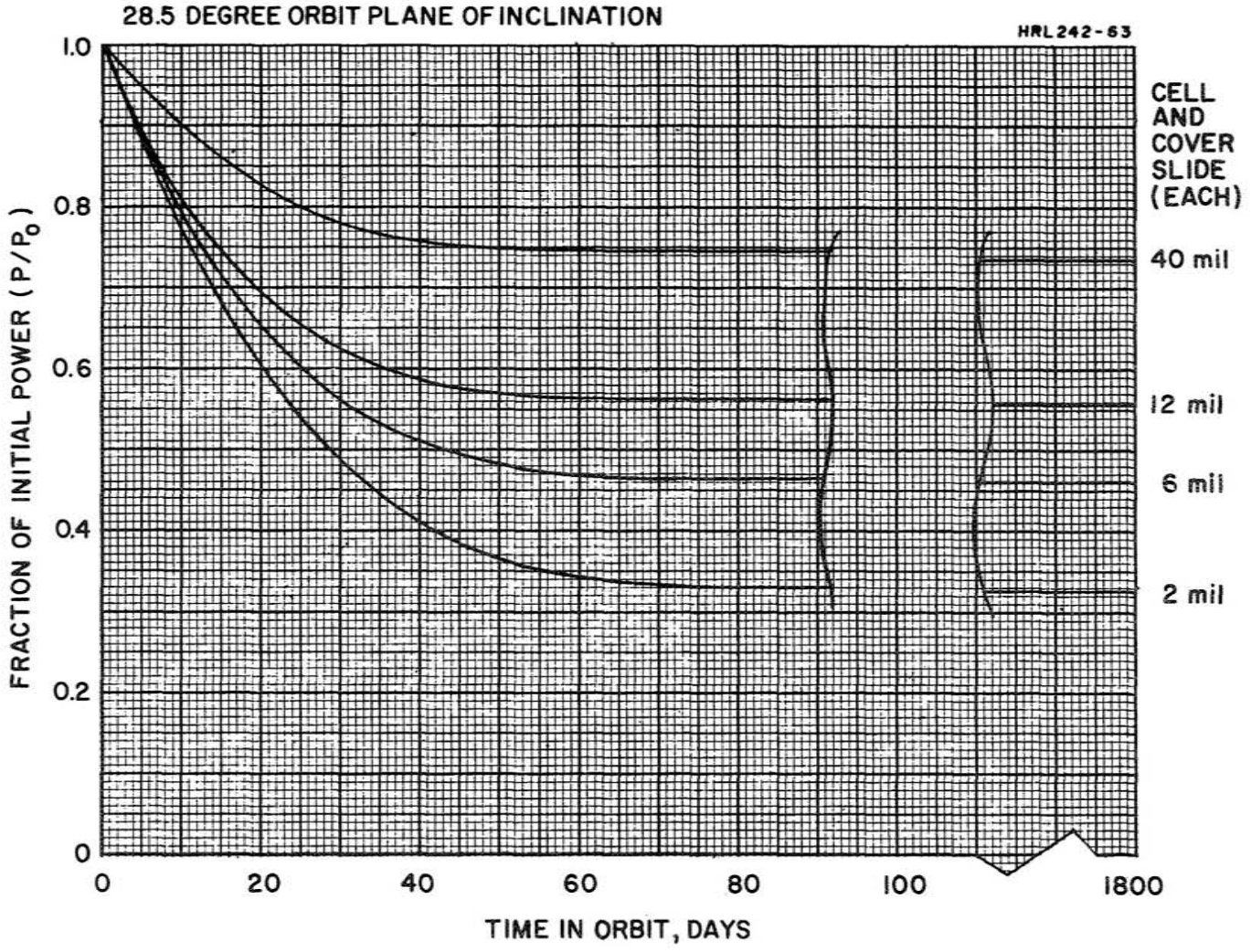

Fig. 33. Fraction of initial power versus time in orbit (- 3 σ).

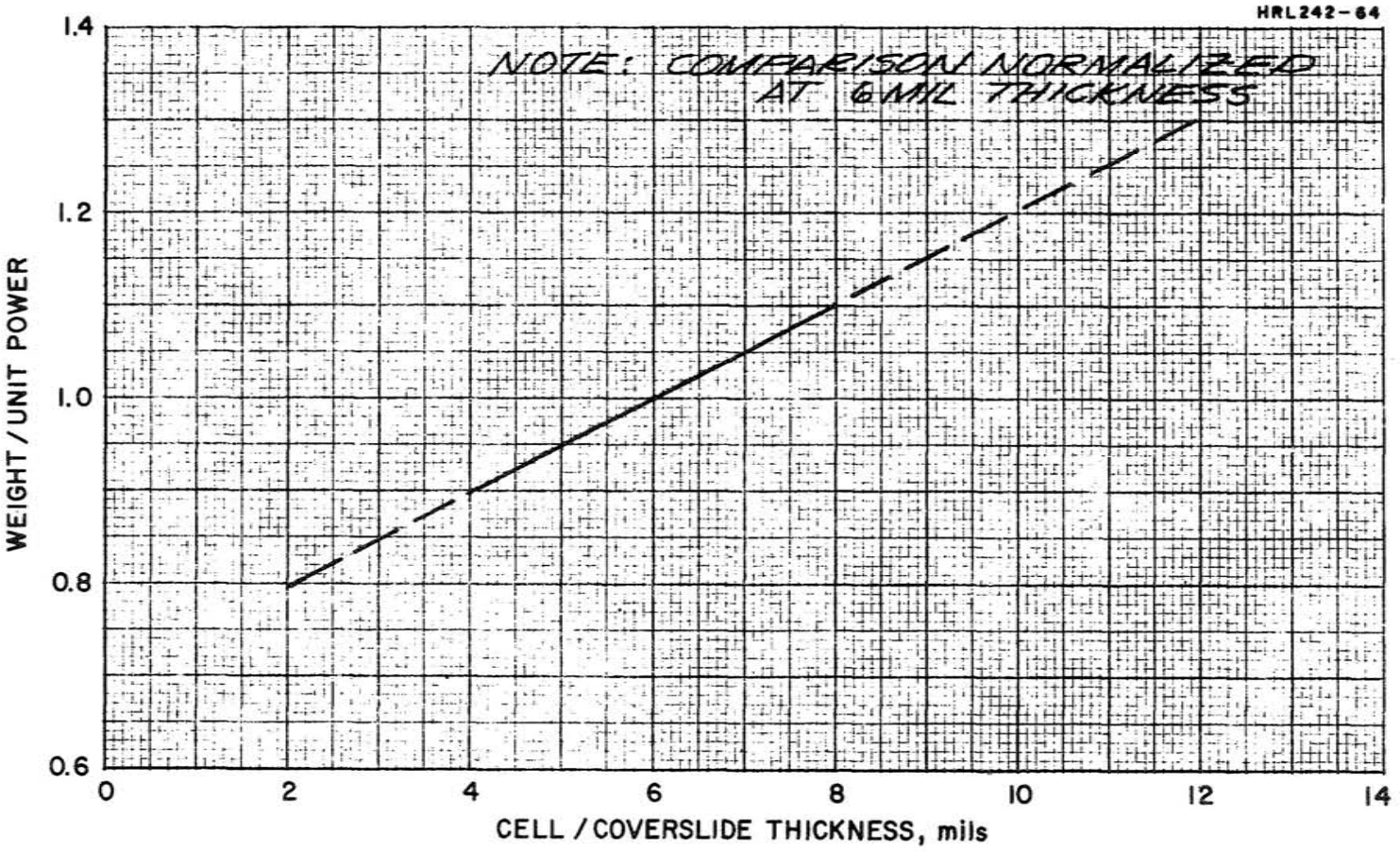

Fig. 34. Weight-efficiency trend as a function of cell and cover slide thickness (28.5° orbit inclination, end of life - 3 σ).

catastrophic failure can result through permanent shorting. For most organic insulators such shorting results from carbon residues which provide a permanent conductive path that cannot be restored to a non-conductive condition. Certain materials such as ceramics and silicone compounds have high resistance to the formation of residues in the presence of electrical discharge and, therefore, should be employed in array construction to minimize the potential for surface breakdown due to the formation of conductive paths.

The general aspects of electrical breakdown in the bulk and along the surfaces of insulators and methods for limiting the electrical stresses which cause breakdown are now discussed.

(1) Bulk Breakdown - Bulk breakdown results from electrical stresses within the dielectric due to voltage gradients and may be characterized by any of the following processes:

- Intrinsic breakdown
- Thermal breakdown
- Inclusion induced breakdown
- Electrolytic deterioration
- Emission discharge

Each of these processes is discussed in turn.

Intrinsic breakdown results from electron avalanche of sufficient magnitude to completely destroy a section of dielectric existing between two electrodes. The voltage levels for intrinsic breakdown are established in the absence of all other causes of bulk breakdown, and represent the highest recorded breakdown levels in experiments where other effects have been minimized. As a result, intrinsic values are of little use in design for cases where the presence of other factors such as pre-breakdown discharge, heating, and geometry exist. The usefulness of intrinsic data is limited to comparisons between materials; however, even this application must be tempered by an understanding of the other modes of breakdown.

Thermal breakdown occurs in the presence of excessive electrical power dissipation within the dielectric due to a nonzero conductivity. This dissipation causes an increase in temperature which either thermally decomposes the dielectric or excites electrons into the conduction band. In the case of electron excitation, electrons are accelerated by the electric field, resulting in charge multiplication and electrical discharge. Materials having low resistivities or containing substances which lower the resistivity are generally more susceptible to thermal breakdown if the internal power dissipation increases the bulk temperature. This process also depends on the ability of the dielectric component to dissipate heat. Therefore, thin insulating layers having large heat conductivities have small susceptibility to thermal breakdown. Once the thermal breakdown

process is initiated, it is progressive, leading to complete failure unless the conditions causing the process are removed. Thermal breakdown is a common failure mode for organic insulation such as is expected to be utilized with a high voltage solar array.

Inclusion-induced breakdown generally results from a redistribution and intensification of stresses within the dielectric. These stresses are concentrated in regions of high permittivity or resistivity, such as gas pockets or included matter, which become the sites for initiation of breakdown.

Gaseous inclusions or voids are a common cause of dielectric failure in solids and may be expected in the construction of a high voltage array. Electrical breakdown due to voids is dependent upon void size, dielectric thickness, gas presence, type of gas, and applied voltage. It has been found that this type of breakdown is related to the well-known Paschen breakdown in gases (see Fig. 30). In this case the high electrical stress in a gas filled void is relieved by an electrical discharge. Because of the conductivity of the dielectric material, the electrical stress will slowly be re-established until further discharging occurs. Assuming a typical dielectric material and a pressure of 1 atm in a void, the minimum void diameter which is expected to result in failure is approximately 4×10^{-4} cm (0.8 mil). The level of damage depends on the energy dissipated per discharge and the total number of discharges, which depends on the RC time constant of the configuration. In some cases the void may enlarge, due to repetitive discharging, until the pressure within it decreases to a point where breakdown no longer occurs and no further damage is incurred. However, this situation depends on the insulating material, initial conditions, geometry, etc.

The life of insulating material subject to this type of discharging (or corona) is limited to a degree which must be determined experimentally for a given situation. Corona measurements can give some indication of the soundness of insulation, and sensitive detection equipment is available (Refs. 19, 20). In addition, proper design and visual inspection can aid in elimination of this mode of electrical breakdown.

Electrolytic deterioration causes another mode of bulk dielectric failure. The intrinsic conductivity of most dielectrics, including those proposed for the high voltage array, is based upon electron-hole pair mechanisms. In this form of conductivity the dielectric remains unaltered as a result of current flow. However, the presence of contaminants, which are generally ionic, can result in electrolytic processes which cause breakdown. In this case, breakdown results either from direct dielectric destruction or from the production of conditions for electrical discharge and subsequent failure. Conditions leading to gradual deterioration include the formation of gases and the redistribution of ionic matter. Substances that have demonstrated the referenced deteriorating effect on insulating materials are chloride ions, silver, and rosin flux

residues (Ref. 21) (ambietic acid salts). Electrolytic deterioration is not considered to be a primary source of dielectric failure for the high voltage array.

The final mode of bulk dielectric failure to be considered is emission discharge. The emission phenomenon involves a low level discharge of a randomly recurrent nature in which the momentary current increases by some exponential power of the voltage. The effect occurs in the absence of voids or excessive heating, although the advanced stages of breakdown, to which the emission phenomenon can lead, may be a function of thermal mechanisms (Ref. 22). Various studies have shown that emission discharges are damaging, with dielectric failure the ultimate result. If the voltage is increased above the emission inception level, the discharge and deterioration rates are accelerated, reducing the time to failure. This may account for the disagreement between pulsed and long term tests on the same materials, which result in higher breakdown levels for the pulsed methods of testing. It should be emphasized that emission discharge has been noted at voltages ranging from 50 to 100% of commonly measured dielectric breakdown voltages. For example, a Kapton film, which was found to exhibit breakdown voltages of 18 kV, produced emission discharge at 14 kV during the same tests.

A further consideration in establishing the dielectric design is the bulk behavior of dissimilar dielectric materials under electrical stress. When dielectrics are placed in series, the electrical stresses are apportioned according to the following expressions:

$$E_1 = \frac{V}{x_1\left(1 + \frac{x_2 k_1}{x_1 k_2}\right)}, \qquad E_2 = \frac{V}{x_2\left(1 + \frac{x_1 k_2}{x_2 k_1}\right)}$$

where E is the electrical stress, V the applied voltage, k the dielectric constant, and x the thickness. These relationships, which are illustrated in Fig. 35 can be used to predict the approximate stress in each material used in a given dielectric design. For example, these relationships indicate that the application of 20 kV across a series combination of 3 mils of silicone resin and 5 mils of Kapton (see Table II) results in electrical stresses of 2000 and 2800 V/mil, respectively. If the design limit for this configuration were assumed to be one half of the stated dielectric strength, this situation would be at the limit of acceptability. It should be noted that the presence of a void adds another, weaker element in series. This example illustrates the importance of such considerations in producing an effective dielectric design.

For dielectrics in parallel (Fig. 35 (b)) the stresses are equal in both materials, and the breakdown will be determined by the material with the lowest strength.

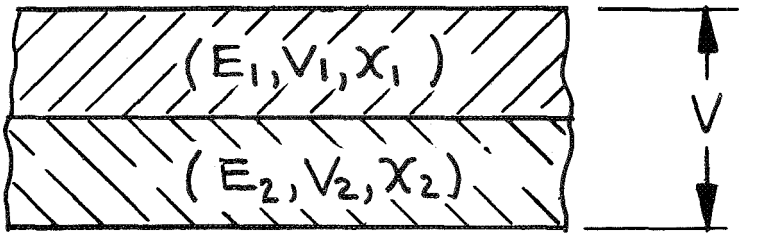

$$V = V_1 + V_2 \quad E_1 = \frac{V_1}{X_1} \quad E_2 = \frac{V_2}{X_2}$$

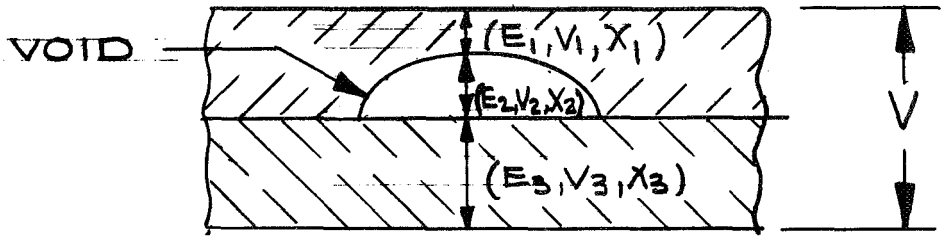

$$V = V_1 + V_2 + V_3 \quad E_1 = \frac{V_1}{X_1} \quad E_2 = \frac{V_2}{X_2} \quad E_3 = \frac{V_3}{X_3}$$

A. SERIES

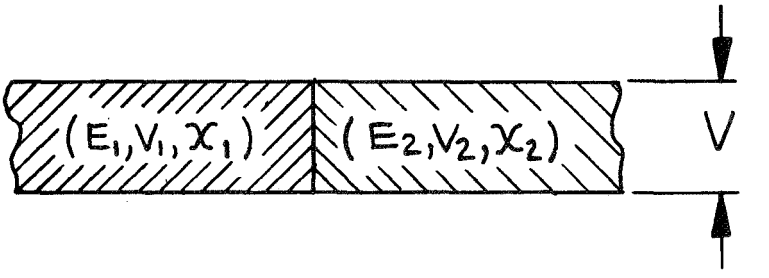

$$V = V_1 = V_2 \quad E_1 = E_2$$

B. PARALLEL

Fig. 35. Electrical stress distributions in dissimilar dielectrics.

Conclusions: An important design principle can be stated concerning the bulk breakdown of dielectric material. Because emission discharges can lead to dielectric failure, the potential at which this process is initiated for a given material would establish the design limit for the dielectric strength.

(2) Surface Breakdown - The surface breakdown of dielectrics is a complex phenomena depending upon many factors. It can be described by two basic processes: flashover (arcing) and tracking.

Flashover occurs when the electric field along a surface exceeds the breakdown strength of the medium or the surface. At a solid-gas interface, in a parallel electric field, flashover is ordinarily initiated by electrical breakdown in the gas which has a lower dielectric strength. Under space conditions, in which the mean-free-path of the gas is greater than the electrode spacing and gas breakdown is precluded, flashover can still occur either by breakdown of the solid or field emission associated with high electric fields at the electrodes. The formation of the well known "Lichtenberg" figures, which have been observed in vacuum is an example of flashover (Ref. 23). The flashover voltage is strongly affected by surface conditions of the cathode, cathode material, dielectric surface (if it influences the cathode) and the characteristics of the dielectric-cathode-vacuum interface (Ref. 24). The breakdown voltage is less sensitive to similar conditions occurring at the anode. For configurations in which a smooth cathode is intimately connected to the interelectrode dielectric (no microscopic cracks exist), the breakdown voltage has been found to be independent of the presence of the surface (Ref. 25).

This effect becomes significant in terms of the high voltage solar array where solar cells with rough surfaces, interconnections, and busses may contribute to flashover. Therefore, the array design must give particular attention to the region of the cathode-dielectric junction where methods must be utilized to preclude the existence of high electric fields.

Although flashover is not directly dependent upon the exposed dielectric surface, the second mode of surface breakdown is related to the characteristics of this surface. Tracking is the formation of a conducting path on a surface which may result from electrical discharges, thermal degradation, or electrolytic degradation. Electrical discharges on or adjacent to the dielectric surface can result in deterioration of the surface and the formation of conductive paths. These discharges may be induced by gaseous inclusions at a surface, conductive or semiconductive contaminants on or in the surface, and excessive electrical stress within the dielectric.

Both thermal and electrolytic deterioration which result in tracking depend upon the mechanisms and conditions previously described under bulk breakdown.

All of the above conditions which lead to tracking could exist on a high voltage array. However, an awareness of their potential existence can result in design considerations and process controls which eliminate their occurrence. For example, the use of semiconducting surface layers or surface treatments which are highly insulating can significantly reduce the tendency to track.

Conclusions: Surface breakdown is an area of primary concern in the design of a high voltage solar array. Particular attention must be given to the vacuum-insulation-cathode junction.

It is possible that the solar cells of a high voltage array will suffer damage resulting from large intermittent currents associated with electrical breakdown of the insulating layers which bound the cells. Normally the electric fields within a solar cell, other than those directly generated by the cell, are quite small. When the array is first operated in space, at high voltage, current will flow to the junction between the solar cells and the insulating layers which bound them (the cell becomes one plate of a capacitor). This current is equal to the current collected on those insulating surfaces which are exposed to the space plasma. The collected current density can be no greater than approximately the electron saturation current density which is not of sufficient magnitude ($j_{esat} \sim 10^{-6}$ A/cm^2) to influence the solar cell operation. At equilibrium the ohmic currents flowing across the insulator-solar cell boundary are even less than this amount. However, should electrical breakdown occur between the exposed insulating surfaces and the solar cell, the capacitance formed by the insulating layer will be discharged with the possibility of high current flow within the cell. For example, if a potential of 16 kV appears across a 0.015 cm (6 mil) thick cover slide, the stored energy is approximately 10^{-2} J. This amount of energy, if deposited in the semiconducting material of the solar cell, can vaporize roughly 10^{-6}g of material. A cover slide will charge to the array voltage in as little as 1 sec at low altitudes and, therefore, as much as 1 g of material could be vaporized in ten days. At synchronous altitude many years would be required to decompose a similar amount of material due to the slower surface charging of insulating layers by plasma currents. In actuality it is expected that the energy stored in an insulating layer will be dissipated over a sufficiently large area that only minor heating of the cell will result.

None of the above electrical breakdown phenomena have been investigated for the environmental conditions and materials of interest for the operation of a high voltage solar array. The bulk breakdown strength of typical insulating materials may be significantly influenced by continued exposure to the space radiation environment. In addition the effect of surface discharging over a long period of time is not clear. For example, repetitive surface discharging of solar cell cover slides may impair their optical transmission. In any case, experimentation is required to determine the importance of these effects for the particular application.

(3) Methods of Limiting Voltage Gradients in Insulators - Because electrical breakdown is a major factor in determining the design of a high voltage solar array, various means must be considered for reducing to a tolerable level the voltage gradients which cause breakdown. The simplest approaches involve providing adequate spacing between regions of different potential, sufficient thickness for insulating layers, and voltage block layouts that minimize electrical stresses. An example of the last approach is illustrated in Fig. 36, where two possible arrangements of 12 voltage blocks connected in series on an array panel are shown. The magnitudes of the voltage differences appearing between the blocks are indicated by the circled numbers. Because the configuration shown in Fig. 36 (b) involves smaller voltage differences, it would represent the preferred choice.

Based on presently available data, it is expected that insulating layers of the same thicknesses as used with conventional solar arrays will be sufficient to withstand the large voltage gradients associated with a high voltage solar array. However, the effect of long exposure to the space environment may result in a deterioration of insulator properties and an increased susceptibility to electrical breakdown. If future experimentation indicates that this is the case, further reduction of electric fields will be necessary. In this situation use of the previcusly mentioned approaches may result in increased array weight and may not be allowable, depending on the constraints of the proposed mission. A number of other approaches which have been investigated for application in this area, are:

- Conductive surface films
- Conductive insulators
- Dielectric shielding
- Self-neutralization
- Encapsulation

These approaches are discussed below.

(a) Conductive surface films: Electric fields within the bulk and along the surface of an insulating layer can be greatly reduced by application of a conductive surface film that is electrically connected to the substrate. This method is applicable to the cover slide of solar arrays which protect the solar cells from the space environment, and to the backing layers which provide mechanical support as well as protection. It is clear that the conductive film must not be continuous because this would result in short circuiting of the array. An example is illustrated in Fig. 37, where conductive films are employed to reduce the electric fields both within the cover slides and the substrate. In this case the voltage across the cover slides is zero and the maximum voltage across the substrate is the voltage generated by the number of solar cells backed by a continuous film area. Because the film has approximately the same potential as

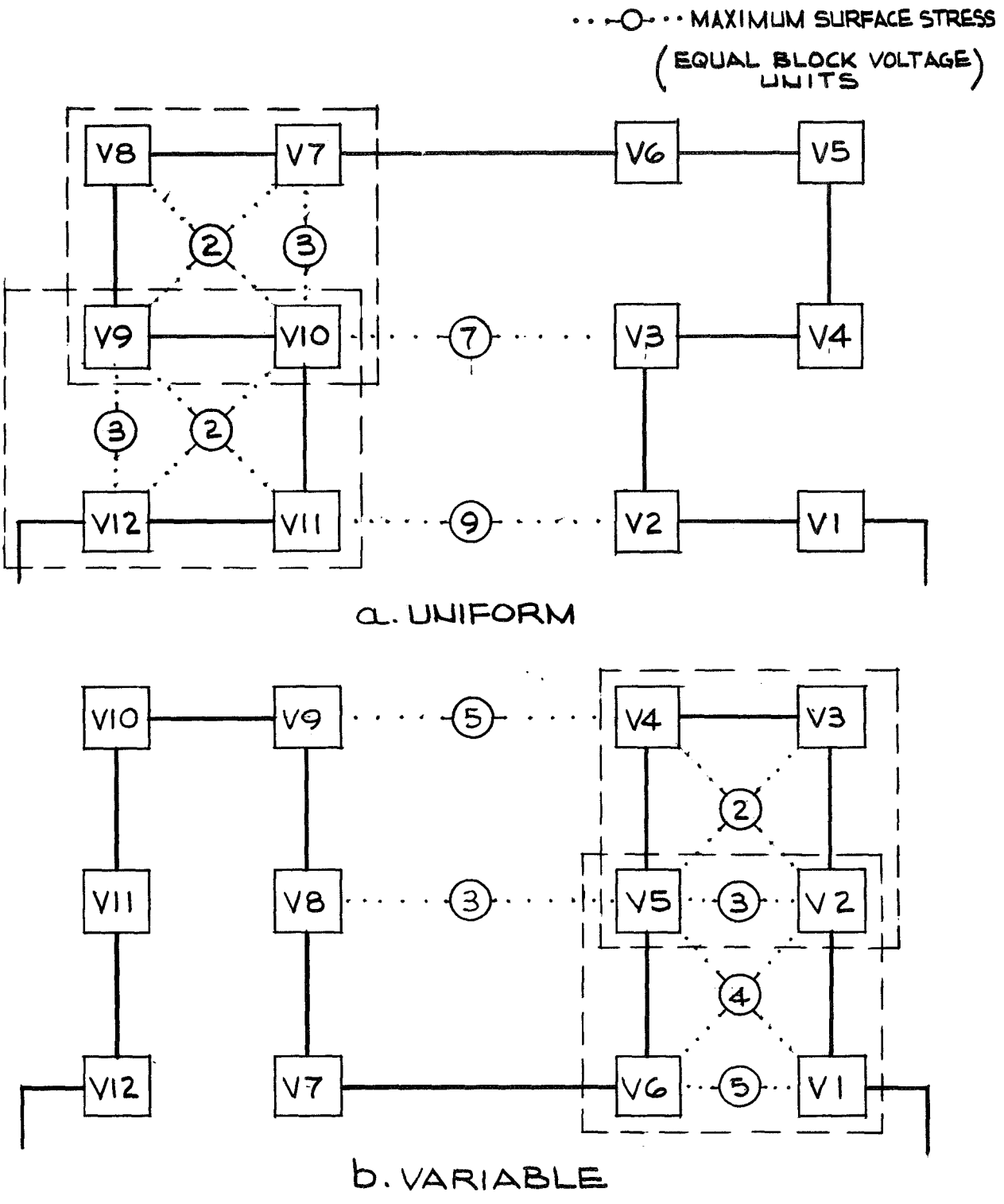

Fig. 36. Influence of voltage source locations on the surface gradients.

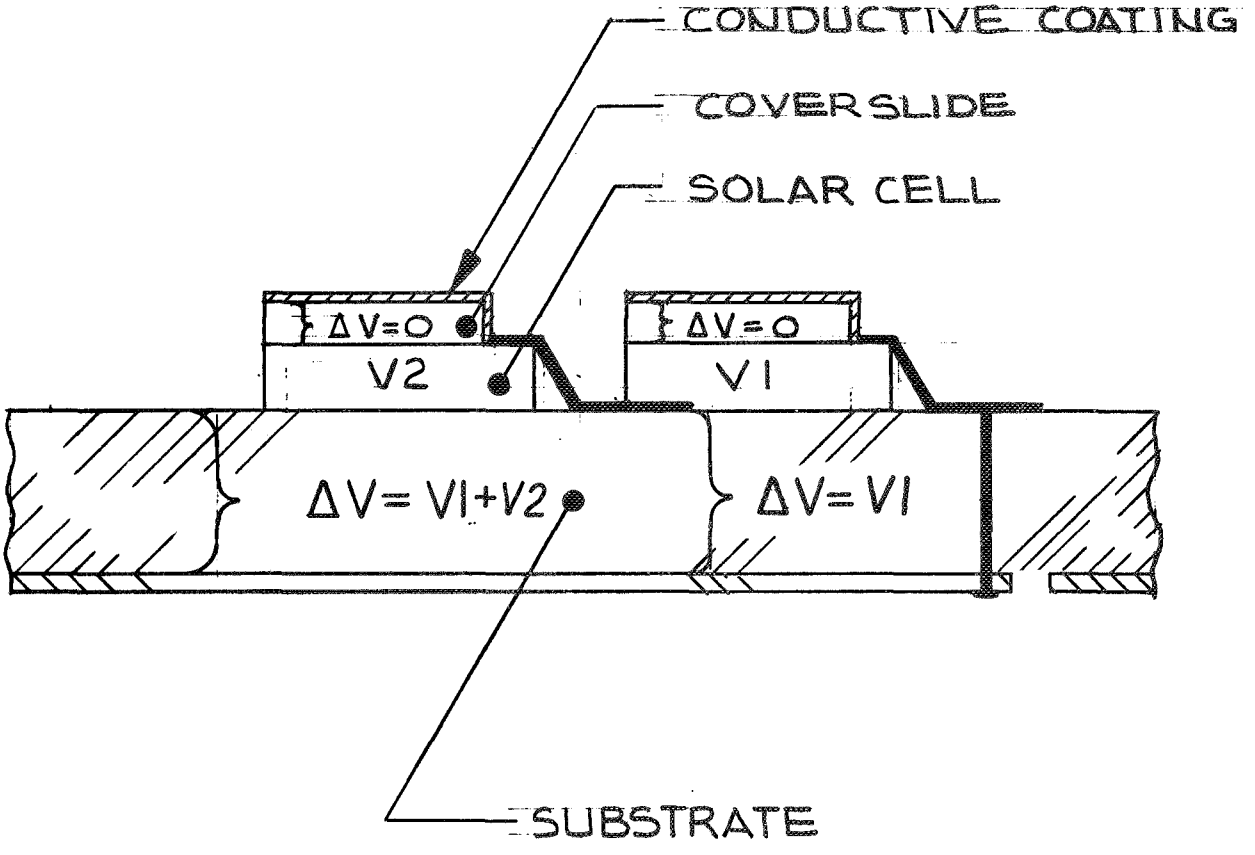

Fig. 37. Electric stress for biased dielectrics.

the substrate, plasma ions can be collected at high energies and, therefore, attention must be given to the effects of sputtering. It will be seen later that films must have thicknesses on the order of 1 μm in order to not be completely eroded during an orbit raising mission. As discussed in Section III, alternate regions of conducting and insulating material which are exposed to the space plasma (the case for exposed tabs and an insulating cover slide) give reduced plasma current collection compared with a completely conductive surface. Therefore, it can be expected that a conductive film will result in an increase in the power losses of an array. In addition, the radiant emissivity of the film may be such as not to degrade the thermal properties of the array.

Films used with nontransparent insulating layers can be composed of any material which will satisfy the above requirements. However, films employed with transparent layers also must be transparent and must not suffer discoloration or transmission losses as a result of exposure. The following transparent conductive films have been investigated.

- Thin metallic films such as aluminum. These films are not expected to suffer radiation damage; however, films which are thick enough to have significant electrical conductivity have transmission losses greater than 20%. In addition, the small required thickness ($\sim$ 50 Å) makes them susceptible to sputtering damage.

- Semiconducting films such as SnO_2. These films have high transmission (> 90%) and good conductivity, and are thick enough ($\sim$ 1 μm) that sputtering would not be a problem. However, it is expected that exposure to the space radiation environment will result in a decrease in transmission with time. Experimentation is required to determine the importance of this effect.

- Coating No. 343, Sierracin Corporation, Sylmar, California. This coating has metallic conduction properties although it is not a metal (the composition is company proprietary). The transmission is greater than 80%. The properties of this film with respect to radiation damage are unknown and experimentation is required.

(b) Conductive insulators: The use of conductive insulators results in a reduction of electrical stresses by providing a current leakage path between the substrate and the exposed surfaces of the insulating layer. In order to provide a 50% decrease in the electric fields in the bulk of an insulating layer 0.015 cm (0.006 in.) thick when the substrate potential is 8 kV, the resistivity of the insulating material must be 3×10^{15} Ω-cm at an altitude of 300 km (assuming zero sheath thickness and an incident current density equal to j_{esat}). Impurities must be added to the insulating material in order to achieve such resistivities. Because the associated conduction process is ionic (i.e., current is carried by impurity ions)

the resistivity will increase with time as current passes through the material and the properties of the material may change as ions are collected at the electrodes. In addition, the optical transmission of transparent insulating layers may decrease in time due to color center formation associated with the presence of impurities. Therefore, this method of reducing electrical stresses does not appear to be attractive; however, experimentation would be required to determine the characteristics of various materials for a particular application.

(c) Dielectric shielding: The possibility of using a dielectric shield has been studied as a possible means of reducing electrical stresses in insulating layers. In this approach either the insulating layers of the array are separated from their substrate by a small distance or a dielectric sheet is placed around the array with a vacuum space in between. Because vacuum is a good dielectric, it is possible that electric stresses could be distributed between the vacuum and the insulating layers, therefore reducing the stresses in the latter over that encountered with no vacuum space. However, charged particle penetration of thin insulating films, photoemission, and secondary emission processes can result in current passage across the vacuum space. This eventually will cause most of the electric stresses to reappear in the insulating layers (unless they are more "conductive" than the vacuum space). In addition, this approach suffers many deficiencies due to the difficulty to deployment, outgassing problems (gas pressure may build up in the vacuum space unless openings are supplied in the surrounding dielectric shield), and optical deterioration. The above considerations indicate that this approach is not very attractive as a means of limiting electrical stresses.

(d) Self-neutralization: The motion of charges (which are released by secondary and photoemission processes) between insulating surfaces and surrounding conducting areas may provide an effective current leakage mode between insulator surfaces and their conductive substrates, as discussed earlier. This process has been investigated as a possibility for providing "self-neutralization" of insulator surface charge and a decrease in electrical stresses. However, as previously described (Section IV-A), this process does not provide leakage under all conditions and, therefore, it does not appear to be a good over-all method of limiting electrical stresses. It is possible that this approach could be used over small regions of parameter space, but this would depend on the specific application.

(e) Encapsulation: The encapsulation of exposed conductors is the final method presented for the control of breakdown, and is shown in Fig. 38. An advantage of encapsulation would be the closer allowable spacing of conductors. However, this is offset by the possibility of electrical discharge resulting, for example, from the existence of voids in the encapsulant. Such discharging (pinhole arcs) could produce permanent and catastrophic failure. The trade-off in weight between encapsulating and nonencapsulating arrays is dependent upon the relative levels at which the surface and the encapsulants

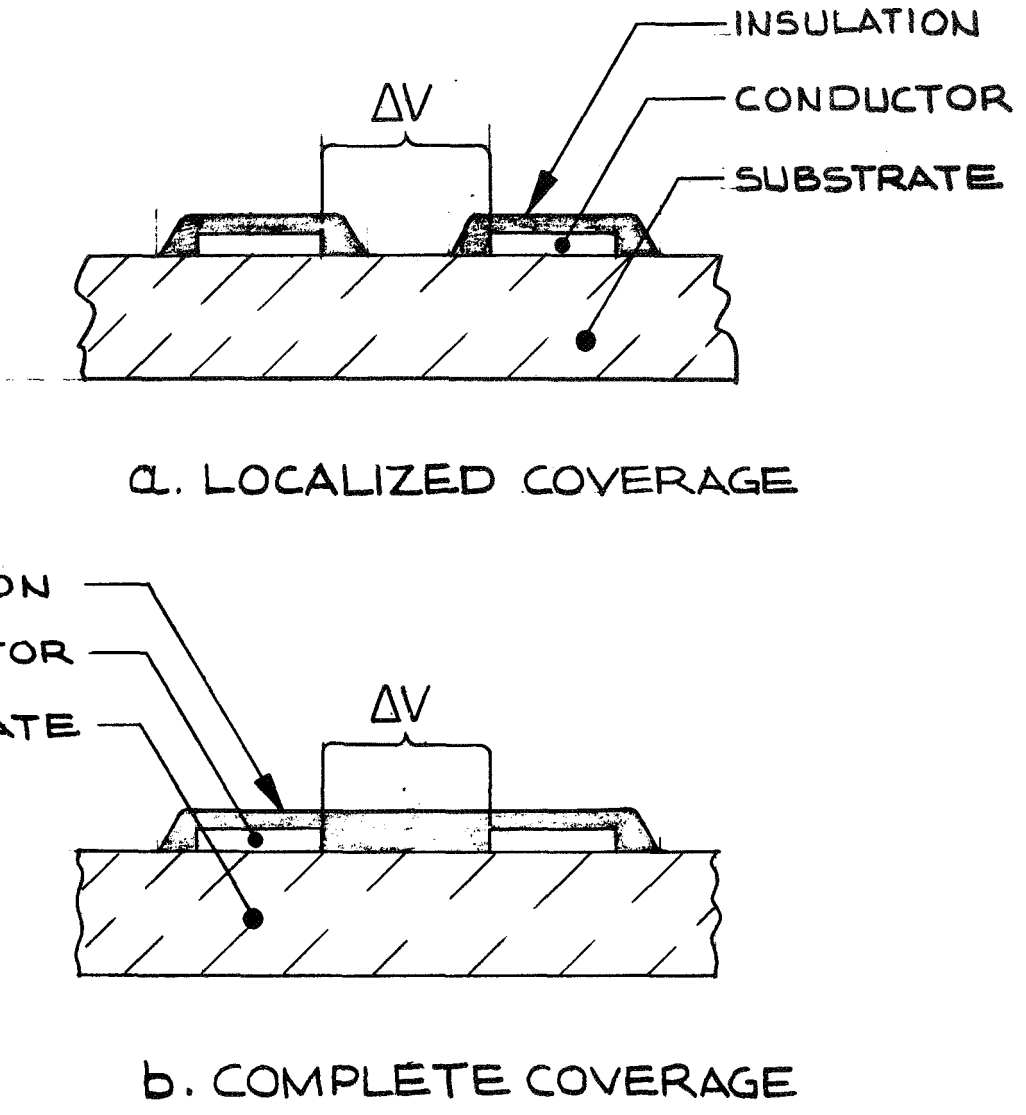

Fig. 38. Technique for insulating exposed busses.

can be stressed and the amount of encapsulant required. (One may expect a 1 to 3% array weight increase due to encapsulation.)

A combination of encapsulation and spacing (see Fig. 38 (a)) can be used, but there is still the chance of voids which can lead to breakdown. For this reason, the spacing between busses would have to be the same as for bare busses, but the weight would be greater.

Because the surface breakdown in space approaches the bulk breakdown, encapsulation is not likely to be necessary. It would probably be employed only as a technique to control plasma losses.

Conclusion: It is seen from the above discussion that conductive surface films offer the best possibility for limiting electric fields in insulators. However, experimentation is required, particularly in the case of transparent conductive films, to determine the efficacy of this approach.

b. Outgassing of Materials

Array materials which outgas or vaporize at a high rate give rise to the possibility of Paschen breakdown. Breakdown can occur when the mean free path λ of the gas is comparable to or smaller than the distance between array elements which exist at different potentials. The largest distances are the most critical, since they can lead to breakdown at the longest mean free paths and, thus, at the lowest pressures. On an array, the largest applicable distance is the span ℓ. For the purpose of estimating the maximum tolerable rate of outgassing, we take λ to be equal to ℓ. Under equilibrium conditions, which will be assumed to exist, the mean free path λ and outgassing rate μ are related via the vapor pressure p (see, for example, Ref. 26) as follows:

$$\lambda = \frac{kT}{\sqrt{2}\ \pi d^2 p} \tag{8}$$

$$\mu = \left(\frac{m}{2\pi kT}\right)^{1/2} p \tag{9}$$

where k is the Boltzmann constant, T is the gas temperature, m is the mass, and d is the diameter of a gas molecule.

Combination of (8) and (9) yields

$$\mu = \frac{1}{2\pi}\left(\frac{mkT}{\pi}\right)^{1/2} \frac{1}{\lambda d^2} \tag{10}$$

With T = 400°K, m = 1.62×10^{-22} g (equivalent to a molecular weight of 100), d = 10^{-7} cm, and $\lambda = 10^{3}$ cm, one obtains a maximum tolerable outgassing rate of 2.6×10^{-8} g/cm^2 sec or 8.3×10^{-5} g/cm^2 hour. Figure 39 compares this limit with empirically observed outgassing rates for RTV and Kapton. It can be seen that with RTV only the first few hours are critical, while with Kapton, there is absolutely no danger of breakdown.

c. Temperature

Temperature affects the performance of a high voltage array, in part, through its influence on the properties of dielectrics. All dielectrics show a decreasing dielectric strength and electrical resistivity and an increasing deterioration rate with increasing temperature. However, the magnitude of these effects varies greatly from material to material. The importance of the change in breakdown potential can be reduced if the material properties chosen for design are based upon the maximum operating temperature. The major concern involving changes in resistivity is that a primary dielectric (i.e., the material intended to support the most stress) will not become secondary, thereby placing the major stress across another material when the temperature shifts. The effects of this redistribution of stress may be minimized by using materials whose properties are essentially independent of temperature over the operating range of the array. Degradation of a dielectric due to electrical discharge will be accelerated by increased temperature because of the increased thermal energy in the material. Therefore, the maximum expected temperature must be employed in array design for reliability studies and determination of dielectric requirements.

Secondary temperature effects which could influence the high voltage array include the introduction of differential strains in the array materials and variations in outgassing rates. Differential strains are important only if they lead to separations and voids which act as sites for electrical discharge. Such occurrences have not been demonstrated in practice. However, strains causing open circuits are possible and should be studied for large array applications. The effects of outgassing rates have already been discussed. It is sufficient to state that these rates increase rapidly with temperature.

d. Radiation

Radiation effects on dielectrics in the presence of large electric fields are not well defined by experimental studies. This lack of information includes both primary effects on electrical discharge and breakdown characteristics and secondary effects such as changes in mechanical, thermal, and optical properties.

Most radiation studies to date have been limited to low and moderate energy x-rays which do not produce detectable changes in the breakdown potential for low loss materials such as Teflon TFE (Ref. 27). It has been determined, however, that both particulate and wave radiation, such as will be experienced in space, can produce electron-hole pairs, excited states, and ionization in dielectrics which can lead to both temporary and permanent alteration of material properties. For example, experiments have demonstrated

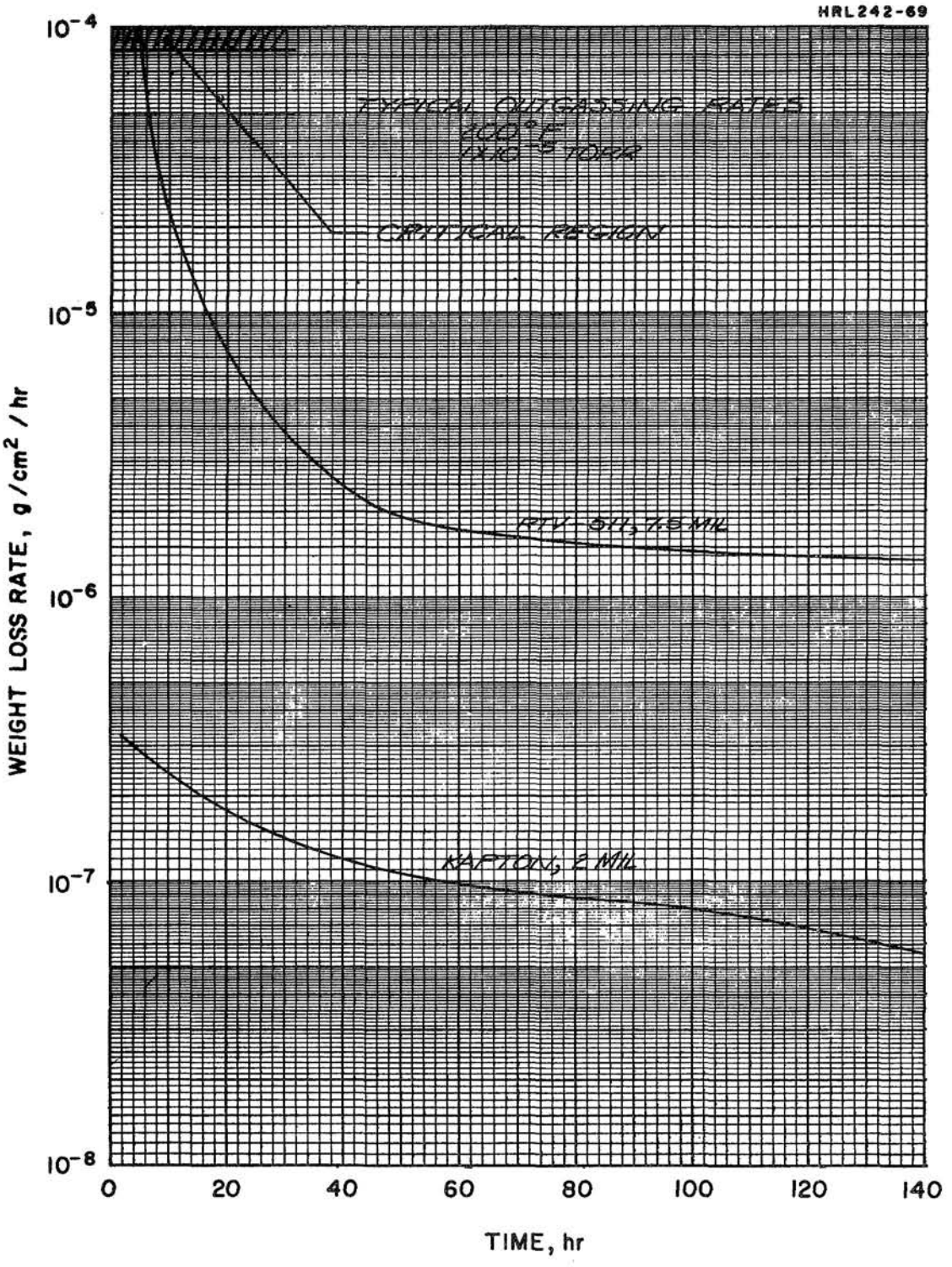

Fig. 39. Typical outgassing rates (200°F, 1 x 10^{-5} Torr).

a factor of ten to a hundred increase in electrical conductivity in some dielectrics due to proton and electron radiation. It must be emphasized, however, that radiation studies have not yet been performed in the presence of large electric fields. Such fields, which could significantly alter the results of any radiation studies, must be included in future experiments.

It is not known whether radiation-induced conductivity in dielectrics is a result of thermal breakdown, electrical discharge, or BIC (see Section III); however, studies indicate that the increased conductivity is temporary and depends only upon the decay rate of the activated condition after removal of the radiation source. Such a temporary effect would be most significant in the denser regions of the radiation belts or during bursts of energy such as from a solar flare, and should be considered in establishing test conditions for radiation effect studies.

The permanent effects of radiation on dielectric materials are well known and documented with less emphasis on electrical changes than mechanical. These permanent effects are cumulative; however, it should be noted that while most materials show continued degradation, certain materials degrade and then begin to improve in some properties. Kapton, a polyamide, demonstrates this characteristic with respect to dielectric strength. Under continuous radiation, Kapton's dielectric strength decreases to approximately 6000 V/mil at 10^6 rad and increases to 6710 V/mil when the dosage reaches 10^8 rad. If such minima occur for a given dielectric during the projected array life, they must be employed for design purposes.

An attempt to establish dielectric requirements with regard to radiation effects results in the following recommendations:

- Select materials that exhibit minimum radiation damage, considering types, intensities, and total dosage.
- Allow liberal design margins for unknown effects, such as changes in electrical discharge inception voltages.
- Define further studies to investigate areas of uncertainty critical to the successful operation of a high voltage solar array.

Conclusions: Properties considered important in the selection of suitable array materials are:

- Dielectric strength
- Volume resistivity
- Dielectric matching characteristics

- Effects of surface and bulk breakdown
- Temperature dependence
- Radiation effects
- Outgassing characteristics
- Ease of application.

The materials selected on the basis of these properties are grouped below in terms of the array element for which they are considered. Electrical, physical, and radiation resistance properties are summarized in Tables II, III, and IV, respectively.

(1) Substrate- Materials considered:

- Kapton, an aromatic polyamide
- Mylar, a polyester
- Nomex, an aromatic polyamide
- Teflon, (polytetrafluorethylene).

Kapton is chosen because of its high dielectric strength and high volume and surface resistivities. It also exhibits lack of temperature dependence over the array operating temperature range (-200°C to + 100°C), and a generally superior radiation resistance (initial physical damage inception level 10^8 rad). The major disadvantage of Kapton is that its absorptivity increases under ultraviolet radiation while its emissivity remains constant. This will result in increased temperature both within the dielectric and on the array.

Although Mylar exhibits electrical and physical properties comparable to those of Kapton at room temperature, dielectric characteristics show a marked temperature dependence. It is also considerably less radiation resistant than Kapton.

Nomex, a calendered paper, has a lower dielectric strength than either Kapton or Mylar. It is known to contain gas inclusions which would be detrimental to its use as a space dielectric.

The limitations of Teflon are poor radiation resistance, tendency to cold flow, and the requirement of extensive and critical surface treatment in preparation for bonding to other materials.

(2) Adhesives - Materials considered:

- RTV 655 Methyl-Phenyl Silicone (cell-substrate)
- RTV 602 or R-63-489 Dimenthyl silicone (cell-cover slide)

TABLE II

Electrical Properties of Selected Dielectric Materials

	Electrical Breakdown Characteristics				Electrical Resistance		Dielectric Constant
	Dielectric Strength, V/mil	Thickness, mils	Frequency, Hz	Arc Resistance, sec	Volume Resist., Ω-cm	Surface Resist., Ω/square	
Kapton	7,000	1	60	180	10^{18}	10^{16}	3.5
	3,600	5	60				
Teflon (TFE)	3,000	1	60	360	10^{18}	10^{13}	2.1 - 2.3
	900	100-250	60				
Nomex	900	2	D. C.	130	10^{16}		2.0 - 2.6
Mylar	7,000	1	60	10	10^{18}	10^{16}	3.25
XR63489	2,000	5	60		10^{15}	10^{13}	2.88
RTV602	2,500	10	D. C.		10^{15}	10^{12}	3.0
RTV577	1,500	10	D. C.	300	10^{15}	10^{12}	4.1
RTV511	1,500	10	D. C.	300	10^{15}	10^{12}	4.1
RTV655	2,500	10	D. C.		10^{15}	10^{12}	3.0
Epoxy-Polyamine	3,000	5	D. C.	120	10^{13}	10^{11}	3.5 - 5.0
Epoxy-Polyamide	2,000	5	D. C.	120	10^{13}	10^{11}	4.0
Glass (Quartz)	5,000	4		High	10^{19}	10^{19}	3.78
	5,000	8					
Parylene "N"	6,500	1	D. C.		10^{17}	10^{15}	2.6
Parylene "C"	3,700	1	D. C.		10^{17}	10^{16}	3.0

TABLE III

Physical Properties of Selected Dielectric Materials

Material	Density, g/cm^3	Modulus of Elasticity (psi x 10^{-5})	Transition Temperature, °C	Outgassing Characteristics	
				Gas Load (% of total weight)	Rate Avg. ($g/cm^2/hr$ -90°C)
Kapton	1.42	4.3	227	1.0	1.0-3.0 x 10^{-7}
Teflon (TFE)	2.1-2.3	5.8	164	0.1	
Nomex	2.15	2.0	77	1.5	
Mylar	1.40	5.5	Glass 75 Trans130	0.4	
XR 63489	1.08		-120	2.0	1.05-5.0 x 10^{-6}
RTV602	.99		-60	2.0	1.0-5.0 x 10^{-6}
RTV577	1.35		-130	2.0	1.0-5.0 x 10^{-6}
RTV511	1.18		-130	2.0	1.0-5.0 x 10^{-6}
RTV655	1.07		-130	2.0	1.0-5.0 x 10^{-6}
Epoxy-Polyamine	1.0	4.0-6.0	Approx 0	1.0	10^{-7} - 10^{-6}
Epoxy-Polyamide	1.1	4.0-6.0	Approx 0	1.01	10-7 - 10^{-6}
Glass (Quartz)	2.2	---		0	0
Parylene "N"	1.12	3.5	60-75		
Parylene "C"	1.29	4.0	80-100		

TABLE IV

Radiation Damage Levels (Refs. 2 and 17)
(Where no damage is shown no data are available)

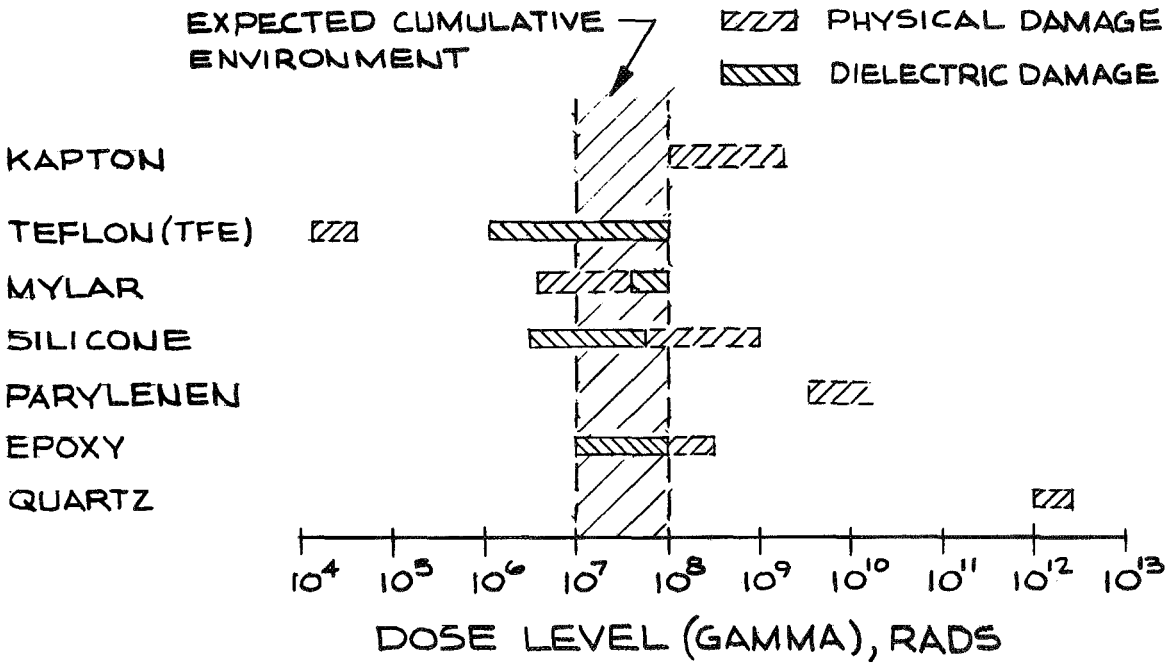

- RTV 511, Methyl-Phenyl Silicone, filled
- RTV 577, Methyl-Phenyl Silicone, filled
- flexible epoxy-polyamine
- flexible epoxy-polyamide

A methyl-phenyl silicone was chosen as the cell-substrate adhesive. It was selected because of the requirements for flexibility and operation over wide temperature excursions. Methyl-phenyls exhibit low transition temperatures and high elongation, which reduce stress within joints and the probability of separations. In addition, these materials show only a slight dependence of volume resistivity upon temperature. Volume resistivity changes by only a factor of 10^2 over the projected temperature range of the array. The dielectric strengths of methyl-phenyls are good, ranging from 1500 to 2500 V/mil. The selected methyl-phenyl, RTV-655, is chosen because it is a clear transparent substance which permits backside inspection for voids and improved array thermal control through backside emission.

The major limitation of both polyamine and polyamide epoxies is their rather severe temperature dependence. Both epoxies can be expected to exhibit a factor of 10^6 to 10^8 resistivity change over the array operating temperatures.

The selection of RTV 602 or R63489 as the cell-cover slide adhesive is based upon the successful use of this material for cover slide attachment. Its properties are also suitable for high voltage design.

(3) Encapsulants - Materials considered:

- RTV 655, Methyl-phenyl silicone
- Parylene C, poly (chloropara-xylylene)
- Parylene N, poly (para-xylylene)

The selected candidate for encapsulating or coating the array for surface discharge protection is RTV 655. Its superior qualities, as described above, apply also to encapsulation.

The Parylenes are a new class of coatings formed by a vapor phase polymerization under vacuum conditions. In the industry, it is felt that they cannot be recommended as a practical solution for coatings on localized areas. The nature of the deposition process is such that all exposed surfaces become coated with a continuous film. This results in a requirement for considerable masking and film cutting to achieve a localized coating. If a complete and uniform coverage of the complete array or large areas of the array, including cells, was determined necessary and feasible, parylene would become a prime candidate. Under such conditions the type N polymer would be preferred. It has a higher dielectric strength and electrical

resistivity, and exhibits less temperature dependence. However, if solar cell cover slides were to be coated, it should be stated that type C has the superior optical transmission properties. However, the undegraded optical transmission is still poor for solar cell applications, and its change due to particulate radiation is unknown. The physical properties of the two parylenes are comparable. Experience with the parylene process makes it, at best, a second choice to RTV 655.

The epoxy polyamines were not considered for encapsulation purposes. The reasons for avoiding them in high voltage applications were stated earlier.

(4) Cover Slides- Material considered: Fused Silica.

A review of the dielectric and optical properties of fused silica resulted in its choice as the cover slide material. The possible problems resulting from surface electrical discharge effects on the optical properties of quartz are unknown; this area should be subjected to future study. Figure 40 presents the dielectric breakdown voltage of fused silica as a function of the thickness. It is seen that a 6 mil thick cover slide, for example, can easily withstand the expected electrical stresses associated with a high voltage solar array.

(5) Busses - Materials considered:

- Copper ribbon
- Aluminum ribbon
- Copper wire, round
- Aluminum wire, round.

Ribbon copper was chosen as the bus material on the basis of the ability to readily form reliable interconnections, availability of variable dimensions for given cross-sectional area, smaller associated electric fields than for circular geometry, and the need for flexibility.

(6) New Materials and Processes - Based upon the proposed configurations and the problems previously described for a high voltage array, it may become necessary to reconsider and add to the selection of materials as follows:

- Conductive or semiconductive coatings for both cover slides and substrate capable of dissipating surface charge (see earlier discussion).
- Conductive or semiconductive adhesives for cell-substrate attachment, such that there is effectively no electrical stress within the adhesive.
- Metallization and photochemical etching techniques for producing conductive films or grids on the array.

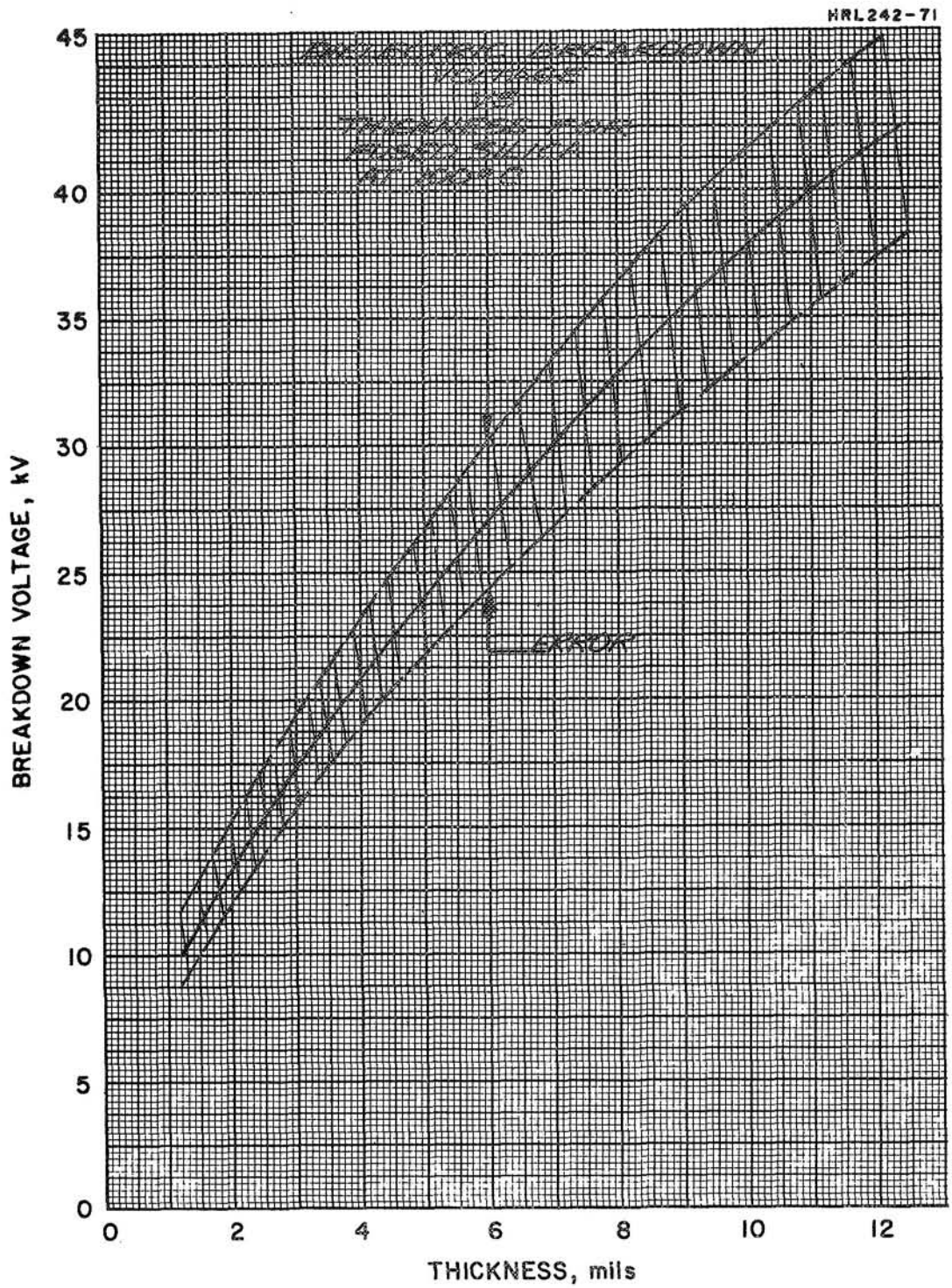

Fig. 40. Dielectric breakdown voltage as a function of thickness for fused silica at 100°C.

It must be emphasized that the necessity for developing these or other materials is related to further experimentation on the baseline dielectric configuration, which is discussed next.

4. Array Configuration

The general aspects of the array configuration are discussed in this subsection. Consideration is given to flexible versus foldout designs, array and panel configurations, cell layout, the location of busses, conductor spacing, and finally, alternative dielectric configurations.

A high voltage solar array can be developed that is either flexible or foldout. The advantages and limitations of these two possibilities are presented in Table V in terms of general design requirements. The results of this comparison indicate that a flexible array is superior to a foldout array in the case of high voltage applications.

Possible array configurations are shown in Fig. 41. Two types of rollout and one type of a foldout array are illustrated. Based on mission requirements, the size of each panel would be 21 by 120 ft for the two-panel configuration and 15 by 85 ft for the four-panel array. The panels in the four-panel arrangement are shown separated from the spacecraft to prevent ion-engine exhaust impingement on the panel during orbit raising.

Three basic configurations for a given panel of the four-panel rollup array are shown in Fig. 42. Each assumes a basic cell block that will deliver 0.94 A at 1 kV at end of life. Many other arrangements are possible. The type 3 configuration is the simplest from a design and fabrication point of view. Types 1 and 2 allow varied distribution of potential gradients over the panel. Such variations were considered from the possibility of minimizing plasma effects as discussed in Section II.

Longitudinal and transverse series cell layouts are shown in Fig. 43. The directions are relative to the drum for a rollup array. In terms of cell cracking and optimum reliability, the transverse layout is preferred.

Methods of locating the buses on both the front and back of the array are shown in Fig. 44. Placing buses on the back of the array and beneath the solar cells would impose severe insulation requirements for the array because of the high electric fields in the substrate. Electrical breakdown in this case also would result in shorting between active elements and could result in array failure. The primary advantage in backside location is a reduction in array size. Eliminating all buses from the backside would require positioning of buses outboard of the cells; however, with the buses located on the front of the array, breakdown between active elements could occur only as a result of surface mechanisms. Such an approach allows a larger safety margin in dielectric design because of the smaller electrical stresses, and thereby reduces insulation requirements. The frontside location of buses is preferred.

TABLE V

A Comparison Of Flexible and Foldout Array Configurations

	Advantages	Limitations
Flexible	Minimum substrate thickness based primarily on dielectric requirements Buses located on substrate Visual inspection of critical areas such as adhesive bonds Simplified plasma screen deployment mechanism	Control electronics either mounted on deployment mechanisms or requiring special techniques to mount on array
Foldout	Control electronics mounted in substrate or frame	Increased substrate thickness(typically) Possible Paschen breakdown for foam or honeycomb in substrates Bus location on frame requiring increased insulation, or special jumper techniques to interconnect frames if mounted on substrates Limited visual inspection of critical areas Complicated plasma screen deployment techniques

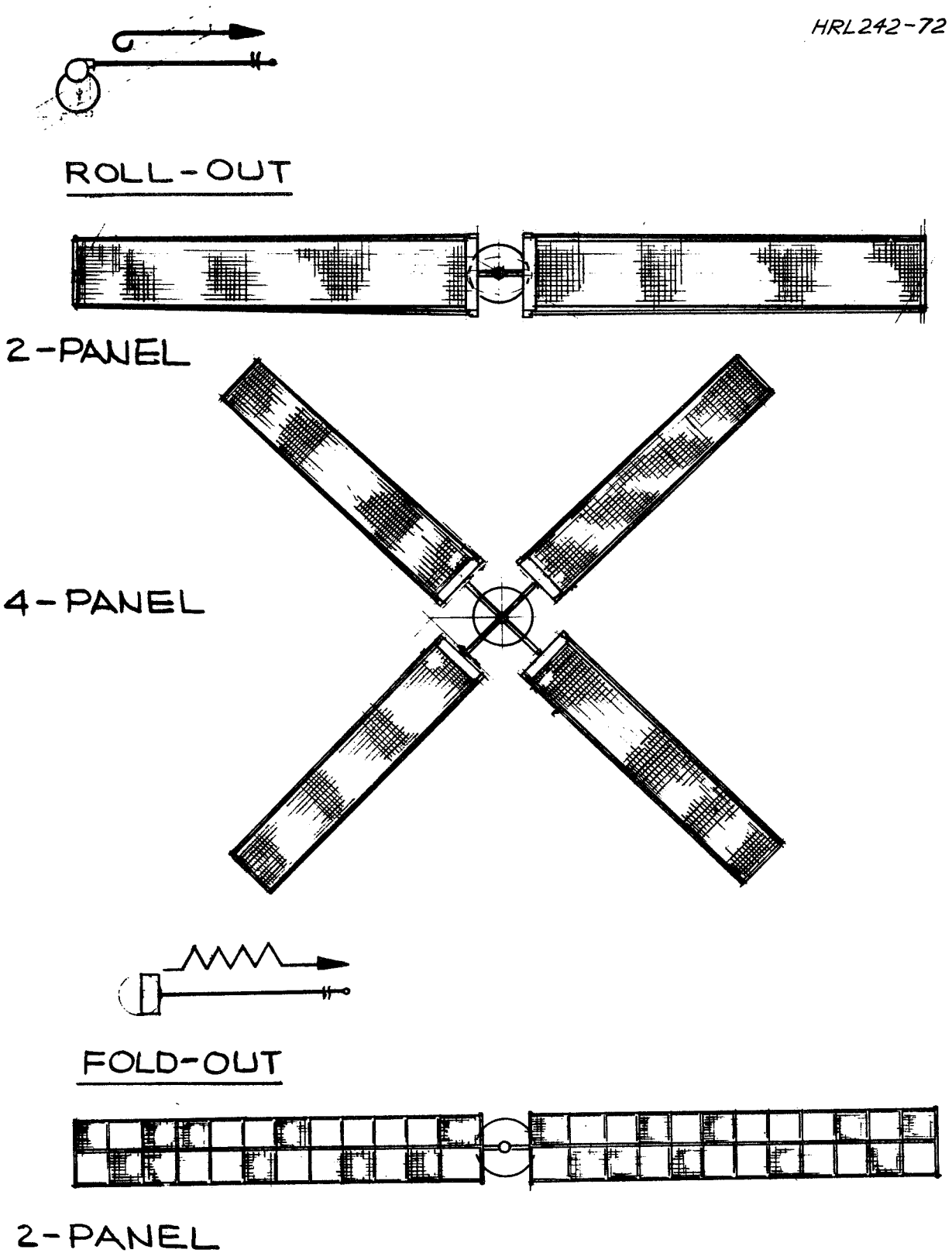

Fig. 41. Typical solar array configurations.

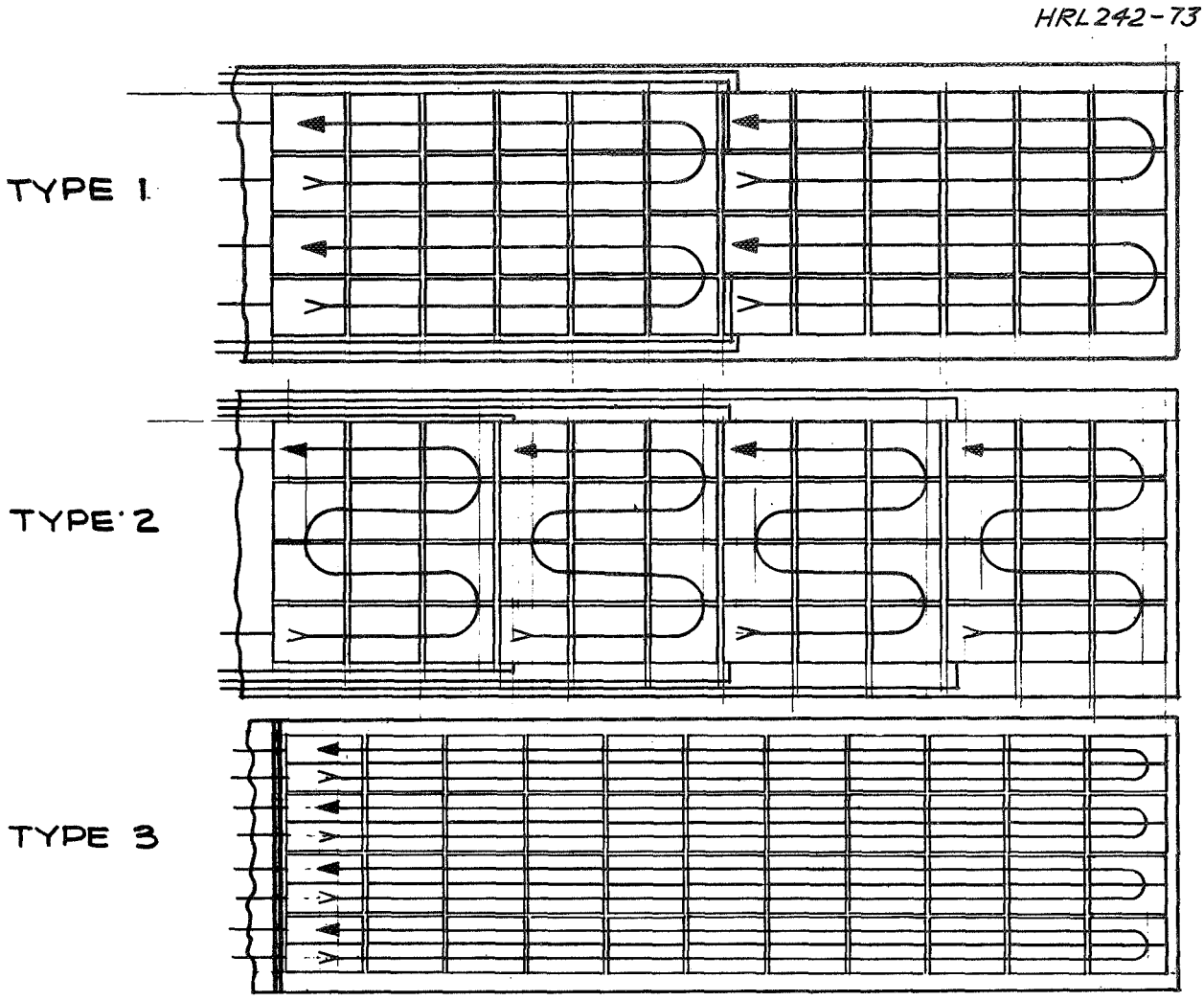

Fig. 42. Typical solar panel layout concepts. Assume basic cell blocks deliver 0.94 A at 1 kV at end of life (smaller blocks can be used with minor changes).

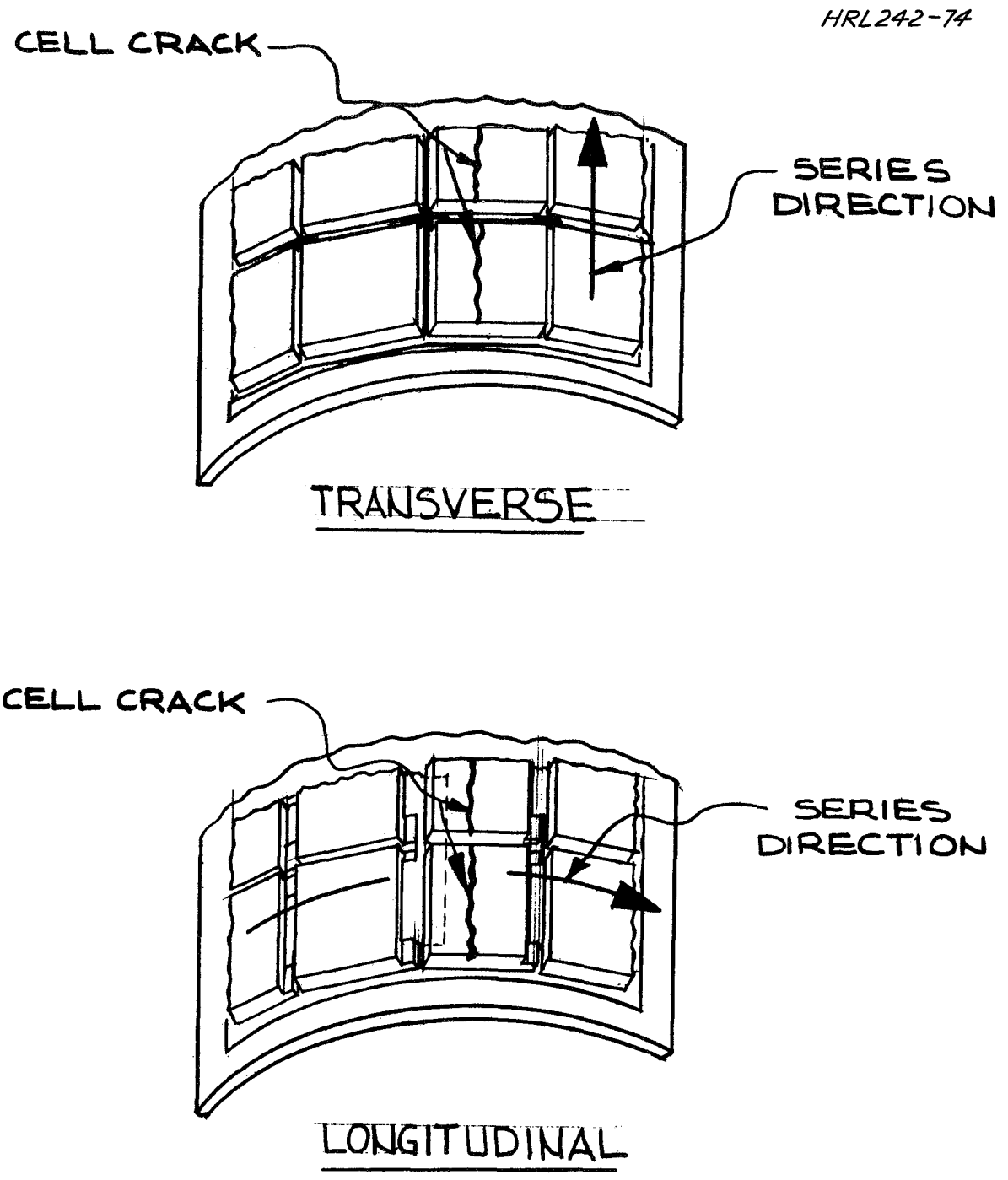

Fig. 43. Expected open cell failures as a function of series orientation.

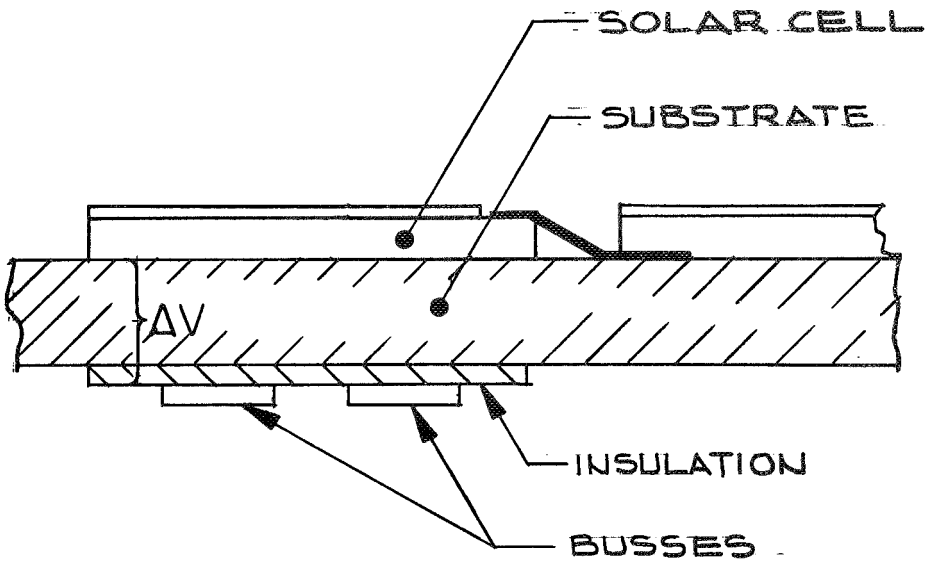

a. BACKSIDE POSITIONING

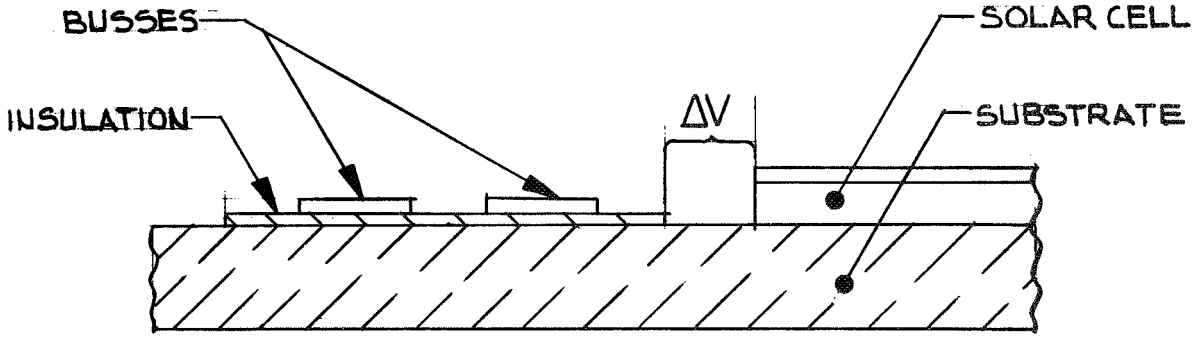

b. FRONTSIDE POSITIONING

Fig. 44. Location of buses on the high voltage array.

The mechanisms of surface breakdown and the control of voltage gradients which have been discussed previously lead to the establishment of permissible stress values for design spacing purposes. The proposed level is 50 to 100 V/mil in the spacing of conductors. These values are less than one-tenth of the measured breakdown levels in vacuum, and thereby permit the design of an array with high dielectric reliability. Two other factors are important in establishing these limits: (1) atmospheric testing must be permissible and (2) the critical spacing of conductors in fabrication must be minimized.

Three detailed dielectric configurations for a high voltage array are presented in Fig. 45. Each employs a flexible dielectric film substrate and adhesives for bonding cells and cover slides. Fiberglass cloth, which is used between cells and substrate in certain low voltage arrays, has been eliminated because it is a major source of voids.

Configuration A of Fig. 45 forms the baseline design. It utilizes only the substrate and the adhesive for the control of stresses through the dielectric. If it becomes necessary to reduce electrical stresses in the substrate, configuration A may be modified by the addition of a conductive film on the backside of the substrate.

Configuration B employs a method for eliminating electrical stresses with the adhesive. Such stresses could lead to failures in the adhesive which might propagate into the substrate, causing the latter to fail. The stresses are eliminated by the use of the conductive adhesive and a conductive film on the frontside substrate surface. This configuration eliminates the danger inherent in interfacial separations between the substrate and adhesive, which could result in a site for discharge.

Configuration C involves the minimum electrical stress through all dielectric layers. Both the tops of the cover slides and the bottom of the substrate are biased by means of conductive films. There will be no stress through the cover slide, and the maximum stress through the substrate is limited by the size of the biased conductive zones on the back of the array.

Although configuration A is the baseline design, configurations B and C are presented in lieu of experimental determination of the permissibility of failure through the dielectric between nonactive areas of the substrate. All three configurations assume that the conductor spacing criterion developed above is sufficient to support the electrical stresses; however, if subsequent breadboard tests disprove this assumption, encapsulation and/or the depressed current collector techniques could be adapted to these configurations.

5. Reliability

The two primary considerations with respect to the reliability of a high voltage solar array concern failures due to open circuit and short circuit conditions.

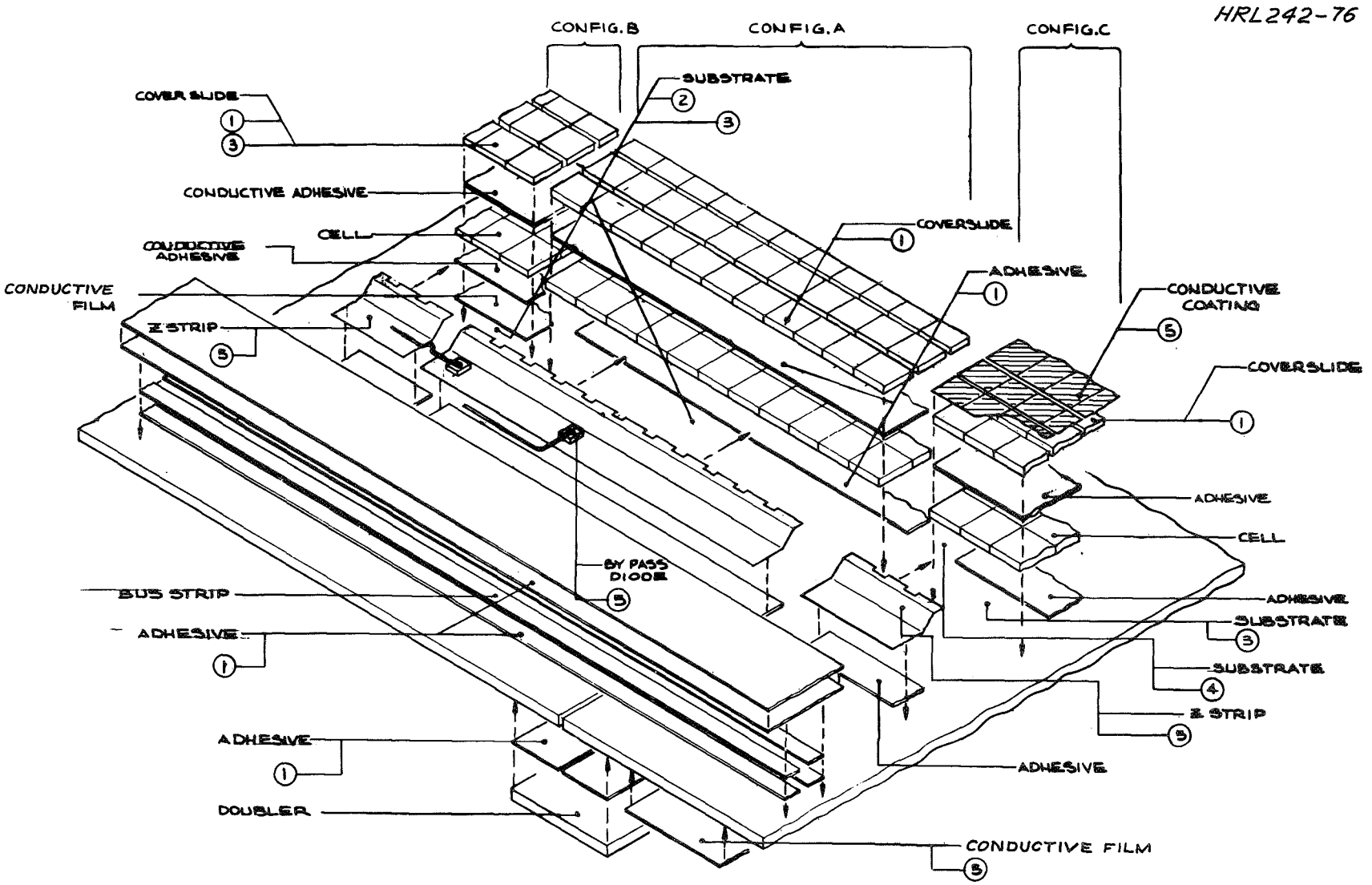

Fig. 45. Solar array dielectric problem areas.

a. Open Circuit Failures

Open circuit cell or wiring failures have a much greater degrading effect on high voltage solar array performance than is the case for low voltage arrays because the former requires a very large number of cells in series compared with the number in parallel. The larger number in series increases the probability of failure in a given cell string, and the smaller number in parallel reduces the capability of the array to compensate for failures by a shift of operating point on the I-V curve.

Figure 46 demonstrates this latter effect, which is critical for loads that are essentially constant current in nature. If a load were operating at the maximum power point for a row of seven parallel cells and one cell were to fail open, the I-V curve for the row would drop to six-sevenths of its original current level. If the load is not able to also shift downward then, instead of the row operating at its original +0.45 V, it will operate at -40 V, resulting in a considerable loss in power. This loss is not only intrinsically detrimental, it is also power which must be dissipated by the solar cells. The resultant heating of the cells and interconnections has been demonstrated to be potentially damaging.[30]

An effective means to solve this problem is to incorporate bypass diodes in parallel with the solar cell rows.(A typical diode available for this application is approximately 0.10 cm^2 and has a voltage drop of 1.1 V at 1A.) These diodes provide an alternative current path in the event that a failure occurs which results in back-biasing a portion of the array. The ratio of diodes to cell rows to be used depends on the cell failure rate, ratio of number of cells in series to number in parallel, and the acceptable degradation in total array performance.

The failure rate, which has been assumed for solar cells in a flexible array, is 3.0×10^{-8}/hr, or 0.001314 for a five year mission, which is four times that expected for a rigid array. This number can be considered accurate only within ± one order of magnitude due to a lack of adequate experience with this type of array in space; however, it can be used as an indication of the effect on performance of varying the number of cells in parallel and the number of diodes used.

Figure 47 shows the effect of varying the number of cells in a parallel row while holding the number of rows per diode (constituting a bypass module) to one. Here the failure rate increases with increasing numbers because,as the number of cells in a parallel row increases, the probability of failure also increases. This tendency of decreasing reliability with increasing parallel cells continues up to eight cells. Below this point, only one open circuit cell failure is necessary to back-bias the remaining parallel cells, but for eight or more in parallel, two cells must fail simultaneously in order to back-bias those remaining. The probability of the latter occurrence is, of course, much less, and this is reflected in the figure.

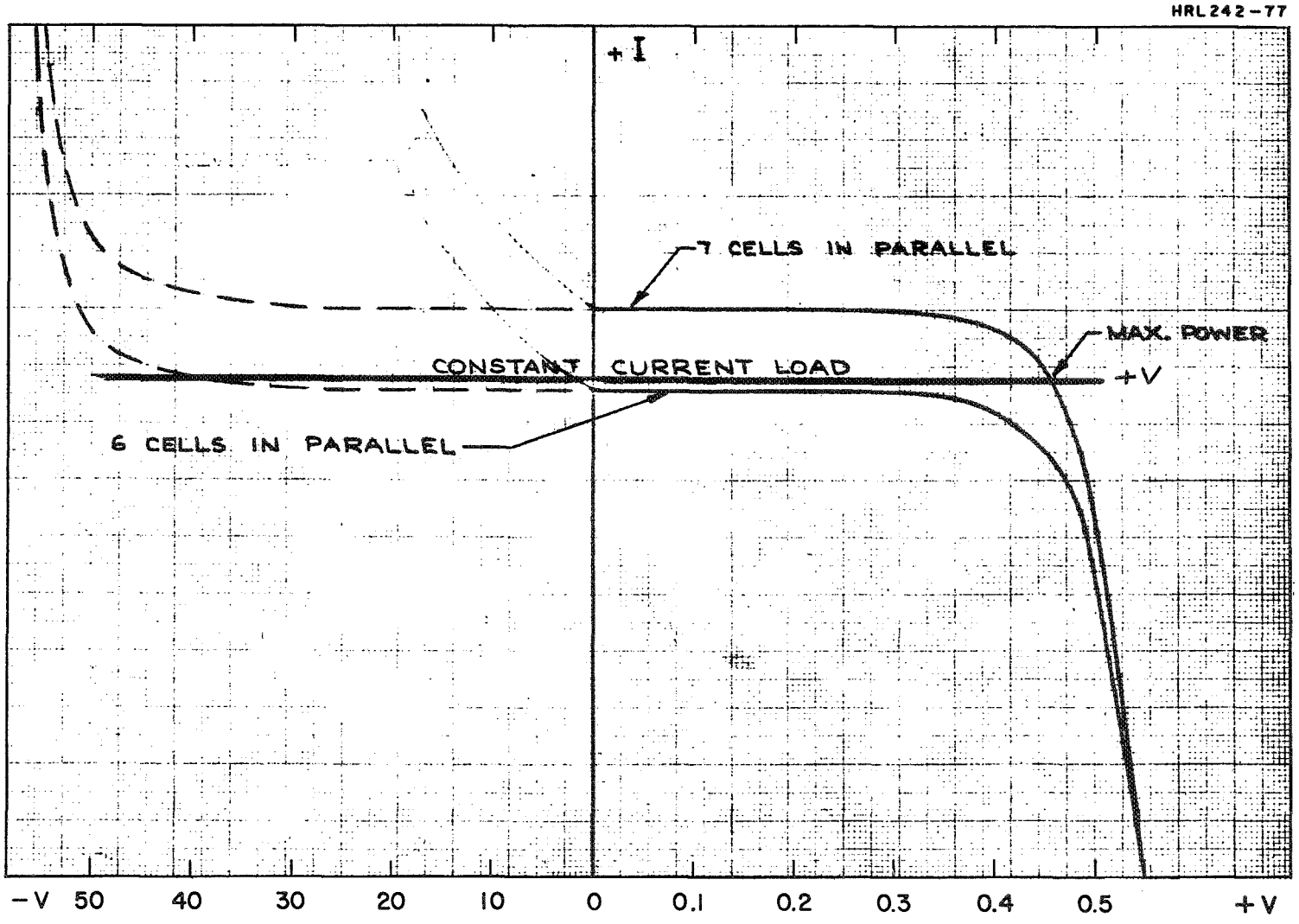

Fig. 46. Effect of open circuit cell failure — back-biasing of remaining cells in parallel.

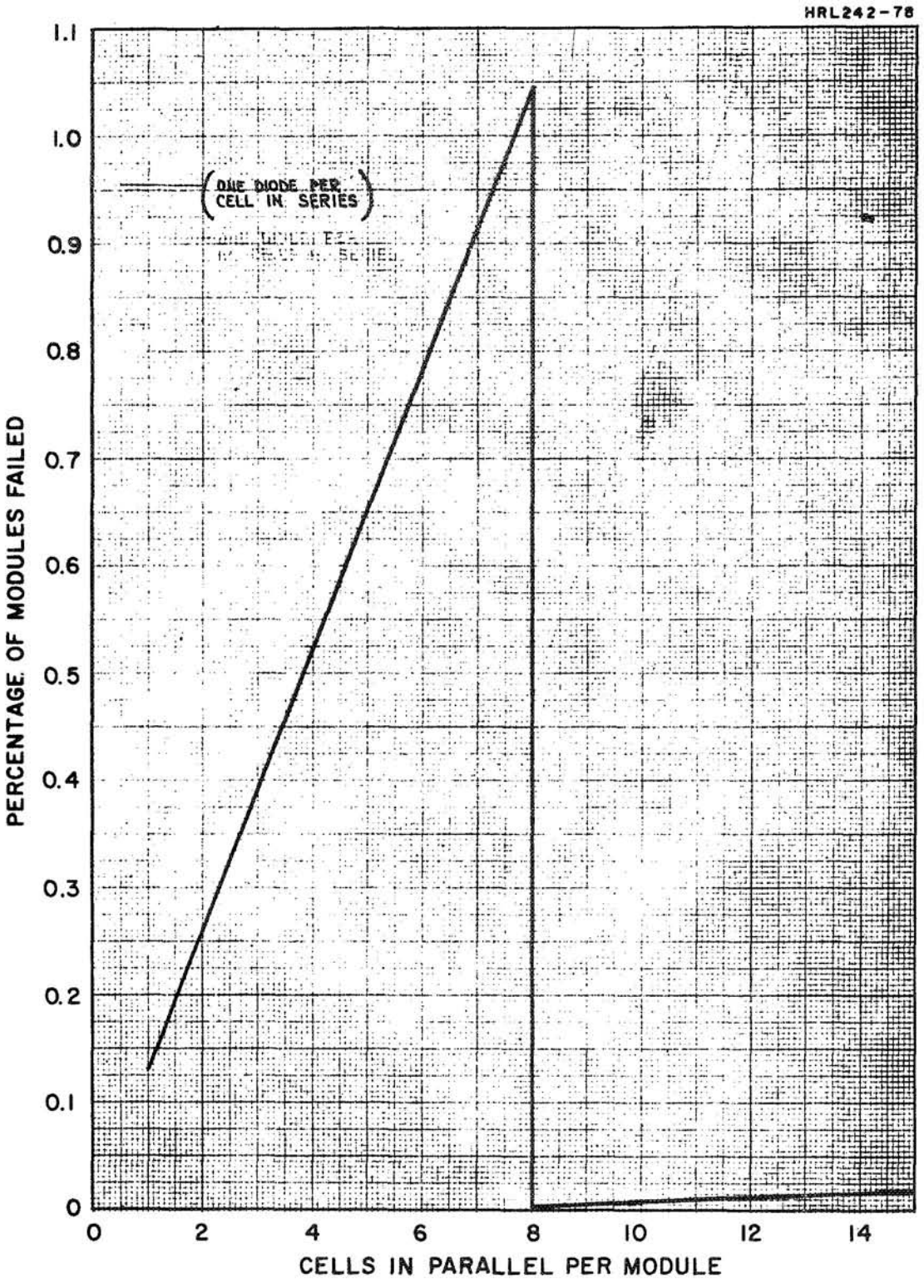

Fig. 47. Module failure (bypass) rate as a function of the number of cells in parallel (see Appendix J).

Figure 48 illustrates the anticipated failure rate as a function of the number of series cells bypassed per diode. As would be expected, the probability of a failure within a given module increases with the number of cell rows bypassed. The curves also are presented as a function of cells in parallel, showing the same trend as in Fig. 47.

For a configuration using the full 14 cells in parallel per row, the anticipated bypass module failure rate is shown in Fig. 49 (see Appendix I). If a decision were made to allow no more than a 1% failure rate, it can be seen that there could be no more than 65 rows in a module which were connected in parallel with a bypass diode. The selected configuration has 50 rows per module.

b. Short Circuit Failures

The risk of failures due to short circuiting is greatly reduced by utilizing a dielectric substrate. The pressence of high voltages, however, makes the danger sufficient to be of continued concern because any failure can be catastrophic. Aside from the use of insulation, other means may be utilized to offset this danger. Isolation devices can be placed between all blocks of cells and the main bus, and all panel wiring and buses should be configured so that there are no crossovers. Smaller blocks of cells (lower in current and/or voltage) also can be used which would result in better failure isolation and more circuit flexibility. However, because of the increased total length of boundaries across which shorting can take place, the risk of failure increases with the ability to isolate it. In addition, more switches and buses would be required and the system would be more complex. For these reasons, and because of the general nature of this study, only voltage blocks of 1 kV have been considered.

The device used for isolation in case of failure has two basic requirements: (1) the isolation must occur very quickly in order to quench any arcing which might further damage the array, (2) the isolation must be reliable enough to last for a full five year mission without allowing the arcing to resume.

6. Fabrication

As a part of the high voltage array study, problems associated with the fabrication process were isolated. Fabrication problems are defined as those which relate directly to the processing methods and only indirectly to the basic material properties. However, these problems affect the final product and can influence array performance. Problem areas, array effects, probable occurrence, allowable levels, and methods of problem elimination are summarized in Table VI.

It is expected that fabrication procedures will conform to conventional flexible array fabrication with emphasis on cleanliness, inspection (to isolate voids and separations) and safety as described in a following section. The final panels should be fabricated from segments of the substrate with cell groups attached, rather than

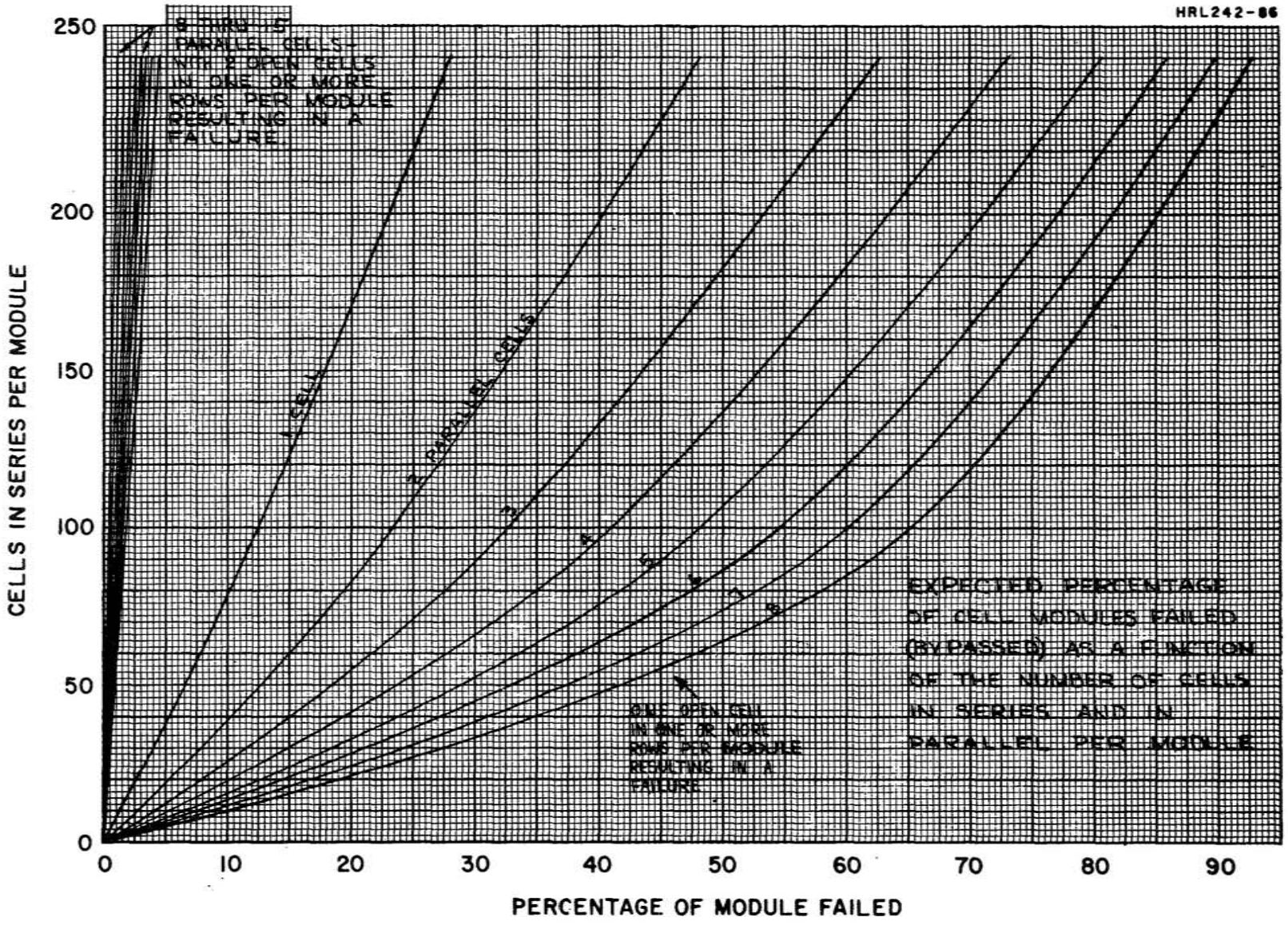

Fig. 48. Expected percentage of cell modules failed (bypassed) as a function of the number of cells in series and in parallel per module.

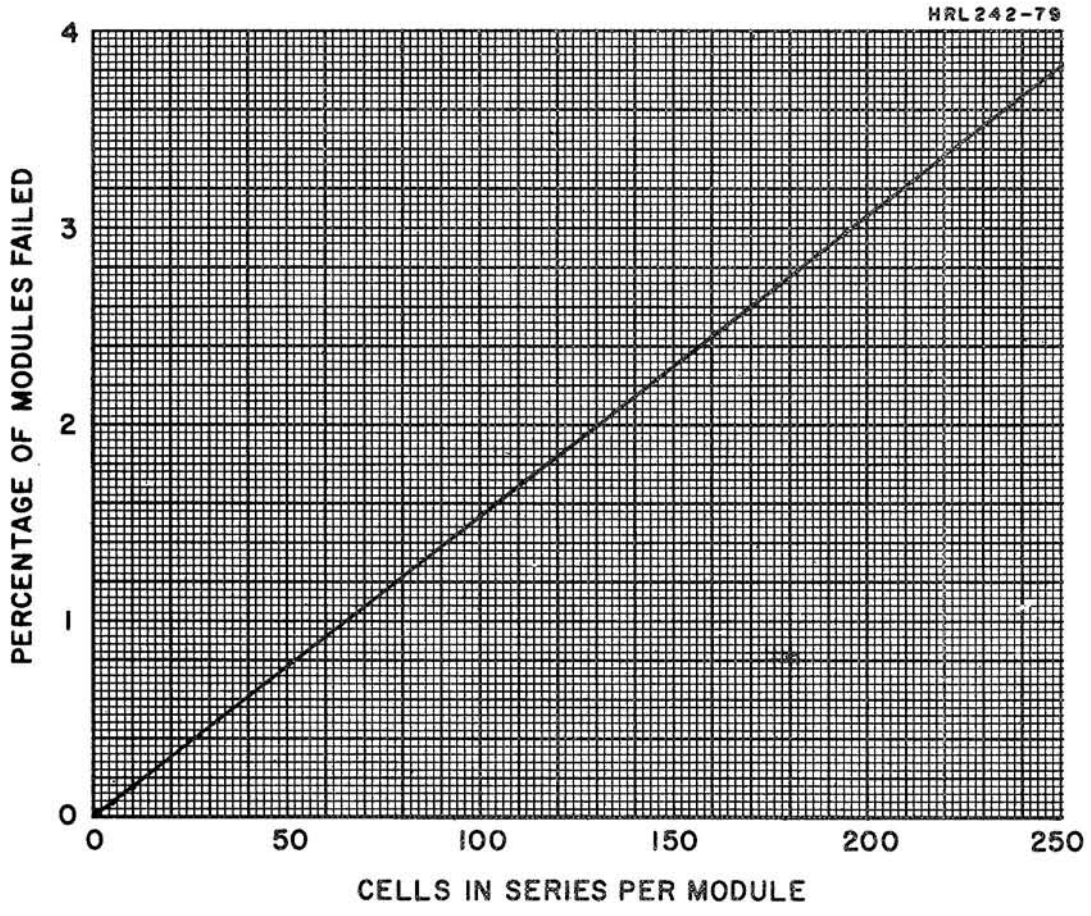

Fig. 49. Module failure rate as a function of number of cells in series per bypass diode (14 cells in parallel).

TABLE VI

Fabrication Problems and Considerations

Type of Problem	Effects	Probable Occurrence[a]	Allowable Level	Method of Detection	Method of Elimination
Voids					
Cover slides	Possible electrical discharge site; dielectric erosion.	0 to 1	Not allowed at erosion level.	Visual.	Rejection of cover slide.
Cover slide adhesive	Site for initiation of dielectric failure.	0 to 2	Established by electrical stress in given area volts/mil.	Visual.	Rejection process control.
Cell adhesive with scrim	Site for initiation of dielectric failure.	8 to 10	Established by electrical stress in given area volts/mil.	Electrical, emission discharge methods.	Reduced by viscosity control, conductive adhesive.
Cell adhesive without scrim	Site for initiation of dielectric failure.	1 to 8	Established by electrical stress in given area volts/mil.	Electrical, emission discharge methods.	Reduced by viscosity control and degassing
Laminated substrate	Site for initiation of dielectric failure.	0 to 2	Established by electrical stress in given area volts/mil.		Resin control, roll lamination.
Substrate film.	Site for initiation of dielectric failure.		Established by electrical stress in given area volts/mil.		
Separations					
Adhesive	Similar to voids.	All adhesive areas 1 to 4	Established by electrical stress in given area volts/mil.	Visual electrical stress, ultrasonic.	Process control, viscosity.
Cracks and Tears					
Substrates	In high stress area acts as void, mechanical.	1 to 2	Small surface cracks allowed-otherwise treated as voids.	Visual.	Controlled bend radii, processes, repair.
Wrinkles					
Substrate, substrate adhesive	Cracks upon flexure.	5 to 10	Wrinkles not producing cracks	Visual, radius gauge.	Flat working surfaces, handling control.
Contamination					
Environmental	Electrical shorts, leakage currents, outgassing.	1 to 2		Surface resistance, electrical.	Cleaning procedures, handling, storage.
Fabrication	Electrical shorts, leakage currents, outgassing.	5 to 10		Visual, electrical fluorescent, surface resistance.	Post operative cleaning methods, inspection.
Process Control					
Conductive coatings	Shorts, electrical stresses	0 to 1	Established by electrical stress in given area volts/mil.	Electrical stress.	Process controls, repair techniques.
Electrical interconnections	Opens, intermittent.		Opens or intermittents not allowed.	Electrical, visual (under flexed conditions.	Process controls, rework.

a) Scale: 10-7 Severe, always 6-3 Moderate, limited 2-0 Light, slight

laying cells on the total panel substrate. The segments should be butted together with adhesive as a final step in the process. Such an approach has the advantages of allowing post-fabrication performance testing on large panel segments (eight sectors isolated from one another) as well as easy replacement of a segment of the panel in case of failure during fabrication or testing, and prior to flight. The sector size constraint is established by the test plane of a typical pulsed xenon solar simulator. Segments will be interchangeable, with minor changes, in order to fulfill switching requirements of the total array.

7. Testing

The basic testing philosophy and procedure are taken from past industry experience with the development and testing of large flexible arrays. Areas of concern for the high voltage array are

- facility limitations
- array protection
- high voltage effects
- critical tests.

a. Facility Limitations

The large size of an array providing 16 kV and 15 kW at end of life establishes test constraints. Present pulsed xenon solar simulators will just accommodate one sector as shown in Fig. 50. This suggests post-fabrication testing of individual sectors followed by the assembly of several into a panel.

Problems with size are encountered also in full solar-thermal-vacuum tests for the completed panel which will be approximately 15 by 85 ft. It is proposed, based on past flexible array performance, that under thermal vacuum conditions all system functions be tested without deployment of the panels. The panel will be deployed following thermal-vacuum tests and partially illuminated to provide a qualitative check of the total power subsystem operation.

b. Array Protection

A concern in the development of flexible arrays is the minimization of the weight increase associated with array protection from nonflight loading conditions. The array operates under less than 1g conditions in space, but it must be assembled, handled, tested, transported, and stored under 1g conditions. Deployment of the panel for full panel tests under ambient conditions requires adjunct protection. Several methods have already been developed for panel deployment, which should be applicable to the high voltage array with minimal changes.

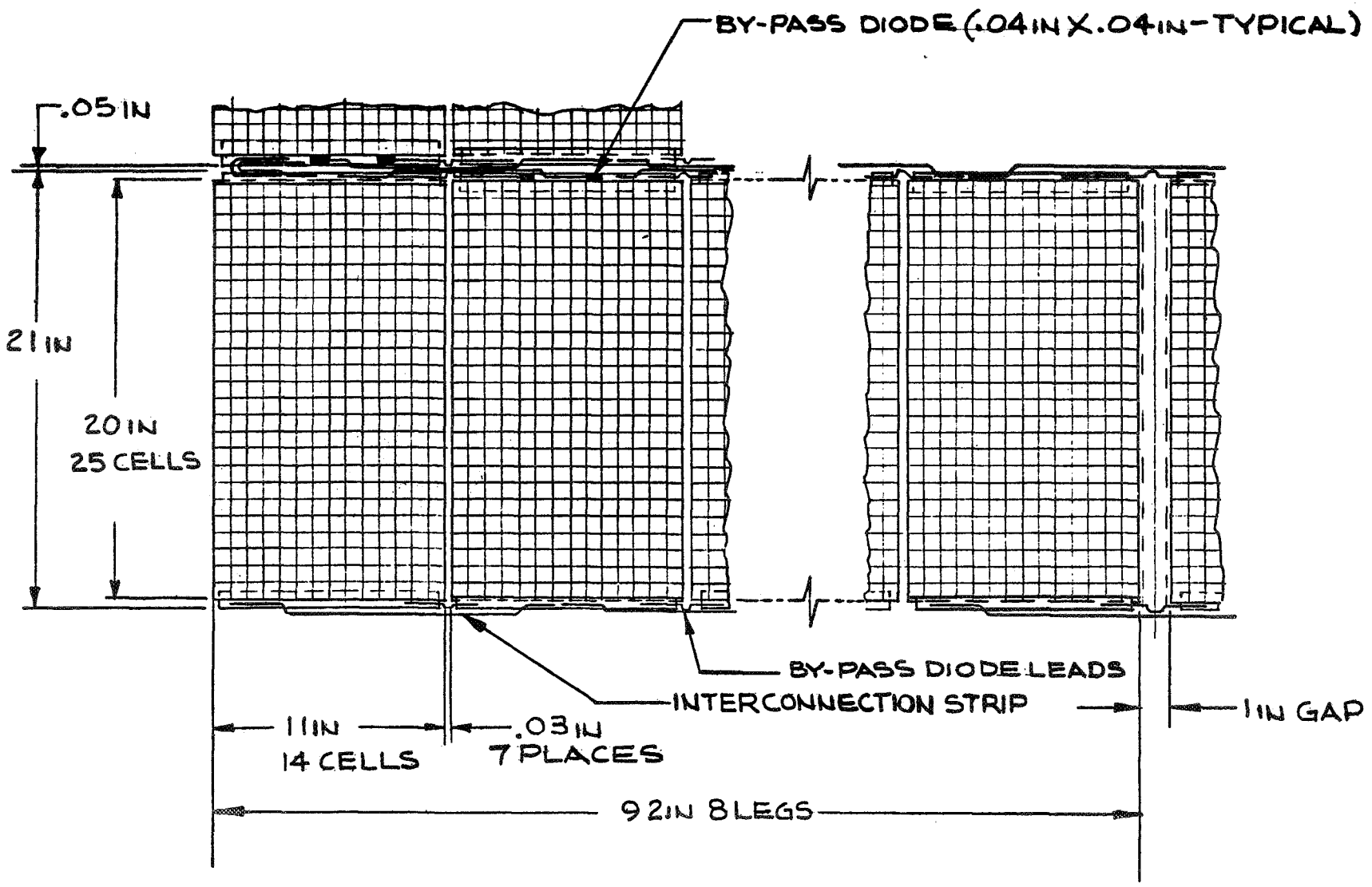

Fig. 50. Sector, conceptual design.

c. High Voltage Effects

The dielectric configurations chosen for the array have been evaluated in terms of test requirements. The array configurations developed will allow ambient testing of the panels under high voltage conditions. This capability is extremely important in light of the size constraints placed upon full panel S-T-V tests, and results in low weight penalties.

d. Critical Tests

Critical testing of the array must be performed in an environment which simulates the conditions encountered out of eclipse and which includes thermal shock and sinusoidal vibration.

8. Safety

a. "Safe" Current-Voltage Levels

Because the discomfort level for electric shock varies from person to person, the definition of a "safe" current-voltage level for solar cell groups is extremely difficult. However, the following tentative guidelines are established:

- To minimize the danger of severe shock, the maximum current drawn by an individual should be less than 8 mA.
- The resistance measured between two electrodes placed on the skin varies from 500 Ω to 5000 Ω. Normal dry hand resistance may be assumed to be 3000 Ω.
- Past experience with 2 cm x 2 cm n on p cells indicates a wide variation in cell output under ambient (fluorescent) lighting conditions. Short circuit current values near 3 mA/cell are realistic, although values which are a factor of ten lower have been experienced. The ambient voltage output varies from 0.3 to 0.5 V/cell at open circuit.

Employing the above guidelines, basic cell groups sized from 3 in parallel by 100 in series to 14 in parallel by 50 in series may be handled with standard safety procedures.

b. Safety and Fabrication

The basic building block for the panel segment is the sector with 200 cells in series by 14 cells in parallel (Fig. 50). Once the sector is fabricated, safety procedures related to severe shock hazard become imperative. It is important that the sector be treated in the same way as a normal 110 V ac power line.

The point in fabrication at which the danger is highest is during the joining together of panel segments to form the final panel. Although methods such as ambient light filtering and shadowing have been considered, the severe shock hazard dictates that cell groups (subsector) should be shorted and that cell groups should be isolated from one another prior to the final step in the fabrication process.

c. Safety and Testing

As indicated above, the basic building block, the sector, must be treated with the same respect as a 110 V ac power line under ambient lighting. Normal steady-state simulation to determine I-V performance at 1 solar constant would produce a much more severe hazard. However, pulsed xenon systems allow large area tests at 1 solar constant without severe hazard to personnel. With a pulse length of less than 500 μsec, the energy delivered by a sector during a single pulse at 1 solar constant is too small to cause bodily harm.

Full panel tests will require careful control. The physical shorts and isolation incorporated on the panel during the final step of fabrication must be removed with greatest care. The array has been designed for full panel tests in air; however, the high voltage hazard to personnel remains.

d. Techniques for Safety

A number of techniques and devices have been explored to enhance safety. They remain secondary, not primary. These techniques are listed for completeness; feasibility determination requires further study:

- Standard cells used to monitor the "safe" current level during fabrication
- Ambient light filtering in fabrication and testing areas
- Partial deployment and shadowing of the panel
- Partial illumination during full panel tests.

The hazard that might be created by static charge buildup during fabrication and testing has not been ascertained. It remains to be determined whether techniques for charge control will be required.

C. CONCEPTUAL DESIGN

In this section a conceptual design of a high voltage solar array is discussed which represents a distillation of the various design factors examined in the preceeding portions of this study.

1. Array Configuration

The conceptual design utilizes 985,600 solar cells mounted on four rollup panels (Fig. 41), each of which has dimensions of approxi-

mately 15 by 85 ft. The panel configuration, shown in detail in Fig. 51, consists of four voltage blocks, each providing 1 kV at 0.94 A at end of life, which can be switched to achieve any desired combination. The blocks are so arranged that no buses are required on the array; this is important with regard to the control of dielectric failure.

A panel is formed by joining eleven panel segments which are fabricated separately. The panel segments are interchangeable in order to allow easy and inexpensive replacement in case of pre-launch failure. The segments, in turn, comprise eight of the sectors shown in Fig. 50, which have dimensions that allow testing with a pulsed xenon solar simulator.

The conceptual design utilizes a cell layout with transverse interconnections (Fig. 43) in order to minimize the effects of potential cell cracking during panel roll-up. Open circuit failures of solar cells are compensated for by the use of bypass diodes connected in parallel with each group of 50 series-connected solar cells. Failure isolation devices are employed to compensate for short circuits.

The spacings between active elements are chosen sufficiently large ($\cong$ 0.6 in.) to permit testing in air.

2. Materials

The dielectric material design is based on the following rules:

- The design strength for all dielectric materials is taken to be the emission discharge onset potential, a value between 50 and 100% of the commonly measured dielectric breakdown voltages. A safety factor of two is added as an extra margin.
- The maximum operating temperatures are assumed in determining design dielectric thicknesses.
- All dielectric materials are designed to a maximum beginning-of-life voltage of 30 kV.
- Voids between active elements of the array are unacceptable.

The recommended materials are:

Item	Materials
Substrate	Kapton, 0.012 cm thick (5 mil)
Solar Cell	2 x 2 cm n on p, 10 Ω-cm, 0.015 cm thick (6 mil)
Cover slide	Fused silica, 0.015 cm thick (6 mil)
Cell-Substrate Adhesive	RTV 655
Cell-Cover slide Adhesive	RTV 602 or R63-487

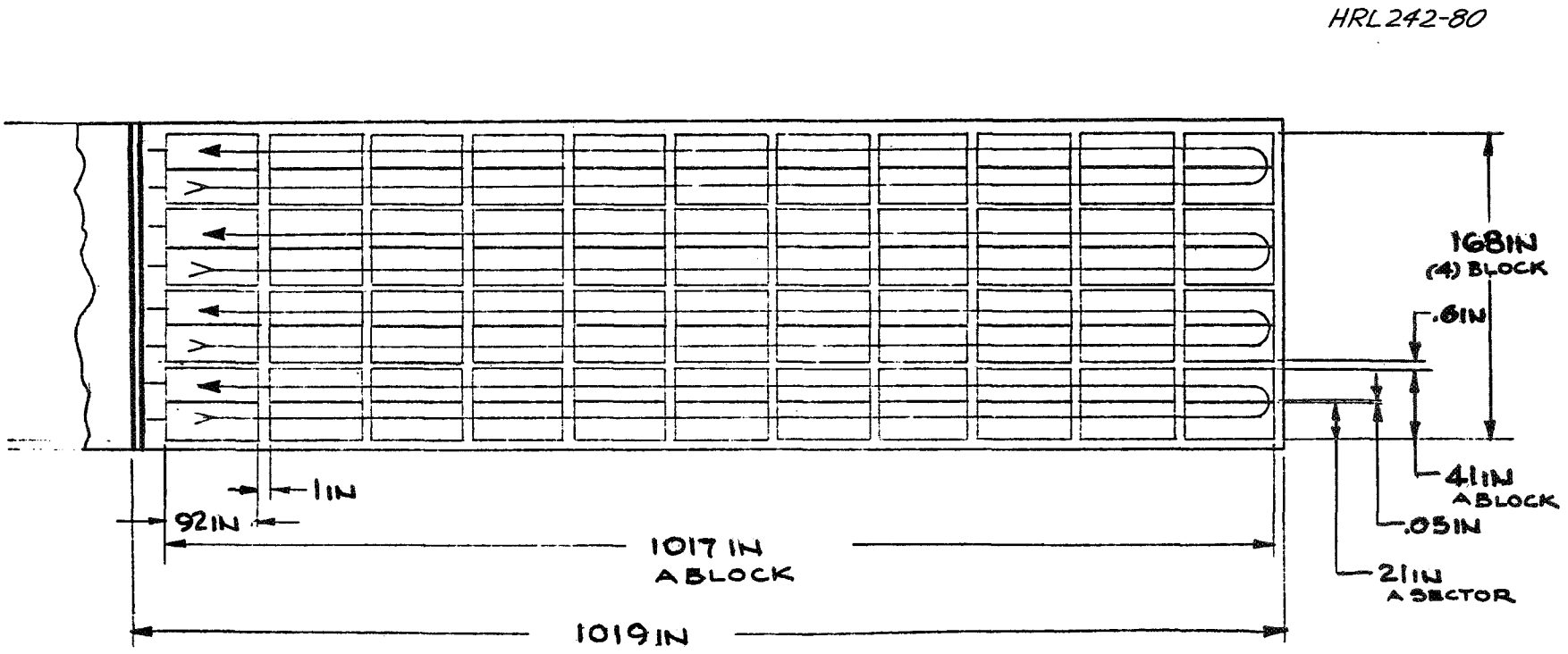

Fig. 51. Panel, conceptual design.

Item (cont.)	Materials (cont.)
Encapsulant (if required)	RTV 655
Buses	Copper ribbon
Interconnects	Copper
Conductive grid on back of substrate	VDA

3. On-Orbit Performance

The performance predictions are based upon a computer program which statistically takes into account the following factors: temperature, intensity, radiation, fabrication loss, cover slide transmission loss, and instrumentation allowance. Figure 52 shows the total array I-V characteristics at beginning of life and at end of life, together with three sigma deviations from the nominal. Array sizing is dependent upon end of life minus three sigma winter solstice maximum power to meet the 16 kV, 15 kW requirement of the mission at the end of five years in space.

The extra high voltage produced as the cold array comes out of the eclipse is of basic concern to the array design. A post-eclipse performance curve is shown in Fig. 53. The worst case voltage is approximately 50 kV at open circuit. To protect the array from this temporary high voltage, it is planned to isolate the blocks from one another and switch them to short circuit. This approach allows the array to warm up (a period of minutes) and permits voltage stresses to be controlled without resorting to increased insulation and the additional required weight. Following warm-up, the array will be switched back to the spacecraft loads. At the lowest altitudes, the power losses due to plasma leakage are expected to be 20-30% at 2 kV. A number of methods are proposed to reduce these losses.

4. Methods of Plasma Loss Reduction

For those missions where the plasma losses become unacceptably large (low altitude missions with relatively high output voltages), one of the following earlier discussed methods for loss reduction must be considered:

- complete array insulation
- depressed plasma collectors
- biased screen grid.

At present, not enough is known about the merits of each of these methods to single out one as a preferred choice. Conceptual designs of the depressed plasma collector method and of the biased screen grid method are shown in Figs. 54 and 55. Incorporation of the

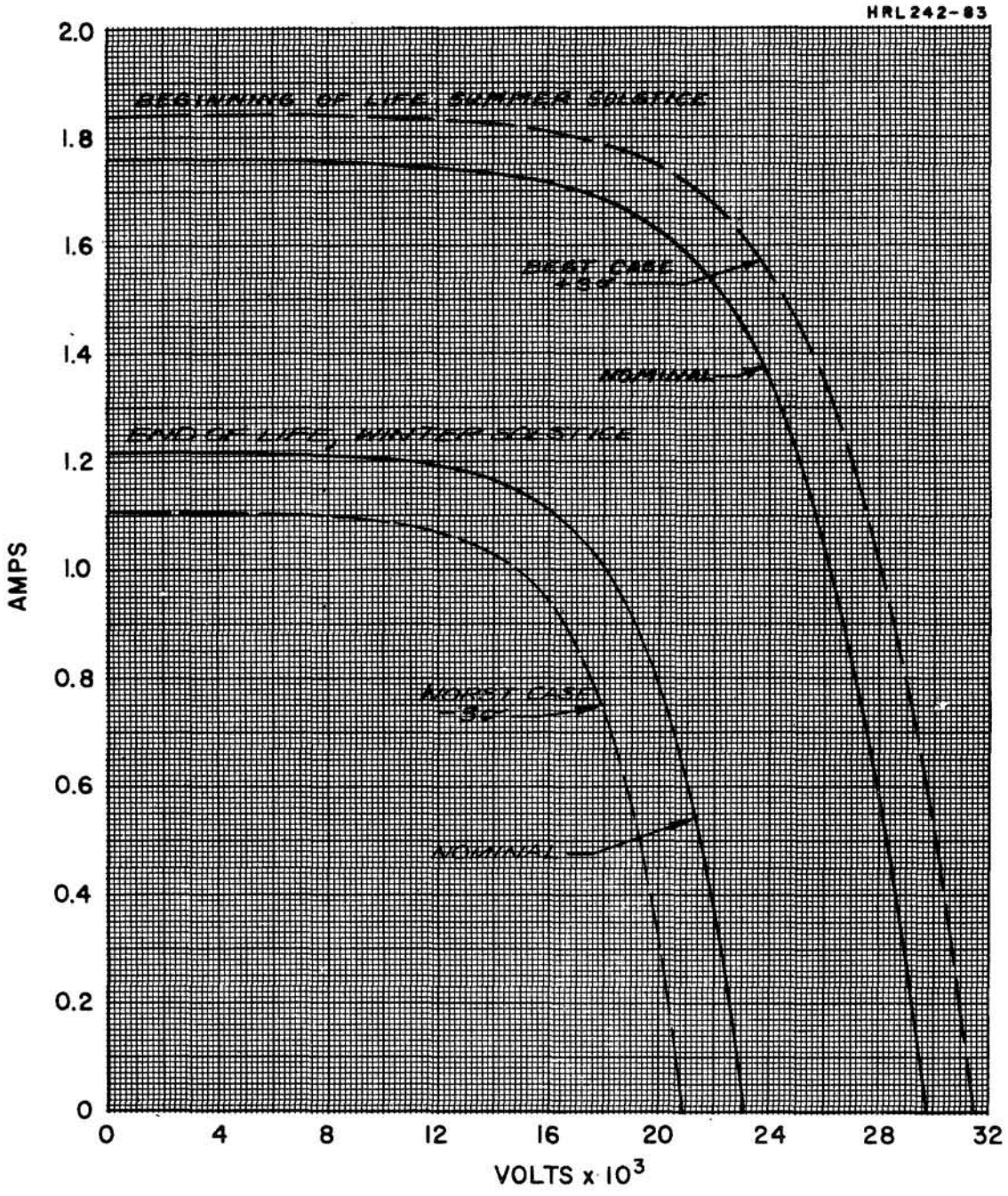

Fig. 52. High voltage solar array performance optimization for 16 kV.

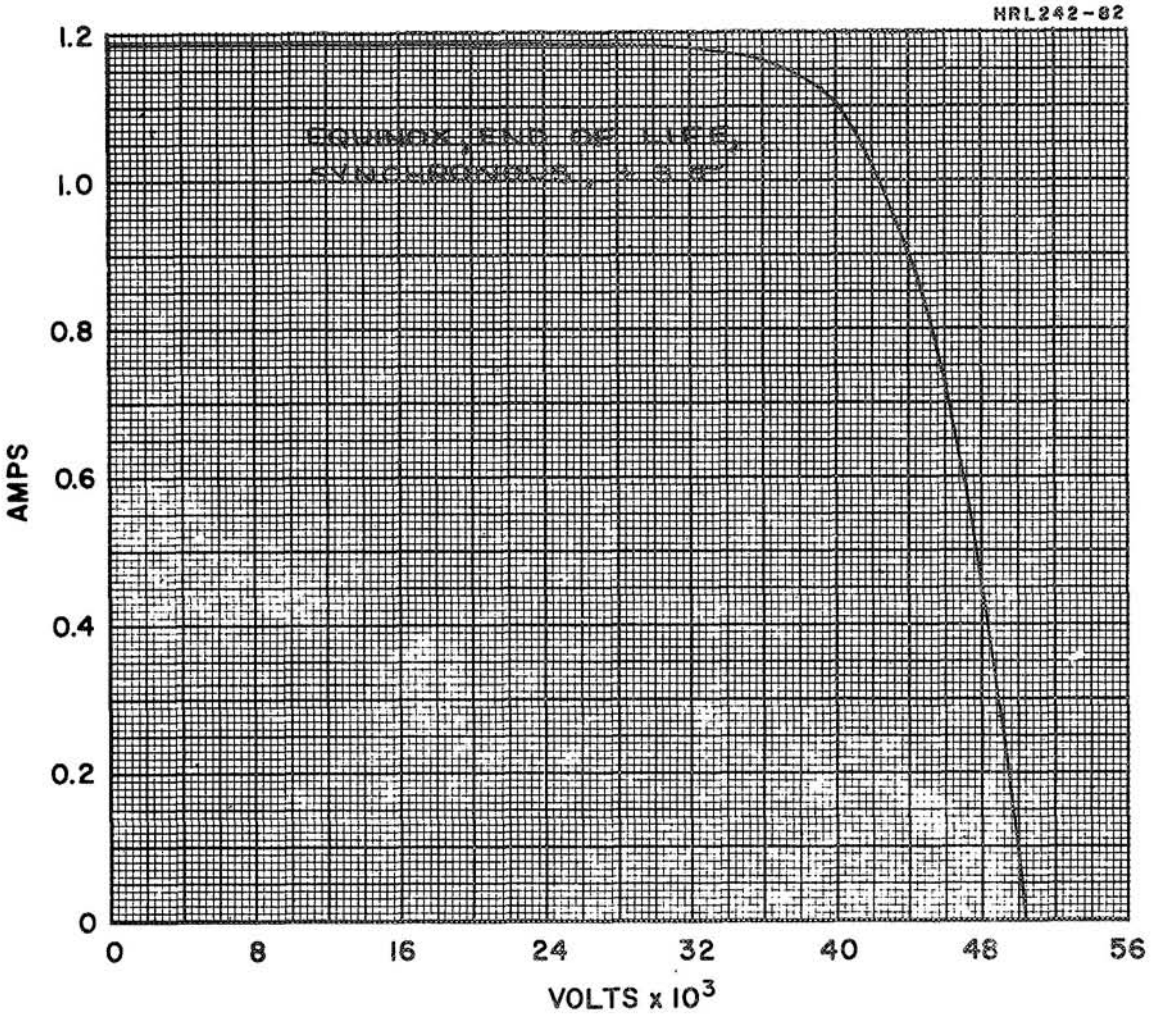

Fig. 53. High voltage solar array post-eclipse performance.

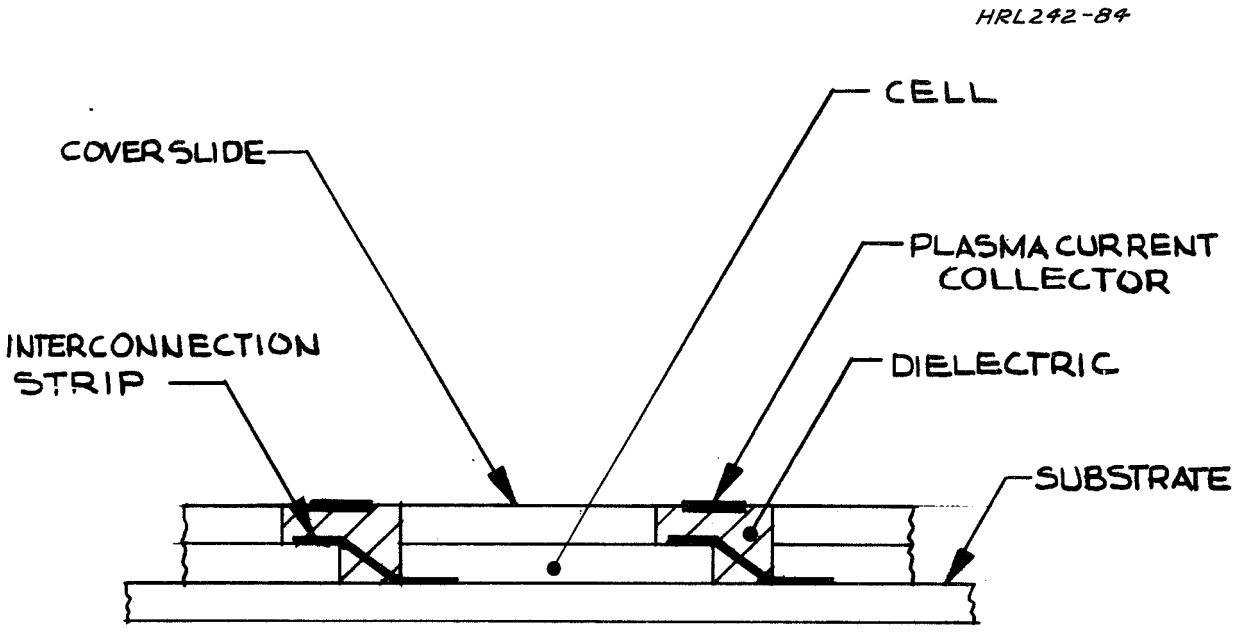

Fig. 54. Depressed current collection concept.

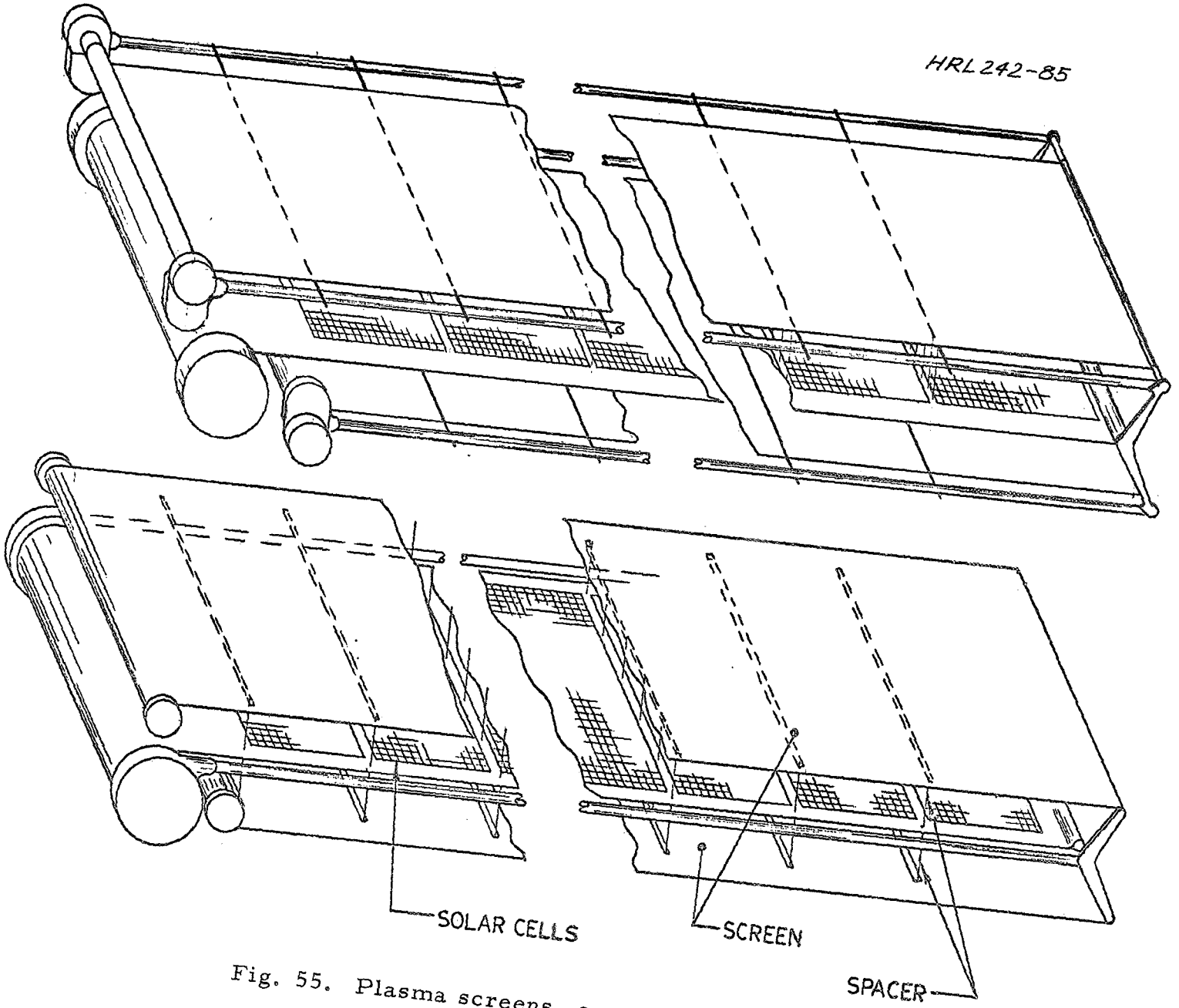

Fig. 55. Plasma screens, conceptual design.

complete array insulation method can be accomplished by filling the gaps between cover slides with an encapsulant (for example, RTV 655).

D. CONCLUSIONS

As far as can be concluded from the present design exercise, high voltage solar arrays can be configured much like conventional arrays. Dielectric breakdown considerations require a small increase in substrate thickness (from about 3 to 5 mils) and a modest increase in cell block spacing (to 0.6 in.); however, neither is expected to have a major impact upon array weight or size (< 5%). The weight penalty associated with an optional screen grid also is not considered severe. The fact that high voltage arrays require smaller buses and less power conditioning suggests that they may even enjoy an over-all weight advantage against conventional arrays.

V. PROPOSED FUTURE STUDY TASKS

During the work reported here a number of tasks have become apparent which are desirable for a demonstration of the feasibility of high voltage arrays. These tasks are predominantly of an experimental nature, even though they should be complemented by analysis. The recommended tasks, many of which have already been mentioned in earlier parts of this report are summarized below.

A. OBJECTIVES

Future studies should accomplish the following over-all objectives:

- Determine through experimentation the solar cell materials and configurations best suited to withstand the dielectric stresses arising from high voltage operation of solar arrays.
- Determine experimentally the discharge and plasma current leakages for solar cell configurations with mostly insulating surfaces, including an assessment of the conditions under which pinhole breakdown occurs.
- Provide a breadboard model incorporating the essential features of a preferred solar array embodiment, and yield performance and accelerated life tests in a simulated space environment.

B. DETAILED TASK DESCRIPTION

The above listed objectives require the following experimental and theoretical investigations.

1. Dielectric Material Experiments

a. Measure the state of charging of a dielectric (cover slide or backing layer) in a simulated space plasma environment.

Objective: to determine the actual dielectric stress levels across cover slides and backing layers.

Method: measure the displacement currents across the dielectric, using a pickup electrode attached to the rear of the dielectric.

Parameters; current density and energy of electrons and protons bombarding the surfaces, intensity and spectral distribution of photon radiation, and magnitude of the potential applied to neighboring conducting surfaces (tabs) which may collect or emit secondary electrons.

b. Measure bulk and surface dielectric breakdown in a simulated space plasma environment.

Objective: to determine the thicknesses of cover slides and backing layers required for high voltage operation and to establish safe distances between solar cells and buses which are maintained at different potential levels.

Method: measure voltages at which breakdown occurs under bombardment with electrons and protons, and inspect dielectric materials microscopically for tracks and pinholes.

Parameters: current density and energy of bombarding electrons and protons, intensity of photon radiation, preradiation doses with energetic particles, surface contamination (e.g., with mercury), number and size of voids, artificial pinholes (simulating micrometeroroid tracks), mechanical stress levels, temperature.

Control Experiment: perform static breakdown measurements with cover slides and backing layers sandwiched between test electrodes and compare results with plasma breakdown measurements.

c. Determine the consequences of dielectric breakdown.

Objective: to find the conditions under which dielectric breakdown leads to self-sustained pinhole arcs and to observe whether this leads to a deterioration of solar cell output.

Method: measure discharge currents after breakdown occurs, inspect dielectric for damage, measure cell output.

Parameters: current density and energy of bombarding electrons and protons, surface contamination, temperature.

d. Investigate conductive coatings and conductive cover slide materials.

Objectives: to determine whether the charges on cover slides can be conducted away, thereby reducing dielectric stresses

Method: measure potential differences between front and rear surface by the displacement current method under electron and ion bombardment

Parameters: conductive coating materials and thicknesses, conductive cover slide materials and thicknesses, intensity of bombardment

2. Current Loss Experiments

a. Measure the current losses of a high voltage solar array model in a simulated space plasma

Objective: to determine the current losses of an array which utilizes the most promising dielectric surface configuration

Method: measure current losses in a properly scaled laboratory experiment

Parameters: plasma density, voltage of the array

b. Compute the trajectories of the attracted plasma particles for an array surface with varying ratios of insulated to conducting area

Objective: provide a comparison for the above experiments and find the most promising configuration

Method: self-consistent computer analysis, utilizing modified Stanford program

c. Investigate the conditions under which pinhole breakdown occurs

Objective: determine feasibility of total insulation concept for leakage elimination

Method: expose insulated surface to plasma with bias applied

Parameters: plasma density, bias voltage

d. Assess leakage reduction concepts

Objective: determine usefulness of (1) total insulation, (2) depressed collector, (3) biased screen

Method: expose suitably motified array model to plasma

Parameters: plasma density, bias voltage collector geometry and voltage, screen geometry and voltage.

e. Cross-field discharge properties of a high voltage solar array

Objective: determine whether in the presence of the Earth's magnetic field the array may be enveloped by a Penning discharge which results in additional loss currents

Method: measure voltages at which discharge occurs

Parameters: magnetic field strength and orientation, gas density, background plasma density

3. Breadboard Model Tests

Objective: to determine the operational performance and durability of a high voltage solar panel

Method: construct a breadboard panel comprising several strings of solar cells with buses, bypass diodes, blocking diodes, regulation devices, and switches and expose to fluxes of electrons, protons, photons, and energetic particles

Parameters: intensity of electron and proton fluxes, of photon and energetic particle radiations, panel temperature, and background gas.

C. FACILITIES AND APPARATUS

The proposed experiments must be carried out in a sufficiently large vacuum chamber, so large, in fact, that plasma sheaths remain smaller than the chamber dimensions. For ionospheric plasma densities of $10^6/cm^3$ and with 95% insulated arrays, the sheath widths will be in the range between 40 and 100 cm depending upon voltage. A vacuum tank of about 3 m diameter and of at least comparable length should suffice. The pressure should not exceed 10^{-6} Torr in order to prevent volume ionization within plasma sheaths, but it need not be lower than 10^{-7} Torr.

The choice of a suitable plasma source is of considerable importance. To simulate ionospheric conditions, the source should be capable of generating oxygen, nitrogen, and hydrogen ions with a thermal energy of a few electron volts and of densities between 10^4 and $10^6/cm^3$. The spacecraft velocity should be simulated by impressing a directed energy of about 100 eV upon these ions. Sources which can satisfy these requirements are (1) rf plasma sources, (2) the electron-bombardment source originated at Lewis Research Center and recently developed into prototypes at Hughes, and (3) photo-ionization plasma sources. The duoplasmatron is not considered useful because it delivers ions with too high kinetic energies and with too narrow beam widths.

REFERENCES

1. F. F. Chen, Plasma Diagnostic Techniques, R. H. Huddlestone and S. L. Leonard, Eds. (Acdemic Press, New York, 1965), p. 128.

2. I. Langmuir in Collected Works of I. Langmuir, G. Suits, Ed. (Pergamon Press, New York, 1961), Vol. 4, pp. 32 ff.

3. L. M. Linson, J. Geophys. Res. 74 , 2368 (1969).

4. W. Knauer and R. L. Poeschel, Proc. VII Intern. Conf. on Ionized Gases, Vol. II, p. 719, 1966.

5. U. Samir, Am. Phys. Soc. Plasma Phys. Meeting, Los Angeles, 1969.

6. H. Heil, Phys. Rev. 164, 887 (1967).

7. R. K. Cole, H. S. Ogawa, and J. M. Sellen, Paper No. 69-262, AIAA 7th Elec. Prop. Conf., Williamsburg, Va. 1969.

8. P. A. Redhead, J. P. Hobson, and E. V. Kornelsen, The Physical Basis of Ultrahigh Vacuum (Chapman and Hall, London, 1968), p. 222.

9. G. W. Morey, The Properties of Glass , Reinhold, New York, 1954), p. 465.

10. E. I. DuPont de Nemours and Co., Literature on Kapton.

11. W. Ehrenberg, et al., Brit. J. Appl. Phys. 17 , 63 (1966).

12. Ibid.

13. L. Pensak, Phys. Rev. 75 , 472 (1949).

14. B. Kazan and M. Knoll, Electronic Image Storage (Academic Press, New York, 1968), p. 33.

15. B. M. McCormac, Earth's Particles and Fields (Reinhold, New York, 1968). p. 33.

16. Redhead, et al., op. cit., p. 192.

17. G. Carter and J. S. Colligon , Ion Bombardment of Solids (American Elsevier, New York, 1968).

18. T. W. Reynolds and E. A. Richley, Paper No. 69-270, AIAA 7th Elec. Prop. Conf., Williamsburg, Va., 1969.

19. J. H. Mason, "Dielectric Breakdown in Solid Insulators," in Progress in Dielectrics (J. Wiley, New York, 1959), p. 30.

20. ASTM D1868.

21. L. L. Alson, High Voltage Technology (Harwell-Oxford, London, 1968) pp. 178-181.

22. R. J. Holbrook, unpublished work.

23. K. Arnold, private communication.

24. M. J. Kofoid, AIAA Trans. 79, 999 (1960).

25. L. J. Frisco, "Dielectrics for Satellites and Space Vehicles," Final Report, Contract DA-36-039-SC-78321, 1 March 1959 to 28 February 1962.

26. S. Dushman, Scientific Foundations of Vacuum Techniques (J. Wiley, New York, 1962).

27. A. Von Hippel, Dielectric Materials and Applications (MIT Press Wiley and Sons, New York, 1954), p. 153.

28. Space Materials Handbook, 3rd ed. (Lockheed Missile and Space Company, 1968).

29. "The Effects of Radiation on Electrical Insulating Materials", REIC Reports No. 46 and 47, Battelle Memorial Institute, Columbus Laboratories, Columbus, Ohio.

30. F. A. Blake and K. L. Hensen, "The 'Hot Spot' Failure Mode for Solar Arrays,"IEEE Intersociety Energy Conversion Engineering Conference Record, 1969, pp. 575-581.

APPENDIX A - THE PARTICLE AND FIELD ENVIRONMENT OF EARTH

A. NEAR EARTH ENVIRONMENT

The space surrounding earth (over distances to which the earth's magnetic field extends) is occupied by a number of neutral and charged particle components. At altitudes below about 100 km most particles are electrically neutral. With increasing altitude, the degree of ionization increases rapidly as a result of photoionization in the upper atmosphere. The resulting "thermal plasma" extends out from the ionosphere into the geomagnetic cavity along lines of force of the geomagnetic field. A second, independent, space plasma component, the so-called "plasma sheath," is located in the auroral zones and extends into the tail of the geomagnetic cavity. It is composed of particles which are believed to stem from the solar wind and which may enter the tail of the cavity as a result of ∇B drifts. A third magnetospheric charged particle component is the radiation belt population. Its electrons and ions are presumed to be of solar origin also, and are believed to have entered the magnetosphere along the tail. The above mentioned particle components are described in detail below.

1. Neutral Atmosphere

Composition: The higher atmosphere is mainly composed of O, He, and H. With increasing altitude the mean molecular weight decreases from about 25 at 200 km to near 1 at 5000 km. The details of this dependence are tabulated by Johnson (Ref. A-1).

Density: The density of the upper atmosphere varies strongly with time. Figure A-1 gives maximum and minimum particle densities as a function of altitude as recorded in Ref. A-1.

Temperature: The temperature of the upper atmosphere generally increases with altitude. At 200 km altitude the lowest average nighttime temperature is about 600°K;at 2000 km it is about 700°K. The corresponding highest daytime temperatures are 700°K and 1800°K. Detailed temperature profiles are given in Ref. A-1.

2. Thermal Plasma

Composition: The thermal plasma consists of equal numbers of electrons and ions. Most of the latter are protons; however, with decreasing distance from earth, increasing numbers of He^+, O^+, and N^+ are present (Ref. A-1).

Density: The plasma density distribution near earth, in the ionosphere, has been measured by radio transmission and with Faraday cup plasma collectors (Ref. A-1). The resulting particle fluxes are shown in Figs. A-2 and A-3. Information about the plasma state in the outer regions of the geomagnetic cavity has been obtained with the help of Faraday cup collectors aboard IMP-1 (Ref. A-2) and IMP-2

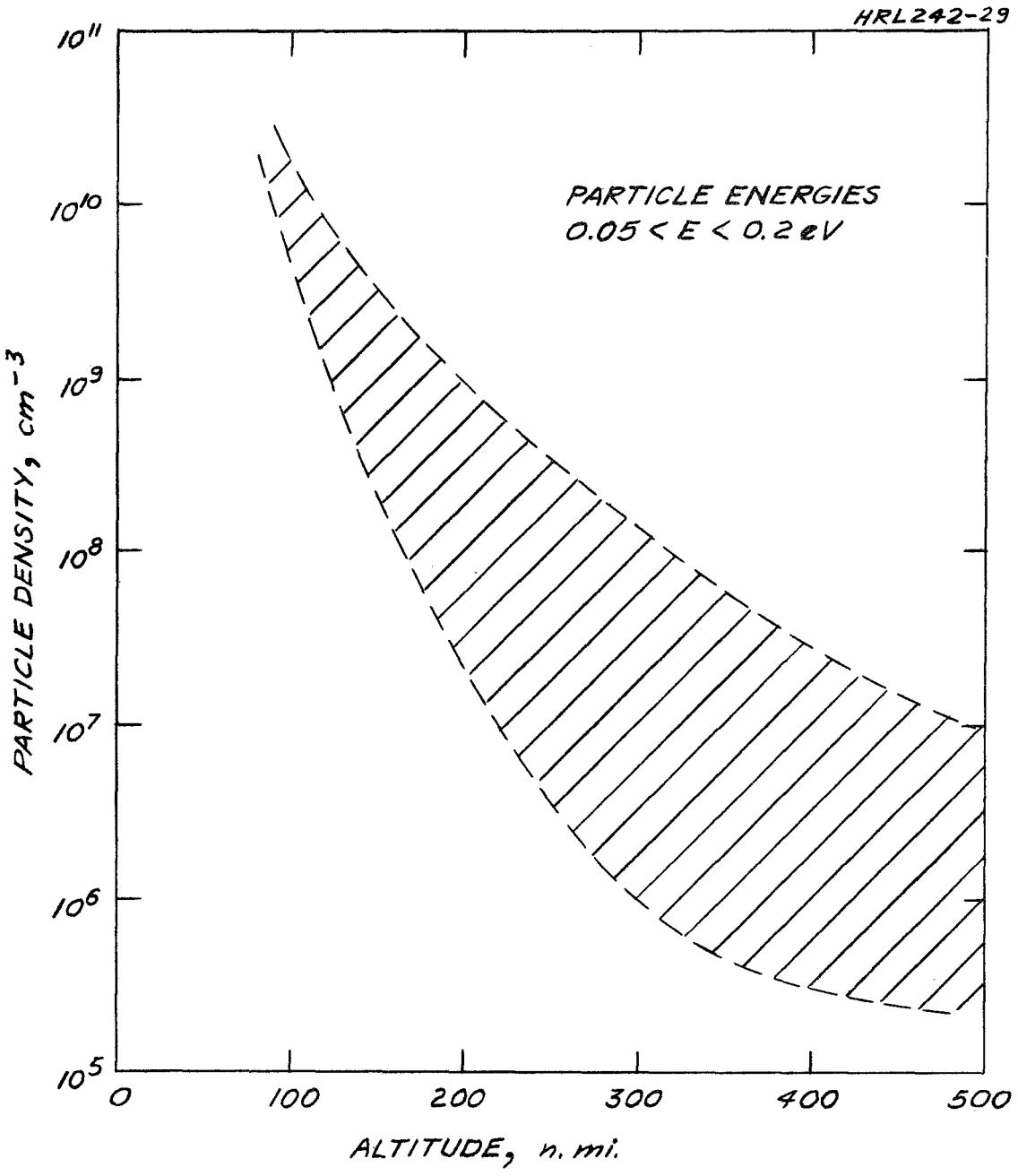

Fig. A-1. Atmospheric density distribution; the range indicates the difference between daytime, maximum sunspot cycle, and nighttime, minimum sunspot cycle.

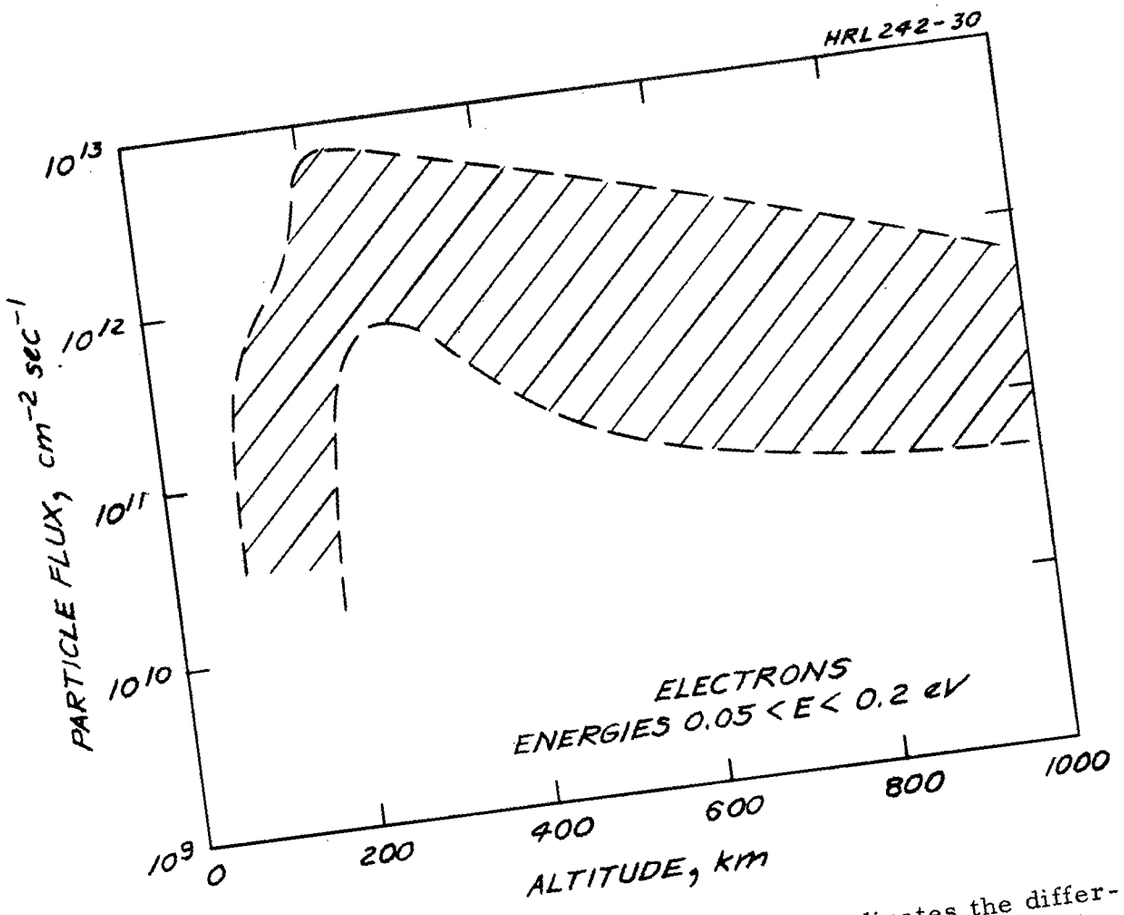

Fig. A-2. Ionosphere electron fluxes; the range indicates the difference between daytime maximum sunspot cycle and nighttime minimum sunspot cycle.

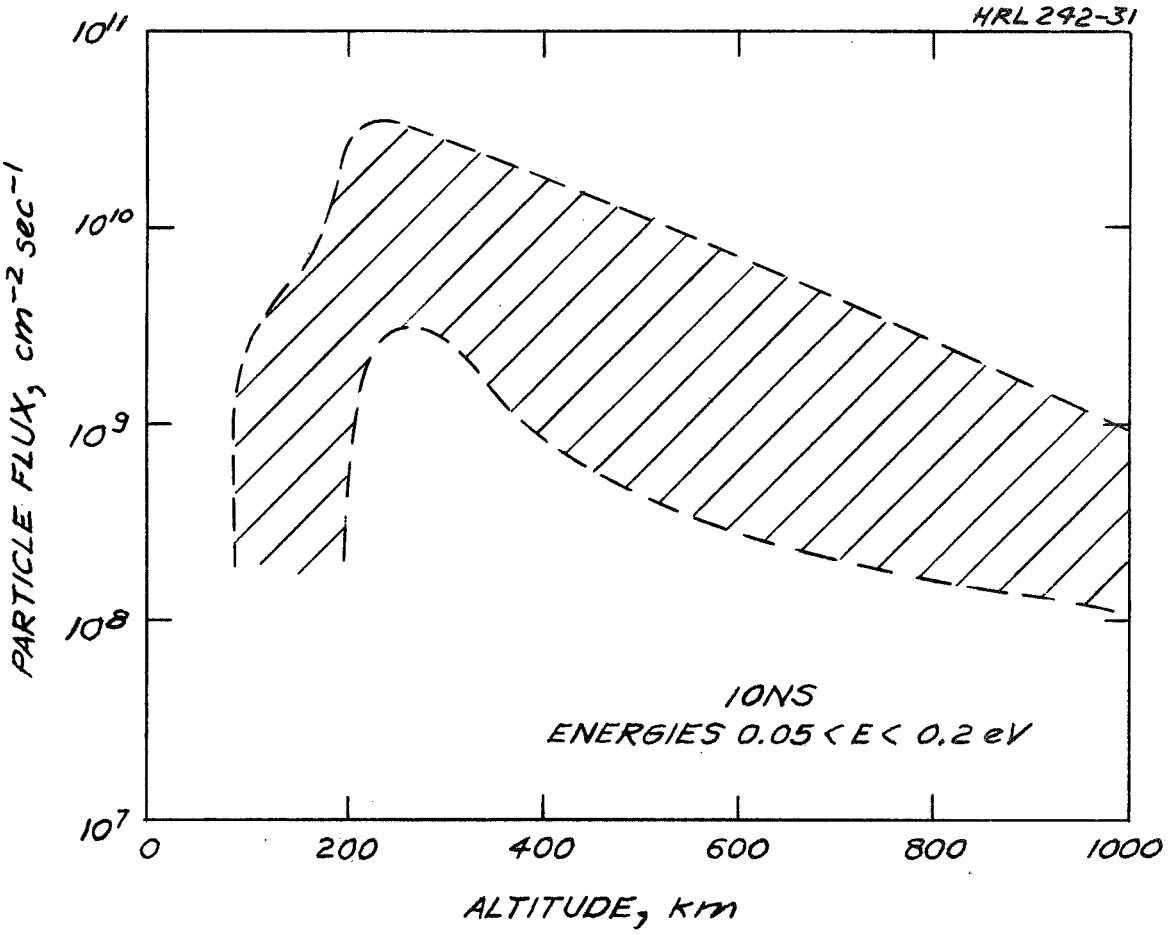

Fig. A-3. Ionosphere ion fluxes; the range indicates the difference between daytime maximum sunspot cycle and nighttime minimum sunspot cycle.

(Ref. A-3), and also from measurements of the whistler propagation along geomagnetic field lines (Ref. A-4). Results based upon both types of measurements are given in Fig. A-4.

Energy: IMP-2 (Ref. A-3) measurements have also provided information about electron and ion energy distributions. The electrons were found to have energies in the range from 1 to 5 eV, and ions in the range from 1 to 10 eV.

3. Plasma Sheath (Including Auroral Particles)

Composition: The plasma sheath is essentially a neutral plasma with equal numbers of protons and electrons.

Density: The density of the plasma sheath has been measured by Vela (Ref. A-6) satellites as well as OGO-1 and OGO-3 (Ref. A-6). The results are shown in Figs. A-5 and A-6.

Energy: According to the Vela measurements the particle energies are in the range of 10^2 to 10^4 eV for protons and of 10^2 to 10^5 eV for electrons.

4. Radiation Belts

Composition: The radiation belts are composed predominantly of energetic protons and electrons.

Particle Fluxes: The proton and electron fluxes associated with the radiation belts have been measured by various satellites. Much of the available information was obtained with Pioneer-6 (Ref. A-7) and Explorers-12,-14, and-15 (Ref. A-8). The collected data are summarized in Fig. A-7.

Energy: Information obtained with the above named satellites points to energy ranges of 10^4 to 10^8 eV for protons and 10^4 to 10^7 eV for electrons. Generally, the energy increases with decreasing distance from earth.

5. Geomagnetic Field

The geomagnetic field is approximately a dipole field up to distances on the order of about 5 earth radii. Beyond this distance the solar wind disturbs the earth's magnetic field, as shown in Fig. A-8.

6. Geoelectric Field

Many regions of the magnetosphere contain electric fields. The approximate strength and orientation of these fields are known only in the ionosphere. There, the largest fields occur in the auroral zones and are associated with electrojets. Within these jet streams the field strength reaches maximum

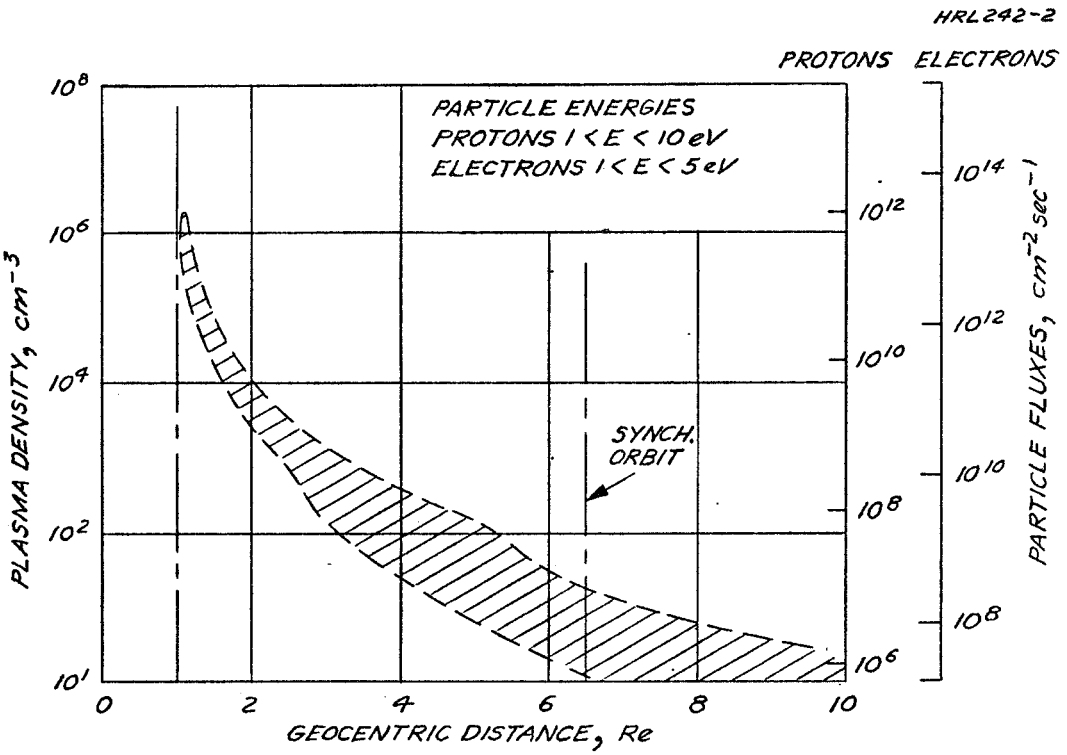

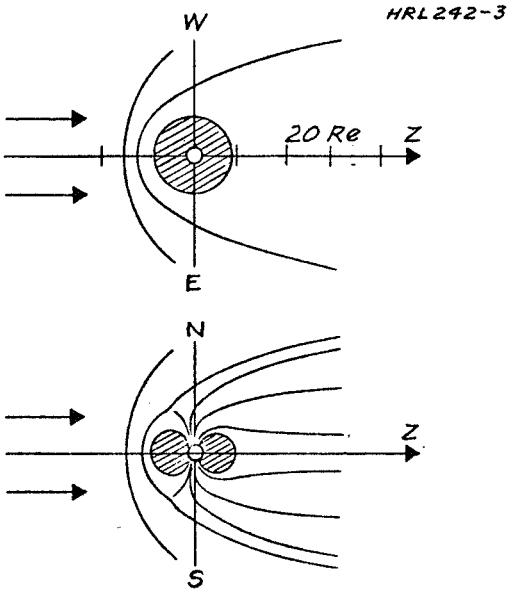

Fig. A-4.
Thermal plasma distribution along the z-axis within the geomagnetic cavity. The range shown indicates temporal fluctuations and measurement uncertainties.

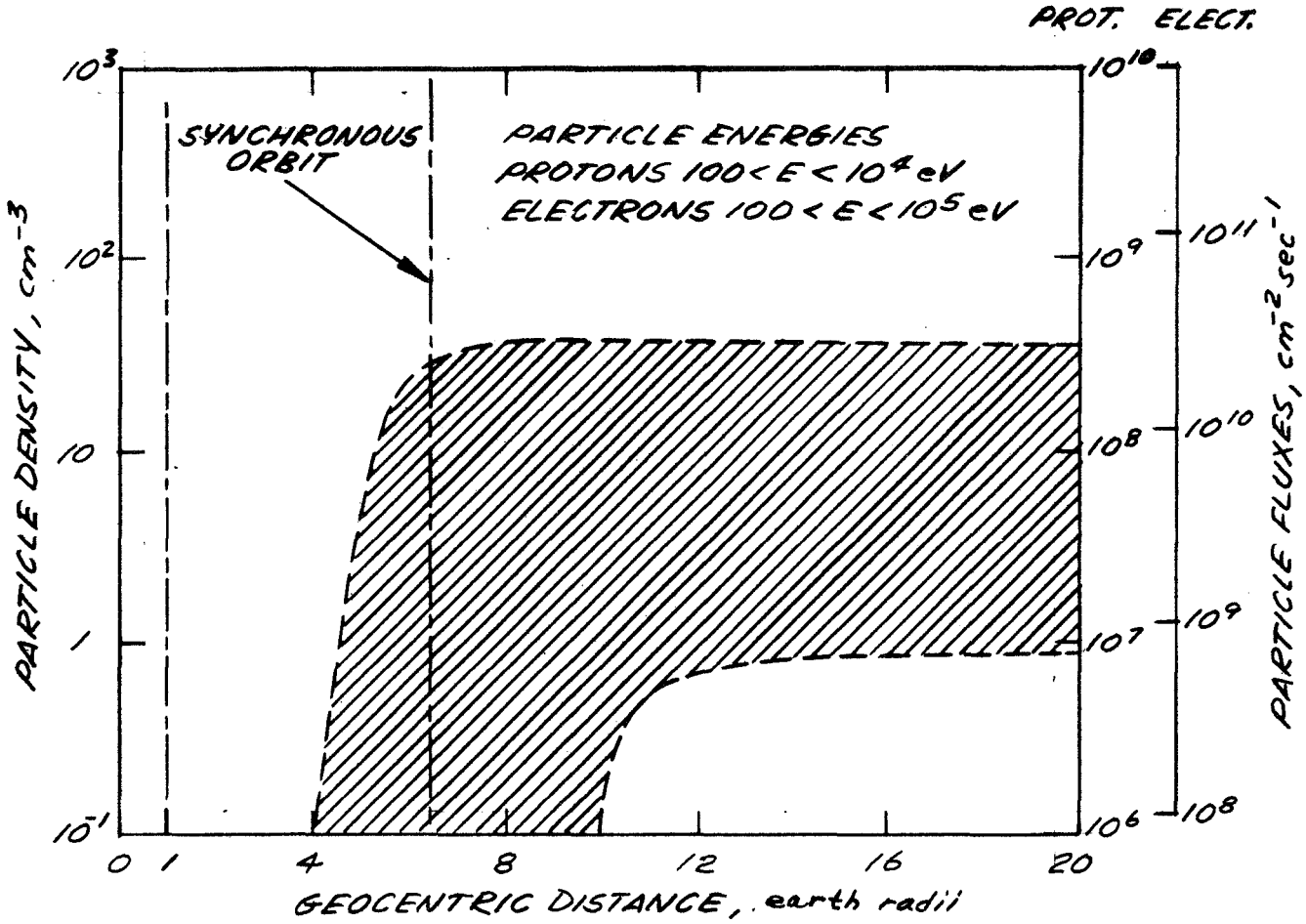

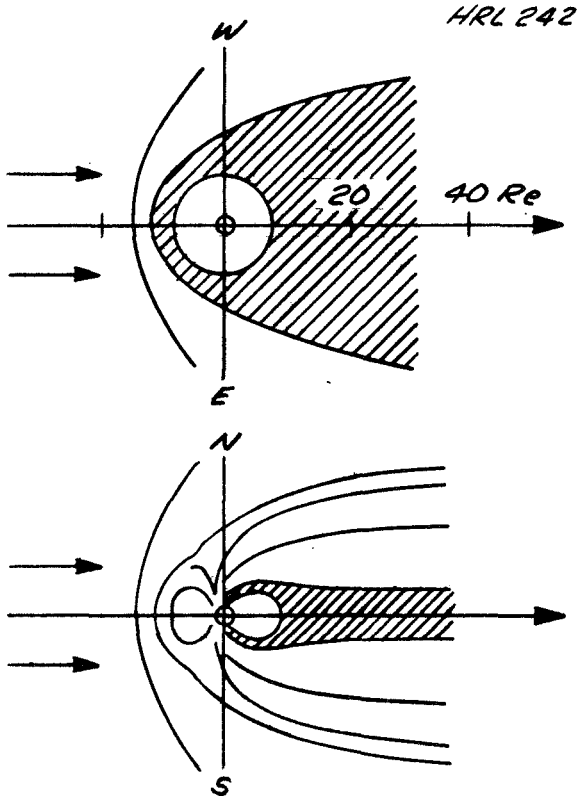

Fig. A-5.
Plasma sheath particle population along the z-axis of the geomagnetic cavity. The range of values indicates temporal fluctuations and measurement uncertainties.

HRL 242-34

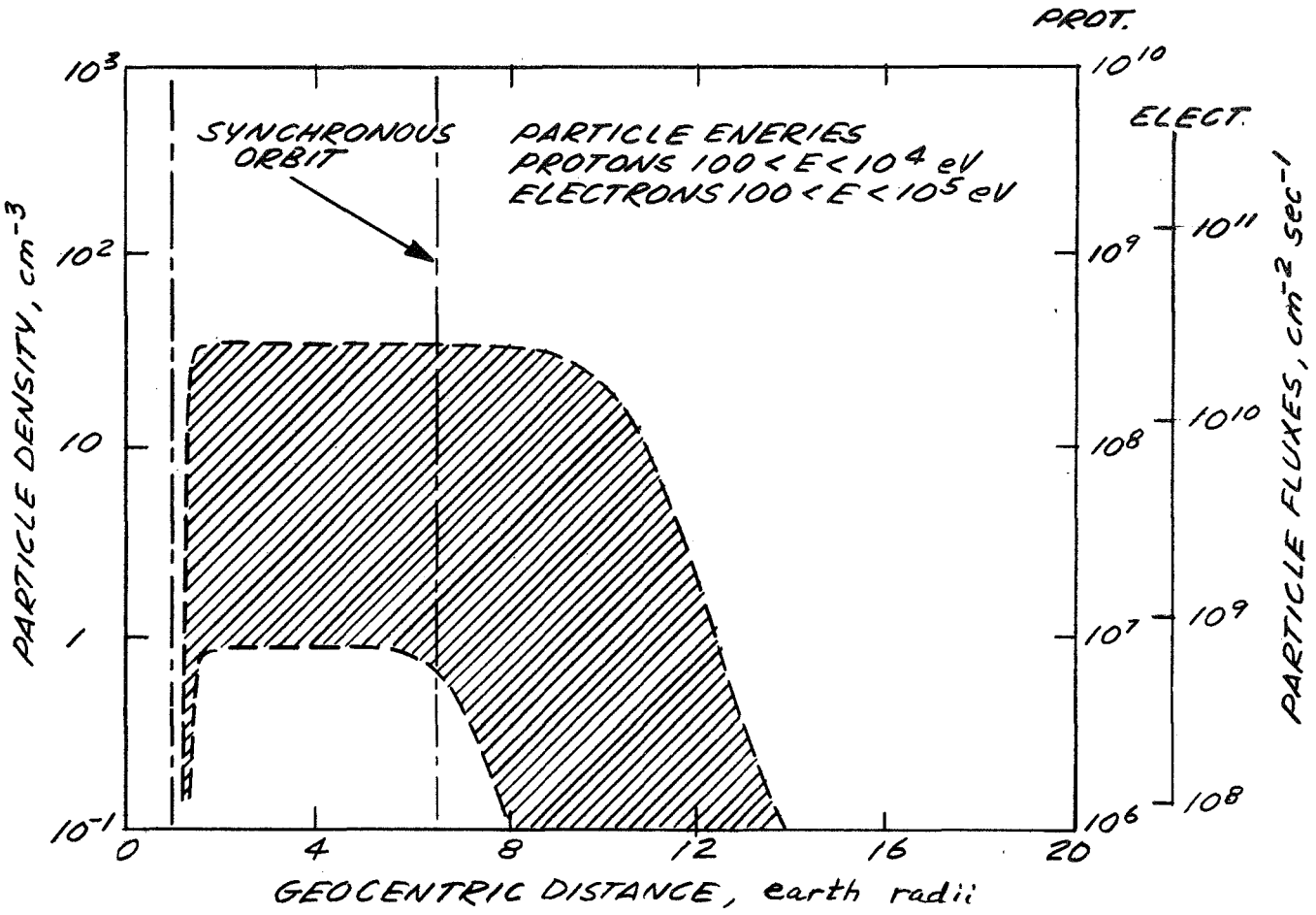

HRL 242-35

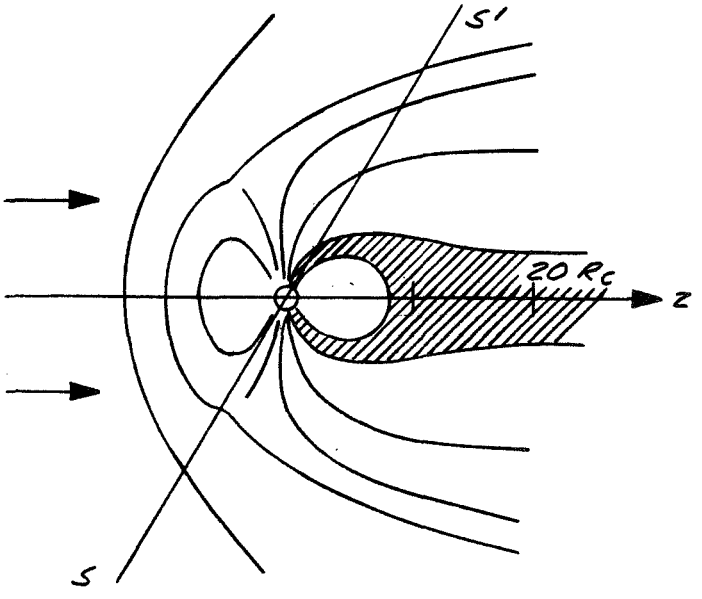

Fig. A-6.
Auroral zone particle population (along axis s-s'). The range shown gives temporal fluctuations and measurement uncertainties.

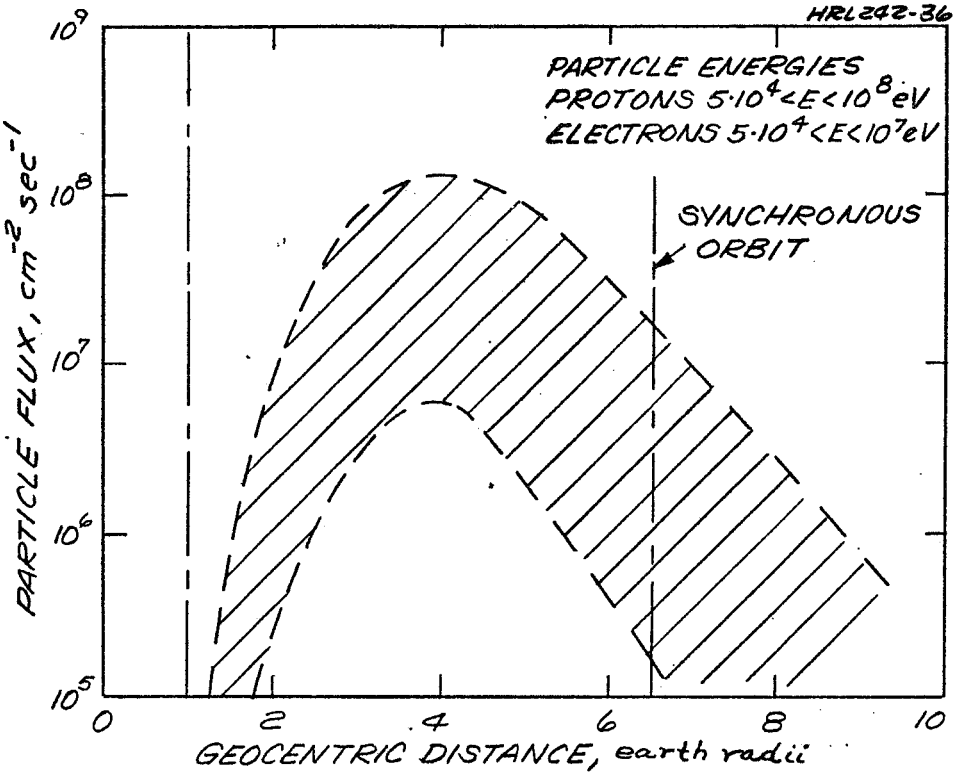

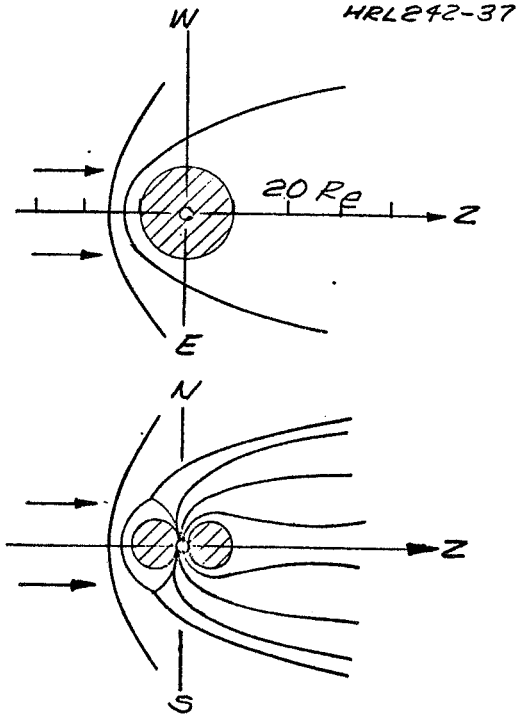

Fig. A-7.
Radiation belt particle fluxes along z-axis. The range shown indicates temporal fluctuations and measurement uncertainties.

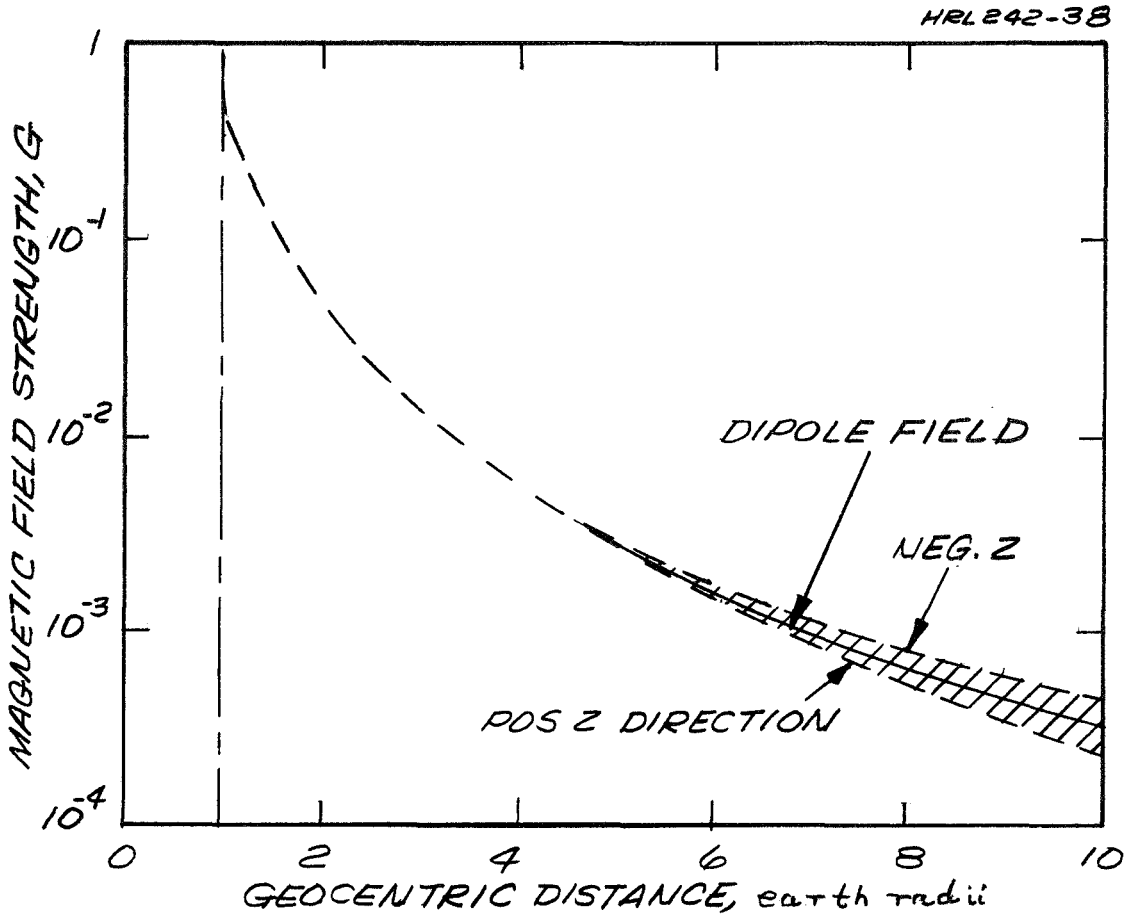

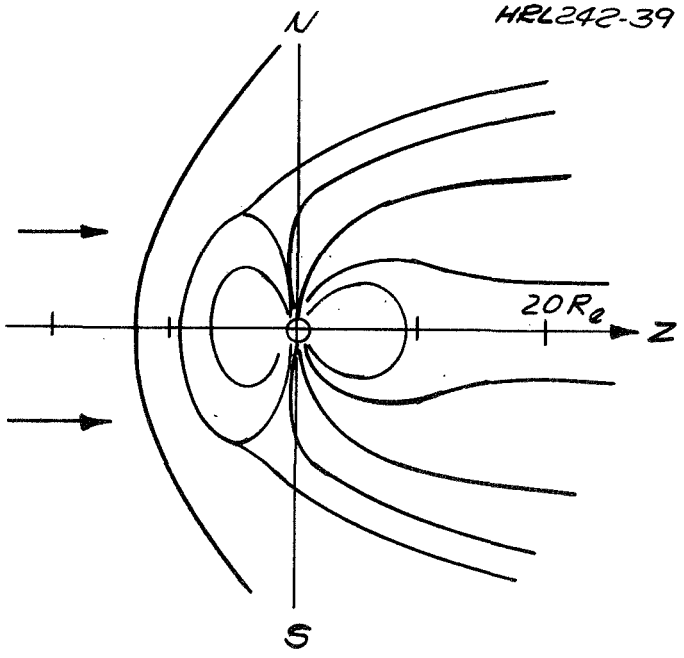

Fig. A-8.
Geomagnetic field along z-axis of geomagnetic cavity. The range of values shown indicates difference between front and back of cavity.

values on the order of 1 V/m (above 100 km altitude). Electric fields in the outer and predominantly in the rearward regions of the geomagnetic cavity are believed not to exceed 10^{-3} V/m.

7. Micrometeoroids

The earth is surrounded by a "dust cloud" of micrometeoroids. The density near earth (within about 1 earth radius) is about two orders of magnitude larger than that in interplanetary space. Meteoroid fluxes near earth as a function of size, obtained from flight data on many spacecraft, have been collected by Moroz (Ref. A-9) (see Fig. A-9). The penetration frequency of 2024-T3AC aluminum by near-earth meteoroids was estimated by Naumann (Ref. A-10). The dependence of the penetration rate upon thickness of the aluminum layer is given in Fig. A-10.

B. SOLAR WIND

The solar wind is a streaming plasma which originates in the solar corona. The corona expands continually and generates a supersonic ionized particle stream which carries along a magnetic field. The solar wind flows around earth at a distance of about 10 earth radii and is deflected away from the earth's surface by the geomagnetic field. The region of deflection, the so-called "bow shock," contains a thermalized solar wind plasma.

Composition: On the average the solar wind is neutral, i.e., it consists of equal numbers (per unit volume) of ions and electrons. Measurements on Mariner-2 (Ref. A-11), IMP-2 (Ref. A-12), Vela-2, Vela-3 (Refs. A-13, A-14), and Pioneer-6 (Ref. A-15) have disclosed the following average ion composition: protons 96%, He^{++} 4%, He^{+} 1%. With time the He^{++} proportion varies over a range from less than 1% to above 15%. Some higher mass ions are also present. Their total number amounts to less than 0.5%. So far, the following ion species have been identified O^{+5}, O^{+6}, and O^{+7} (Ref. A-16).

Density: The particle density of the solar wind near earth has been measured by Mariner 2 (Ref. A-11), IMP-1 (Ref. A-17), IMP-2 (Ref. A-12), Vela-2, and Vela-3 (Ref. A-13), Venus-3 (Ref. A-18), Pioneer-6 (Ref. A-15). The average density at 1 AU is about 5 particles/cm^3. Temporal fluctuations reach maximum values of about 100 particles/cm^3 (during solar eruptions) and minimum values of 0.1 particles/cm^3. Determinations of the solar plasma density near the surface of the sun, obtained with the aid of radio wave refraction measurements, indicate that the plasma density decreases approximately as r^{-2} with distance from the sun (see Fig. A-11). The thermalized solar wind within the bow shock is shown in Fig. A-12.

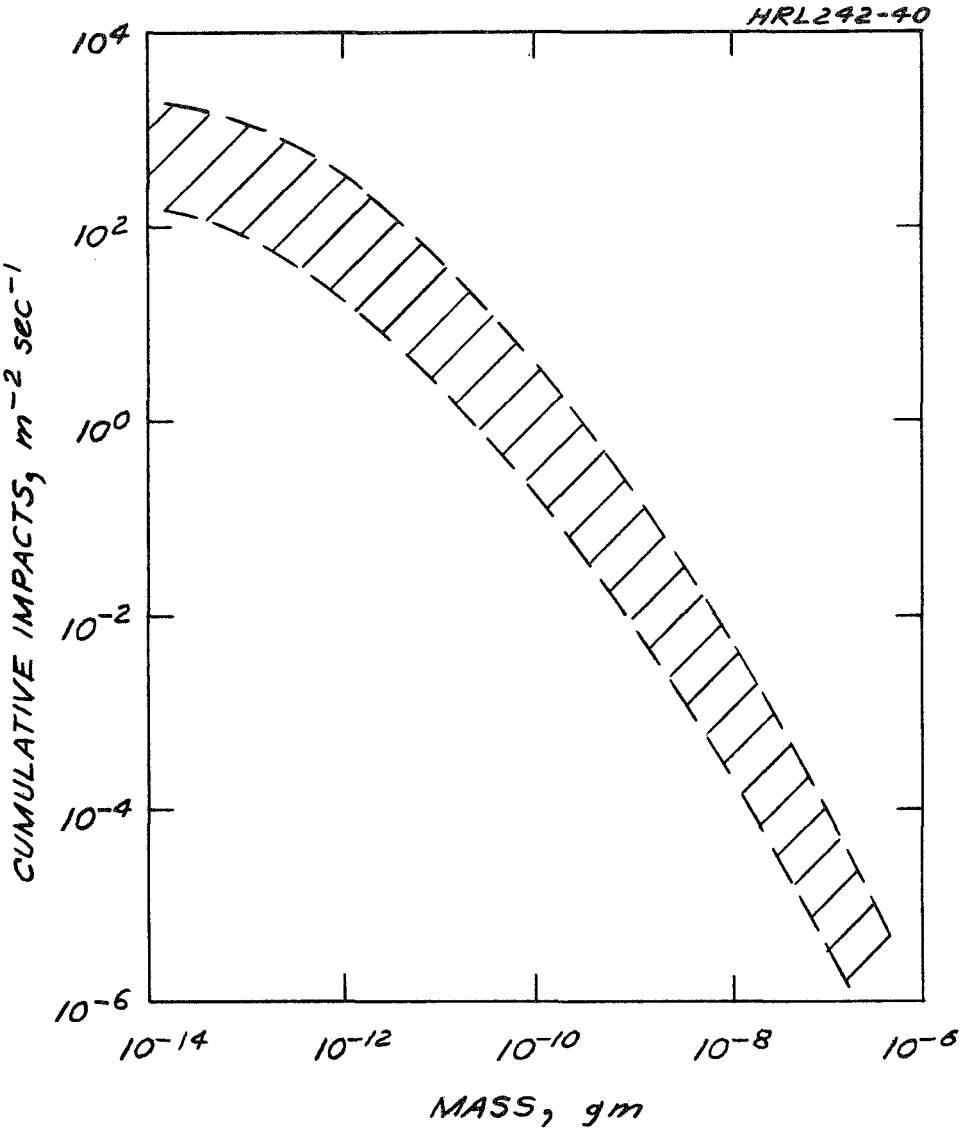

Fig. A-9. Meteoroid fluxes near earth, based upon data collection given by Moroz (Ref. A-9); the range indicates experimental and temporal uncertainty.

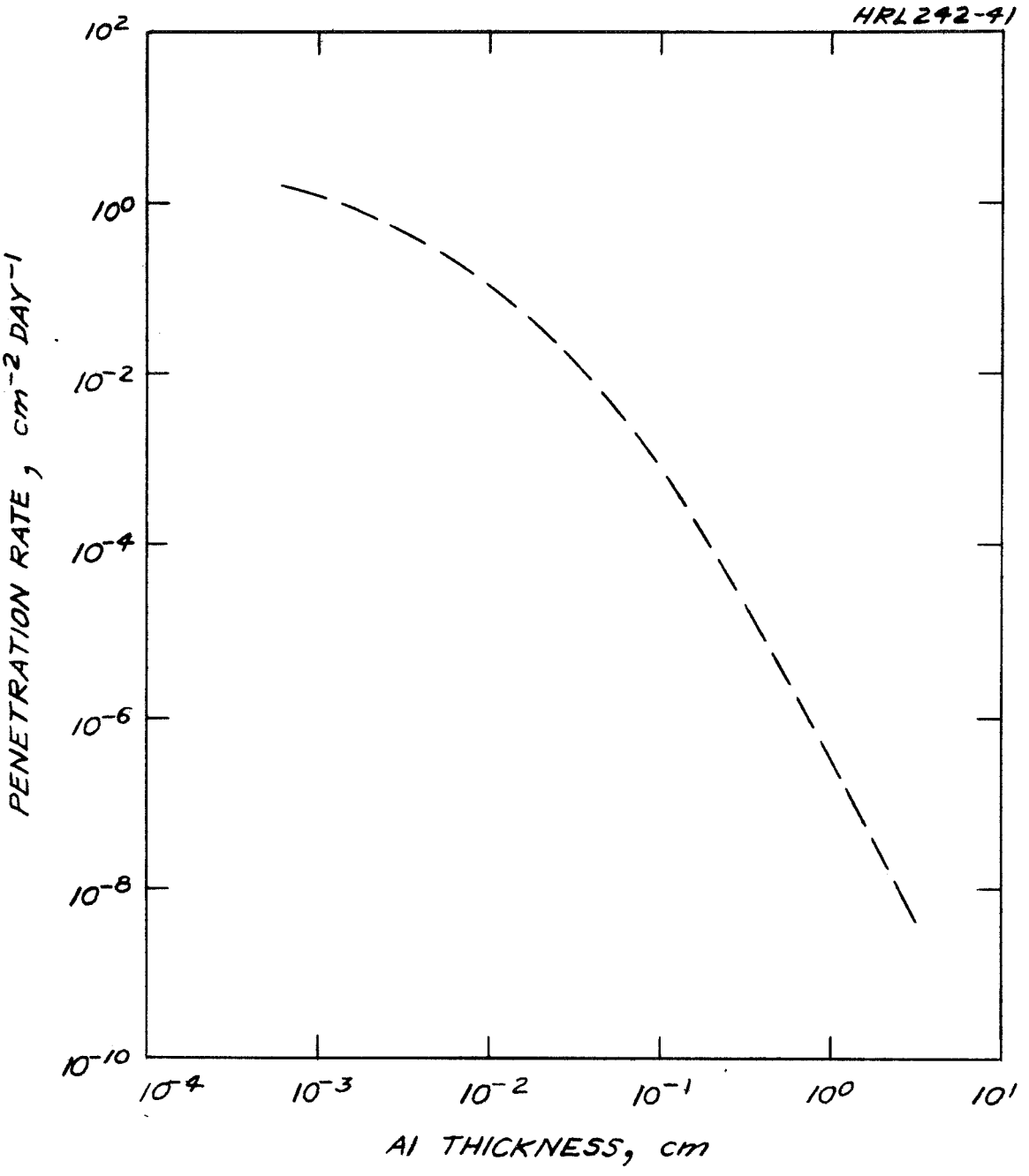

Fig. A-10. Estimates given by Naumann (Ref. A-10) of the penetration frequency of 2024-T3 Al by meteoroids in near earth orbits.

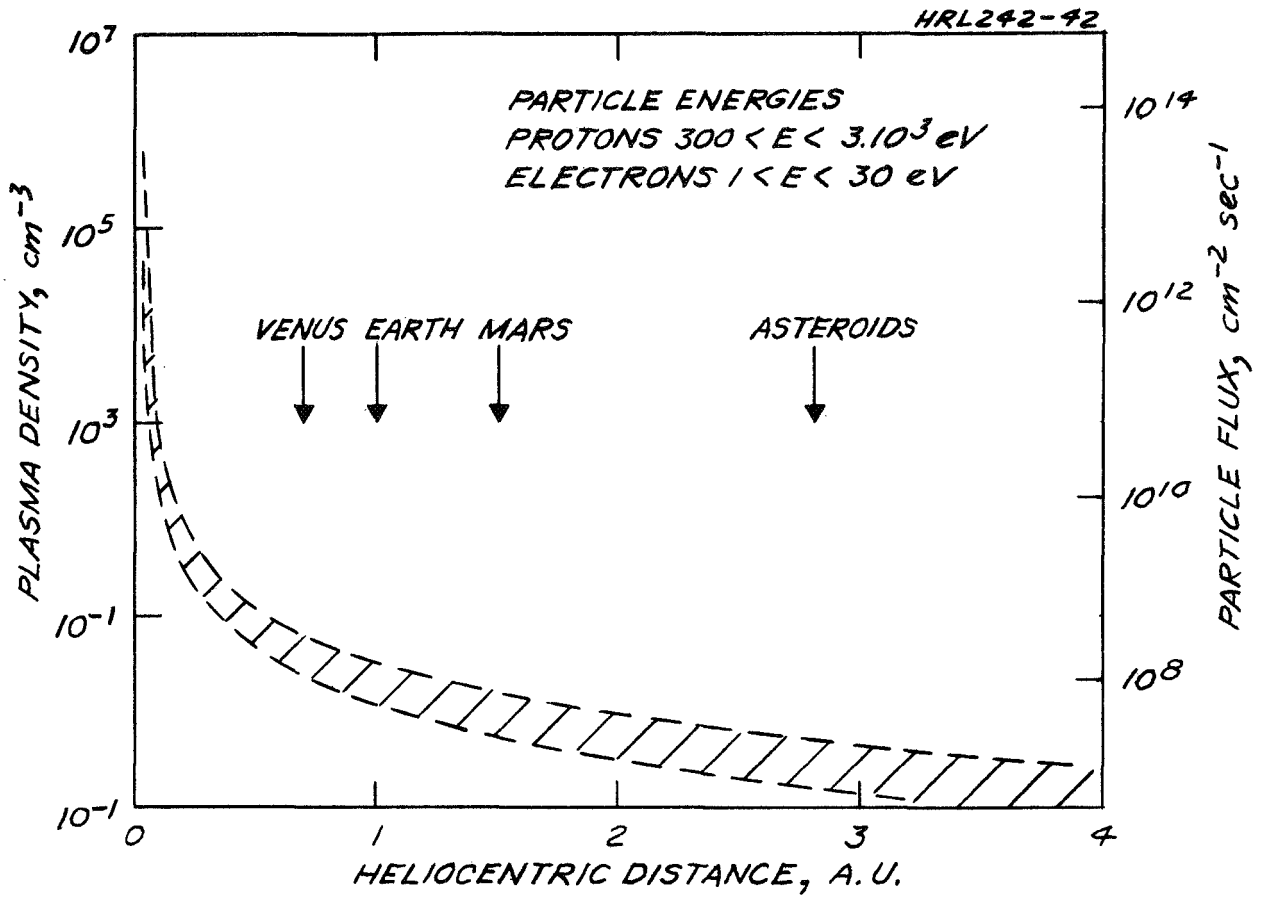

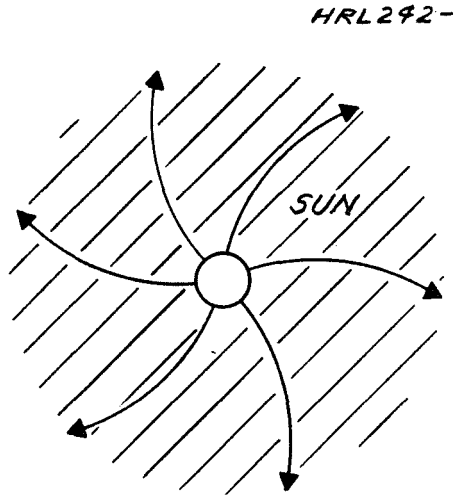

Fig. A-11. Solar wind distribution as a function of distance from sun. The range indicates temporal fluctuations and measurement uncertainties.

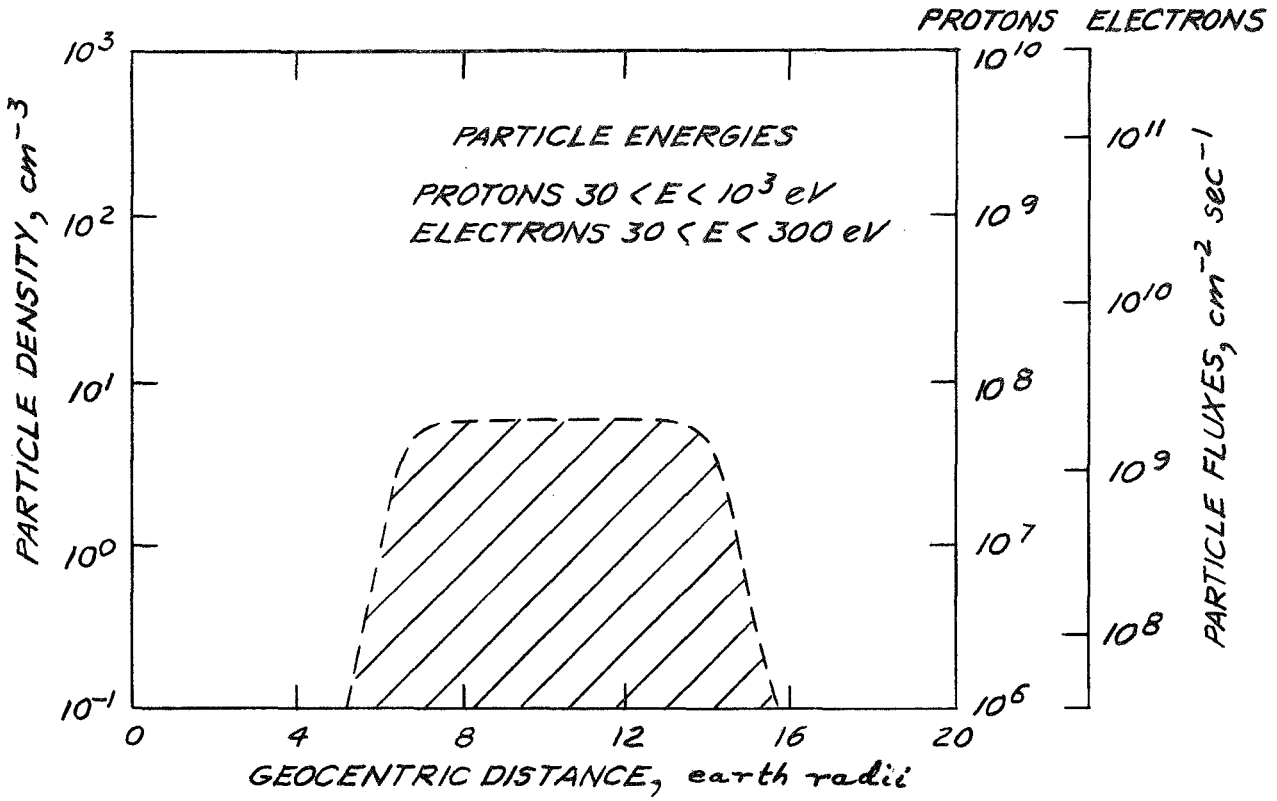

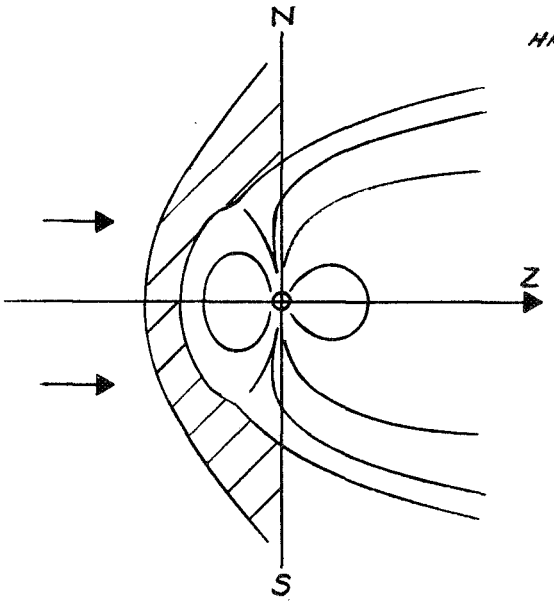

Fig. A-12. Thermalized solar wind between bow shock and magnetospheric boundary along z-axis (toward sun). The range indicates temporal fluctuations and measurement uncertainties.

Velocity: Solar wind directed velocity measurements were performed aboard Mariner-2 (Ref. A-11), IMP-1 (Ref. A-17), IMP-2 (Ref. A-12), Mariner 4, Vela-2 and Vela-3 (Ref. A-13), Venus-3 (Ref. A-18), and Pioneer 5 (Ref. A-15). According to these observations the ions are radially outbound from the sun and move with an average velocity of about 300 km/sec. During solar eruptions the velocity can increase to above 1000 km/sec.

Temperature: Ion temperature measurements on Mariner-2 (Ref. A-11), IMP-2 (Ref. A-12), Vela-2 and Vela-3 (Ref. A-13), and Pioneer 6 (Ref. A-15), have shown average ion temperatures on the order of 2 to 5 x 10^4 °K. Recent indications are that, in the radial direction, the ion temperature may be several times higher than in the transverse direction. During storms, the ion temperature was found to exceed 10^5 °K. To date, neither electron temperatures nor directional electron velocities have been measured. However, it is likely that electron and ion temperatures are comparable. (A directed electron velocity equal to the directed ion velocity would constitute a small fraction of the thermal electron velocity, estimated at about 5 eV, and therefore would be a minor factor.)

Magnetic Field: Observations of the solar magnetic field near earth indicate a 27-day periodicity. Because the sun rotates once every 27 days it is suggested that a linkage exists between the magnetic field near earth and certain surface portions of the sun. During the 27-day cycle the magnetic field undergoes several reversals. Periods between reversals last on the order of 5 to 10 days.

Magnetic field measurements were undertaken aboard Pioneer-5 (Refs. A-19, A-20), Mariner-2 (Ref. A-11), IMP-1 (Ref. A-12), Mariner-4, IMP-3 and Pioneer-6 (Ref. A-15). The average field strength was found to be about 5 γ (= 5 x 10^{-5} G). Variations are typically in the range 1 to 10 γ during quiet periods.

C. INTERSTELLAR MEDIUM

The interstellar medium pervades galactic space outside the influence spheres of stars. The influence sphere of the sun, for example, is believed to extend to distances between 10 and 100 AU. There, a boundary is expected to exist at which the solar wind pressure becomes equal to the interstellar pressure. The properties of the interstellar medium are not well established; the following numbers represent crude estimates (Ref. A-21).

Composition: The prevailing particle component of the interstellar medium is neutral hydrogen. A small percentage of ionized atoms such as sodium and calcium is also present. The latter particles provide enough free electrons to render the medium a rather good conductor. In addition, the interstellar medium contains a cosmic ray population which consists primarily of energetic protons.

Density and Energy: Observations of the 21 cm line suggest that the interstellar hydrogen gas has an average density on the order of 1 atom/cm^3. The gas temperature is estimated to be about 100 ^oK. Cosmic rays appear at an average density on the order of 10^{-10} particles/cm^3, and they possess a median energy of about 10^{10} eV.

Magnetic Field: The galactic magnetic field strength is estimated to be in the range 1 to 10 μG. The field configuration is not known.

REFERENCES

A-1. W. B. Hansen Satellite Environment Handbook, (Stanford Press, Stanford, 1965), pp. 38-39.

A-2. G. P. Serbu, Space Res. 5, 564 (1965).

A-3. G. P. Serbu and E.T.R. Meier, J. Geophys. Res. 71, 3755 (1966).

A-4. D. L. Carpenter, Res. Geophys. 2, 415 (1964).

A-5. J. T. Gosling, et al., J. Geophys. Res. 72, 101 (1967).

A-6. V. M. Vasyliunas, J. Geophys. Res. 73, 2839 (1968).

A-7. J. A. Van Allen, Nature 183, 430 (1959).

A-8. L. R. Davis, et al., Space Res. III, 365 (1962).

A-9. W. A. Cosby and R. G. Lyle, NASA, Special Publications 78 (1965).

A-10. R. J. Naumann, NASA Technical Note D-3717 (1966).

A-11. M. Neugebauer and C. W. Snyder, J. Geophys. Res. 71, 4469 (1966).

A-12. J. H. Wolfe, R. W. Silva, and M.A. Myers, Space Research (Spartan Books, New York), (1966), Vol. VI, p. 680.

A-13. T. H. Coon, Radiation Trapped in the Earth's Magnetic Field, McCormac, Ed. (Randel, 1966), p. 231.

A-14. A. T. Hundhausen, et al., J. Geophys. Res. 72, 87 (1967).

A-15. T. H. Wolfe, et al., J. Geophys. Res. 71, 3329 (1966).

A-16. S. T. Bame, et al., Phys. Rev. Lttrs 20, 393 (1968).

A-17. T. H. Wolfe, et al., J. Geophys. Res. 71, 1319 (1966).

A-18. K. I. Gringauz, et al., Paper presented at Inter-Union Symposium on Solar Terrestrial Phys., Belgrade, 1966.

A-19. P. T. Coleman, et al., Report Inst. Geophys. Planet Phys., University of California No. 501, 1966.

A-20. P. T. Coleman, et al., Report Inst. Geophys. Planet Phys. University of California No. 504, 1966.

A-21. E. N. Parker in Plasma Astrophysics, P. A. Sturrock Ed, (Academic Press, New York, 1967), p. 242.

APPENDIX B - CURRENT COLLECTION BY A SPHERICAL PROBE

The current collection rates by a spherical probe from an isotropic plasma for the case where the plasma sheath is large compared with the probe radius can be determined as follows:

According to Langmuir, the space charge limited current I between concentric spheres of radius a and r_o, with a voltage V applied between both is given by

$$I = \frac{4\sqrt{2}}{9} \left(\frac{e}{m}\right)^{1/2} \frac{V^{3/2}}{\alpha^2} \qquad \text{(cgs units)} \qquad \text{(B-1)}$$

where α is a complicated function of a and r_o. For cases where $r_o >> a$, α can be expressed as

$$\alpha^2 \cong 2\ (1.11\ r_o/a - 1.64)^{3/2} \qquad \text{(B-2)}$$

or, still more approximately, by

$$\alpha^2 \cong 2.32\ (r_o/a)^{3/2} \qquad \text{(B-3)}$$

Equations (B-1) and (B-3) together yield

$$I = 0.27 \left(\frac{e}{m}\right)^{1/2} (a/r_o\ V)^{3/2} \qquad \text{(B-4)}$$

If a biased probe attracts charges from a plasma, the collected current must just match the random arrival current at the sheath edge (ignoring pre-sheaths). This then requires that

$$I = 4\ \pi\ r_o^2\ j_r \qquad \text{(B-5)}$$

where j_r is the random current density of the attracted species in the plasma. Combination of (B-4) and (B-5) yields

$$r_o = \left[\frac{1.08}{\pi} \left(\frac{e}{m}\right)^{1/2} \frac{(aV)^{3/2}}{j_r}\right]^{2/7} \qquad \text{(B-6)}$$

for the plasma sheath radius. The current collection is obtained by introducing (B-6) into (B-5):

$$I = 4\ \pi \left[\frac{1.08}{\pi} \left(\frac{e}{m}\right)^{1/2}\right]^{4/7} (a\ V)^{6/7}\ j_r^{3/7} \qquad \text{(B-7)}$$

This is the desired expression for the collection of charged particles from an isotropic plasma. Equation (B-7) is valid for both electrons and ions; however, different values for the mass m must be used. Equation (B-7) applies to all cases where the impact parameter p is larger than the sheath radius r_o.

APPENDIX C - ELECTROLYTIC TANK STUDIES

An electrolytic tank simulation technique was used to determine the plasma boundaries and leakage currents for two geometries intermediate between the high and low plasma density limits in which the sheath width was either much smaller or larger than the solar array. In the tank, the spacecraft was modeled by a wedge section of a unipotential circular disc, while the plasma boundary was simulated by a curved metal electrode. A dielectric strip was placed in the plane of the disc between the disc and the plasma boundary to insure that no flux lines crossed the plane of symmetry. The space charge simulation currents were calculated for an assumed emitted current and trial plasma boundary position; the potential distribution was then measured and the emitted current distribution was calculated from the measured potential. This procedure was iterated until the measured and calculated currents were in agreement.

The two cases solved in the tank had plasma sheath thicknesses comparable to the size of the disc. The first case had a sheath thickness (on the axis) equal to the disc diameter, while the second case had a sheath thickness (on the axis) equal to the disc radius. In the former case the final plasma boundary was very nearly spherically shaped with a slight inward bowing at the equator. In the second case the plasma boundary was oval. The plasma boundary for case II is shown in Fig. C-1. The leakage currents calculated for these two cases have been converted to power loss and plotted in Fig. 4 of this report. It is seen that the computed points lie close to the curve extrapolated between the low and high density plasma cases.

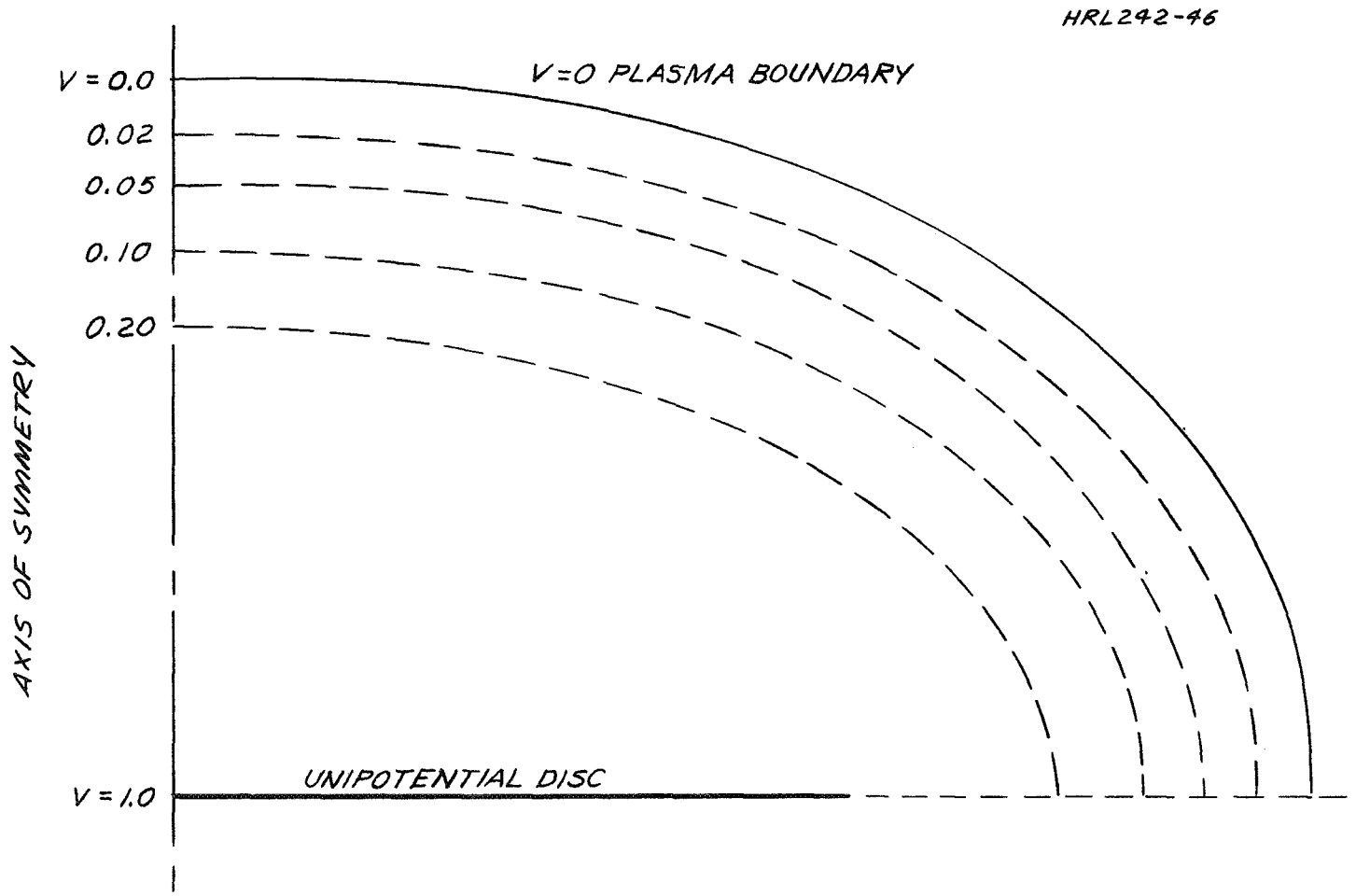

Fig. C-1. Case II plasma boundary found in electrolytic tank.

APPENDIX D - DISC MODEL

An analytic model has been developed which accounts for the fact that the array is actually a disc rather than spherically shaped. The basis for this method which is valid in the low plasma density limit was originally suggested by Matricon (Ref. D-1) and has been used by Ivey (Ref. D-2) to find the space charge limited current flow from planes, cylinders, and spheres to unsymmetrically shaped anodes. The method consists in finding the space charge free capacitance of the unsymmetrical geometry and equating it to the capacitance of a planar, cylindrical, or spherical diode. From this, an equivalent anode position is found which is then used in the expression for the space charge limited current for the particular geometry applicable. For our case we desire the current from an outside emitting sphere to an inside concentric disc. It is required that the plasma density be low enough that the plasma boundary is actually spherically shaped and that it is far enough away from the disc that the vacuum equipotentials are nearly spherically shaped. It is shown in Ref. D-3 that the equipotentials around such a charged disc are oblate spheroids near the disc, while for distances greater than approximately a disc diameter away from the disc the equipotentials are very nearly spherically shaped. The electrostatic capacitance for a disc of radius r_d surrounded by a sphere of radius r_o is given by

$$C_{disc} = \frac{8\,\varepsilon_\sigma\, r_d}{1 - \frac{2}{\pi}\cot^{-1}\frac{r_o}{r_d}}$$

while concentric spheres have a capacitance given by

$$C_{sp} = \frac{4\pi\varepsilon_o\, r_o\, r_e}{r_o - r_e}$$

where r_o and r_e are, respectively, the outer and inner sphere radii. By requiring that $C_{disc} = C_{sp}$, we can calculate an "equivalent" inner sphere radius r_e. Table D-1 shows normalized r_o/r_e values for various ratios r_o/r_d. It also shows the total current and current density at the emitting sphere for a disc radius of 10^3 cm. Because the total current is a function of r_o/r_d only (at a fixed voltage), the current density for other disc radii r_d is given by multiplying $J(r_o)$ by $(10^3/r_d)^2$.

REFERENCES

D-1. M. Matricon and S. Trouve, Onde Elec. 30, 510 (1950).

D-2. H. Ivey, J. Appl. Phys. 24, 1966 (1953).

D-3. P. Moon and D. Spencer, Field Theory for Engineers D. Van Nostrand, New York (1961), p. 276.

TABLE D-1

Concentric Sphere Configuration with same Electrostatic Capacitance as Disc-Sphere Configurations with $a = 10^3$ cm, together with total current and current density at outer sphere for V = 2000 V

r_o/r_d	r_o/r_e	I, A	$J(r_o)$, A/cm^2
2.0	3.21	0.881	1.75×10^{-8}
2.5	4.0	0.527	0.661
3.0	4.78	0.361	0.32
3.5	5.54	0.273	0.177
4.0	6.33	0.206	0.102
4.5	7.1	0.165	0.0653
5.0	7.9	0.138	0.044
6.0	9.95	0.0904	0.02
7.0	11.0	0.076	0.0123
8.0	12.75	0.061	0.0076
9.0	14.2	0.0504	0.00494
10	15.8	0.0437	0.0035

APPENDIX E - DIGITAL COMPUTER TRAJECTORY CALCULATIONS

A. INTRODUCTION

The trajectories of charged particles in the vicinity of an array with insulating surfaces (except for tabs) have been studied for charged particles originating either at the plasma boundary or at the array. First attempts at this problem used the electrolytic tank and the analog computer to trace trajectories, but it was found the fields were so weak at distances away from the array comparable to a fraction of the width of a solar cell that the trajectory tracer electronics were masked by noise. It was then decided to solve the problem on the digital computer. The model used for this analysis is shown in Fig. E-1. The array was assumed to be a "stripe" pattern of infinite extent in the x direction with no variation in the y direction. All distances were normalized to the width of one solar cell (~ 2 cm), taken as a single period in the x direction. Because the area of the cell tabs represents about 5% of the total cell area, the "average" potential seen by the space plasma (for an array voltage of + 2000 V) is approximately 100 V (see main text). In the densest regions of the ionosphere this leads to a sheath width of about 40 cm, or a normalized z of 20. For most trajectory calculations z was taken to be 20.

B. DESCRIPTION OF POTENTIAL

At the surface of the array the potential is shown in Fig. E-1. Because it is periodic in the x direction, first attempts at representing the potential characterized by sharp positive peaks separated by wide zero potential valleys resulted in a Fourier series of the form

$$V(x,z) = \sum_n a_n \cos nx \, e^{-nz} + Az$$

The applied field A is necessary to make the potential vanish at $z = z_o$ (the plasma boundary). However, when the above series was differentiated to produce the electric field components, it was found that the series was very slowly converging near the tab boundary where the field behaves as the derivative of a delta-like function. It was found that a much better representation of the potential could be obtained by using a Fourier integral representation.* In this method the potential of a single tab at $x = 0$ was evaluated in closed form. The potentials of tabs placed at $x = \pm 1, \pm 2 \ldots$ then were summed up producing a good approximation to the potential over the region $-0.5 \leq x \leq 0.5$. The potential so derived for the region $-0.5 \leq x \leq 0.5$ was then extended periodically over the entire x axis. The computer was programmed to compute the potential at, for example, $x = 10.4$, by using the previously evaluated potential at $x = 0.4$. In practice it was found that a very good approximation was obtained by adding the contributions from ten adjacent tabs.

* This method was suggested by Dr. R. Seliger

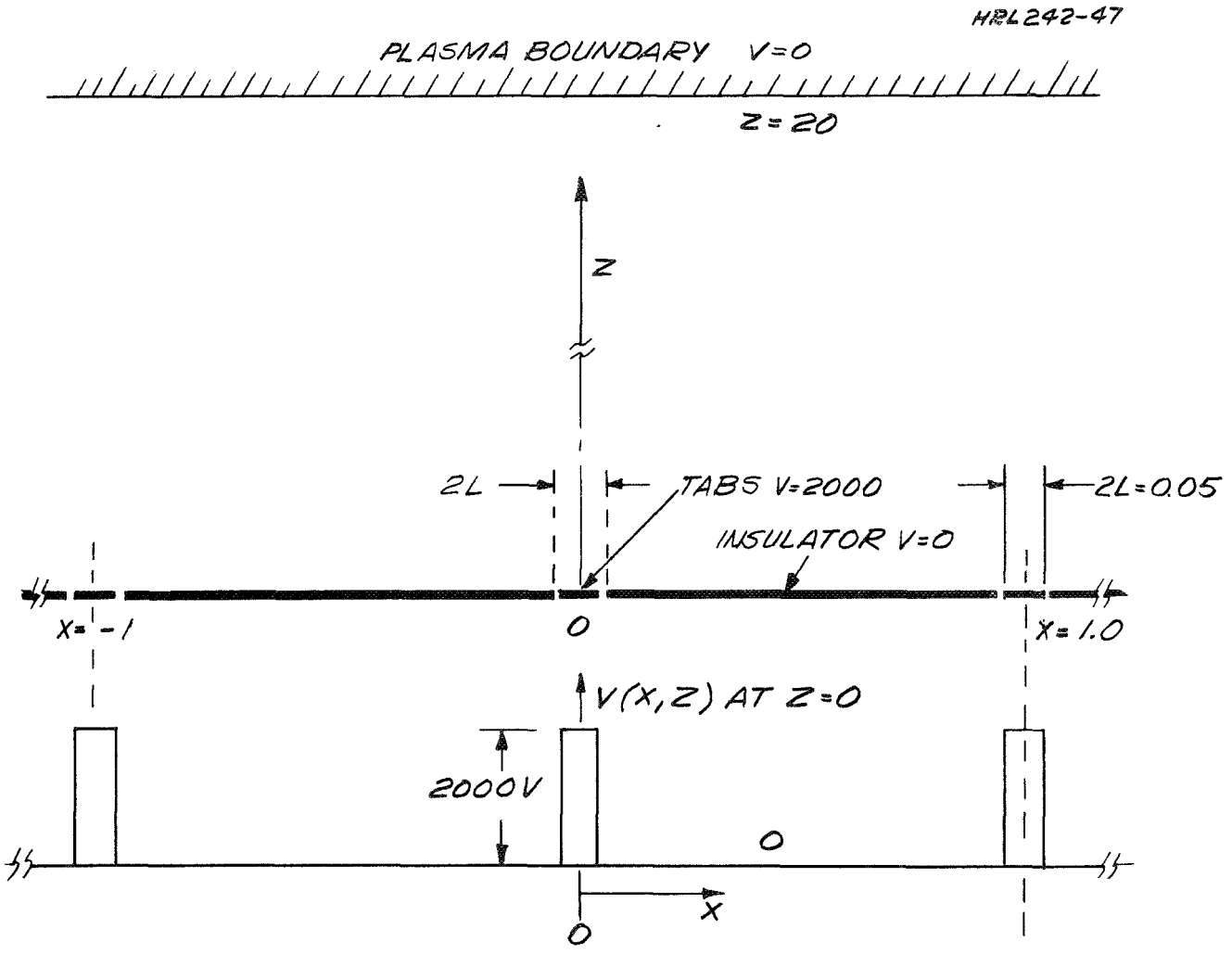

Fig. E-1. Array-plasma geometry used for digital computer trajectory calculations.

It can be shown that the following equation satisfies Laplace's equation for the above derived potential distribution (as, in fact, for any arbitrary potential V (x, 0) along the x axis)

$$V(x,z) \quad \frac{1}{\pi} \int_{-\infty}^{\infty} V(\xi, 0)\, d\xi \int_{0}^{\infty} e^{-\lambda z} \cos(\xi - x)\lambda \, d\lambda$$

For the case of a single tab placed at the origin

$$\begin{aligned} V(x,0) &= 0 && x < -1 \\ V(x,0) &= V && -1 < x < 1 \\ V(x,0) &= 0 && x > 1 \end{aligned}$$

using

$$\int_{0}^{\infty} e^{-\lambda z} \cos(\xi - x)\, \lambda \, d\lambda = \frac{z}{(\xi-x)^2 + z^2}$$

V becomes

$$V(x,z) = \frac{Vz}{\pi} \int_{-\ell}^{\ell} \frac{d\xi}{(\xi-x)^2 + z^2} = \frac{V}{\pi} \left[\tan^{-1}\left(\frac{1+x}{z}\right) + \tan^{-1}\left(\frac{1-x}{z}\right)\right].$$

By superposition, the potential of an array of tabs placed at x = 0, x = ± 1, x = ± 2...x = ± N is given by the following series:

$$V(x, z) = \frac{V}{\pi} \sum_{-N}^{N} (\tan^{-1} u + \tan^{-1} \bar{u}) + Az$$

where

$$u = \frac{1 + (x - N)}{z} \quad \text{and} \quad \bar{u} = \frac{1 - (x - N)}{z}$$

As with the Fourier series representation, the applied field A is necessary to make the potential vanish at $z = z_o$. A graph of this potential as a function of x is shown in Fig. E-2 for different z positions. The rapid decay in the z direction is shown in Fig. E-3 where the potential is plotted as a function of x for x = 0 (over a tab) and x = 0.5.

C. TRAJECTORY CALCULATIONS

The trajectory calculations were performed on the GE635 computer using a program written to solve the following two dimensional equations of motion. (e/m was taken as 1 because the scale for time is arbitrary.)

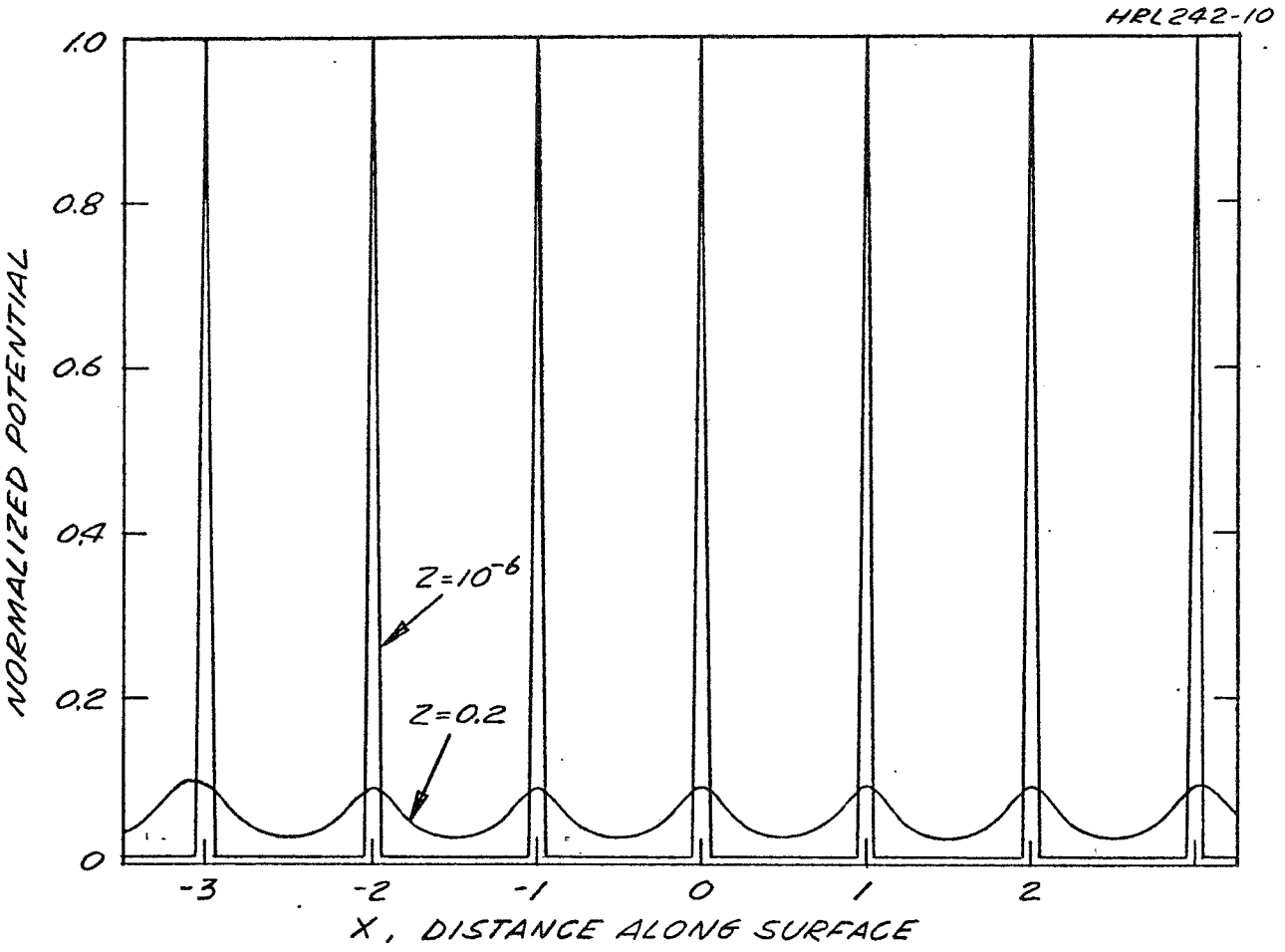

Fig. E-2. Normalized potential as a function of distance along surface for different z positions.

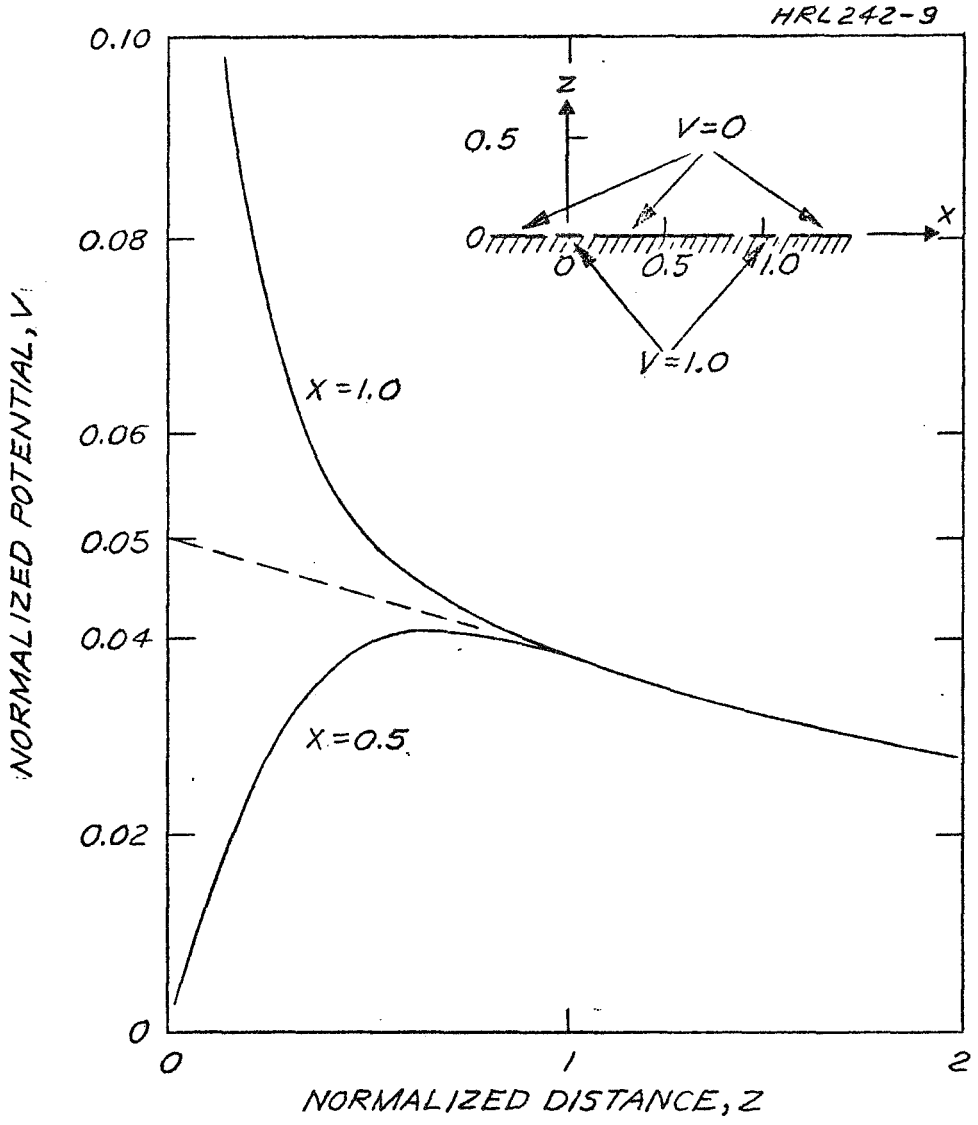

Fig. E-3. Potential as a function of z for x = 0 (over a tab) and x = 0.5 (over an insulator).

$$\frac{dv_x}{dt} = E_x = \frac{-\delta V(x,z)}{\delta x}$$

$$\frac{dx}{dt} = v_x$$

$$\frac{dv_z}{dt} = E_z = \frac{-\delta V(x,z)}{\delta z}$$

$$\frac{dz}{dt} = v_z$$

subject to the initial conditions

$$x = x_o, \quad z = z_o$$

$$\dot{x} = \dot{x}_o, \quad \dot{z} = \dot{z}_o$$

$$\text{at } t = 0$$

These four simultaneous first order equations were integrated with respect to time using a Library subroutine which uses the Adams-Moulton method of integration. This routine uses a variable step size Δt to keep the truncation error less than a predetermined amount. The input to the trajectory program are the initial positions x_o, z_o and velocity $\dot{x}_o$, $\dot{z}_o$ of the electrons (ions). A trajectory computation was stopped when $z < 0$ (collected on array) or $z > z_o$ (collected by plasma). The outputs of the program are CALCOMP plots of the trajectories.

D. RESULTS

1. Electrons Emitted from the Plasma Boundary with Normal Velocities

In this case a uniform distribution of electrons in the region $0 < x < 1$ was directed toward the array with initial energies of 2, 10, and 20 eV at the plasma boundary at $z = 20$. Typical trajectories for these cases are shown in Figs. E-4. We see that, for normal incidence, the tabs collect all electrons on the first pass even though the electrons are energetic enough to be collected on the insulator at $V = 0$ (they were emitted with > 0 initial velocities). We also find that low energy electrons are attracted toward the tabs sooner than electrons emitted with high initial energy. An extreme case was run with an initial energy of 100 eV; in this case the electrons travel in practically straight lines toward the array and nearly all are collected on the insulator. However, in actual practice this could not happen because the insulator would charge up to a potential sufficiently negative to repel all further electrons.

2. Electrons Emitted from the Plasma Boundary with Isotropic Velocity Distribution

For this case groups of electrons were emitted at the plasma boundary at $z = 20$ at uniformly spaced x positions between the center of a tab and the center of a insulator ($x = 0.1, 0.2, 0.3, 0.4, 0.5$). Each group had electrons leaving at a series of uniformly spaced angles, defined as $\theta = \tan^{-1} z_o/x_o$, ranging from 90^o (normal incidence) to 9^o (nearly oblique incidence). For all these cases the electrons had initial total energies of 2 eV which is in the range expected for electrons associated with the thermal plasma. The results of a typical trajectory calculation at a fixed x position is shown in Fig. E-5. We see the appearance of the trajectories are quite different than those obtained in the previous case (initial trajectories normal to plasma boundary). In the present case many electrons miss the tab on the first pass and are reflected from the array. These particles then make wide parabolas in the uniform field region, much like particles thrown up in a gravitational field. When they return to the array some are collected but many make additional loops before being

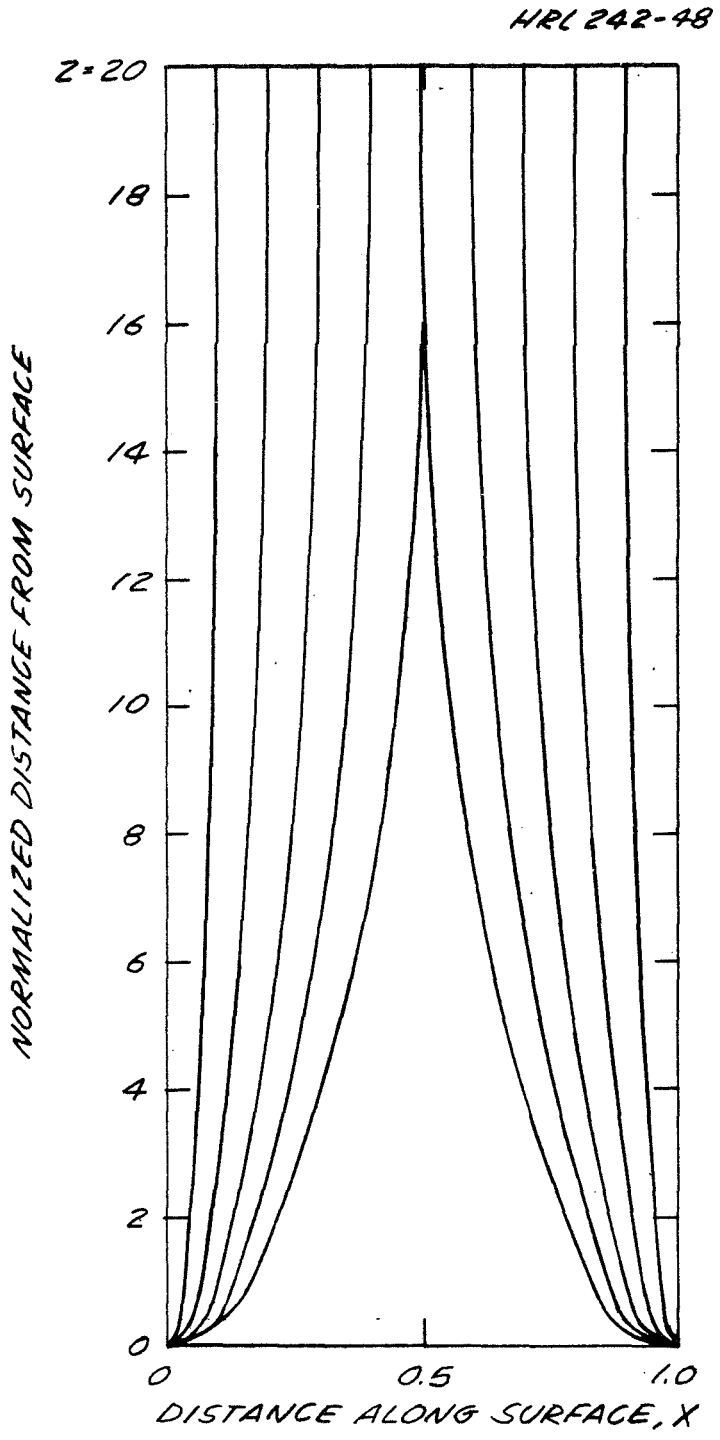

Fig. E-4. Computer generated trajectories of electrons emitted from plasma boundary at x = 20 with 10 eV initial energy.

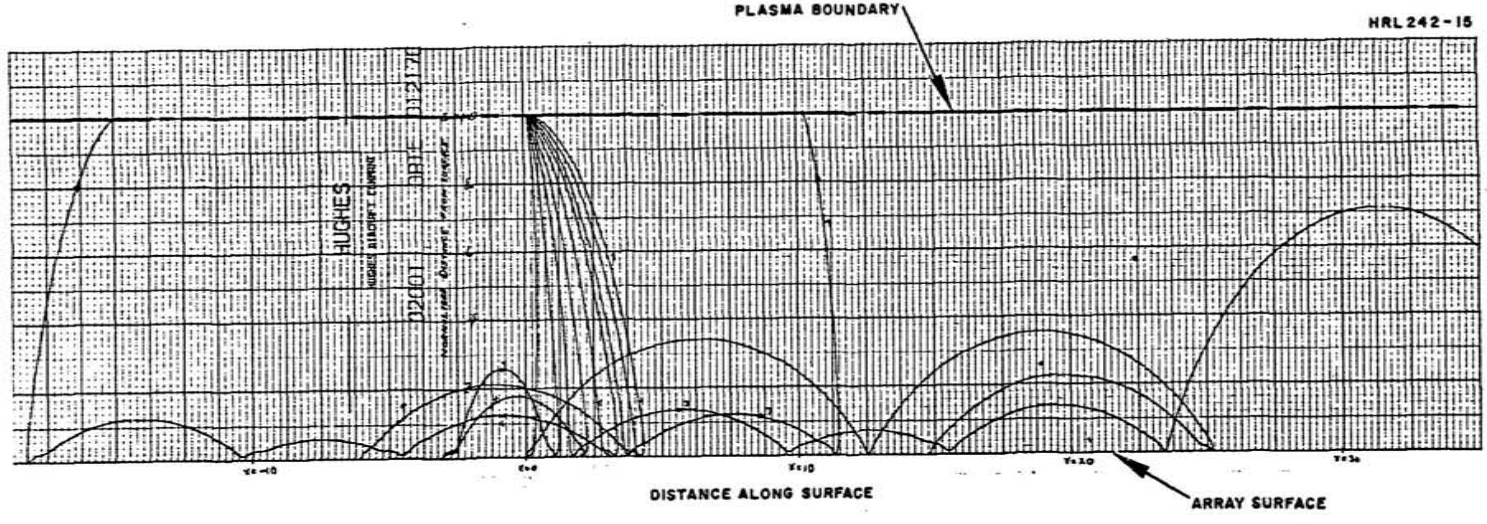

Fig. E-5. Trajectories of attracted plasma electrons; surface is 95% insulating, tabs are at 2000 V.

collected on the tabs or on the array. A few of the particles are reflected from the array at nearly normal incidence; these particles then are reflected back into the plasma. The general description of the trajectories is so complicated that a statistical averaging was used to characterize their behavior. The following data summarize the results of 77 trajectories leaving the plasma boundary at z = 20:

56 or 73% were collected on the tab
15 or 19.5% were collected on the insulator
6 or 7.8% were reflected back into the plasma
63 loops were performed (on the average, about 1 loop per trajectory).

Because the effect of looping is to add negative space charge and because in reality the collection rate on the insulator could not be 19% (because it would charge up negatively enough to repel incoming electrons), a modified plasma sheath thickness of z = 10 was used to determine whether the collection rate was strongly dependent on sheath thickness. Results of 54 trajectory calculations for this modified sheath thickness are summarized below:

33 or 60.1% were collected on the tab
10 or 18.5% were collected on the insulator
11 or 20.4% were reflected back into the plasma
79 loops were performed (on the average, about 1.4 loops per trajectory).

Comparing these averages with the z = 20 case, we see that the main effect of bringing the plasma boundary closer is to increase the number of electrons reflected back into the plasma at the expense of those collected on the tabs. The percentage collected on the insulator (this could not occur in practice because of the previously mentioned arguments) is nearly the same. From the results of the above calculations it is concluded that with the decrease in plasma sheath width trapping becomes less important and the current approaches the value determined by the one-dimensional theory.

3. Secondary Electrons (Ions) Emitted from the Tabs

For the case of a negative array it was decided to investigate the trajectories of secondary electrons released from tabs by impacting ions and photons. Trajectories were calculated for an array voltage of -2000 V. The results for electrons emitted normal to the tab with an initial energy of 2 eV are shown in Fig. E-6. We see that all electrons are collected by the plasma, even though the electrons which are emitted at the edge of the tab leave at quite oblique angles. The latter group of electrons still receives sufficient z directed motion upon leaving the tab not to be collected by the insulator. These results are also applicable to secondary ions leaving the tabs of a positive array. It is concluded that particles which are released from conducting regions of the array (solar cell tabs, etc.) are never collected by insulating areas (cover slides, etc.)

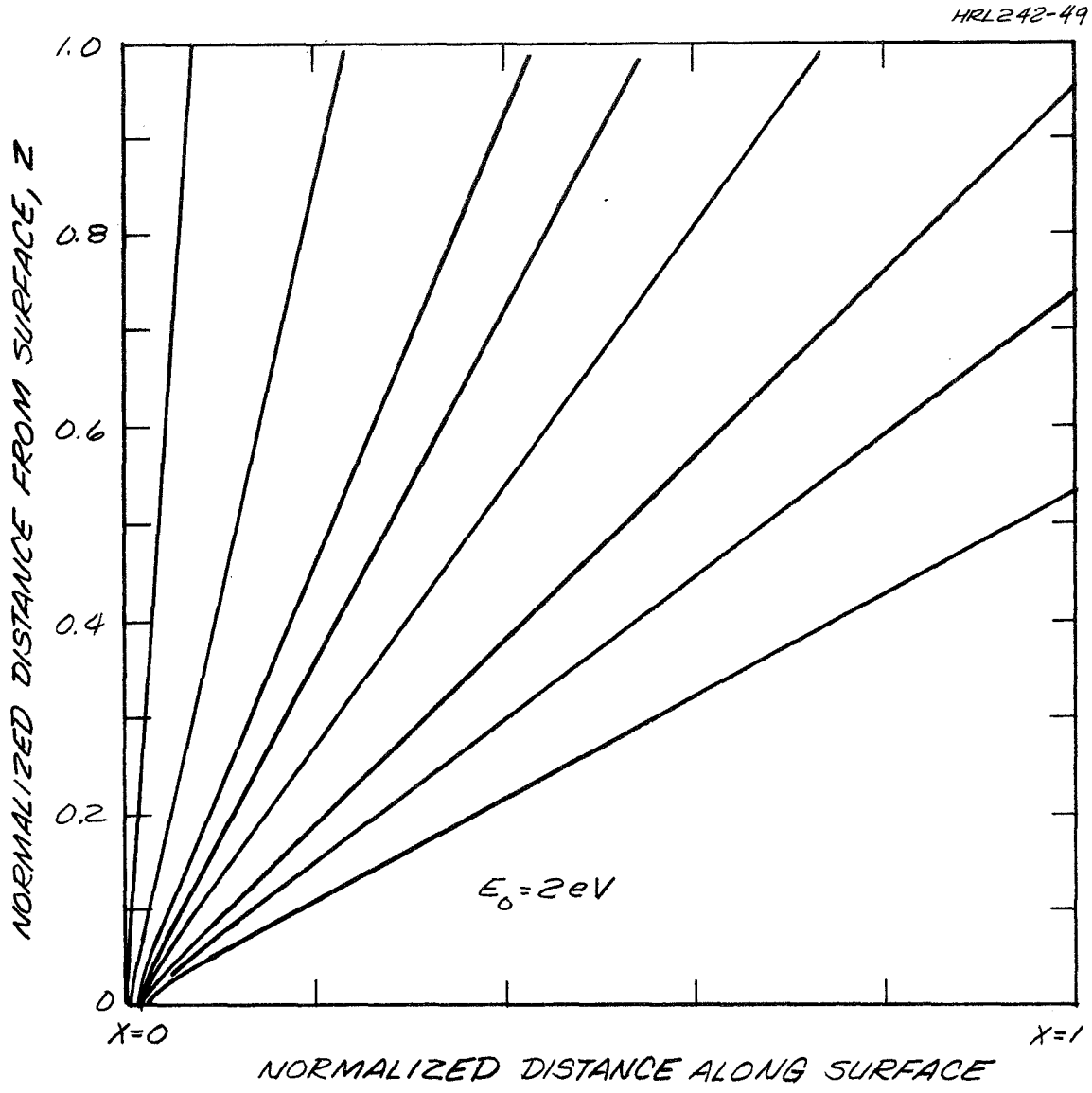

Fig. E-6. Computer generated trajectories of electrons emitted from (negative) tabs with 2 eV initial energy. Plasma boundary at z = 20.

4. Secondary Electrons (Ions) Emitted from the Insulator

The result of trajectory calculations for electrons leaving the insulating surface regions of a positive array is shown in Fig. E-7. For this case, electrons were emitted from the region $0 < x < 0.5$ with 2 eV initial energy in the normal direction. The trajectories are similar in appearance to those for particles emitted from the plasma boundary with oblique angles. In this case the particles are repeatably reflected from the array, making wide loops before being collected. Out of ten electrons leaving the insulator,

5 or 50% were collected on the tabs
2 or 20% were collected back on the insulator
3 or 30% were collected on the plasma.

Sixteen loops were performed, so that on the average there were 1.6 loops per trajectory. The principal effect of looping is to add negative space charge and bring the plasma boundary closer. This increases the collection rate of the plasma at the expense of the tab collection rate. In the present case this would not change the collection rate of the insulator and, thus, it is expected that an equilibrium condition will be established in which the insulator potential adjusts itself to a value such as to reduce the collection of secondary electrons by the tabs to zero. This means that the insulating surface potential tends to rise. The degree to which this happens depends upon the ratio of photoemitted electron current reaching the tabs to plasma electron current attracted to the insulator surfaces. A noticeable rise in insulator potential is expected to occur only in a very tenuous plasma environment.

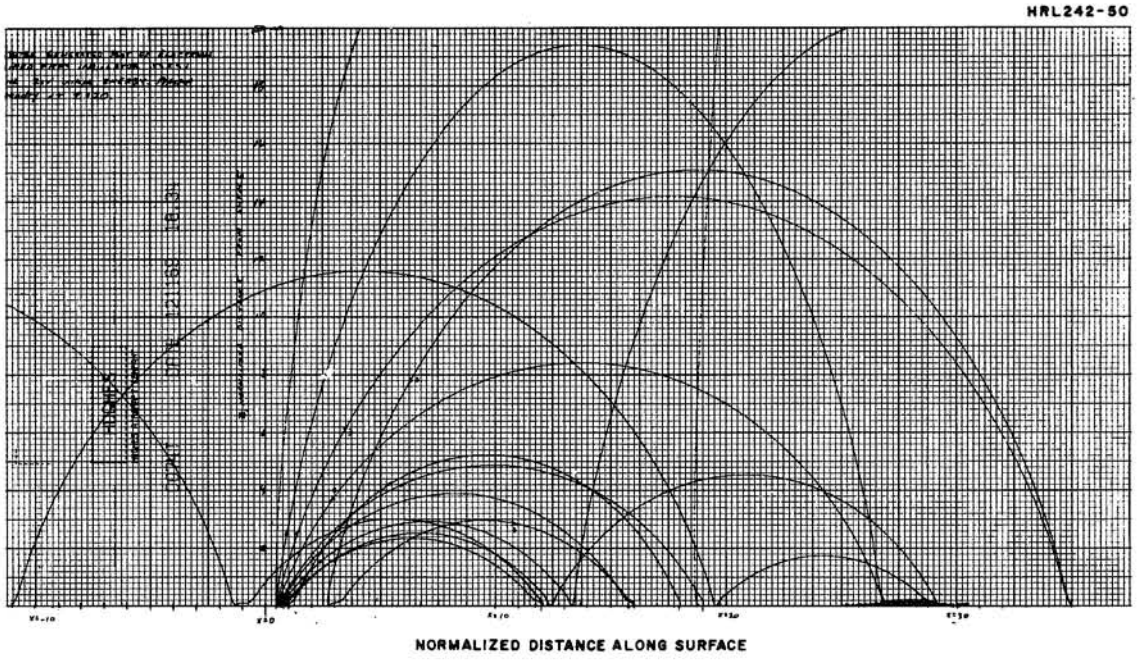

Fig. E-7. Computer generated plot of electrons emitted from insulator $0.5 < x < 1$ with 2 eV initial energy plasma boundary at $z = 20$.

APPENDIX F - THRUST BEAM CURRENT LEAKAGE

The effect of the thrust beam on the current collection to the array was investigated using a digital computer program developed at HRL by G. Nudd and K. Amboss under a JPL contract (JPL Contract No. 952129). This program has been used extensively at HRL for both electron gun and ion optical studies. It is a version of W. Herrmannsfeldt's Stanford program (Ref. F-1) modified to handle arbitrarily shaped emitters of either planer or axial symmetry. To use this program, a closed boundary of the problem is drawn over a square mesh which is limited to 100 mesh points on the horizontal axis and 60 mesh points on the vertical (R) axis, with not more than 3600 total mesh points. The boundary points are specified in sequence using a coding method which specifies the Δr and Δz from a mesh point to the boundary. Either the potential (Dirichlet boundary) or the normal derivative (Neumann boundary) is specified for each boundary point. The program calculates the finite difference equations for each mesh unit within the problem and proceeds to generate the solution to Poisson's equations which match the boundary conditions. The space charge limited current at the emitter is first calculated using the Laplacian fields. Trajectories are then calculated for 27 rays until each ray strikes the boundary. As a ray crosses a vertical mesh line, the space charge contribution is calculated and distributed to the two mesh points above and below the point where the ray is crossed. The potential is then calculated including this space charge and a new value of the space charge limited emitter current is calculated. The entire procedure is repeated, and new trajectories are calculated. In practice, the solution converges after 4 or 5 iterations. The program can also calculate trajectories, including space charge, for particles emitted with nonzero initial velocities at arbitrary angles of emission. However, in this case the amount of current must be specified because the program cannot calculate the current with nonzero E field at the emitter. The outputs of this program are the perveance, CAL-comp plots of the trajectories, and the equipotentials including space charge.

For thrust beam leakage current computations, the electron emitting ion beam was modeled by an emitting cone with a half angle of 15^{o} and having a 1 m diameter at the array. The array was assumed to be a 20 m diameter unipotential disc at + 2000 V. Furthermore, the plasma sheath surrounding the array was assumed to be the sheath geometry found in the electrolytic tank (Case I) for a unipotential disc at + 2000 V at an altitude of $\approx$ 3 Re. Figure F-1 shows the computer generated trajectories for this model. Note that most of the electrons are collected on the outer portions of the disc and that the electrons emitted from the downstream portion of the cone miss the edge of the disc and are presumably collected on the opposite side. The calculated perveance for this geometry was

$$P = 12 \times 10^{-6} \text{ A/V}^{\frac{3}{2}}$$

which corresponds to a leakage current of 1.07 A at 2000 V. The current at other array voltages has been calculated using $I = PV^{3/2}$ and converted to a power loss plotted in Fig. F-2. We see that at 2 kV the power loss repre-

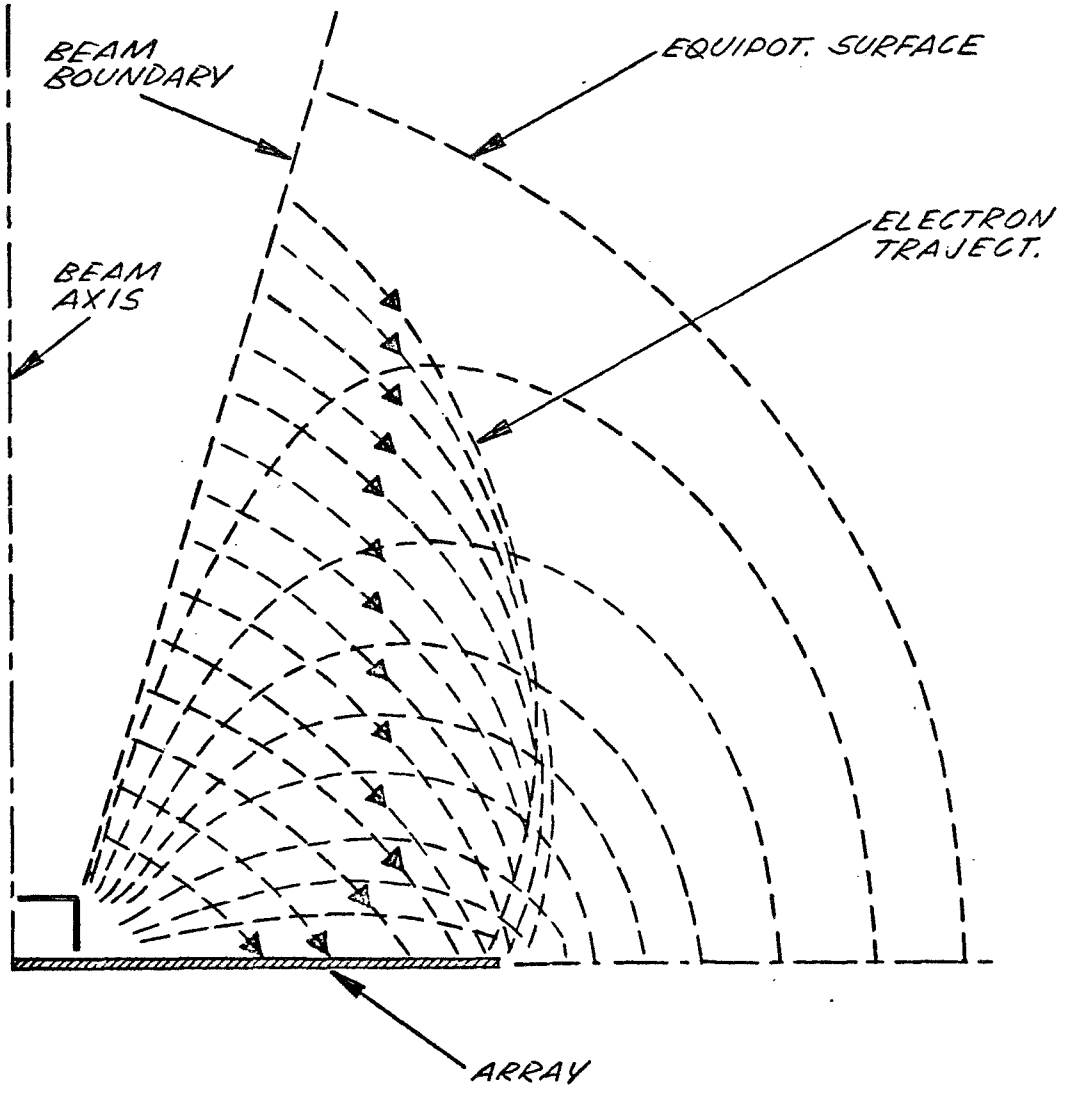

Fig. F-1. Computer plot of electron trajectories emitted space charge limited from ion beam $P_{calc} = 12 \times 10^{-6}\ A/V^{3/2}$.

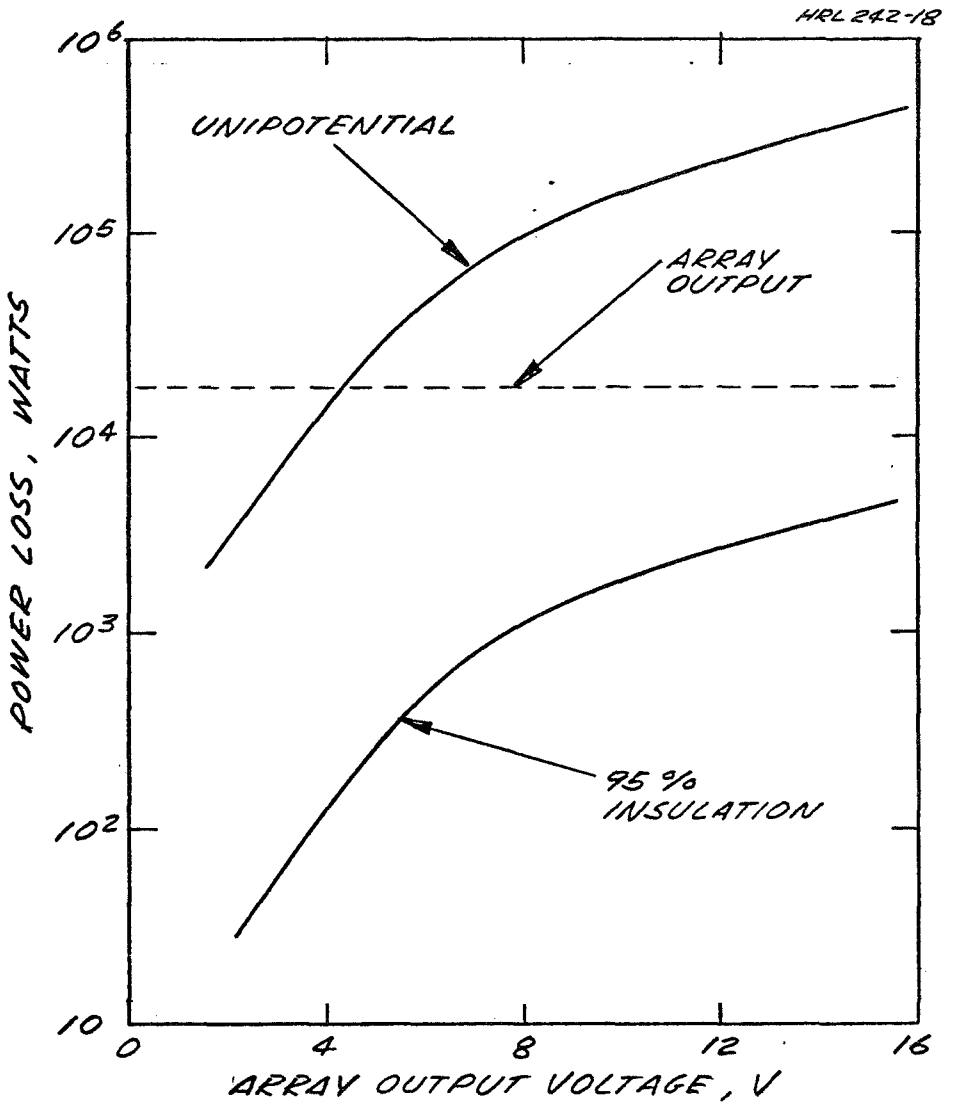

Fig. F-2. Power loss contributed by leakage current from thrust beam.

sents ~ 12% of the array's output while at ~ 5 kV it is equal to the array's output. In making these calculations, we have neglected that, at voltages higher than 2 kV, the sheath width becomes larger so that the actual currents would be somewhat higher because the emitting cone becomes longer; the opposite is true for array voltages below 2 kV.

In estimating the power loss for the checkerboard model in which ~ 95% of the array's area is an insulator floating at plasma potential and in which the tabs, with 5% of the area, are at the array voltage, we have scaled the unipotential disc currents down by a factor dependent on the "average" effective potential of the checkerboard model. Thus, for the above model at distances of one or two "periods" from the array (2 to 4 cm), the effective potential is ~ 5% of the tab (array potential). The currents for the checkerboard model are thus related to the currents found for the unipotential model as follows:

$$I_{CB} \simeq I_{disc}\,(0.05)^{\frac{3}{2}} \qquad \frac{I_{disc}}{89.6}$$

We have multiplied these currents by the actual array voltage to arrive at a power loss for this model. We see in Fig. F-2 that the power loss is negligible for array voltages up to 16 kV. All computed losses are quite conservative because of the previously mentioned reduction of the effective emitting area of the thrust beam as the plasma sheath width becomes smaller.

In the previous discussions, we have assumed that the electrons were emitted normal to the cone shaped ion beam boundary with zero initial velocity. To simulate more accurately a neutralized ion beam in which the injected electrons make zig-zag motions as they bounce off the beam boundaries, we have run the previous unipotential disc case with electrons having 15 eV total energy (corresponding to approximately the neutralizer coupling voltage) of which 10 eV is directed in the downstream direction and which arrive at the beam boundary with an energy of 1 eV directed normal to the boundary. For this calculation we injected the current previously calculated by the computer for the zero initial velocity case. The calculated trajectories for the second case are shown in Fig. F-3. We see that only the two electrons nearest the plasma boundary escape while all others are collected, even though they make wide excursions before heading toward the disc. Thus we conclude that, for the unipotential + 2000 V disc, the currents collected with zero initial velocity and with 10 eV tangential velocity are virtually identical. However, for the checkerboard model in which a 2000 V array voltage would be seen as 100 V by the emitted electrons, we would expect that with 10 eV tangential energy a larger portion of the emitted electrons would escape. Thus, the previously calculated power losses for the checkerboard model, found to be small even for the zero initial velocity case, would be still smaller if tangential velocities were included.

REFERENCE

F-1. W. B. Herrmannsfeldt, "Poisson Equation Solving Program," USAEC Tech. Rept., Contract AT (04-3)-400, September 1965.

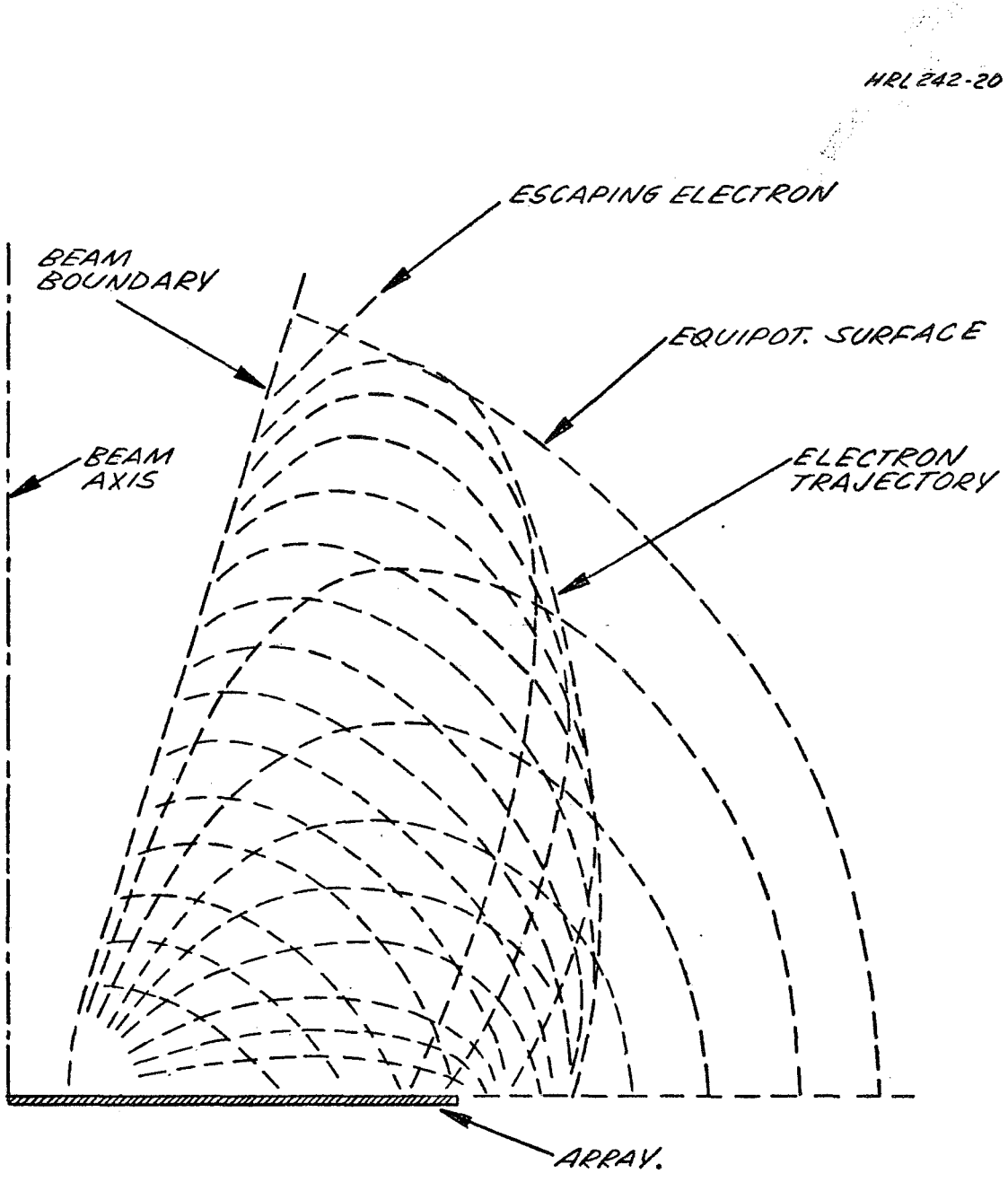

Fig. F-3. Computer plot of electron trajectories from ion beam with electrons having 10 eV initial tangential energy in downstream direction.

APPENDIX G - REDUCTION OF SOLAR ARRAY POWER LOSSES USING A GRID

A partially insulated high voltage solar array of conventional design, which floats electrically in the space plasma, will suffer power losses due to current leakage through the plasma, as discussed earlier. At low altitudes such losses can be a substantial percentage of the total power output and, therefore, it is of interest to consider methods of limiting these losses. The use of a transparent conductive grid to surround and shield the array has been studied in this regard. The problem is very similar to that of a standard triode electron tube with the additional equilibrium constraint that the total current collected from the plasma by the array is zero (the current flows in at one end of the array and out at the other). One approach toward a current controlling grid is to use a relatively fine, conductive screen (1 cm grid wire spacing) surround it with the entire array, and electrically connect it to the most negative end of the array. The total current collected by this configuration (including the grid) is zero with a grid potential which is slightly negative with respect to the plasma. This leads to a reduction in current leakage from the plasma as is easily understood with reference to Fig. G-1. Plasma ions are attracted to the negative biased grid; however, as a result of the high grid transparency, most ions pass through the grid without being collected. Because most of the array is positive with respect to the plasma, the ions which pass through the grid are reflected before reaching the array surface and again pass through the grid into space with only a small probability of collection by the grid. The small portion of the array which is negative also collects ions; however, the total collected ion current is much less than that of an unshielded array. The condition that the total collected current is zero means that the ion current to the grid is balanced by an equal electron current to the positive portions of the array across the grid. Because the grid holds back most of the arriving electrons, the total leakage current is reduced.

The potential distribution of the array and the dimensions of the grid system are illustrated in Figs. G-2 and G-3 for an array model which assumes that the array potential varies linearly from one end to the other. The total output voltage of the array is V. The potential (to be determined) of the most negative end of the array with respect to the plasma is V_o. The length of the array is L and z_o is the position on the array at which the array potential equals the plasma potential. The local potential of the array is denoted by V_a. In Fig. G-3, the grid wires are parallel and of radius t. The thickness of the plasma sheath is ℓ'. To achieve the desired operation the following conditions must be satisfied:

$a >> t$, for high transmission, where a is the wire separation
$\ell' >> a$, so the plasma does not leak through the grid.

In addition, the following reasonable assumptions are made to achieve simplicity in the calculations:

$L >> \ell'$ (this is true for the altitude range over which the major losses occur)

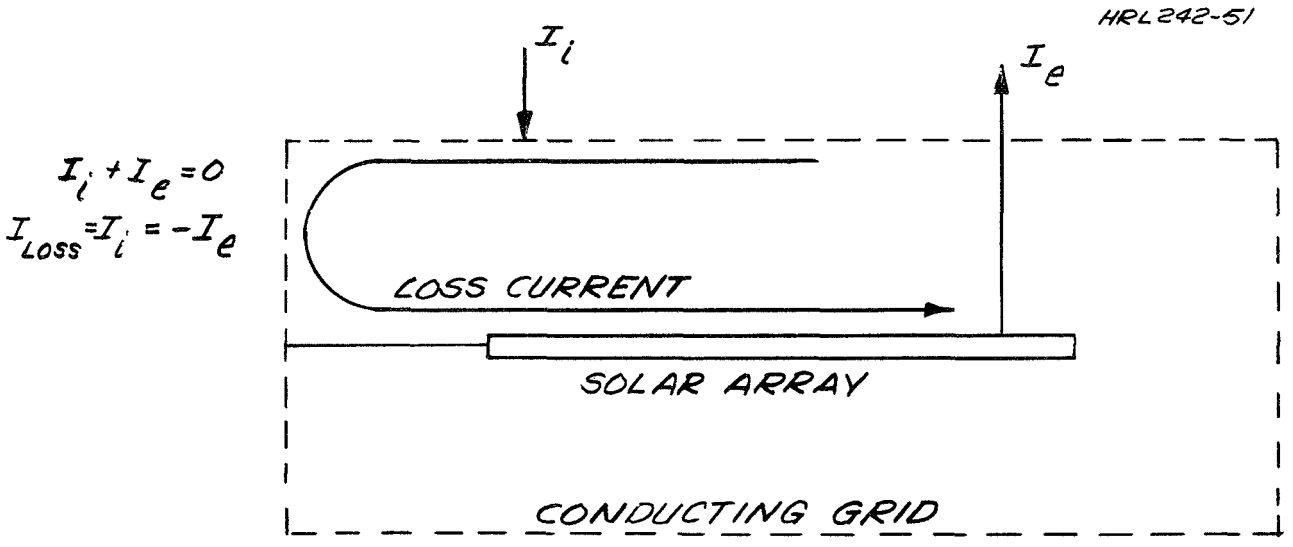

Fig. G-1. Basic grid configuration.

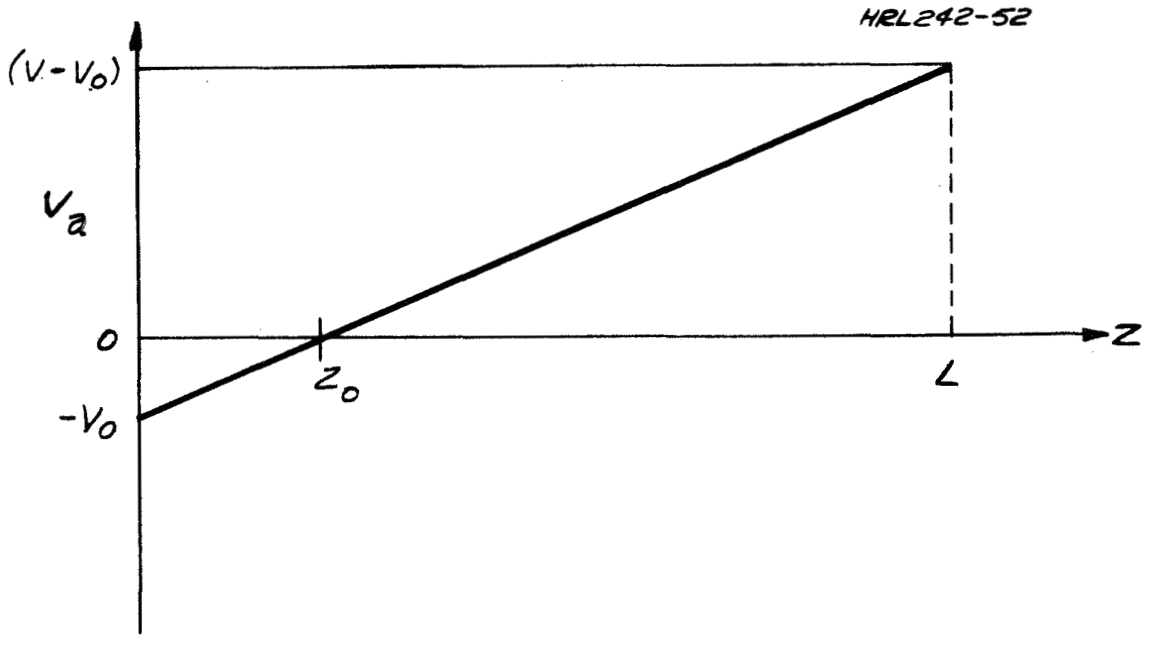

Fig. G-2. Dependence of array potential on position for a floating array.

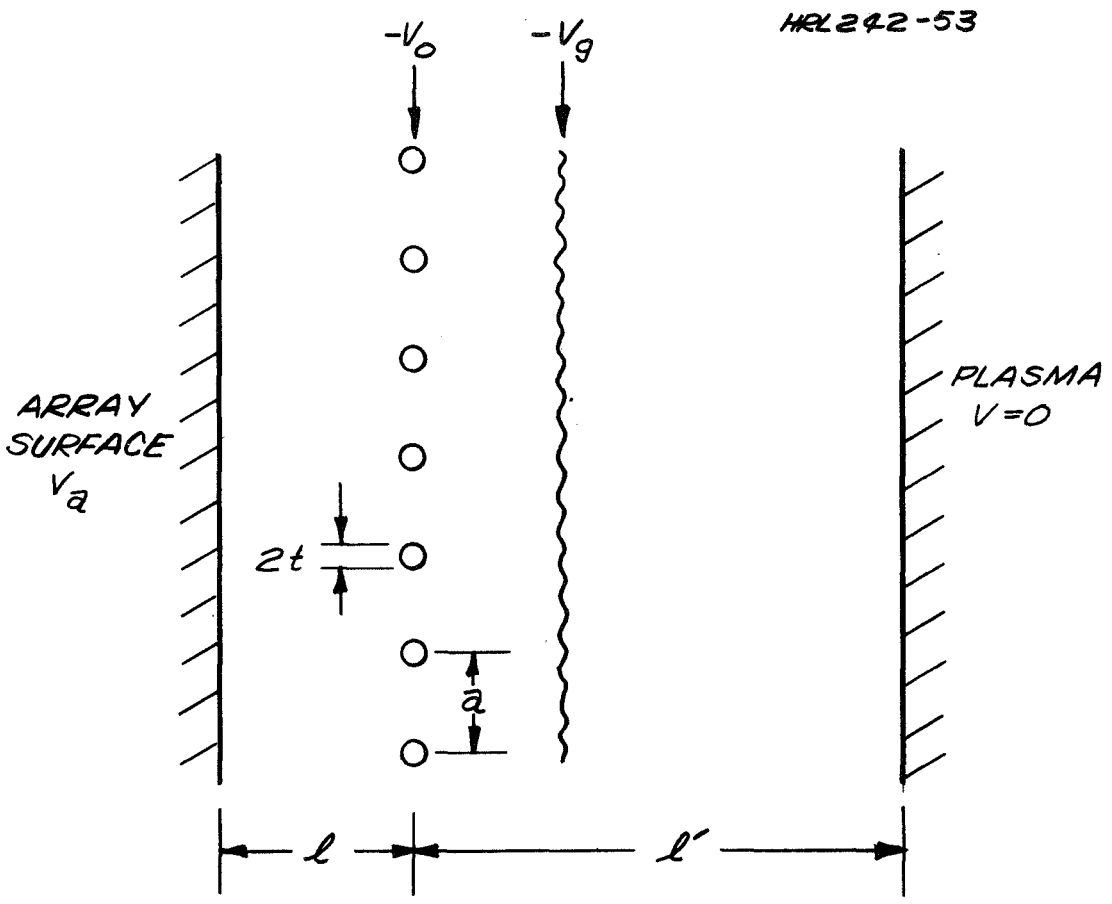

Fig. G-3. Dimensions and potentials for the shielded array model.

$$\ell \gg a$$
$$T_i = T_e \equiv T$$
$$V \gg kT_e$$
$$L \gg l,$$

and space charge can be neglected.

The problem of determining the plasma loss currents is very difficult as a result of the complicated potential distribution near the grid wires and the energy distribution of the plasma particles. In order to simplify the calculations a new potential V_g is defined. This is the potential of an imaginary plane, unipotential surface, parallel to the array surface, which has the same macroscopic influence on plasma particle motion as would the grid. The potential V_g is assumed to be related to the other system potentials by the relation

$$V_g = \alpha \left(\frac{V_a}{\mu} - V_o\right),$$

where μ is the amplification factor for a triode (when the grid potential is equal to $-\mu^{-1}$ times the anode potential, the electric field at the cathode is zero) (Ref. G-1) and α is an unknown factor expressing the effectiveness of the grid. It is expected that α lies in the range 0.1 to 1.0.

The potential which the grid attains is obtained by setting the sum of the ion and electron currents collected from the plasma equal to zero. The total collected ion current I_i can be written as

$$I_i = j_{isat}\ d\left[z_o + \int_{z_o}^{L} 2\varepsilon' dz\right]$$

where j_{isat} is the ion saturation current density, d is the width of the array, and ε' is the opacity of the grid for ions. The first term in brackets represents the ion current collected on that portion of the array which is at a negative potential. The second term represents the collection of ions on the grid wires; the factor 2 is due to the two transits which the ions make through the grid. The quantity ε' is not equal to the optical opacity ε but must be determined as in the theory of particle collection by electrostatic probes (Ref. G-2). With the observation that ions do not "see" individual grid wires until they are within a distance of approximately $a/2\pi$ from the grid, where the potential is approximately equal to V_g, it can easily be shown that

$$\frac{\varepsilon'}{\varepsilon} = \left(\frac{V_o}{V_g}\right)^{1/2}$$

and, therefore, the result for the collected ion current is

$$I_i = j_{isat}\ dL\left[\frac{V_o}{V} + \frac{\varepsilon}{\alpha^{1/2}}\ \frac{2\mu V_o}{V}\left(1 - \sqrt{1 - \frac{V}{\mu V_o}}\right)\right].$$

The total collected electron current I_e is written as

$$I_e = -j_{esat}\, d \int_o^L \varepsilon^{\frac{-eVg}{kT}}\, dz$$

Performing the required integration gives

$$I_e = -j_{esat}\, dL\, \varepsilon^{\frac{-e\alpha V_o}{kT}\left(1 - \frac{1}{\mu}\right)}\, \frac{kT\mu}{e\alpha V}\left(\varepsilon^{\frac{e\alpha V}{\mu kT}} - 1\right),$$

Setting the sum of I_e and I_i equal to zero gives an expression for V_o. The loss current I can then be simply equated to the ion current (or electron current) which is obtained by using the expression for V_o in the equation for I_i. Using the following values for the various system parameters

t	=	0.0025 cm
ℓ	=	50 cm
α	=	0.1-1.0
a	=	1 cm
μ	=	50 (Ref. G-3)
kT	=	0.5 eV
V	=	16 kV,

one obtains

$$\frac{V_o}{\mu V} \approx 1 \text{ and } \frac{e\alpha V}{\mu kT} >> 1$$

with the result that the ratio I/I_o, where I_o is the loss current without a grid can be written as

$$\frac{I}{I_o} = \frac{1}{\mu} + \frac{4\varepsilon}{\alpha}\, 1/2$$

For the above parameters this ratio has values in the range 0.03 to 0.08.

Thus, it is seen that a large (a factor of ten or more) reduction in the plasma loss current can be achieved by using a grid.

It should be noted that the effects due to trapping of ions in the potential well of the grid wires has not been included in the above calculations due to the vastly increased difficulty in analysis. Experiments are required to determine the influence of such effects on the efficacy of the grid.

REFERENCES

G-1. K. Spangenberg, Vacuum Tubes (McGraw-Hill, New York, 1948) p. 125

G-2. R. H. Huddlestone and S. L. Leonard, Plasma Diagnostic Techniques (Academic Press, New York, 1965), p. 128

G-3. L. Pensak, Phys. Rev. 75, 472 (1949).

APPENDIX H - SECONDARY EMISSION AND PHOTOEMISSION PROCESS IN FUSED SILICA

The following is a detailed discussion of the important charged particle emission processes for fused silica as determined from existing experimental data.

A. SECONDARY ELECTRON EMISSION BY ION IMPACT

Few data are available concerning the emission of secondary electrons due to ion impact. However, Batanov (Ref. H-1) has obtained results for a molybdenum glass of unknown composition which is expected to have characteristics similar to those for fused silica. He found that the secondary emission coefficient (the number of secondary electrons per incident ion) varies linearly with ion energies up to 3 keV. For He^+ and H_2^+ ions the emission coefficient saturates at approximately 15 keV with yields of 2 for He^+ and 4 for H_2^+. The bulk of the secondary electrons have energies less than 10 eV.

B. ION EMISSION DUE TO ION IMPACT

Ions which are incident on a surface can be reflected or cause the emission of both positive and negative secondary ions (the emission of neutral particles will be discussed later). Batanov (Ref. H-2) has investigated ion emission resulting from positive potassium ion bombardment for a number of dielectric materials, including a molybdenum glass of unknown composition. He found that the yield (number of emitted ions per incident ion) of positive ions from glass decreased from approximately 0.15 at low primary energies to zero for incident energies greater than 1 keV. Results obtained with a number of dielectrics indicate that the yield depends markedly on the surface preparation and past history of ion bombardment; however, it can be generally stated that the maximum positive ion yields are in the range 0.1 to 0.3 and have nonzero values at low primary energies. The bulk of the emitted ions have energies in the range 0 to 40 eV. The yield of negative ions was found to be less than 0.02 for molybdenum glass and zero for freshly cleaved crystals of NaCl and KCl. These results suggest that the emission of secondary negative ions by positive primary ions is very weak for clean surfaces. Based on these results, fused silica will be assumed to have properties similar to those obtained by Batanov for glass samples.

C. SECONDARY ELECTRON EMISSION BY INCIDENT PRIMARY ELECTRONS

The emission of secondary electrons from fused silica has been discused by a number of authors. The results of Hackenberg and Brauer (Ref. H-3) for fused silica and pyrex (for comparison) are illustrated in Fig. H-1. The maximum yield is 2.4 and occurs at an incident primary energy of 400 eV. The secondary yield has a value of unity for primary energies of approximately 80 and 2,800 eV.

The results of Mueller (Ref. H-4) for fused silica, which extend to larger primary energies, are given in Table H-1. Mueller found that the pri-

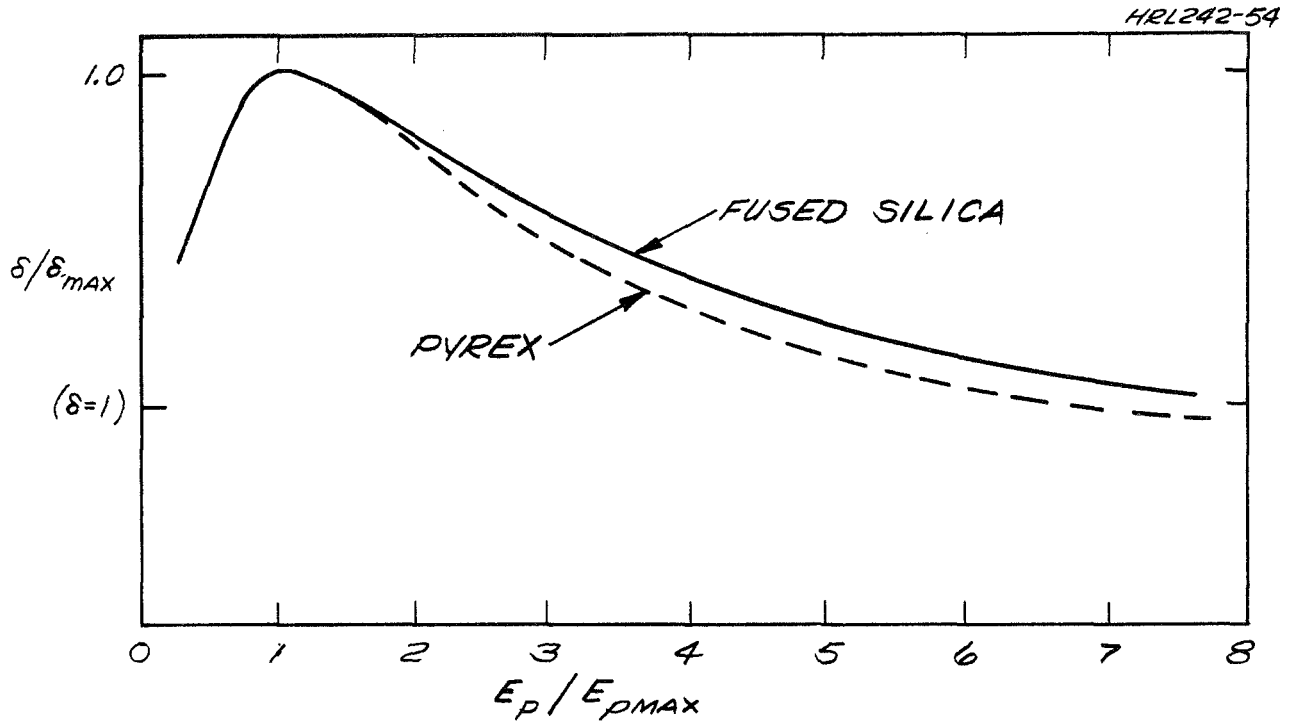

Fig. H-1. The secondary electron yield for incident primary electrons of energy E_p.

mary energy for unity secondary yield, which he found to occur at 2.30 to 2.65 keV, is constant over a sample temperature range of 100°C to 385°C. Similarly, the maximum secondary yield was found to be constant to within 2.3% over the temperature range 240°C to 420°C. The energy distribution of the secondary electrons is peaked at approximately 4 eV and the bulk have energies less than 10 eV.

Data for other materials are given by Redhead, et al. (Ref. H-5).

D. PHOTOEMISSION

Measurements performed with borosilicate and soda glasses have demonstrated that the photoemissive properties are strongly dependent on the impurity content of the glass (Ref. H-6). In particular, the quantum efficiency (number of electrons per incident photon) was found to be proportional to the concentration of sodium. For borosilicate glass, containing 4% sodium, the quantum yield was 10^{-4} for incident wavelengths of 2537 Å, 10^{-3} for radiation generated by a glow discharge ($\lambda < 1200$ A), and less than 10^{-8} for wavelengths longer than 3300 A.

TABLE H-1

Results for Fused Silica (From Mueller, Ref. H-4)

Primary electron energy (keV)	Secondary Yield
0.4	2.2 - 2.4
2.3 - 2.65	1.0
3.6	0.82
4.9	0.63
6.4	0.53
8.1	0.46
10.0	0.41

These results are roughly the same as those obtained for metals (Ref. H-7) which yield a photoelectric current density of approximately 2×10^{-9} A/cm^2 at 1 AU (Ref. H-8). Thus, for commercial fused silica, which contains less than 0.1% sodium, the expected photoemitted current density is expected to be less than 5×10^{-11} A/cm^2 at 1 AU (Ref. H-9). Because the solar spectral intensity is low at short wavelengths, most of the photoelectrons have energies on the order of several electron volts.

REFERENCES

H-1. G. M. Batanov, Soviet Phys.-Solid State 2, 1839 (1960); 4, 1306 (1963).

H-2. G. M. Batanov, Soviet Phys.-Solid State 3, 471 (1960); 4, 1306 (1963).

H-3. O. Hackenberg and W. Brauer, "Secondary Electron Emission from Solids," in Advances in Electronics and Electron Physics, (Academic Press, New York, 1959), Vol. 11, p. 413.

H-4. C. W. Mueller, J. Appl. Phys. 16, 453 (1945).

H-5. P. A. Redhead, J. P. Hobson, and E. V. Kornelsen, The Physical Basis of Ultrahigh Vacuum (Chapman and Hall, London 1968), p. 159.

H-6. V. K. Rohatgi, J. Appl. Phys. 28, 951 (1957).

H-7. I. Langmuir in Collected Works of I. Langmuir, G. Suits, Ed. Pergamon Press, New York 1961), Vol. 4, pp. 32ff.

H-8. G. P. Serbu, Space Res. 5, 564 (1965).

H-9. J. R. Hutchins III and R. V. Harrington, Encyclopedia of Chemical Technology, 1966, Vol. 10, p. 533.

APPENDIX I - SPUTTERING

A partially insulated high voltage solar array may be subject to sputter damage resulting from the impact of photoplasma ions which have been accelerated by the intense electric fields associated with the array. For solar arrays with voltage capabilities up to 16 kV, which are of interest under the present contract, the maximum range of energies for ions incident upon array surfaces is approximately 0 to 16 keV.

The rate at which a surface is eroded by the impact of energetic ions is dependent on the type of ions and their energies, as well as the composition of the surface. To calculate the sputtering rate of a given surface due to the incidence of energetic photoplasma ions, it is necessary to determine the ionic composition of the plasma and then to sum the contributions to the sputtering rate by each ionic species. The scarcity of data concerning plasma composition and sputtering yields (the number of ejected atoms per incident ion) for various ions and target surfaces will require the use of a number of approximations. Calculations and considerations are presented below which have been employed to determine the sputtering rates for various metal surfaces and a characteristic insulator (fused silica).

Some experimental and theoretical data are available for the ionic composition at low altitudes (Ref. I-1); however, the densities of the various ion species vary in time. To obtain the expected density ranges for the various important ionic constituents, it is assumed that the fractional composition is constant and that it can be obtained from existing data. The density ranges are then obtained by employing the charge neutrality requirement and setting the sum of the ionic densities equal to the extremes of the electron density range, which is well known. Table I-1 gives the density ranges for the main ionic species for several altitudes.

TABLE I-1

Density Ranges

Altitude, cm	H^+, cm^{-3}	He^+, cm^{-3}	N^+, cm^{-3}	O^+, cm^{-3}
400	29 to 5.4 x 10^2	29 to 5.4 x 10^2	3.9 x 10^3 to 7.2 x 10^4	7.8 x 10^4 to 1.4 x 10^6
600	87 to 2.6 x 10^3	6.1 x 10^2 to 1.8 x 10^4	1.7 x 10^3 to 5.2 x 10^4	1.7 x 10^4 to 5.2 x 10^5
1000	1.1 x 10^3 to 1.3 x 10^4	2.2 x 10^3 to 2.6 x 10^4	7.3 x 10^2 to 9 x 10^3	4.4 x 10^3 to 5.2 x 10^4
3.4 x 10^4 (synch. alt.)	1 to 20	<< 1	<< 1	<< 1

To determine the flux of the individual ionic species incident on the target surface, it is assumed that the surface is plane and infinite and that each species arrives with its ion saturation flux density

$$S_i = \tfrac{1}{4} n_i \bar{v}_i$$

where n_i and $\bar{v}_i$ are the density and average velocity of the i^{th} ion species. The average velocity depends on the temperature T_i and mass M_i of the ion species as given by

$$\bar{v}_L = \left(\frac{8}{\pi} \frac{kT_i}{M_i}\right)^{1/2}$$

At the low altitudes T_i is the same for all ion species and is equal to the temperature of the electrons (Ref. I-2). Therefore, at a given low altitude v_i depends only on the ion mass.

The emitted flux of sputtered atoms expressed in atoms/cm^2-sec is simply given by

$$S_a = \sum_i \gamma_i(x) S_i \qquad \text{(I-1)}$$

where γ_i (x) is the sputtering yield of the i^{th} ionic species incident on a given target surface labeled x. The sputtering rate of the target surface, expressed in Angstroms per second, is given by

$$S = s \frac{W_a}{\rho N_o} \times 10^8 \qquad \text{(I-2)}$$

where W_a is the atomic weight of the target material, ρ is the target density, and N_o is Avagadro's number.

An extensive tabulation of sputtering yields is not available; however, good estimates can be obtained from existing experimental results. Detailed consideration has been given to silver, which is representative of conductors, and fused silica, which is expected to be characteristic of insulators, because of the relatively greater amount of data available for these materials.

The sputtering of silver by light ions has been studied by Gronlund (Ref. I-3). The results indicate that

$$\gamma_{H^+}\ (Ag) \cong 0.03 \quad \text{and} \quad \gamma_{He^+} \cong 0.40$$

over an incident ion energy range of 2 to 16 keV. Estimates of the sputtering yields due to the impact of N^+ and O^+ ions on silver have been obtained from the results of Rol (Ref. I-4) and the data tabulations of Carter (Ref. I-5). For example, Rol found γ_{N^+} (Cu) = 2.0 over an incident ion energy range of approximately 2 to 16 keV, and from Carter it is found that

$$\frac{\gamma_{D^+}(Ag)}{\gamma_{D^+}(Cu)} = 1.7$$

Assuming that this ratio holds for N^+ ions incident on silver and copper, one obtains γ_{N^+} (Ag) = 1.7 x 2.0 = 3.4. Similar considerations were employed to obtain γ_{O^+} (Ag) = 4.3.

The sputtering rates for silver obtained from the above results are given in Table I-2 for several altitudes and plotted in Fig. 29. At the lower altitudes the sputter rate is due primarily to O^+ impingement, and at high altitudes H^+ is dominant.

TABLE I-2

Sputtering Rates for Silver

Altitude, (km)	S, (Å/yr)
400	7×10^3 to 1.2×10^4
600	1.7×10^2 to 5.3×10^3
1000	6.3×10^1 to 7.2×10^2
3.4×10^4 (synch. alt.)	1.2×10^{-3} to 2.4×10^{-2}

Rough estimates of the sputtering rate for other conducting target materials in relation to silver can be obtained by inspection of tabulated sputtering yield data and use of eqs. (I-1) and (I-2). Table I-3 gives the approximate factors by which the sputtering rate for silver should be multiplied in order to obtain the rate for the listed conducting materials.

TABLE I-3

Sputtering Rates for other Metals

Material	Fraction of Sputtering Rate of Silver
Sn	0.5
Cu	0.3
Ni	0.2
Mo	0.1
Al	0.6

There are very few available data concerning the sputtering of fused silica and other insulators. Study of the sputtering of fused silica by Kr^+ ions has shown that the sputtering yield is 1 molecule/ion for ions of 5 keV energy and 2 molecules/ion for ions with energies in the range 10 to 25 keV (Ref. I-6). The sputtering yields for ions which compose the space plasma are obtained from the approximate relationship (Ref. I-7).

The remainder of the calculation of the sputtering rate is the same as for silver. The results are given in Fig. 30.

REFERENCES

I-1. F. S. Johnson, Satellite Environment Handbook (Stanford University Press, Stanford, 1965), p. 1965.

I-2. Ya. L. Al'pert, et al., "Space Physics with Artificial Satellites," Consultants Bureau, 1965.

I-3. H. Heil, Phys. Rev. 164, 887 (1967).

I-4. P. K. Rol, et al., Physica 26, 1000 (1960).

I-5. G. Carter and J. S. Colligon, Ion Bombardment of Solids (American Elsevier, New York, 1968), p. 310.

I-6. Carter and Colligon, op. cit.

I-7. P. K. Rol, et al., Physica 26, 1009 (1960).

APPENDIX J - FAILURE RATE DETERMINATION FOR BYPASS MODULES

Assuming that any open circuit failures that take place on the array occur in a random manner, calculations based on the binomial distribution can be used to determine module failure rates. The development of the final equation, which was then incorporated in a computer program, is given below:

E	=	total expected number of failures
P	=	probability of failure
R	=	reliability
c	=	cell
r	=	row
m	=	module
N	=	number of modules per block
K	=	number of modules failed
S	=	number of cell rows in series per block
F	=	maximum allowable cell failures per row without going into bypass mode (F = 0 for 1 to 8 cells, and F = 1 for 8 to 15)

$$P_K = P(K:N) = \frac{N!}{(N-K)!\,K!} P^K R^{N-K} \text{ (binomial distribution)}$$

$$E_m = \sum_{K=0}^{N} K \frac{N!}{(N-K)!\,K!} P_m{}^K R_m{}^{N-K}$$

$$P = 1 - R_S$$

$$R_m = (R_r)^{\frac{S}{N}}$$

$$P_m = 1 - (R_r)^{\frac{S}{N}}$$

$$E_m \sum_{K=0}^{N} K \frac{N!}{(N-K)!\,K!} 1 - (R_r)^{\frac{S}{N}}{}^K \; (R_r)^{\frac{S}{N}}{}^{N-K}$$

$$\text{Failure Rate} = \frac{E_m}{N}$$

R_r is calculated from

$$P_r(K_c:N_c) = \sum_{K_c=0}^{F} \frac{N_c!}{(N_c-K_c)!\,K_c!} P_c{}^K R_c{}^{N-K}$$

$$R_r = 1 - P_r$$

The body of the computer program is shown in Fig. J-1.

```
100 PRINT "PAR. CELLS"
110 PRINT
120 PRINT "N=1","10","44","440","4400"
130 PRINT
140 PRINT
150 READ Q,A
160 PRINT Q
165 PRINT
170 READ N
175 LET P=0
180 LET C=0
190 LET B=1
200 LET B=A*B
210 LET C=C+1
220 IF C=4400/N THEN 240
230 GØTØ 200
240 FØR K=1 TØ N
250 LET E=(1-B)↑(K/2)
260 LET F=N-K
270 LET G=B↑(F/2)
280 LET H=N
285 LET R=N-1
290 LET I=1
295 LET S=1
300 LET I=SQR(H)*I
310 LET H=H-2
320 IF R=N-K THEN 340
323 LET S=SQR(R)*S
325 LET R=R-2
327 IF H=N-K THEN 340
330 GØTØ 300
340 LET J=K
350 LET L=1
360 LET L=SQR(J)*L
370 LET J=J-1
380 IF J=0 THEN 400
390 GØTØ 360
400 LET Ø=K*I/L*E*I/L*S*E*S*G*G
420 LET P=Ø+P
430 IF Ø<P*1E-4 THEN 460
440 NEXT K
460 PRINT P,
470 IF N=4400 THEN 130
480 GØTØ 170
620 END
```

Definitions:

Q = Number of cells in parallel per row.

A = Reliability of a row.

N = Number of modules per block.

P = Total expected number of module failed.

Fig. J-1. Failure rate determination for bypass modules.

The assumption that cells fail randomly on a flexible solar panel has been supported by the results of limited testing performed by HAC on one of its own developmental panels in connection with another program. This panel was subjected to repeated roll-up cycles under different simulated pre-launch tensions and was also exposed to repeated launch type vibration exposures. The resulting failures, which were essentially all in cover slide cracking, followed almost exactly a random pattern.

There were three cells per parallel row, and the ratio of actual failures to predicted failures was as follows:

Number of Cells Failed per Row	Ratio of Actual to Predicted
1	1.01
2	0.90
3	2.00*

* Not statistically representative because there was only one occurrence, while 0.5 was predicted.